Computational modelling and analysis of the flow and performance in hydrocyclones

Author:
Ghodrat, Maryam

Publication Date:
2014

DOI:
https://doi.org/10.26190/unsworks/17028

Computational Modelling and Analysis of the Flow and Performance in Hydrocyclones

Maryam Ghodrat

A thesis submitted in fulfilment of the requirements for the degree of

Doctor of Philosophy

UNSW
AUSTRALIA

Lab for Computer Simulation and Modelling of Particulate Systems
School of Materials Science and Engineering
Faculty of Science
The University of New South Wales

March 2014

PLEASE TYPE

THE UNIVERSITY OF NEW SOUTH WALES
Thesis/Dissertation Sheet

Surname or Family name: Ghodrat

First name: Maryam | Other name/s:-

Abbreviation for degree as given in the University calendar: PhD

School: Materials Science and Engineering | Faculty: Science

Title: Computational modeling and analysis of the flow and performance in hydrocyclones

Abstract 350 words maximum: (PLEASE TYPE)

Hydrocyclones have been widely used to separate particles by size in many industries. Their flows are complicated and involve multiple phases: liquid, gas, and particles of different sizes and densities. A two fluid model, facilitated with the mixture model, has been used to study the flow in hydrocyclones under wide range of conditions and used here to study the effects of geometrical configuration and material properties of cyclones operated at different feed solids concentrations. The variables considered include geometrical configurations such as dimensions and shape of body, cone and vortex finder as well as particle density.

The outcome shows a smaller cyclone results in an increased cut size, decreased pressure drop, sharper separation and higher water split. Both large and small spigot diameters lead to poor separation performances. Accordingly, an optimum spigot diameter can be identified depending on feed solids concentration. It is also shown that for all considered hydrocyclones, a better separation performance can be achieved by the operation at lower feed solid concentration.

Further research shows that cyclone performance is sensitive to both length and shape of conical section. A longer conical section leads to decreased inlet pressure drop, d50, and Ep, and an increased water split. When cone shape varies from concave to convex, a compromise optimum performance for the cyclone with a convex cone is observed with a minimum Ep and relatively small pressure drop and water split. A new hydrocyclone featured with a long convex cone is then proposed which can improve the performance of the conventional cyclone. The key characteristics of flow in a hydrocyclone are then investigated when vortex finder geometry including diameter length and shape varies. It has been shown that a compromise optimum performance can be identified with relatively small inlet pressure drop, Ep, and water split.

Discussion is then extended to flow behaviour analysis under the effect of different density fractions. The origin of flow pattern and the motion of coal particles have been predicted and discussed. The effect of coal density variation on operational conditions and performance of the large diameter hydrocyclones are also studied in this work.

ORIGINALITY STATEMENT

'I hereby declare that this submission is my own work and to the best of my knowledge it contains no materials previously published or written by another person, or substantial proportions of material which have been accepted for the award of any other degree or diploma at UNSW or any other educational institution, except where due acknowledgement is made in the thesis. Any contribution made to the research by others, with whom I have worked at UNSW or elsewhere, is explicitly acknowledged in the thesis. I also declare that the intellectual content of this thesis is the product of my own work, except to the extent that assistance from others in the project's design and conception or in style, presentation and linguistic expression is acknowledged.'

Signed ....

Date 31/3/14 ....

COPYRIGHT STATEMENT

'I hereby grant the University of New South Wales or its agents the right to archive and to make available my thesis or dissertation in whole or part in the University libraries in all forms of media, now or here after known, subject to the provisions of the Copyright Act 1968. I retain all proprietary rights, such as patent rights. I also retain the right to use in future works (such as articles or books) all or part of this thesis or dissertation.

I also authorise University Microfilms to use the 350 word abstract of my thesis in Dissertation Abstract International (this is applicable to doctoral theses only).

I have either used no substantial portions of copyright material in my thesis or I have obtained permission to use copyright material; where permission has not been granted I have applied/will apply for a partial restriction of the digital copy of my thesis or dissertation.'

Signed ....

Date 31/3/14 ....

AUTHENTICITY STATEMENT

'I certify that the Library deposit digital copy is a direct equivalent of the final officially approved version of my thesis. No emendation of content has occurred and if there are any minor variations in formatting, they are the result of the conversion to digital format.'

Signed ....

Date 31/3/14 ....

To my parents and my sister

ABSTRACT

Hydrocyclones have been widely used to separate fine particles by size in many industries. Their flows are complicated by the presence of swirling flow, turbulence, air core and segregation, and involve multiple phases: liquid, gas, and particles of different sizes and densities. A two-fluid model, facilitated with the mixture model, has been extended and used to study the complicated liquid-gas-solid flow in hydrocyclones under a wide range of conditions. In the model, the strong swirling flow of the cyclone is modelled using the Reynolds stress model. The interface between liquid and air core and the particle flow are both modelled using the so called mixture model. The solid properties are described by the kinetic theory. The applicability of the proposed approach has been verified by good agreement between the measured and predicted results. It is used here to study the effects of geometrical configuration and material property for hydrocyclones operated at feed solids concentrations from 4% to 30 % (by volume), which is well beyond the range reported before.

The systematic studies for better designing and controlling of the hydrocyclone process are few and the fundamentals governing the complicated liquid-gas-solid flow in a hydrocyclone are still poorly understood, particularly at different feed solids concentrations and particle densities though being extremely important in practice. On the other hand, lack of comprehensive studies of the flows and performance in hydrocyclones of different geometrical configurations under wide range of feed solids concentrations is indisputable.

In addition the effect of particle density distribution that represents a foremost difference between several major coal types is another area that requires further fundamental research work. It is also important to note that the current research in classification technology based on the particle densities is largely inadequate and efforts should be made to establish a better understanding of the impact of fine particle classification.

Based on these shortcomings, a two fluid model (TFM) facilitated by Mixture model is extended and used to describe hydrocyclone flows and performances under a wide range of flow conditions. A systematic study of the geometrical, operational and material

variation effects on the flows and performances of hydrocyclones operated at wide range of feed solid concentrations is carried out. The key characteristics of the multiphase flows in hydrocyclones are examined in terms of the flow field, pressure drop, and amount of water split to underflow (defined as the ratio of the volumetric water flow rate of the underflow to that of the feed stream), separation efficiency and underflow discharge type. The variables considered include geometrical configurations such as dimensions and/or shape of body, cone and vortex finder as well as particle density.

The outcome of the work shows that the multiphase flows in a hydrocyclone vary with cyclone size and spigot diameter, leading to different performance. For given particles of different sizes, when cyclone body size is increased varied within a certain range, the separation efficiency decreases with the increase of cyclone size, correspondingly the cut size increases, whereas the water split and hence the by-pass flow decreases. Both large and small spigot diameters may lead to poor separation performances. Accordingly, an optimum spigot diameter can be identified depending on feed solids concentration. It is also shown that for all the considered hydrocyclones, a better separation performance and a smoother running state can be achieved by the operation at a lower feed solid concentration.

Further research on geometrical variables shows that cyclone performance is sensitive to both length and shape of conical section. A longer conical section length leads to decreased inlet pressure drop, d_{50}, and E_p, and at the same time, increased water split. When cone shape varies from concave to convex styles gradually, a compromise optimum performance for the cyclone with a convex cone is observed with a minimum E_p and relatively small inlet pressure drop and water split to underflow. Based on the numerical experiments, a new hydrocyclone featured with a long convex cone is proposed which can improve the performance of the conventional cyclone at all the feed solids concentrations considered.

The key characteristics of flow in a hydrocyclone are then investigated when vortex finder geometry including diameter length and shape varies. It has been shown that a compromise optimum performance can be identified with relatively small inlet pressure drop, E_{p}, and water split. It is also found that the effect of vortex finder length on separation efficiency is much less significant than diameter and shape, which shows opposite trends at low and high feed solids concentrations. The results obtained in this part of the work expounded using the predicted tangential and axial velocities and solid volume fraction.

Discussion is then extended to flow behaviour analysis under the effect of different density fractions. The origin of a flow pattern, and the motion of coal particles have been predicted and discussed. Moreover, the key performance features of the flow are examined in relation to the instability of fluid flow. The effect of coal density variation on operational conditions and performance of the large diameter hydrocyclones are also studied in this work.

ACKNOWLEDGMENTS

The research presented in this thesis was carried out at the Lab for Simulation and Modelling for Particulate System (SIMPAS), School of Material Science and Engineering, The University of New South Wales, Australia.

I am deeply indebted to all those who have provided me the support, advice and encouragement during my study. I would like to specially thank my supervisor, Professor Aibing Yu, for giving me the opportunity to carry out this research project, teaching me how to do scientific research, and for always keeping my best interest in mind and my co-supervisor Dr Shibo Kuang for his continuous support. This work would not be possible without their guidance and inspiration. I also wish to thank Dr. Andrew Vince for his much helpful advice and guidance.

I wish to thank University of New South Wales, Australian Research Council (ARC) and Minco Tech for providing me with postgraduate scholarship, and financial support for this work.

Thanks also to my friends and colleagues in the "Lab for Computer Simulation and Modelling of Particulate Systems" for providing me with much help in my study. I am also grateful to the staff of School of Materials Science and Engineering in UNSW for their various helps during the course of my study.

Special thanks to my beloved mother and father and my sister for their love, encouragement and support, which have always been a source of inspiration in my work.

LIST OF PUBLICATIONS

JOURNAL PAPERS

1. M. Ghodrat, S. B. Kuang , A. B. Yu , A. Vince , G. D. Barnett , and P. J. Barnett., Computational Study of the Multiphase Flow and Performance of Hydrocyclones: Effects of Cyclone Size and Spigot Diameter. *Published in Industrial & Engineering Chemistry Research, 2013, 52, 16019-16031*

2. M. Ghodrat, S. B. Kuang, A. B. Yu, Andrew Vince., "Numerical analysis of hydrocyclones with different conical section designs" , *Minerals Engineering ,Volume 62, July 2014, Pages 74–84*

3. M. Ghodrat, S. B. Kuang, A. B. Yu, Andrew Vince., "Numerical analysis of hydrocyclones with different vortex finder configurations" , *Minerals Engineering, Volume 63, August 2014, Pages 125–138*

4. M. Ghodrat, S. B. Kuang, A. B. Yu, A. Vince "CFD study of the effect of coal density on multiphase flow and performance of hydrocyclone" .To be submitted.

CONFERENCE PAPERS

5. M. Ghodrat, S. B. Kuang, A. B. Yu, A. Vince, G. D. Barnett, P. J. Barnett, 'CFD study of the multiphase flow in classifying hydrocyclone: Effect of cone geometry', *Ninth International Conference on CFD in the Minerals and Process Industries, CSIRO*, **Melbourne, Australia**, 10-12 December 2012.

6. M. Ghodrat, S.B. Kuang, A.B. Yu, A. Vince, G.D. Barnett and P.J. Barnett., 'Numerical analysis of hydrocyclones with different conical section designs'. In *MEI* Conferences: Physical Separation '13: Falmouth, Cornwall, UK, 2013

7. M. Ghodrat, S.B. Kuang, A.B. Yu, A. Vince, G.D. Barnett and P.J. Barnett., 'Numerical analysis of hydrocyclones with different vortex finder designs' In MEI Conferences: Computational modeling '13: Falmouth, Cornwall, UK, 2013

8. M. Ghodrat, S.B. Kuang, A.B. Yu, A. Vince "CFD study of the effect of coal density on the multiphase flow and performance in large diameter classifying", the second Australia-China Joint Symposia on Minerals and Metallurgy", Sydney ,Australia , 23-25 July, 2014.

TABLE OF CONTENTS

LIST OF FIGURES

LIST OF TABLES

NOMENCLATURE

C_D	fluid drag coefficient
d	particle size, m
$D_{T,ij}$	turbulent diffusion term
e_{kk}	restitution coefficient between particles
E	Young's modulus, Pa
a_r	radial acceleration, m/s^2
a_k	Acceleration of phase k, m/s^2
E_p	Ecart probable
f_{drag}	fluid drag force, N
g	Gravitational acceleration, 9.81 m/s^2
N	number of computational cells on the radial direction
t	time, s
p	pressure drop, pa
s	scale factor
r	radial distance, m
u	fluid velocity, m/s
x_i	Cartesian coordinate
Re	Reynolds number
R_f	amount of water split to underflow
D_c	body diameter, mm
D_o	vortex finder diameter, mm
D_u	spigot diameter, mm
F_D	defined by Eq. (11)
g	acceleration due to gravity, ms^{-2}
k	kinetic energy, m^{2}s^{-2}
L_c	cylinder length, mm
L_i	inlet side length, mm
L_p	cone length, mm
L_t	vortex finder thickness, mm
L_v	vortex finder length, mm
P_{ij}	stress production term

u	instantaneous velocity, ms^{-1}
v	instantaneous velocity, ms^{-1}
w	instantaneous velocity, ms^{-1}
u'	Dispersion velocity, ms^{-1}
$\bar{u}$	time average velocity in axial direction, ms^{-1}
x	axis, m
α	volume fraction
σ_t	Prandtl-Schmidt number
η_t	turbulent diffusivity
$\gamma\Theta$	collisional dissipation of energy, J
$\phi_{l,k}$	Energy exchange between the l^{th} solid phase and the k^{th} solid phase, J
Θ	granular temperature, m^2/s^2
ε_{ij}	dissipation term
ϕ_{ij}	pressure strain term
τ	particle relaxation time
μ	fluid viscosity, $kgm^{-1}s^{-1}$
ρ	density, kgm^{-3}
ζ	normally distributed random number

SUBSCRIPTS

c	corrected
col	collision
cut	cut size
dr	drift velocity
k	phase *k*
l	phase *l*
L	liquid
t	Tangential
d	solid phase
i, j, k	1,2,3
m	Mixture
p	Particle
q	q^{th} phase

CHAPTER 1

INTRODUCTION

.

A hydrocyclone is a type of separation equipment used for solid–liquid and liquid–liquid systems. It is used to separate dispersed particles from a continuous fluid as the effect of a swirl flow, and has been used in many mineral processing and mining industries. Since the Second World War, there has been a rapid growth in the use of hydrocyclones in the chemical, mineral, coal and powder-processing industries. The reasons for this popularity lie in the design and operational simplicity, high capacity, low maintenance and operating cost and the small physical size of the device. A typical hydrocyclone consists of a cylindrical section with a central tube connected to a conical section with a discharge tube. An inlet tube is attached to the top section of the cylinder. The fluid being injected tangentially into hydrocyclone causes swirling flow and thus generates centrifugal force within the device. This centrifugal force field brings about a rapid classification of particulate material from the medium in which it is suspended.

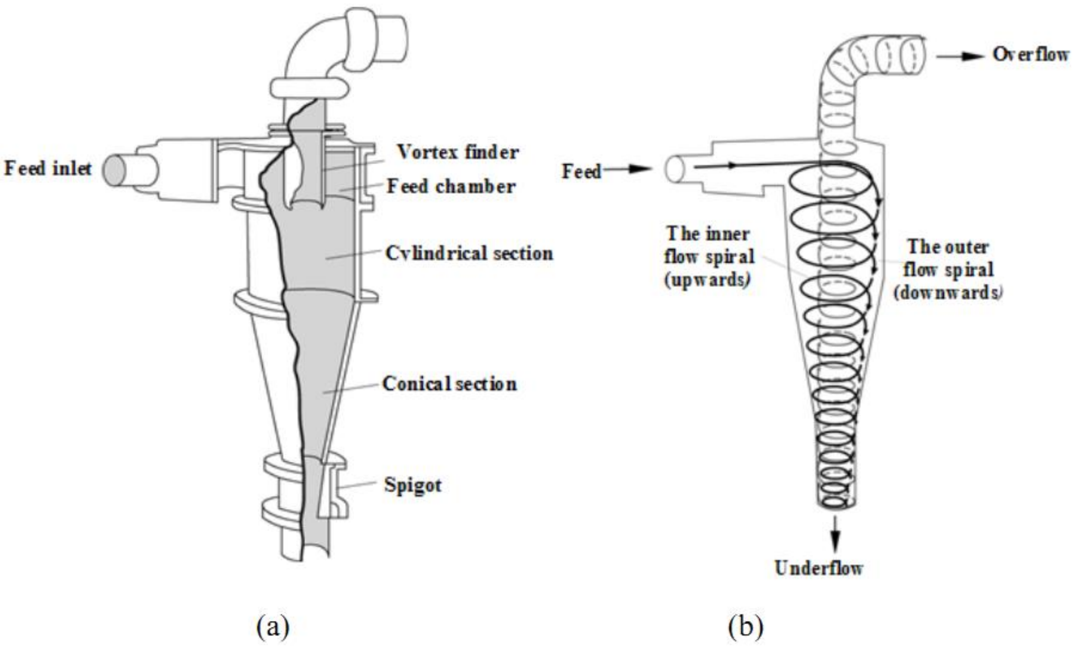

Fig 1.1 Schematic diagram of a hydrocyclone

Fig 1.1 shows the classic configuration and typical flow in a hydrocyclone. The centrifugal field generated by the high circulating velocities creates an air core on the axis that usually extends on the underflow opening at the bottom of the conical section through the vortex finder to the overflow at the top. In order for this to occur the centrifugal force field must be several times larger than the gravitational one. Particles that experience this centrifugal field will tend to move outwards relative to the carrier fluid because of their relatively greater density. The larger, heavier particles will migrate rapidly to the outside walls of the cylindrical section and will then be forced to move downward to the inside of the conical wall. Small particles will, on the other hand, be dragged inward by the fluid as it moves towards the vortex finder.

The flow in a hydrocyclone is very complicated with the presence of swirling turbulence, air core and segregation, and involves multi phases: gas, liquid, solid particles of different sizes. To date, there are few mathematical models that can fully define the cyclone flow and performance.

This complexity of flow behavior in a hydrocyclone has led designers to rely on empirical equations for predicting the equipment performance as a function of geometrical, operational and materials variables.

Many empirical models have been developed to predict the hydrocyclone performance, especially in the mining and mineral processing industry. These models quantify the misclassification of particles and predict the operational characteristics.

In the past, a number of variations and modifications of the geometrical variables to the basic design of hydrocyclone have been examined by various investigators to find out optimal models for different industrial applications, and many empirical equations and models have been formulated to describe the equipment performance.

However, these models suffer from the inherent deficiency as they could only be used within the extremes of the experimental data from which the model parameters were determined. Different sets of experimental data leads to different equations even for the same basic parameters which would not lead to much improvement in the understanding of the fundamentals of cyclones under different conditions.

In view of this shortcoming, mathematical models based on fluid mechanics are highly desirable. Alternatively cyclones can be modelled more fundamentally by CFD (Computational Fluid Dynamics). Computational fluid dynamics provides a means of predicting pressure and velocity profiles, turbulent quantities and other flow related quantities under a wide range of design and operating conditions. Today CFD offers an alternative way to obtain insight into the physical processes and flow interactions of solid particles in hydrocyclones. However the complex nature of the flow and particle interactions makes the development of a computational model for hydrocyclones a challenge. To date, multiphase models have been successfully applied in hydrocyclones to predict the Lagrangian motions of spherical particles. These models are applicable to low feed solid concentration levels as they neglect the particle-particle interactions. In this work, an effort has been made in simulating hydrocyclones by a recently developed two-fluid model facilitated by the mixture model to infer a better flow and performance analysis. In the model, both fluid (liquid and air) and solid phases are treated as interpenetrating continua. Particles of different sizes or densities represent different phases. However, the mixture of gas, liquid and solids is represented by a single phase with mixture properties, and allows certain slipping velocities between different phases. The model is used to systematically study the geometrical effects on the flows and performance in hydrocyclones operated at a wide range of feed solid concentrations. The findings from this study should be useful not only for establishing a comprehensive picture about the effects of cyclone geometrical variables but also for designing and controlling hydrocyclones.

Proposed research

The overall aim of this PhD project is to extend and utilize a recently developed two fluid flow model (TFM) facilitated by the mixture model to systematically study the geometrical, operational and material variation effects on the flows and performances of hydrocyclones operated at a wide range of feed solid concentrations. In the past, a number of variations and modifications have been made to the basic design of hydrocyclone to find out optimal models for different industrial applications, and various empirical models have been formulated to describe the equipment performance (Bradley, 1965; Svarovsky, 1984; Chen et al., 2000; Kraipech et al., 2006). However, systematic studies for better designing and controlling the hydrocyclones process are few. Hence in the first step of this research the cyclone size and spigot diameter are focused considering that they are often investigated under specific conditions for the purpose of industrial applications (O'Brien et al., 2000; Rong, 2007; Atkinson and Swanson, 2008). The findings from this part of the study should be useful not only for establishing a comprehensive picture about the effects of cyclone size and spigot diameter but also for designing and controlling hydrocyclones.

As the second objective of this study, hydrocyclones of different conical configurations have been studied under a wide range of feed solids concentrations using the developed (Two Fluid Model) TFM model facilitated by the mixture model. This part of the PhD project aims at gaining a better understanding of the effects of the conical part on the flow and performance of hydrocyclones, and identifying possible methods to improve the cyclone performance which is classified into two parts, first the effects of the cone length is studied and second the effect of the conical section shape is investigated. On this base, a new hydrocyclone design is proposed.

The third objective of this research is to control the flow within the pre-separation space of the hydrocyclone by properly changing the dimension and shape of the vortex finder, with the aim of improving cyclone performance such as energy utilization and particle separation efficiency. This part of the study focused on the optimum dimension of the vortex finder with respect to length, diameter and shape.

The final aim of this dissertation is to understand and investigate the effect of changing material properties of coal based on density variation on the flow feature and performance of the large diameter industrial hydrocyclones. The overall aim is the evaluation of the size separation performance of a large diameter (1m) classifying cyclone under a number of different operating conditions which could be encountered in normal plant operation. The outcomes from this part of the project allow coal preparation engineers to evaluate the potential of incorporating large diameter cyclones into plant circuits, and assess the resulting processing and cost improvements.

Thesis structure

The above-mentioned work and its objectives are addressed in this thesis which consists of 7 chapters.

Chapter 2 reviews some of the related previous works, including the operational principles, flow pattern and mechanisms of particle separation in hydrocyclones. Besides, some experimental investigation, theories of separation and mathematical modelling in hydrocyclones are reviewed.

Chapter 3 focuses on a parametrical study of the effect of different dimensions of body construction, including cyclone size and spigot diameter. It shows that the suggested two fluid model (TFM) facilitated by the mixture model can satisfactorily describe the flow and performance of a standard hydrocyclone, including the formation of an air core when feed solids concentration is up to 30 % (by volume). The predicted flow features are examined in terms of the flow field, pressure drop, and amount of water split to underflow (defined as the ratio of the volumetric water flow rate of the underflow to that of the feed stream), separation efficiency and underflow discharge type. Discussion is then extended to other flow behaviour in hydrocyclones, including the structure of air core, and the motion of particles of different sizes.

Chapter 4 presents a numerical analysis of hydrocyclones with different vortex finder configurations. A wide range of feed solids concentrations is considered and the effects on the separation efficiency, pressure drop and split ratio is discussed.

Chapter 5 proposes to extend that work by examining the effects of vortex finder diameter, length and shape on hydrocyclone flow and performance under dilute and dense regimes. The working principle of the vortex finder is explored by analysing the internal flow in a hydrocyclone.

Chapter 6 discusses the mechanisms of coal particle separation at different densities and feed solids concentration within large body diameter hydrocyclones. The simulated flow features allow estimates to be made of pressure drop, amount of water split (defined as the ratio of the volumetric water flow rate of the underflow to that of the feed stream), and partition curves (shows the fraction of a material of a specific size in the feed to that reports to the coarse product stream (underflow)) for coal particles of different sizes and densities. The estimates is compared favourably with industrial scale measurements of a 1000 mm diameter hydrocyclone operating under similar conditions and on this base, the effect of particle density that represents the foremost difference between several major coal types is studied in this chapter. The results were then analysed in terms of flow patterns, partition performance and energy consumption indices.

Chapter 7 presents the conclusions of the research. The practical implications of the results of the research work as well as the suggestions for further work are discussed.

It should be noted that although there is a logical sequence throughout the thesis, each chapter is self-contained and can also be treated as an independent contribution.

CHAPTER 2

LITERATURE REVIEW

2.1 Introduction

The hydrocyclone is an important and popular mechanical separation device used to separate dispersed solid particles from a liquid suspension fed to it by centrifugal action. It is widely used in the mineral and coal industries because of its simplicity in design and operation, high capacity, low maintenance and operating costs, as well as its small physical size. A typical hydrocyclone consists of a cylindrical section with a central tube called a vortex finder which is connected to a conical section with a discharge tube called spigot or apex. An inlet tube is attached to the top section of the cylinder. The fluid being injected tangentially into the hydrocyclone causes swirling and thus generates centrifugal force within the device. This centrifugal force field brings about a rapid classification of particulate material based on size from the suspended liquid and gas .The commonly used conventional hydrocyclone is shown in Fig. 2.1.

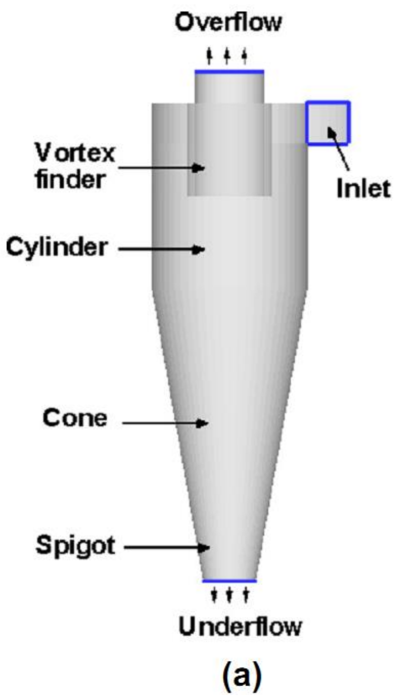

Fig. 2.1 Schematic diagram of a hydrocyclone

The separating action of a hydrocyclone treating particulate slurry is a consequence of the swirling flow that produces a centrifugal force on the fluid and suspended particles. The feed slurry is injected tangentially into the hydrocyclone at high velocity, to produce a large centrifugal force field (Fig. 2.2). The feed moves down the wall rapidly and generates a helical vortex, which extends beyond the lower end of the vortex finder.

This swirling flow is highly turbulent and three-dimensional. In the centrifugal field, the particles move relative to the fluid with respect to the balance of centrifugal and drag forces acting upon particles in the radial direction, such that classification occurs. The coarser or heavier particles move toward the wall and are swept downward to the apex of the cone. The fluid phase which carries the smaller or lighter particles approaches the apex and reverses in the axial direction spiralling upward and leaving the hydrocyclone through the vortex finder. Along the axis, an area of low pressure is created by the very high angular momentum. This may cause the formation of a rotating free liquid surface at the centre. If the hydrocyclone is open to the atmosphere, air is inhaled through the apex and forms an air core. In that case, the pressure at the air-liquid interface is equivalent to the atmospheric pressure.

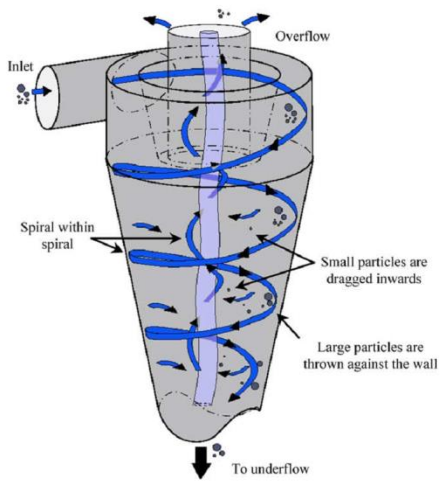

Fig. 2.2 Spiral flow pattern in a hydrocyclone

The flow within a hydrocyclone is quite complex. This complexity is mainly because this flow is strong swirling turbulent multiphase flow. The complexity of flow processes has led designers to rely on empirical equations for predicting the equipment performance. These empirical relationships are derived from an analysis of experimental data and include the effect of operational and geometric variables. A number of classifying cyclone models has been developed over the past two decades (Asomah and Napier-Munn, 1997; Nageswararao, 1999). Although many efforts have been made to study experimentally the flow in hydrocyclones (Yoshioka and Hotta, 1955a; Bradley, 1965; Svarovsky, 1984) little detailed flow information was generated until the availability of laser Doppler anemometry (LDA). It is well known that the

LDA technique is expensive, largely limited to the dispersed liquid phase, and at present suitable only for laboratory-scale studies rather than industrial design and application. All in all empirical models normally suffer from their inherent deficiency as they can only be used within the limits of the experimental data from which the empirical parameters were determined. In view of these shortcomings, mathematical models based on the basic fluid mechanics are highly desirable to intensify innovation. The CFD technique is gaining popularity in process design and optimization as it provides a good means of predicting equipment performance of the hydrocyclone under a wide range of geometric and operating conditions; it also offers an effective way to design and optimize the hydrocyclones.

In this Chapter, a comprehensive review of the operational principles, the experimental investigations, empirical model and theories of separation, computational modelling of hydrocyclones flow and particle motions is described. The general performance of a hydrocyclone is affected both by design variables, namely, the cyclone dimensions, and by operating variables, namely, the feed pressure and the physical properties of feed solids in the following sections, the flow regime within a cyclone is discussed qualitatively and the effects of different variables upon the capacities and solids separation characteristics of cyclones are discussed quantitatively.

2.2 General principles of the operation of the hydrocyclone

The principle operation of the hydrocyclone is based on the concept of the terminal settling velocity of a solid particle in a centrifugal field. Particles in a swirling flow move with a terminal velocity relative to the fluids movement in the flow. The terminal velocity determines if the particle is collected or lost. The terminal velocity is equivalent to a particle settling under steady-state conditions in the earth's gravitational field, except that in a cyclone the gravitational field is replaced by a radial directed centrifugal force field. Understanding of the terminal velocity for a particle in a cyclone is therefore essential. Newton's law for a particle moving in a flow field is the mass times acceleration and the sum of forces acting on the particle, (mass × acceleration)=(body force)+(fluid drag) +(unsteady force terms), where the body force is normally due to gravitational field or centrifugal force. The term centrifugal force is as mentioned not a real force. Hence the above force balance is performed in a reference coordinate system rotating with the particle. The unsteady force terms accounts for the acceleration of the particle relative to the fluid and the fluid drag accounts for the drag of the particle as it moves with steady velocity relative to the fluid. When a particle enters the separation space in the cyclone the particle is in influenced by an outward directed centrifugal force and an inward directed drag force. At the point where the incoming fluid starts to experience rotation and the solids first experience centrifugal force directed radially outwards, the separation space in the cyclone starts.

Many Separation process are based on the difference in settling velocity of high density and low density particles. An upwards current of fluid specially separates fine particles in the overflow, leaving the high coarse particles to exit in the underflow. For Spherical particles there are well-established equations for predicting the terminal free-settling velocity u_t as a function of particle diameter d and density ρ, fluid density ρ_f and viscosity μ and gravitational acceleration (Rhodes, 2008) .These depend on which settling regime the particle is in. In the Stocks' law regime, where velocity forces dominate $(\mathrm{Re}_t = u_t \rho_f d / \mu < 1)$

$$u_t = \frac{d^2(\rho_p - \rho_f)g}{18\mu} \tag{2.1}$$

Numerous empirical correlations are available for the intermediate regime $(1 < \mathrm{Re}_t < 500)$. For instance, one based on Vance and Moulton (1965) is:

$$u_t = 0.153 \frac{d^{1.14}(\rho_p - \rho_f)^{0.71} g^{0.71}}{\mu^{0.43} \rho_f^{\ 0.29}} \tag{2.2}$$

In Newton's law regime $(500 < \mathrm{Re}_t < 10^5)$:

$$u_t = 1.74 \left(\frac{d(\rho_p - \rho_f)g}{\rho_f} \right)^{1/2} \tag{2.3}$$

Empirical correlation that covers the full range up to $(\mathrm{Re}_t < 10^5)$ is also available

Barth (1956) calculated the terminal settling velocity for static particles, based on the exact balance between the centrifugal force and the drag force. The collection efficiency for any particle size is determined from the ratio of its settling velocity to the terminal settling velocity of the static particle.

The centrifugal separation is produced by the motion of the slurry, induced by the tangential introduction of the feed material. Its principle of operation is based on the concept of the terminal settling velocity of a solid particle in a centrifugal field. The following picture describes the conditions in an operating hydrocyclone. The feed enters tangentially into the cylindrical section of the hydrocyclone and follows a circulating path with a net inward flow of fluid from the outside to the vortex finder on the axis. The centrifugal field generated by the high circulating velocities creates an air core on the axis that usually extends on the spigot opening at the bottom of the conical section through the vortex finder to the overflow at the top. In order for this to occur the centrifugal force field must be several times larger than the gravitational one. Particles that experience this centrifugal field will tend to move outwards relative to the carrier fluid because of their relatively greater density. The larger, heavier particles will migrate rapidly to the outside walls of the cylindrical section and will then be forced to move downward to the inside of the conical wall. Small particles will, on the other hand, be dragged inward by the fluid as it moves towards the vortex finder. The solid separation occurs in the passage of the suspension along the barrel of the hydrocyclone, to form thickened slurry at the outer wall, which then leaves the hydrocyclone as a continuous stream from its discharge nozzle.

Fig. 2.3 shows the classic configuration of hydrocyclones. It consists of a cylindrical upper body with a central tube called vortex finder and a conical lower body with a discharge tube called spigot. This configuration has been used during the last 80 years. The centrifugal separation is generated by the motion of the slurry, induced by the tangential introduction of the feed material.

The conditions in an operating hydrocyclone can be described by reference to Fig. 2.3 and Fig. 2.4. The feed enters tangentially into the cylindrical section of the hydrocyclone and follows a circulating path with a net inward flow of fluid from the outside to the vortex finder on the axis. The circulating velocities are very high and these generate large centrifugal fields inside the hydrocyclone. The centrifugal field is usually high enough to create an air core on the axis that often extends from the spigot opening at the bottom of the conical section through the vortex finder to the overflow at the top. In order for this to occur the centrifugal force field must be many times larger than the gravitational field.

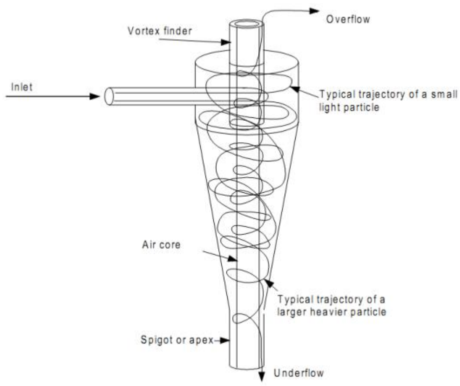

Fig. 2.3 Typical particle trajectories in a hydrocyclone

Particles that experience this centrifugal field will tend to move outwards relative to the carrier fluid because of their relatively greater density. The larger, heavier particles will migrate rapidly to the outside walls of the cylindrical section and will then be forced to move downward on the inside of the conical wall. Small, light particles, on the other hand will be dragged inwards by the fluid as it moves toward the vortex finder. The drag force experienced by any particle will be a complex function of the hydrodynamic conditions inside the hydrocyclone and the shape and size of the particle. The classification action of the hydrocyclone is determined by the net effect of the two competing forces that act on every particle; the outward centrifugal force and the inward drag force. A rough guide to the effect of various operating variables on the performance of the device can be established using the so-called equilibrium orbit hypothesis. Any particle that experiences equilibrium between these two forces inside the hydrocyclone will have an equal chance to exit through either the underflow or the overflow because they will tend to circulate on a circular orbit in the hydrocyclone and will be moved toward one or other outlet by random impacts with other particles and the random eddy motion in the highly turbulent flow field inside. An orbit on which a particle experiences a balance between the centrifugal and drag forces is called an equilibrium orbit.

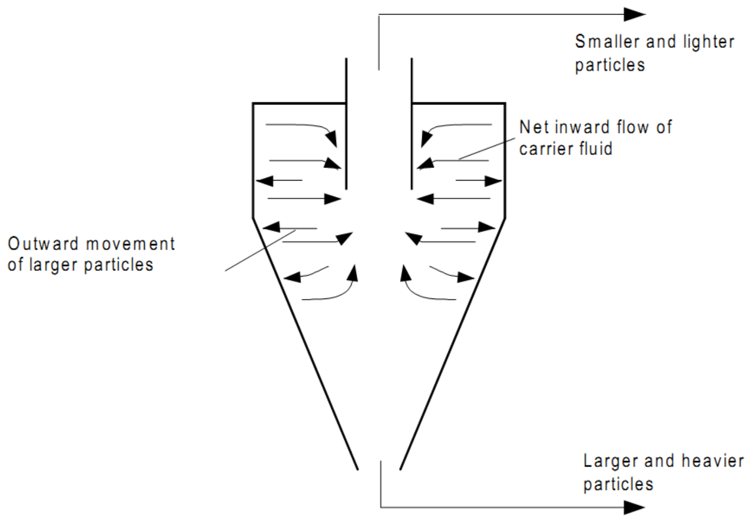

Fig. 2.4 Schematic representations of the net flow of water and the counter flow of larger particles in the hydrocyclone

To describe the underlying physics behind hydrocyclones operation, the theory concerning the separation procedure should be defined in more detail. As mention earlier the flow behavior in a hydrocyclone is highly swirling and multiphase structure. Because of strong swirling flow acting on fluid element, the element accelerates toward the center as it rotates. This acceleration is called centrifugal acceleration which caused by a force called centrifugal force. The centrifugal force, acts away from the rotating axis and is similar to gravity. The magnitude of the force is equal to the mass of the element times the centrifugal acceleration.

It is important to note that mass forces acting on particles due to an internal or external field of acceleration is the base of separation in hydrocyclones so for separation to take place there should be a density difference between the fluid and the particles.

Basically the swirl motion is created when a fluid enters the cyclone inlet under pressure. The fluid then moves axially downwards in the outer vortex in the cylindrical section of the cyclone. As it moves into the lower part of the conical section, the fluid is forced into the inner vortex which moves axially upwards, and exits through the vortex finder (the overflow). The particles in the fluid are flew out to the wall in the cylindrical section and stays in the downward outer vortex through the conical section until they exit through the underflow (Fig. 2.5). The particles suspended in the fluid are separated due to size and specific gravity (density). The swirl flow creates a vortex in the cyclone that give rise to a low pressure zone along the vertical axis, called the inner vortex. The vortex flow in the cyclone consists of two vortices; one downward outer region and one inner upward region, Fig. 2.5. Stokes law tells us that heavy fast settling particles move to the wall of the cyclone and follow the flow out through the underflow. The lighter and slower settling particles move into the low pressure zone in the center of the cyclone, and follow the overflow up along the axis and exit through the vortex finder. This proves that gravity does not significantly affect the separation in cyclones, except in large cyclones used to separate large particles, it is the flow itself. Hence the cyclones do not need to be operated in vertical position.

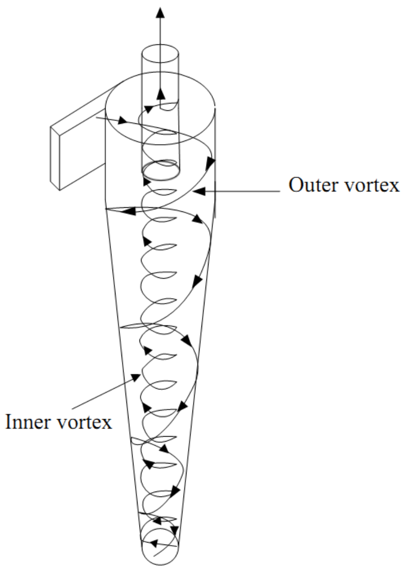

Fig. 2.5 Sketch of the two flow patterns in a reversed-flow cyclone (Cortés and Gil, 2007), The inner upward directed vortex pass out through the vortex finder. The outer downward directed vortex passes out through the underflow.

2.3 Flow pattern

2.3.1 Fluid flow pattern

The separating action of a hydrocyclone is a consequence of the swirling flow that produces a centrifugal force on the fluid and suspended particles within the hydrocyclone. Hydrocyclones have no rotating parts and the essential twisting flow is formed by pumping the fluid tangentially into a standing cylindrical body. In general the fluid within the cyclone body has a circular symmetry with the exception of the region in and around the inlet duct. The feed slurry is injected tangentially into the device at high velocity, to produce a large centrifugal force field. The feed moves down the wall rapidly and generates a helical vortex, which extends beyond the lower end of the vortex finder. This swirling flow is highly turbulent and three-dimensional. The inward fluid moves in an outer helical flow into the outer portion of the cone where it begins to feed across towards the centre. The downward flow on the other hand leaves through the underflow orifice in the spigot of the cone whereas the rest reverses their vertical path and rise via the inward helical flow and out through the vortex finder.

In the centrifugal field, the particles move relative to the fluid with respect to the balance of centrifugal and drag forces acting upon particles in the radial direction, such that classification occurs. The coarser or heavier particles move toward the wall and are swept downward to the spigot of the cone. The fluid phase which carries the smaller or lighter particles approaches the spigot and reverses in the axial direction spiralling upward and leaving the hydrocyclone through the vortex finder. Along the axis, an area of low pressure is created by the very high angular momentum. This may cause the formation of a rotating free liquid surface at the centre. If the hydrocyclone is open to the atmosphere, air is inhaled through the spigot and forms an air core. In that case, the pressure at the air-liquid interface is equivalent to atmospheric pressure.

The flow field inside the hydrocyclones has been the objective of several studies; see e.g. (Bradley, 1965) and (Svarovsky, 1984). In the early days intrusive probes were used for measuring the local flow velocity (e.g. (Yoshioka and Hotta, 1955a; Lilge, 1962)). Later advance studies solely used optical methods, e.g. (Kelsall, 1952b), or (Svarovsky, 1984; B. Dabir, 1986). The flow in a hydrocyclone is often described as a combination of an outer helical downward flow and an inner helical upward flow. In steady-state, a radial displacement of the fluid is necessary for the flow to change direction from downward to upward flow. Some authors claim that this radial flow uniformly takes place over the entire length of the cyclone as depicted in Fig. 2.6 e.g. (Svarovsky, 1984; B.A.Wills, 1997). Conversely, (Kelsall, 1952b) based on visual observations stated that most of the radial flow seems to occur around the opening of the vortex finder.

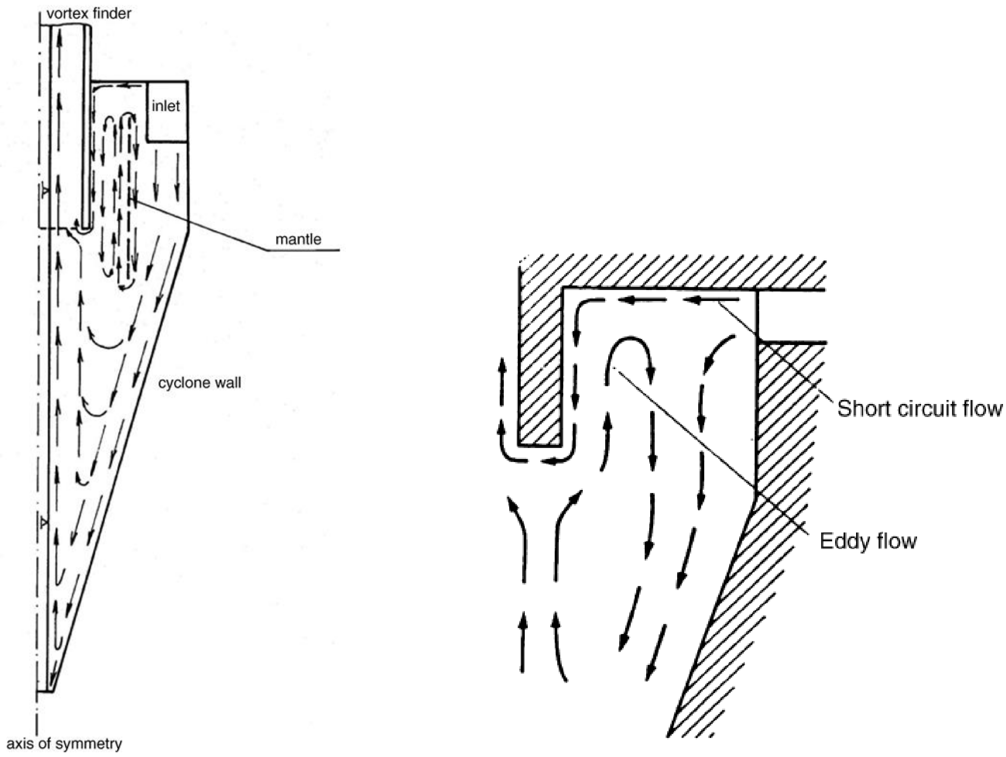

(a) (b)

Fig. 2.6 (a) Schematic 2D-representation of the flow field (Svarovsky, 1984), (b) Depiction of the short circuit and eddy flows (Bradley, 1965).

Friction at the roof of the hydrocyclone causes the swirling flow to locally slow down. Lower tangential velocities coupled with the higher pressure far out in the hydrocyclone will cause a short circuit flow. It flows directly from the feed inlet along the roof and down the outside of the vortex finder, see Fig. 2.6. The separation efficiency of a hydrocyclone is obviously impaired when part of the feed flow is taking this shortcut to the vortex finder which is one of the reasons why the vortex finder is protruding into the cylindrical section of the hydrocyclone. Monredon (1992) measured the internal velocity field of several hydrocyclone geometries using LDV, and compared their separation efficiency which was also linked to the experimental findings with an efficiency predicting numerical model. They found that an involute type of inlet reduced the short circuit flow from the inlet to the vortex finder, and hence increased the efficiency. The relative confinement of the vortex in a hydrocyclone may augment the propensity to form secondary circulatory flow patterns. Bradley (1965) visualized circulatory eddy flow (Fig. 2.6) by pumping small amounts of dye into a transparent hydrocyclone. The dye had the tendency of becoming trapped in eddies. Even multiple eddies next to the vortex finder have been reported by (Svarovsky, 1984) (Fig. 2.5(a)). Dabir and Petty (1986) found sharp opposing axial flows inside the vortex finder which were probably generated by a geometrical constriction further up in the vortex finder (Fig. 2.7).

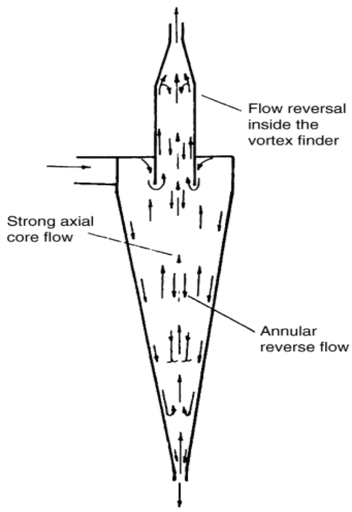

Fig. 2.7 Annular counter current axial flows inside both the conical section of the hydrocyclone and the vortex finder (B. Dabir, 1986).

Ohtake (1987) reported eddies that are similar to the findings of Bradley (1965), see Fig. 2.8. These neighbouring multiple eddies create a flow interface with little radial fluid flow, designated ‘mantle’ in Fig. 2.6 and Fig. 2.8.

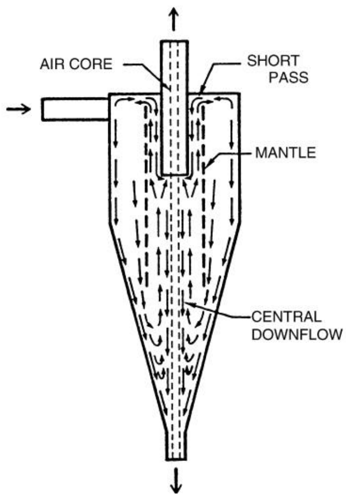

Fig. 2.8 The flow pattern visualized with tracer injections .(T. Ohtake, 1987).

At the centre axis of the hydrocyclone, the low pressure supports the formation of a rotating air-column, the air-core. The geometry and the stability of the air-core have been empirically found to have a strong influence on the operational state of the hydrocyclone, (Knowles et al., 1973; Davidson, 1995a; Williams et al., 1995; Concha et al., 1996; Chu et al., 2004; Neesse and Dueck, 2007; Sripriya et al., 2007; Doby et al., 2008; Evans et al., 2008; Gupta et al., 2008) shown in Fig. 2.8. Due to often poor visual access to the air-core at high particle loading, experimental research has to a large extent been directed towards indirect air-core aspects such as the discharge shape of the underflow (Neesse et al., 2004). By using acoustic or optical monitoring of the discharge, the operating state of a hydrocyclone can be controlled (T. Neesse, 2004).

2.3.2 **Particle flow pattern**

The partition of particles happens in the hydrocyclone because of its flow field, but the location where separation occurs is still unclear. This is an area of hydrocyclone where very few experimental researches have been carried out and more work is absolutely needed. Renner (1978) used a sampling probe to examine the size distribution of particles at different positions in a hydrocyclone. They recognized four areas each of which were made of a typical particle size distribution, as illustrated in Fig. 2.9. Region A comprised material matching with the size distribution of the feed, region B included materials similar to the size distribution of the coarse particles , region C same material size to the fine product and region D contained material larger than intermediate size fractions of the feed.

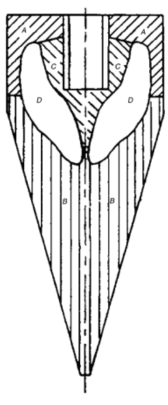

Fig. 2.9 Four regions of similar size distributions within an operating hydrocyclone (Renner, 1978).

Furthermore, Rajamani and Milin (1992) demonstrated that a high solids concentration region occurs in the vicinity of the vortex finder.(Fig. 2.10).

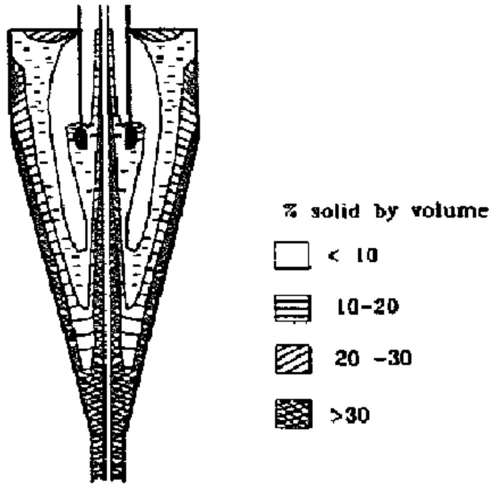

Fig. 2.10 Particle distribution within the hydrocyclone.(Rajamani, 1992).

Dyakowski and Williams (1996) computed the streamline pattern near the vortex finder.(Fig. 2.11). It should be noted that a sharp change in the velocity direction causes an increase in components of the rate of strain tensor, as shown elsewhere (Monredon, 1992).

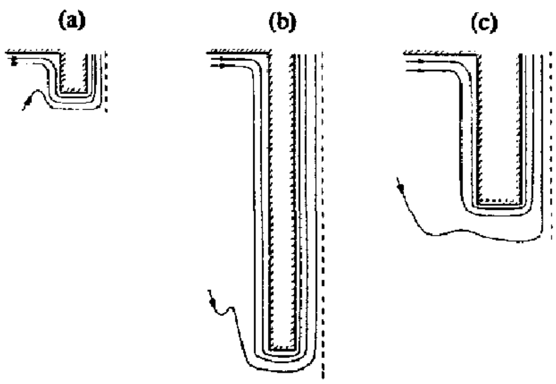

Fig. 2.11 Streamlines pattern, in a meridional plane, in the vicinity of the vortex finder wall. (a) d= 12 ram. L= 18rmn: (b) d= 12 man, L=140 ram (c) d=20mm, L=80mm.

The results observed by Dyakowski and Williams (1996), using electrical resistance tomography made inside a 44 mm hydrocyclone are illustrated in Fig. 2.12. Based on the fact that high conductivity is associated with lower solids concentration, the results show the presence of a ring of particles near the wall and the air-core axially central can be seen. In a more recent paper, Williams et al., (1999) showed axial and radial conductivity distribution and air-core diameter measurements. Based on evidence of Fig. 2.12, it can be concluded that high particle concentration regions exist not only near the hydrocyclone wall but also near the vortex finder and air core.

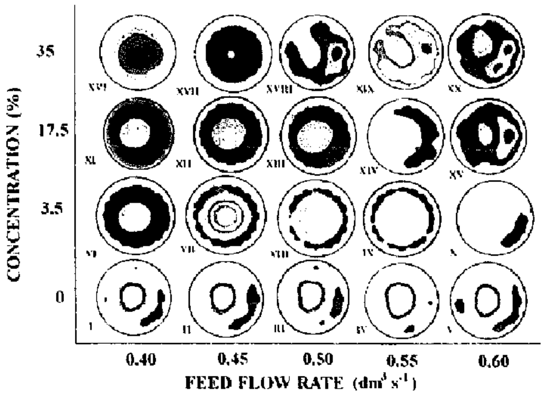

Fig. 2.12.Sequence of resistivity images below the feed inlet region in a 44 mm diameter hydrocyclone operating at various feed flow rates (0.4-0.6 dm^3s^{-1}) and different solids concentrations (0-35 wt%), (Dyakowski, 1996).

In Hsieh's experiment, typical particle of different diameters were chosen to trace the trajectories. The results of his study show that large particles mainly collected near the walls while small particles escaped from the overflow stream of the cyclone. The fine particles cannot move to the wall of the cyclone as the centrifugal force acting on them is smaller than the fluid drag force. A particle of cut size is primarily dragged down by the external downward flow. Simultaneously, the radial velocity pointing to the air core leads the particle to be dragged inward. In this situation, since the particle size is small correspondingly, the inward drag force is larger than the centrifugal force. Accordingly, in some area of the conical section, these particles are caught by the upward inner flow and by pass through the vortex finder or follow the external downward flow to be collected at the underflow. Such a particle is shown to be very unsteady, and it has a higher residence time than other sized particles. Coarse particles on the other hand mainly remain on the conical cyclone wall once their size exceeds a critical value. This phenomenon would cause wear in the hydrocyclone, observed by Bradley (1965). The reasonable explanation is that oversize particles are held by a centrifugal force against the wall when the upward and downward forces on the particles are in balance (Wang et al., 2007).

2.4 Separation behaviour theories

The theoretical foundations of the hydromechanics of separation in a hydrocyclone and related separation processes have been developed for many decades (Svarovsky, 1984). Initially, most of the researchers have made a continuous attempt to derive empirical equations for the separation characteristics of the hydrocyclone from experimental data or, if the data on the flow pattern in the device was roughly reliable (see, e.g., (Ivanov, 1987)). The deterministic motion of single particles was considered in the work of some other researchers such as (Baranov, 1996) and (Ternovsky, 1994). The works along this field of research have shown a number of uniqueness of the particle motion in a hydrocyclone and have allowed investigators to make a general assessment of the effect of some parameters of the hydrocyclone and of the mixture on the separation characteristics.

2.4.1 Equilibrium orbit theory

This theory is based on the laminar flow condition assumption which is originally proposed by Drissen (1951) and Criner (1950). It states that each particle in the hydrocyclone tends to be in equilibrium between two opposing forces, (i) centrifugal force acting towards the wall of the hydrocyclone, and (ii) drag force from the liquid acting towards the axis (Fig. 2.13)

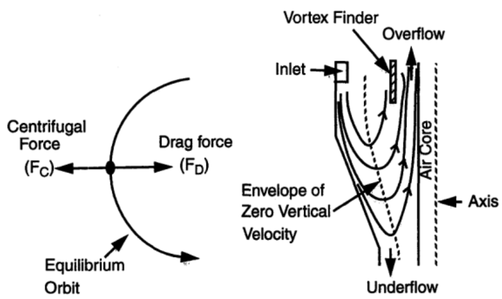

(a)Top view (b) Side view

Fig. 2.13 Explanation of the equilibrium orbit theory of hydrocyclone mechanism (Kawatra et al., 1996b).

The theory assumes that particles of a given size will reach an equilibrium radial orbit position inside the hydrocyclone where their outward terminal settling velocity is equal to the inward radial velocity of the liquid. Accordingly to this theory, larger particles will attain a radial orbit position near the wall, where the axial fluid velocity has a downward direction. These particles will, therefore, leave the cyclone through the underflow. The radial orbit position of smaller particles will be located near the centre, inside the region where the axial fluid velocity is upward. These particles will, therefore, escape through the overflow. The cut size is defined as the particle size whose equilibrium orbit is coincident with the locus of zero vertical velocity of the fluid. Such a particle will have equal chance to escape the hydrocyclone either through the underflow or through the overflow.(Coelho and Medronho, 2001).

2.4.2 **Crowding theory**

The proposed crowding theory (Fahlstroem, 1960) suggested that the cut size is a function of the capacity of the underflow and particle size distribution of the feed. Similarly later a separation model based on turbulence two phase flows was proposed by Schubert (1980). The “crowding theory” states that, except for hydrocyclone operations with low feed solids contents, the separation size is primarily determined by the spigot diameter and by the solids content and size distribution of the feed. The larger particles of the feed are discharged through the spigot up to its capacity limit, and the remaining finer particles are discharged through the vortex finder. Fahlstrom's (1960) experimental results suggest that this effect is controlling when a hydrocyclone is operating with oversize flow stream solids contents greater than 40% by volume.

2.4.3 **Residence time theory**

One of the other well-known theories for particle separation in hydrocyclones is the residence time theory which first proposed by (Rietema, 1961). According to this theory, a particle will be separated as a function of both the position it enters the cyclone and the available residence time. The cut size will be the size of the particle which entering the equipment exactly in the centre of the inlet pipe will just reach the wall in the residence time available (Castilho and Medronho, 2000; Coelho and Medronho, 2001; Cilliers et al., 2004; Nauman, 2008).

2.5 Experimental Investigations

Many empirical models have been developed in recent years to predict the hydrocyclone performance. They use the dimensions of the hydrocyclone and constants related to the characteristics of the slurry to predict the size classification.This section reviews the important empirical models available in the literature for predicting hydrocyclones performance. This reveals the gaps in the models while comparing with the industrial cyclone performance, and helps to examine by using computational flow modelling methods. The first experimental study on the flow of hydrocyclone done by Knowles et al., (1973). He used high-speed movies of anisole droplets moving through a hydrocyclone to determine the velocities of liquid flow. More recently a number of investigators reported their measurements using laser Doppler velocimetry (LDV) and electrical impedance tomography (Doby et al., 2008; Evans et al., 2008).

The first systematic and detailed experiment for predicting hydrocyclones performance was carried out by Kelsall (1952a,1953), who measured radial, axial and azimuthal velocities. Subsequently, mathematical modelling of velocity distributions and pressure drops were carried out by several research workers and various analytical solutions were proposed (Rietema, 1961; Bloor, 1973a,1975; Davidson, 1988; Barrientos, 1993; Dyakowski, 1993). Many researchers have correlated experimental data for hydrocyclones, for example, Lynch’s model (Lynch, 1976), Schubert/Neesse’s model (Neesse, 1991), Svarovsky’s model (Svarovsky, 1984) and Nageswararao’s model (Nageswararao et al., 2004). The key shortcoming of these models is that, when the constants of the model are adjusted for a particular operating condition, the same model cannot be used to predict the condition far from the calibrated conditions. Chen et al., (2000) and Nageswararao et al., (2000) assessed most models for practical applications in their papers.

Various experimental techniques have also been developed in the past decade to study the flows within hydrocyclones (Yoshioka and Hotta, 1955b; Knowles et al., 1973; Hsieh and Rajamani, 1991; Chu and Chen, 1993; Dyakowski and Williams, 1996; Williams et al., 1997; Dai et al., 1999; Inaki Schlaberg et al., 2000; Fisher and Flack, 2002; Bergström et al., 2007; Lim et al., 2010; Marins et al., 2010; Chang et al., 2011; Zhang et al., 2011). The techniques include the Pitot tube technique, (Yoshioka and

Hotta, 1955b) , high-speed camera, (Knowles et al., 1973) , Electrical Impedance Tomography (EIT),(Dyakowski and Williams, 1996; Williams et al., 1997) , Ultrasound Tomography (UT),(Inaki Schlaberg et al., 2000) , Laser Doppler Velocimetry (LDV),(Hsieh and Rajamani, 1991; Chu and Chen, 1993; Dai et al., 1999; Fisher and Flack, 2002; Bergström et al., 2007; Marins et al., 2010; Zhang et al., 2011). Particle Image Velocimetry (PIV),(Lim et al., 2010; Marins et al., 2010) and Positron Emission Particle Tracking (PEPT) (Chang et al., 2011). Their use has led to a better understanding of the complicated flow structures in hydrocyclones.

The most common model is undoubtedly the Plitt model, (Plitt, 1976a) which is regularly utilized for the design of hydrocyclones especially in practice. Plitt (1976a) took the data of Lynch and Rao (1968) and included his own, attained with smaller cyclones up to 150 mm diameter tested with silica flour. This model was based on 297 tests, and many developments have been suggested by Flinthoff et al., (1987) Cilliers and Hinde (1991) and Kawatra.(1996a). It has an enhanced accuracy in comparison to the other empirical models (Chen et al., 2000; Nageswararao et al., 2004).

2.5.1 **The Plitt Model for the Hydrocyclone**

Within the empirical models used to hydrocyclones dimensioning the most widely used model is the one proposed by Plitt (1976b). This model can be used to predict the hydrocyclones operation without additional experimental data for a wide range of operational conditions.

Combining the first industrial database on cyclones generated at The Julius Kruttschnitt Mineral Research Centre (JKMRC) with his own laboratory data, Plitt developed an alternative general-purpose cyclone model. In the Plitt's model, the cyclone model predictions can be determined by utilizing four fundamental parameters expressed in terms of the operating design variables. These parameters include separation cut size, flow split between overflow and underflow, sharpness of separation (which determines the cut precision and thus the quality of the product from hydrocyclones) and pressure drop. By determining these parameters, a complete mass balance together with size distribution of the cyclone products can be achieved.

Plitt used three custom-based cyclones with interchangeable parts, with diameter of 3.2, 6.4 and 15.2 cm. He was able to vary, D_o, D_u ,D_i and H=*L-l* for each cyclone. Apart from these geometrical variables, he has also varied the pressure drop and the feed concentration. When developing his model, Plitt added to his 174 experimental points another 132 tests from Lynch and Rao (1968).

This model is formed by the following equations:

$$S = \frac{34.4\left(\frac{D_u}{D_o}\right)^b \cdot (L-l)^d \cdot (D_u^2 + D_o^2)^c \exp(0.54\varphi)}{(\Delta p)^g \cdot D^{1.11}} \tag{2.4}$$

Where

S = volumetric flow rate in underflow / volumetric flow rate in overflow

D_u = spigot diameter

D_i=Inlet equivalent diameter, by area

D_o = vortex finder diameter

D_c = cyclone diameter

φ= volume fraction solids in the feed

h = (L-l) = vortex finder to spigot distance

$H = (\Delta p)$ =slurry feed head

Plitt recommends the following values for hydrocyclone operating with free discharge a = 3.79, b =3.31, c = 0.36, d = 0.54, f = 1.11, g = 0.24

Plitt described the partition function which requires d_{50}, then correlated d_{50} in terms of the cyclone geometry and the operating variables as follows

$$d_{50c} = \frac{aD_c^{\ b} \cdot D_i^{\ c} \cdot D_o^{\ d} \exp(6.3\varphi)}{D_u^{\ f} \cdot (L-l)^g \cdot Q^i \cdot (\rho_s - \rho)^{0.5}} \tag{2.5}$$

In this equation D_i is the inlet diameter and Q is the volumetric flow rate to the cyclone. Recommended values for the constants are: a = 2.69×103 and b = 0.46, c = 0.6 d = 1.21, f = 0.71, g = 0.38, i = 0.45. With this value of a, d_{50c} from equation (2.5) will be in microns. Comparison of equation (2.5) with equilibrium orbit theory equation indicates that Plitt's model for d_{50c} is consistent with the main conclusions drawn from the equilibrium orbit hypothesis in that d_{50c} varies roughly in proportion to the cyclone diameter (cyclone size to the power $b+c+d-f-g$ = 1.18) and inversely with feed rate to a power less than 1. The 0.5 power dependence on ρ_s-ρ_f in dictates that the interaction between particles and fluid is governed by Stokes' Law but higher values can be used.

The values of the parameters *a* in equations (2.4) and (2.5) are often estimated from experimental data obtained from an existing cyclone installation in order to make the model correspond to the actual operating performance and these parameters can each be multiplied by a separate calibration factor.

In spite of the empirical nature of the Plitt hydrocyclone model it has proved to be robust for practical work.

The equation related to pressure drop from Plitt model is

Pressure drop: $$\Delta p = \frac{1.316 \cdot 10^5 \cdot Q^{1.78} \exp(0.55\varphi)}{D^{0.37} \cdot D_i^{0.94} \cdot (L-l)^{0.28} \cdot (D_u^2 + D_o^2)^{0.87}} \quad (2.6)$$

All units are in SI, Q is the volumetric feed flow rate, φ the solids concentration, fraction by volume, D the cyclone diameter, D_i the inlet diameter (or equivalent by area), L the total length of the cyclone, l the length of vortex finder, D_u the underflow diameter, D_o the overflow diameter, ρ_s the solid density and ρ is the fluid density.

With regard to data from industrial units, the accuracy of the model parameters for Plitt's equations is almost wholly dependent on the precision of the early database of Rao (1966). This was supplemented with data from test work with small (600 or less) diameter cyclones, the vast majority of which were from tests at low (less than or equivalent to 5% by weight) solids, or using water only.

In the Plitt model, the independent variables, the model parameters and the functional (linear power and exponential) relationships are governed purely by consideration of the best fit under the multiple linear regression method used. Plitt's regressions were based on all of the available data and he only included variables in the final model equations if they were significant at the 99% confidence level.

Plitt model is also used by Wang and Yu (Wang and Yu, 2006) to validate their proposed computational fluid dynamic-lagrangian particle tracking model. Because of its computational efficiency, the approach has been used to study hydrocyclones under different geometrical and operational conditions.

2.5.2 **Velocity field**

Flow patterns in hydrocyclones have been studied by many authors (Kelsall, 1952b; Ohashi, 1958; Knowles et al., 1973; Bhattacharyya, 1984; B. Dabir, 1986; Gu, 1987; Hsieh, 1988b; Xu et al., 1991; Hwang, 1993). The first and most cited velocity measurement was studied by (Kelsall, 1952b,1963) using small cyclones with diluted feeds containing fine aluminium particles. Tangential and axial velocity components were measured at selected positions, and radial velocities calculated by continuity equation (Fig. 2.14). The axial velocity measurements as shown in Fig. 2.15 exhibited the recirculating flow at levels above the bottom of the vortex finder and short-circuit flow down the outer wall of the vortex finder to the overflow. So the asymmetry of the axial velocity predominates near the region of the inflow and gradually becomes almost symmetric in the lower part of the cone. Further, there is more than one reversal in the flow direction in the region between the vortex-finder and the hydrocyclone wall, yet debatable; Kelsall’s experimental results are by far the most broadly used data among the hydrocyclone researchers.

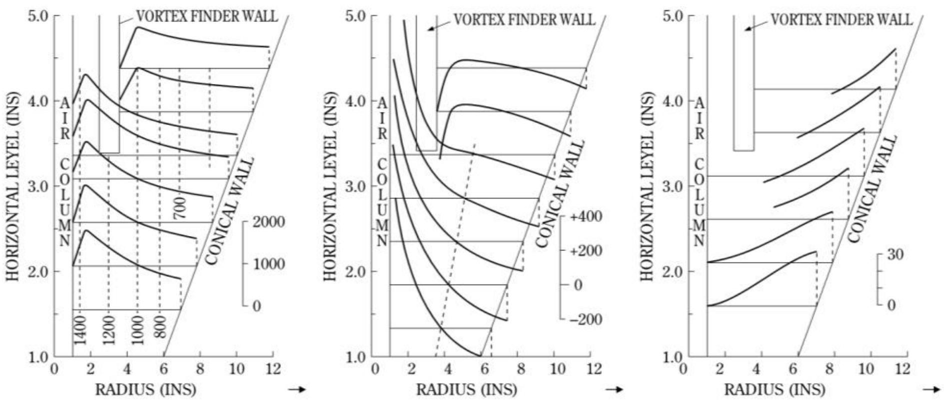

Fig. 2.14 Tangential, axial and radial velocity components according to Kelsall (1963).

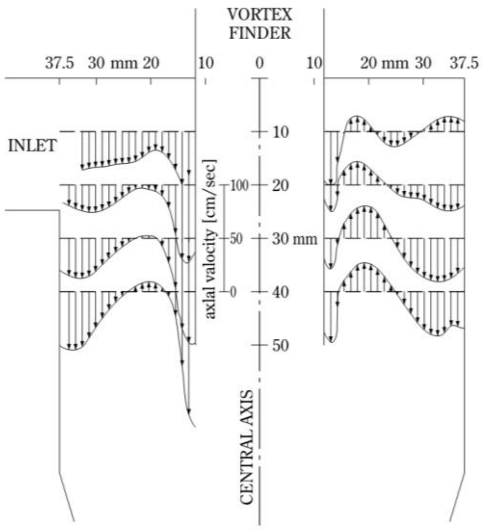

Fig. 2.15 Axial velocity profile in the inlet region, according to Hsieh (1988b).

Knowles et al., (1973) used tracer particles and cine photography for measuring the three-dimensional flow patterns in a 75 mm hydrocyclone working without an air core. It has been found that the profiles of axial and tangential velocities are similar to those detected with hydrocyclones operating with air core. However according to Ohashi and Maeda's observation (1958) the radial velocities profile are relatively small in magnitude.

Bhattacharyya (1984) used a 105 mm hydrocyclone with different inlet and outlet diameters to visualize a photographic techniques with dye injection through the side and end walls of the cyclone. The results illustrated that the locus of zero axial velocity is not affected by the length of the vortex-finder up to 0.6 D_c and is not sensitive to cone angle and relative diameter of apex.

Although these photographic techniques act successfully in unfolding the flow patterns within the hydrocyclone, they usually could not offer detailed information on point velocities, besides the data obtained by these methods are not reliable as accurate analysis of flow reversals and short-circuiting flows cannot be done with such techniques.

Hsieh and Rajamani (1988b) also Monredon (1992) measured and calculated the distribution for the three components of the velocity along the hydrocyclone (Fig. 2.16).

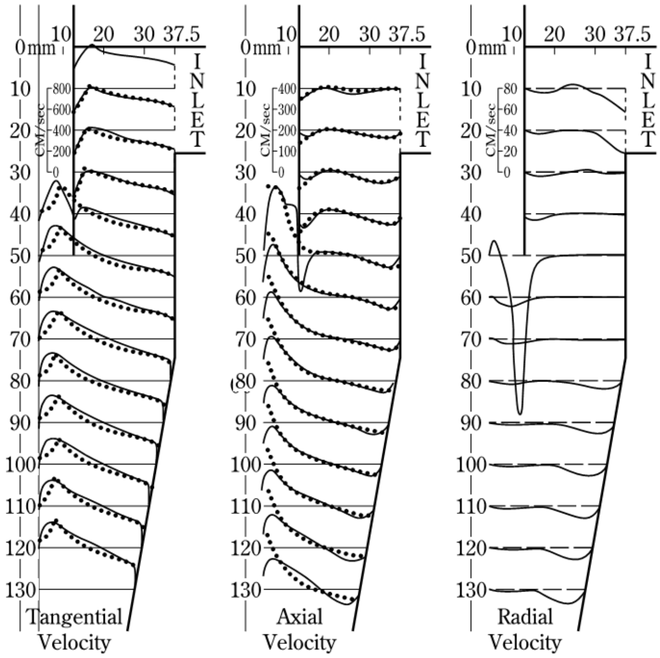

Fig. 2.16.Tangential, axial and radial velocity components according to Hsieh and Rajamani (1988b).

They revealed a detailed report in exposition of tangential and axial velocities for a 75 mm hydrocyclone using the laser Doppler velocimetry technique (LDV). Various proportions of water-glycerol mixtures were used in their experiments to simulate the change of slurry viscosity because of the presence of solid particles in the liquid phase. Tangential velocities measured at 0° and 180° angles, whereas the axial velocities measured at four different angles, 90° apart from each other, to quantify the axisymmetry of the flow, as shown in Fig. 2.17. Various flow reversals have been observed in the area between the wall of the vortex finder and the cylindrical body wall. This research also showed that the short-circuit flows were governing at the back side of the tangential inlet and intensify while fluid viscosity and volumetric flow rate increases.

After Hsieh's (1988b) work , Monredon (1992) used a laser Doppler velocimetry to quantify the velocity profiles within 75 mm and 150 mm hydrocyclone. This work illuminated the effect of design variables (vortex finder diameter and apex diameter and cone angle) on velocity profiles. It revealed that the locus of zero axial velocity (which defined as the dividing line between the upward flow and the downward flow) remained unchanged in the cylindrical section, but moved toward the inside of the conical section, when the vortex finder and apex diameters were enlarged.

With the aid of LDV techniques, fluid flow researches of hydrocyclone have promoted profoundly.

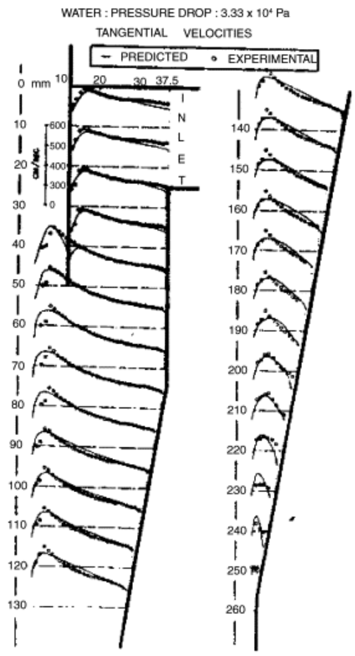

Fig. 2.17 Tangential velocities profiles in a 75 mm hydrocyclone.(Hsieh, 1988b).

Additionally, other investigators used improved techniques to simulate the fluid flow field in hydrocyclones. Ohasi and Maeda (1958) studied the flow patterns by photographing illuminated particles in a 75-mm hydrocyclone. Yoshioka and Hotta (1955a) calculated the tangential velocity in a hydrocyclone, run with a dilute slurry and an air-core, using a one-hole pitot tube. Bradley and Pulling (1959) reported the flow fields by photographic techniques of the movement of a dye injected into transparent hydrocyclones. Lilge (1962) studied the flow fields using pitot tubes of water and magnetite suspensions in a 150 mm, 20° cone angle hydrocyclone. Gu and Li (1987) evaluated tangential and axial velocities of heavy-medium and water cyclones with the aid of laser Doppler anemometry. Luo et al., (1989) calculated three-dimensional velocities in a traditional 82-mm hydrocyclone and resemble the flow fields with those from the water-sealed hydrocyclone, in which the air core was repressed by blocking the spigot with water. Hou et al., (2002) used passive microphones on a hydrocyclone in order to relate the hydrocyclone noise range to a model that anticipates the system reaction to some operating parameters. Chiné and Concha (2000) investigated the fluid flow turbulence field, using LDV, and assumed that the turbulence was not either homogenous or isotropic. Knowles et al., (1973) applied cine photography to calculate the tangential velocity of small anisole droplets with a density close that of water density Dabir and Petty (1986) quantified a forced vortex similar to the central axis of the hydrocyclone. The peak value for the tangential velocity was attained at a radius much smaller than that of the outer vortex finder wall. A comparable qualitative performance was observed by Hwang et al., (1993) by using (LDV) on a hydrocyclone operated without an air-core.

2.5.3 **Air Core**

The air core occurs at the center of the hydrocyclone is an inevitable phenomenon in the rotating flow field. Hydrocyclones form a central air core which extends over the entire length of hydrocyclone. The air core occurs because of the low pressure region in the hydrocyclone drops below atmospheric pressure, which allows air to enter into the cyclone (Nowakowski, 2004). The actual formation of the air core is not known, however the prevalent thought is that the air enters from both outlets and eventually reaches a critical point, which combines the two air vortices (Cullivan et al., 2004). Rietema (1961) noticed that the presence of the air core reduced the pressure drop, thus increasing the economic efficiency of the device. Dyakowski and Williams (1993) showed that the air core is not stationary, but has an oscillatory nature. The oscillations could be caused either by fluctuations in the feed or induced inertial waves (Ovalle, 2005). Delgadillo and Rajamani (2005) investigated the dynamics of the air core using a LES turbulence model. Taking direct measurements of the air core at the outlet is difficult, though non-obtrusive methods have been used by Petersen (1996) and Steffens et al., (1993). Moreover, the geometry and movement of the air core were recognized as being profound indicators of the operational state of hydrocyclones (Neesse et al., 2004; Neesse, 2004). Hence, in recent year’s studies on the air core in hydrocyclones have been the subject of rigorous investigations. Currently, the knowledge on air core performance is incomplete and commonly based on observations in transparent hydrocyclones (Ternovsky, 1994). Air core monitoring using electrical impedance was carried out by Williams et al., (1995). Numerous data have been collected on air-core diameters as a function of hydrocyclone parameters. The measurements were summarised in empirical and semi-empirical formulas in works by Barrientos et al., (1993), Castro et al., (1996), Davidson (1995b), Povarov (1961) and Ternovsky and Kutepov (1994). However, only a few theoretical investigations on the subject were published by Dyakowski and Williams (1995), and Steffens et al., (1993). Hence, the compound procedure of air core formation beginning from instabilities of the multiphase flow up to the stable air core remains poorly understood. For cyclones fed with solid–liquid suspensions, air-core monitoring using electrical impedance has been carried out by Williams et al.,(1995). They successfully used electrical resistance tomography (ERT) to monitor the stability of the air-core. A later development is the use of ERT to monitor separation of oil in a hydrocyclone (Bennett and Williams, 2004). Other non-intrusive air-core tomography techniques that have been tested are, e.g. ultrasonic tomography (Podd, 2000) and X-ray (Cullivan, 2001).

2.5.3.1 Particle motion

Although the geometric structure of a hydrocyclone is simple, the motion of particles inside the hydrocyclone is very complicated. Few researchers studied the motion of solid particles. To understand the separation behavior of hydrocyclones and to obtain a theoretical foundation for structure optimization and efficiency improvement of hydrocyclones, it is essential to make the motion of particles in the hydrocyclones as clear as possible. Most of the experimental works on the motion of solid particles in hydrocyclones have been made by adopting an Euler method, *i.e.*, all the works have been focused on the flow field by studying the motion of particles passing through some fixed positions in hydrocyclones (Kelsall, 1952b; Chu, 1993; Chu et al., 2002). Wang et al.,(2008) investigated the motion of particles in the hydrocyclone by using a Lagrange method, *i.e.*, studying the motion of particles by tracking the particles in the hydrocyclone. Experimental investigations on the motion trajectory of solid particles inside the hydrocyclone have been successfully carried out by using a high-speed motion analyser to track the particle movement. They found for each single particle, the motion trajectory was featured with stochastic characteristics; however, for the overall samples of particles, their motions hold the statistical property. The initial position of particles at the entrance of a hydrocyclone heavily affected the motion trajectory of particles and consequently the separation performance.

2.6 CFD models

This section is a detailed literature review of the existing numerical models used for the performance prediction of hydrocyclones. Previous literature reviews on the numerical modelling of hydrocyclones have been published by (Narasimha et al., 2006b, Narasimha et al., 2007b), Pericleous (1987), Chakraborti &Miller (1992), and Nowakowski et al. (2004).

Three main phenomenon are of interest to the modelling of particle classification in a hydrocyclone: (a) turbulent flow in the cyclone, (b) the effect of air phase on the flow field, and (c) multiphase flow with different particles size ((Narasimha et al., 2006); Hsieh and Rajamani (1991); and Sevilla and Branion (1997)). Numerous works have been carried out in each area, but linking them to develop a broad model for predicting performance of hydrocyclone for industrial applications is of great interest. This section outlines the main development in each of these fields. It should be noted that the CFD model used for fluid flow is Tow Fluid Model facilitated by multiphase mixture model.

2.6.1 **Turbulence modeling in cyclones**

Basic concepts and terminology

In a laminar flow the fluid moves downstream in a smooth and orderly fashion, described as translational motion. When the energy potential (usually pressure gradient) imposed on a laminar flow exceeds a certain amount -the maximum allowable to have the majority of the mass flowing in a translational form- turbulence originates.

In a turbulent flow, the dissipative forces governed by the viscosity of the fluid play a key role in redistributing the mechanical energy into translational and rotational energies. The relevance of this additional rotative fluid motion in turbulent flows on a small particle introduced in the flow is that this particle will describe a larger trajectory than the same particle in a laminar flow for a given geometrical domain.

In order to better comprehend the turbulent transport of particles, some of the important concepts related to turbulent flows, such as vorticity, the presence of rotating structures known as eddies, and the mechanism of turbulence decay will be discussed in this section.

Vorticity, a local property of flows, is defined as twice the local average rotation rate of two initially perpendicular lines following a fluid element (Shirolkar et al., 1996). Therefore, the vorticity of fluid motion is a measure of rotation without deformation. Turbulent flows are characterized by higher levels of vorticity than laminar flows, and because of this augment in vorticity, small particles are carried by turbulent eddies through the flow field. Turbulent eddies, or simply an eddy, is a conceptual idea rather than a physical definition used to refer to rotating structures observed in turbulent flows.

In turbulent flows the vorticity is not only moved around by the flow field, but it is also enhanced by a mechanism called vortex stretching. Due to vortex stretching, the large-scale structures (large-sized eddies) break down to smaller fluid structures (small-sized eddies); this phenomenon leads to the mechanism known as turbulence decay.

In summary, turbulence is the macroscopic and three-dimensional manifestation of inertia and frictional forces caused by the increase in vorticity and strain, which is due to the partition of mechanical energy into rotational and translational energies. The influence of turbulence on small immersed particles is a convective phenomenon that leads to an apparently random spread of the particles through the flow field. One of the most apparent consequences of this influence is the increase in the path described by a particle when it goes from one region in the flow to another. The described path will always be greater for turbulent flows when compared to the path in laminar flows for a given geometrical domain. This is a manifestation of the phenomenon called turbulent particle dispersion.

Overview of the literature on modeling particle in turbulent flows

Industrial hydrocyclones normally run at turbulent flow velocities. The Reynolds number thus is in the range of 510 to 610 (Bradley, 1965). Yet the robust swirling flow, the flow reversal and the flow measure near the underflow stream trigger anisotropy into the turbulence. Most hydrocyclones in mineral processing has an air core and the free surface between the air and the water introduces extra turbulence anisotropy. These features make the CFD modeling of hydrocyclones more difficult and adding of solid particles makes the modelling even more challenging. Lots of researchers have developed models to improve the accuracy of the prediction.

Turbulence models for prediction of very high swirl flow contain empirical constants and are still being developed. The computational cost of such simulations is also very high.

Hsieh (1988b) and (Devulapalli, 1996) modelled hydrocyclones using a 2D axis-symmetric grid where the air core was not set and the air/water interface was treated using a shear free boundary condition. Turbulence anisotropy was integrated into the model by using a modified mixing length turbulence model where a different mixing length constant was used for each component of the momentum equation. Although the model needed calibration it was able to predict velocities measured by these authors using Laser Doppler Anemometry with reasonable accuracy.

k-ϵ models fundamentally make the hypothesis that the turbulence is isotropic as only one scalar velocity fluctuation is modelled. Moreover, the Bousinessq approximation on which the eddy viscosity relies intrinsically implies equilibrium between stress and strain. These assumptions are known to be unrealistic for swirling turbulent flows and this would suggest that k- ϵ models are not appropriate for modeling turbulence in hydrocyclones and this has been shown to be the case by Ma et al (2000), Sevilla and Branion (1997), Petty and Parks (2001), Witt et al., (1999) and Delgadillo and Rajamani (2005) and others. However Dyakowski and Williams (1992) suggested that the k-ϵ model can be used on small (< 44mm radius) hydrocyclones.

Other researchers have used the RNG k- ϵ model with the swirl correction (Fraser (1997) He et al., (1999); Suasnabar (2000); Schuetz et al., (2004), Narasimha et al.,(2005)). However Suasnabar (2000) found that the swirl constant in the RNG model needed to be enlarged to recover predictions but beyond a certain point, further rises caused numerical instability. As an alternative Suasnabar adjusted the constants in the standard k- ϵ model to attain agreement but admitted that this approach is limited. Stress transport models, in particular the full Differential Reynolds Stress model (DRSM), such as that developed by Launder et al., (1975), solve transport equations for each individual Reynolds stress. This enables stress transport models to model anisotropic turbulence and strained flows where the Bousinessq approximation is known to be imperfect.

Although more computationally intensive than k-ϵ models, stress transport models are being used to model turbulence in hydrocyclones.

Boysan et al.,(1982) used an algebraic stress model but the full Differential Reynolds Stress model (DRSM) has been used in more current work. Cullivan and Williams (2001), Slack et al., (2000), Brennan et al.,(2003) have all used variants of the Launder et al., (1975) model. However even here the predictions are not what they could be and there is debate about appropriate modeling options.

Slack (Slack, 2000) found that the Differential Reynolds Stress model gave good predictions of velocities in gas cyclones. However Brennan (2006b), Narasimha et al., (2006), and Delgadillo and Rajamani (2005) found that the DRSM, where the air core was being resolved with the VOF model, under-predicted tangential velocities in simulations of Hsieh's (1988b) 75mm hydrocyclone.

Cullivan et al.,(2003) has suggested that a Differential Reynolds Stress simulation of a hydrocyclone needs to use the Quadratic Pressure Strain correlation of Speziale et al.,(1991) as a minimum. However the author's experience is that velocity predictions from the Speziale model (1991) and the simpler linear pressure strain model of Launder et al., (1975) are much the same once the air core is established. Further Brennan (2006b) also found that the constants in the linear pressure strain correlation need to be adjusted to match velocity predictions. This implies that even the Launder et al., (1975). DRSM has restrictions for this problem.

2.6.1.1 Reynolds's averaging – k-ϵ models and RSM models

The flow in a hydrocyclone is typically turbulent. One of the key features of turbulent flow is it's fluctuations at various length scales. The oscillation can be modelled using Reynolds decomposition where the instant values of the parameters are divided into a mean value and a fluctuating component. To date the backbones of CFD turbulence modeling are k-ϵ models, the Reynolds Stress model and mixing length models. All of these models solve the Reynolds Averaged Equations of motion (RANS). With Reynolds Averaging the equations are averaged over time, which is construed as including all scales of turbulence in the flow. The result is an extra tensor of unknown double correlations called the Reynolds Stress Tensor which is taken as being symmetric and hence covers an additional 6 unknowns for which model equations should be delivered. The first approach to solve this is to accept the Bousinessq estimation. This draws an analogy between the viscous stresses and the turbulent stresses and suggests that the Reynolds Stresses could be calculated by eddy viscosity. As discussed by Wilcox (1998) the Bousinessq approximation is defective, nevertheless the turbulence models, which make use of the Bousinessq approximation, show some achievement in modeling many classes of turbulent flows. However these models are basically empirical. The main approach for calculating eddy viscosity is by mixing length models in which eddy viscosity is assumed to be an algebraic function of the distance from a flow boundary. The Prandtl model (1925) proposes a simple proportionality with an empirical constant. This model gives fairly acceptable predictions for the velocity in fully developed turbulent boundary layers which is mathematically equal to the Law of the Wall by Wilcox (1998). The most common technique for calculating eddy viscosity is to use a two-equation model where an additional transport equation is solved for the turbulent kinetic energy and a second transport equation is solved for the dissipation. The errors in the Bousinessq rough calculation rise due to implicitly makes and assumption that there is a local equilibrium between stress and strain and that the turbulence is isotropic. By modeling transport equations for the individual Reynolds Stresses, Reynolds Stress Models (RSM) do not make the assumption of local equilibrium for stress against strain. Further they relax the assumption of turbulence isotropy because each Reynolds stress is modeled separately, although RSM still average over all scales of turbulence. Wilcox (1998), notes that RSM provide physically accurate estimation for flows which could not be well modeled by k-ϵ models. However RSMs is computationally more demanding and numerically less stable compared to the k-ϵ model as it solves six additional transport equations. Despite of these and other problems, RSMs are now applied in commercial CFD packages with a variety of options.

2.6.1.2 Large Eddy Simulation Model (LES)

Recent developments in computational capability made Large Eddy Simulation (LES) more practical for engineering problems and the fact that LES resolves the large turbulent structures without modeling advises that it should be suitable for modeling cyclones. LES is fundamentally a dynamic simulation and needs a 3D grid.

Slack et al.,(2000) has modeled gas cyclones using LES and established a reasonable predictions of the velocities but the technique needed a finer grid than the DRSM simulation of the same geometry. De Souza and Silveria (2004) modeled the 76 mm hydrocyclone of Debair (1983) but this was without an air core. Both Delagdillo and Rajamani (2005) Narasimha et al.,(2007c), and Brennan (2006b) found that Large Eddy Simulation (LES) gives the best overall velocity predictions although this was more computationally demanding due to finer grid requirements and shorter time steps.

In this model the velocity is decomposed in a different manner than in the k-ϵ and the RSM models. In LES, the large scale turbulent structures are resolved by a filtering operation of the velocity field and the smaller scales or residuals are modelled in a particular manner. A definition for the velocity, defined as the sum of a resolved component u_i and a residual component u'_i, is given by

$$u_i = \bar{u}_i + \bar{u}_i' \tag{2.7}$$

In order to get the resolved component a filtering operation was applied to the governing Navier–Stokes equations. The resulting equations are of the standard form, containing the stress tensor τ_{ij}^{sgs} that arises from the residual motions. The final LES model equations are given as:

$$\frac{\partial \rho}{\partial t} + \rho \frac{\partial \bar{u}_i}{\partial x_i} = 0 \tag{2.8}$$

$$\frac{\partial \bar{u}_i}{\partial t} + \frac{\partial (\bar{u}_i \bar{u}_j)}{\partial x_j} = -\frac{1}{\rho}\frac{\partial \bar{p}}{\partial x_i} + \frac{\partial}{\partial x_j}\left(\mu \frac{\partial \bar{u}_i}{\partial x_j}\right) - \frac{\partial \tau_{ij}^{sgs}}{\partial x_j} + g_i \tag{2.9}$$

The residual stress tensor τ_{ij}^{sgs} contains all information of the subgrid scales or residual and is defined as:

$$\tau_{ij}^{sgs} = \overline{u_i u_j} - \bar{u}_i \bar{u}_j \tag{2.10}$$

The residual stress tensor is modeled most simply by an eddy viscosity model (Smagorinsky, 1963; Piomelli, 2001). The main role of the subgrid scale model is to eliminate energy from the resolved scales into the subgrid scales. The stress tensor is specified as the product of the eddy viscosity and the strain rate, as

$$\tau_{ij}^{sgs} = -\mu_t \left(\frac{\partial \bar{u}_i}{\partial x_j} + \frac{\partial \bar{u}_j}{\partial x_i} \right) \tag{2.11}$$

LES is not well designated to solve the flow near the walls. In order to recover the results, Yakhot et al.,(1989) presented the renormalization group model (RNG). The RNG model is efficacious to model the low-Reynolds-number encountered in transitional flows and close to wall regions with which the molecular viscosity has more impact. The turbulent viscosity is defined as the difference between the effective viscosity and the molecular viscosity:

$$\mu_t = \mu_{eff} - \mu \tag{2.12}$$

The effective viscosity (The effective viscosity of a suspension is defined to be the four-tensor that relates the average deviatoric stress to the average rate of strain (Nunan and Keller, 1984)) is defined as,

$$\mu_{eff} = \mu \left[1 + H \left(\frac{\mu_s^{\ 2} \mu_{eff}}{\mu^3} - C \right) \right]^{1/3} \tag{2.13}$$

The turbulent viscosity , μ_s in the subgrid scale is defined as,

$$\mu_S = \left(C_{RNG} V^{1/3} \right)^2 \sqrt{2 \bar{S}_{ij} \bar{S}_{ij}} \tag{2.14}$$

In Eq.2.8, V is the volume of the computational cell and $\bar{s}_{ij}$ is the strain rate. Typical LES model constant value of C_{RNG} is 0.157 and H (x) is the Heaviside function, defined as

$$H(x) = \begin{Bmatrix} x, x \geq 0 \\ 0, x \leq 0 \end{Bmatrix} \quad (2.15)$$

2.6.2 **Air core models**

A stable flow field is a prerequisite for effective performance in a hydrocyclone. The steadiness of the flow field is dependent upon the feed parameters, such as the feed pressure, the feed concentration etc, but the flow field internal structure also plays a key role on the stability. One of the main internal structures of the flow field, which leads to the stability of operation, is the generated air-core. In hydrocyclones, the high tangential velocity of the fluid in the central region of the device along with the decreased pressure to the value smaller than the atmospheric pressure causes the formation of air-core on the central axis. In the usual models of flow in a hydrocyclone, the interface that bounds the air core is modelled as a fixed cylindrical surface that simplifies the problem greatly. This approximation avoids the necessity of calculating an unknown boundary that modifies; where the field equation must be solved. Nevertheless this simplification can produce bad results.

Literature survey reveals that only limited work has been reported in the literature for formation of air core and measurement of air core diameter. During the 1990s, some investigations were made on the role of the air-core on hydrocyclone operation (Barrientos, 1993; Steffens et al., 1993; Williams, 1995; Castro, 1996; Concha et al., 1996; Romero and Sampaio, 1999). The mathematical models for the air-core developed in the early 1990s could not predict the air-core diameter for an industrial hydrocyclone such as some reported models in the literature:(Tarjan, 1961) and (Svarovsky, 1984). However many models are totally empirical and their validity is suspicious. Dyakowski and Williams (1995) proposed a method to predict the size of the air ore within a hydrocyclone based on calculating the internal pressure distribution by solving a set of conservation equations. The effect of slurry properties, such as bulk viscosity and surface tension and flow conditions are taken into consideration.

Prediction of the air core diameter has been given as a function of various hydrocyclone geometries and operating conditions. A qualitative conclusion based on this model made that the velocity fluctuations at the gas-liquid interface are responsible for the extra surface stresses. These can be described by the surface viscosity which was incorporated into Young-Laplace boundary conditions at the interface. Based on this condition, they found that the higher slurry viscosities are responsible for the air-core decays in the hydrocyclone. Davidson (1995a) developed an expression for the air core diameter in terms of flow variables at the underflow and the overflow which can be applied iteratively during hydrocyclone flow calculations. He analyzed the air core diameter in a hydrocyclone using the physics of uniform density, inviscid flow at each outlet, modified by an empirical factor to account for viscous effects.

Numerical modelling of the air core for liquid phase cyclones has been dealt with in a number of ways. Before the work of Romero and Sampaio (1999), some researchers presumed that the air core has a fixed diameter and applied a slip boundary condition at the phase interface (Hsieh and Rajamani (1991), and Malhotra et al.,(1994)). This is computationally favourable but means that the CFD code cannot predict the air core. Estimating air-core diameter has also been provided by the application of Bernoulli's equation applied with a minimisation procedure (Davidson, 1988; Davidson, 1995a); through the use of an effective air-core interface viscosity (Dyakowski, 1995); as well as through application of Young–Laplace's relation (Concha, 1998). Notably, the latter two approaches offer the potential to account for asymmetric air-core geometry. The air-core shape and diameter predicted in a hydrocyclone by Romero and Sampaio (1999). Based on the Navier-Stokes equations, differential Reynolds stress model (DRSM) utilizes a Young-Laplace type boundary condition at the air-liquid interface and assumes the air-core surface has a cylindrical shape. Although there was reasonable agreement between predicted and experimental results near the free interface, the discrepancy of results were due to insufficient free boundary conditions for the turbulent quantities on the free interface. Pericleous and Rhodes (1986) used the Algebraic Slip Mixture (ASM) model, while Suasnabar (2000), (Cullivan, 2001; Cullivan et al., 2003) and Brennan et al. (2003) used the Volume of Fluid model. Both of these models are implemented in Fluent and are similar in that they both solve an additional transport equation for the volume fraction of each additional phase. The ASM model is designed for dispersed two phase flows and Pericleous and Rhodes (1986) used this model mainly to simulate the slurry phase, but it is interesting to note that it worked for the air core as well. The VOF model is simpler in that it does not have a drift calculation and assumes that the two phases do not interpenetrate. The slip velocity in the ASM model can be disabled so it behaves like VOF with QUICK discretization scheme. Recent studies by Brennan (2006b) and Sripriya et al., (2007) reveal the performance of a hydrocyclone and modeling for flow characterization in the presence and absence of air core, and showed that the separation efficiency increased on suppression of the air core with the insertion of a solid rod. Neese and Dueck (2007) determined the air core diameter by balancing the positive pressure gradient and the centrifugal force in the rotational flow field of a hydrocyclone. Narasimha et al.,(2007c), and Delgadillo and Rajamani (Delgadillo, 2005; Delgadillo, 2009) all used the VOF or Mixture model successfully in simulating the air-core inside the cyclones successfully.

2.6.2.1 VOF Model

The Volume of Fluid model (VOF) (Hirt and Nichols, 1981) and the Mixture model (Manninen et al., 1996) are simplified Eulerian multiphase approaches where the equations of motion are solved for the mixture and additional transport equations for the volume fractions of additional phases are solved. The VOF model and the mixture model solve significantly less transport equations than the full Eulerian approach and thus numerically more efficient. The VOF and Mixture models are implemented in commercial CFD codes such as Fluent with the option of being used for turbulent flows with the turbulence model enabled for the mixture.

The VOF model is intended for modelling flows where there are two or more continuous phases separated by a phase boundary and this makes it suitable for modelling the air core in hydrocyclones (Suasnabar, 2000; Delgadillo, 2005; Narasimha et al., 2006).

The Mixture model (Manninen et al., 1996) is intended for modelling dispersed phases and can incorporate phase segregation which makes it suitable for modelling the solid phases in cyclones, in particular the medium. The Mixture model was used by Brennan et al., (2007) and Narasimha et al.,(Narasimha, 2005; Narasimha et al., 2006;

Narasimha et al., 2007) to simulate medium segregation in a DSM pattern dense medium cyclone and was compared to Subramanian's GRT data (Subramanian, 2002).

2.6.3 **Particle flow modelling**

In general, there are two generic approaches for numerical simulation of particles in a mixture: namely, the Lagrangian approach and the Eulerian approach.[150] The Lagrangian approach treats the fluid phase as a continuum and predicts the trajectory of a single particle in the fluid flow as a result of various forces acting on the particle. In the Eulerian approach, solid particles are assumed to be a continuum. For particles of very small Stokes number, where the slip velocity is very small, a two-phase flow can be approximated as a homogenous single-phase flow. Recently, a so called combined approach of CFD and Discrete Element Method (CFD-DEM) is also developed to study the particle-particle and particle-fluid interactions in the complex industrial units (Chu and Yu, 2008).

2.6.3.1 Lagrangian Particle Tracking approach for cyclones

The Lagrangian approach where the paths of individual particles are tracked based on the velocity predicted by a CFD simulation of the fluid is suited to systems where the dispersed phases are dilute and where the particles interact mostly with the fluid without significantly changing the fluid transport properties. In particular the Lagrangian approach is well suited to systems where small numbers of large particles are encountered. By balancing the forces that act on a particle in motion in a carrier fluid, a particle can be tracked along its trajectory. Additionally corrections of the particle trajectory due to interaction with its surrounding environment can be included. The influence of particles on the fluid can be included by considering a source term in the governing equations of the fluid. Also turbulence dispersion of the particles can be included (Crowe, 1996).

The Lagrangian approach used by Hsiesh (1988b), Hsieh & Rajamani (1991) to predict limestone partition curves (The partition curve relates the weight fraction or percentage of each size fraction found in the feed, which reports to the underflow) for the hydrocyclone geometries used in their studies with good accuracy. However, they only considered the drag and centrifugal forces. Particle dispersion due to turbulence of the fluid was neglected.

He et al.,(1999) and Ma et al.,(2000) employed the Lagrangian approach for dilute systems in cyclones. For such cases the volume occupied by the particles in a computational cell may be neglected. However, the accumulation of solid particles in regions of high fluid strain-rate and low vorticity can result in high values of the local particle concentration, indicating the presence of a significant (local) coupling of the two phases. When solids concentration exceeds 5% by volume, the presence of particles changes the viscosity stresses and results in the generation of the extra inertial stresses.

The Lagrangian approach has however been extended to modelling cyclones at large particle concentrations by Rajamani & Milin (1992), Here the Lagrangian approach was coupled to the fluid system by estimating the slurry concentration from the residence time of the particles in each element of the grid. This concentration was then used to modify the fluid viscosity which was used in the CFD predictions. The method was used the predict limestone partition curves for feeds with up to 35% by weight limestone with good accuracy. The technique also predicted limestone concentrations, but these were not compared to experimental data.

2.6.3.2 The Eulerian-Eulerian Models for cyclones

The Eulerian-Eulerian methodology has been used for modelling higher volume fraction multiphase flows in a hydrocyclone. In this approach, different phases are treated as interpenetrating continua. The model solves different sets of momentum equations for each additional phase simulated. Conservation equations for each phase are derived to obtain a set of equations with regard to momentum, continuity and energy. A study of a hydrocyclone has been carried out by Cokljat et al., (2006) using an Eulerian–Eulerian algorithm coupled with a full Reynolds Stress model. In that study the Reynolds Stress transport equations were solved on the mixture level only. Their results extend the application of CFD to high and medium density cyclones, but this type of study is not currently practical for a general-purpose design tool. In the Eulerian-Eulerian approach, the most common and widely discussed in the literature is the Eulerian two-fluid approach. A more integral approach based on the kinetic theory applied to granular flows (Gidaspow, 1992) has become prevalent recently. Besides a simplified model based on the algebraic calculation of the particle slip velocity (Manninen et al., 1996a) has become widespread especially in cyclone modelling. The simplified Eulerian multiphase approach, i.e., the mixture model approach, (Manninen et al., 1996a) was widely used in hydrocyclone, dense medium cyclone and gas cyclone modelling. Pericleous (1987), Pericleous & Rhodes (1986) and Zughbi et al.,(1991) used this model in hydrocyclone modelling. Nowakowski et al., (2000) presented the concept and principles of applying a multi-continuum model for calculating a hydrocyclone performance. A time scale analysis can provide a quantitative discussion concerning the importance of various types of forces affecting the particle motion. However, modelling a distribution of types and sizes of particles complicates the continuum formulation because separate continuity and momentum equations have to be solved for each size and type. Suasnabar (2000) adapted the full Eulerian approach with granular flow modeling for the particulate phases to model a DSM pattern dense medium cyclone. The technique has also been used more recently by Nowakowski (Nowakowski et al., 2000; Nowakowski, 2004). The full Eulerian-Eulerian interaction between different phases was modeled for hydrocyclones by Cokljat et al.,(2006). His results specified that the small particles remained evenly suspended in the solution. The ratio of amount of particles leaving through the vortex finder and the apex is proportional to the water split ratio in the cyclone. Conversely, most of the larger particles are collected along the wall and leave via the apex at high concentration. Huang (2005a) made an effort in simulating a 3D oil-water turbulent flow in the liquid-liquid hydrocyclone by merging the Euler-Euler approach and Reynolds-stress model (RSM) to handle the anisotropic turbulent two-phase flow with a higher volumetric ratio (over 10%) in the dispersed phase. The model was only tested in liquid-liquid hydrocyclones in which the interactions of droplets with liquid phase are undoubtedly limited. The shortcoming of the full Eulerian multiphase modeling approach is its high computational cost. Additional applications in commercial CFD codes have been restricted to using the k-epsilon/RSM models for turbulence.

2.6.3.3 Combined approach of CFD and Discrete Element Method (CFD-DEM)

The Lagrangian approach is just suitable for dilute flow since it only traces a single particle, and the effect of inter-particle interactions and the reaction of particles on the fluid are ignored. Thus, the effect of medium to coal ratio, which is one of the most important operational parameters in dense medium cyclones, cannot be investigated using the Lagrangian approach. The flow in DMCs is obviously a dense flow because the volume fraction of coal particles in common operation is greater than 10%. In recent years, the so-called combined approach of CFD and Discrete Element Method (CFD-DEM) has been developed (Yu and Xu, 2003) and is able to account for particle-particle and particle-fluid interactions (Tsuji et al., 1992; Xu and Yu, 1997). The CFD-DEM approach has proven to be effective in modelling particle-fluid flow. Chu et al. (Chu et al., 2009a; Chu et al., 2009b) published a series of papers to study the particle-particle and particle-fluid interactions in gas cyclones and dense medium cyclones. The effect of medium to coal ratio and particle flow instability in DMCs were successfully modelled in their work.

2.6.4 The Mixture Models for cyclones

The Volume of Fluid model (VOF) (Hirt 1981) and the Mixture model (Manninen et al., 1996a) are simplified Eulerian multiphase methodologies which use a single-fluid approach. The equations of motion solve for the mixture and additional transport equations for the volume fractions of the additional phases. The VOF model and the mixture model solve less transport equations in comparison to the full Eulerian approach and hence are numerically more efficient. The VOF and Mixture models are applied in commercial CFD codes with the option of being used for turbulent flows with the turbulence model enabled for the mixture. The basic model equations are defined as

$$\frac{\partial}{\partial t}(\rho_m) + \frac{\partial}{\partial x_i}(\rho_m u_m) = 0 \tag{2.16}$$

where u_m is the mass-averaged velocity

$$u_m = \frac{\sum_{q=1}^{n} \alpha_q \rho_q u_q}{\rho_m} \tag{2.17}$$

and ρ_m is the mixture density

$$\rho_m = \sum_{q=1}^{n} \alpha_q \rho_q \tag{2.18}$$

The momentum equation for the mixture can be obtained by summing the individual momentum equations for all phases. It can be expressed as

$$\frac{\partial}{\partial t}\rho_m u_{mi} + \frac{\partial}{\partial x_j}\rho_m u_{mi} u_{mj} = -\frac{\partial p}{\partial x_i} + \frac{\partial}{\partial x_j}\mu_m\left(\frac{\partial u_{mi}}{\partial x_j} + \frac{\partial u_{mj}}{\partial x_i}\right) + \rho g_i + \frac{\partial}{\partial x_j}(\sum_{q=1}^{n}\alpha_q \rho_q u_{dr,qi} u_{dr,qj}) \qquad (2.19)$$

where n is the number of phases and μ_m is the viscosity of the mixture

$$\mu_m = \sum_{q=1}^{n}\alpha_q \mu_q \qquad (2.20)$$

Where $u_{dr,q}$ is the drift velocity for secondary phase q , given by $u_{dr,q} = u_q - u_m$

Davidson (1995a) used the Mixture model by (Manninen et al., 1996a) to resolve particle concentrations in simulations of Kelsall’s (1952a) cyclone. Suasnabar (2000) used both the full Eulerian granular approach (Ding and Gidaspow (1990)) and the Mixture model (Manninen et al., 1996a) to model the distribution of medium in dense medium cyclones. Suasnabar (2000) also found that both Eulerian methods predicted medium segregation qualitatively but the Eulerian granular flow predicted the observed drop in medium concentration at the wall in the bottom of the apex more accurately, they suggested that this phenomenon is mainly due to the full Eulerian granular flow model. The model which was simulated by Bagnold (1954) apply forces on the medium by the gradient in solids pressure in the dispersed phase momentum equation. The Mixture model has also been used to model dispersed phases in cyclone separators at the Julius Kruttschnitt Mineral Research Centre (JKMRC). Originally the Mixture model with the DRSM turbulence model were used by Brennan (2003) to simulate the medium and the air core in a 350mm DSM pattern dense medium cyclone using a single medium size. The basic Schiller and Naumann (1935) drag force law and without viscosity corrections. Brennan (2003) discovered that medium segregation is over predicted while compared to Subramanian’s (Subramanian, 2002) GRT (Gamma Ray Tomography) data. The simulations also predicted that the highest concentration of medium is at the wall and also that a film of pure water is predicted to form just below the air core. Neither of these effects were observed in Subramanian’s (Subramanian, 2002) GRT measurements. Subsequently the modelling was extended in a way that medium is simulated with a size distribution, and wall lift forces based on Saffman’s

(Saffman, 1965) expression included, the Ishii and Mishimi (1984) slurry viscosity model used, and the CFD was used Large Eddy Simulation (Narasimha et al., 2006). In subsequent work (Narasimha, 2007c) a Lagrangian approach is superimposed on the Mixture model simulations (using medium) to build the partition curves for coal particles with sensible correctness. Parallel to this work, the same multiphase CFD approach used to model the classification efficiency of the 75 mm Hsieh (1988b) hydrocyclone (Brennan et al., 2007b) and also the 480 mm JK classifying cyclone (Brennan, 2006b). More recently, Wang et al., (2009) modelled magnetite medium segregation in a dense medium cyclone using the mixture multiphase model combined with the Reynolds stress turbulence model. The validity of the proposed approach was verified by the reasonably good agreement between the measured and predicted results under different conditions. The coal particles were traced by coupling the DEM with CFD multiphase models effectively.

There are many circumstances where hydrocyclone performance and dense flow are intertwined, such as for example when feed solids flow exceeds hydrocyclone capacity during continuous operations. The work reported here, which is part of an ongoing research effort to develop a robust CFD model for prediction of hydrocyclone performance, focuses on hydrocyclone operation at high solids concentration. The paper presents the basic physics framework that accounts for solid–liquid and solid–solid interactions under hydrocyclone's swirling flow. Operating conditions that are past the transition from the spray to rope regime are deliberately chosen for this purpose. Model predictions are validated by comparison with solids split and separation curves measured on a 100 mm diameter hydrocyclone. CFD model predictions permit taking an insightful look at the inside of a hydrocyclone under extreme operating conditions, which would be difficult to achieve experimentally. Velocity profiles, G-force distribution and distribution of solids predicted by CFD are bound to lead to a better understanding of the separation that takes place inside a hydrocyclone, which may eventually help improve hydrocyclone design and performance.

2.6.4.1 The Two Fluid Model (TFM) approach

On the other hand, computer modeling and simulation has been recognized as a promising technique to overcome the problems associated with the experimental measurements. Based on the modeling of the solid phase, the popular mathematical models proposed thus far can be grouped into two categories: the discrete approach at a microscopic level represented by the combined approach of computational fluid dynamic and discrete element method (CFD-DEM) and the continuum approach at a macroscopic level represented by the two-fluid Model (TFM).(Zhou et al., 2010). The CFD-DEM approach has been widely accepted as an effective tool to study particle-fluid systems,(Zhu et al., 2007,2008) with recent efforts made to gas cyclone,(Chu et al., 2011) hydrocyclone,(Zhou et al., 2010) and dense medium cyclone.(Chu et al., 2009,2012). However, at present, it cannot be applied to practical hydrocyclones, where the particle size involved is very small and the number of particles could be billions. To date, discrete modelling of hydrocyclones has been mainly made by the combined CFD and Lagrangian particle tracking (LPT) method.(Hsieh and Rajamani, 1991; Wang and Yu, 2006; Bhaskar et al., 2007b; Mousavian and Najafi, 2009b; Azadi et al., 2010). The CFD-LPT approach, which is actually a simplified CFD-DEM model, traces only a single particle, with the effect of inter-particle interactions and the reaction of particles on the fluid ignored. Because of its computational efficiency, the approach has been used to study hydrocyclones under different geometrical and operational conditions as reviewed by Nowakowski et al., (2004) and Narasimha et al., (2007a) However, it is erroneous as a general model applied to hydrocyclones which may be operated at high solids concentrations.(Slechta and Firth, 1984; Dyakowski and Williams, 1996; O'Brien et al., 2000; Hararah et al., 2010; Zhang et al., 2011).

The Two Fluid Model (TFM) approach can overcome this problem while being computationally more convenient than the CFD-DEM model. It has been increasingly used to study the flows in hydrocyclones.(Nowakowski et al., 2000; Huang, 2005b; Brennan et al., 2007a; Noroozi and Hashemabadi, 2009; Davailles et al., 2012a; Davailles et al., 2012b; Kuang et al., 2012a; Narasimha et al., 2012; Swain and Mohanty, 2013). Generally, the previous TFM studies employ two different ways in describing the phases considered. One applies a full set of conservative equations in regard with momentum and mass to each phase involved.(Nowakowski et al., 2000). It was used to study particle separation (Nowakowski et al., 2000; Davailles et al., 2012a; Davailles et al., 2012b; Swain and Mohanty, 2013) and deoiling (Huang, 2005b; Noroozi and Hashemabadi, 2009) in hydrocyclones. Another is based on the so called mixture model which solves only one set of governing equations for all the phases, with an algebraic slip velocity model for each phase.(Manninen et al., 1996b). This simplification significantly alleviates the computational loading in simulations based on a full TFM model. It has been used by various investigators to study the multiphase flow and related phenomena in hydrocyclones (Brennan et al., 2007a; Kuang et al., 2012a; Narasimha et al., 2012) or in dense medium cyclones.(Narasimha et al., 2007b; Chu et al., 2009; Wang et al., 2009). Kuang et al.(2012a) recently extended the mixture model to study the effect of feed solid concentration based on the cyclone used in Hsieh's experiment.(1988a). Good agreements between model predictions and measurements can also be found in the recent work of Narasimha et al., (2012). Therefore, the TFM facilitated with the mixture model is applicable to a wide range of hydrocyclone conditions. However, to date, comprehensive studies of the flows and performance in hydrocyclones of different geometrical configurations at different feed solids concentrations have not been found in the literature.

In this work, the mixture model reported elsewhere (2012a) is extended to systematically study the geometrical effects on the flows and performance in hydrocyclones operated at a wide range of feed solid concentrations. The cyclone size and spigot diameter are focused considering that they are often investigated under specific conditions for the purpose of industrial applications.(O'Brien et al., 2000; Rong, 2007; Atkinson and Swanson, 2008). The findings from this study should be useful not only for establishing a comprehensive picture about the effects of cyclone size and spigot diameter but also for designing and controlling hydrocyclones.

2.7 Numerical Simulation and the Objectives

2.7.1 **Overview of the model**

To describe the complicated liquid-air-solid turbulent multiphase flows in hydrocyclones, various efforts have been made in the past two decades or so to develop a CFD model based on flow fundamentals (Nowakowski et al., 2004; Narasimha et al., 2007a). Boysan*et al*.(1982) developed one of the first CFD models and showed that the standard k–ε turbulence model was inadequate to simulate flows with swirl because it led to excessive turbulence viscosities and unrealistic tangential velocities.

Recent review of CFD models for hydrocyclones by Narasimhas*et al*. (2007a) manifests that both Reynolds stress model (RSM) and large eddy simulation (LES) can be used to improve the accuracy of the numerical solution. In general, LES provides a better solution for capture of time dependent vortex oscillations and non-equilibrium turbulence (Nowakowski et al., 2004), which will potentially impact upon the separation efficiency. Nonetheless, the successful application of the RSM turbulence model for different studies in cyclone separators has been reported by many researchers (e.g. Wang and Yu, 2006; Bhaskar et al., 2007a; Evans et al., 2008; Mousavian and Najafi, 2009a; Wang et al., 2009; Xu et al., 2009; Wang and Yu, 2010; Chu et al., 2011; Elsayed and Lacor, 2011). Moreover, for industrial scale simulations, RSM model is much more computationally practical compared to LES model as the number of grid in LES (not for RSM) simulations should strictly scale to the 9/4 power of the Reynolds number (Wilcox, 1994) and causes demanding computational efforts. On the other hand, in the existing hydrocyclone's CFD models, volume of fluid (VOF) is widely used to describe the free interface between gas and liquid (Wang and Yu, 2006). The interface can also be predicted by the mixture multiphase model (Narasimha et al., 2006; Brennan et al., 2007a; Wang et al., 2009). It is not clear whether the mixture and VOF give different results or not.

For solid flow in hydrocyclones, Lagrangian Particle tracking model (LPT) is generally applied to trace particles motion (Narasimha et al., 2007a), which usually does not consider particle-particle collision and interaction of particles on fluid in hydrocyclones, and thus valid to a low feed solid concentrations. On the other hand, Brenna *et al*. (2007a) has combined (Large Eddy Simulation) LES model with mixture model to predict partition efficiency of hydrocyclones for classification of limestone at a low feed solid percentage (1.8% by volume). The mixture model treats particles as continuous fluid, which is different in concept from the Discrete Element Model (DEM) and Lagrangian Particle Tracking (LPT) models where particles are discrete elements.

Theoretically, the mixture model can to some degree overcome the problem of Lagrangian Particle tracking model (LPT). However, to date, the reported applications of mixture model to hydrocyclone process are very limited, and thus the applicability of the model to the process under different conditions is not clear.

2.7.2 **Outline of the model**

The numerical model which has been used in this work developed by the UNSW group (Wang and Yu, 2006; Kuang et al., 2012a) .The model is then further extended and modified in this dissertation to describe hydrocyclone flows and performances under a wide range of flow conditions (Ghodrat et al., 2013). The main objectives include systematically examining the existing standard designs of hydrocyclones, optimizing them, and then proposing some new designs. More importantly, this work covers a wide range of feed solids concentrations, which have not ever achieved before but overcome in this project because of the use of new research tool. Also, significant efforts have been made to understand the performance using fluid dynamics such as pressure, velocities, and concentrations of particles of various types using the new CFD model under a wide range of conditions, which are difficult to achieve experimentally if not possible.

In the model the turbulent flow of liquid–gas–solid mixture is modelled by the RSM model, the interface between the liquid and air core and the particle flow are both modelled using a mixture multiphase model, as outlined in Fig. 2.18 (Method II). The widely used LPT model (Method III in Fig. 2.17) is also considered in this work, to be compared with the mixture model. Moreover, the mixture model is examined in detail against the Volume of Fluid (VOF) model in the prediction of fluid velocity, inlet pressure drop, and amount of water split to underflow, which are useful in characterizing hydrocyclone flow and performance. The description of the LPT model has been detailed in the recent work of (Wang et al., 2007; Wang and Yu, 2010).

The mixture model (Manninen et al., 1996a) is a simplified Two Fluid Model (TFM) for efficiently computing the flow of dispersed particles on a CFD cell scale. It allows all the involved phases to be interpenetrating and move at different velocities. The governing equations of mass and momentum conservation are solved only for the mixture of liquid, air and solids as stated by Kuang et al.(2012a). Each sized particles represents one phase. To effect a simulation, an original size distribution of particles is divided into a series of size intervals. Each size interval is represented by a mean size in simulations. The volume fraction of each phase present in the mixture is given according to the continuity equation, considering the relative drift velocity among phases. The same treatment applies to particles of different densities; this issue did not consider in Kuang work nonetheless the model is extended and modified to be applicable for different particle densities in this thesis. This model has been successfully used to model the flow of dense medium in DMCs by the UNSW group (Chu et al., 2009; Wang et al. 2009) and extended in this work to study the separation behaviors of different size and densities particles in hydrocyclones. Notably, in the present model, the solid viscosity is given according to the so-called kinetic theory (Syamlal et al., 1993). The governing equations for the mixture model are detailed in section 2.7.3.

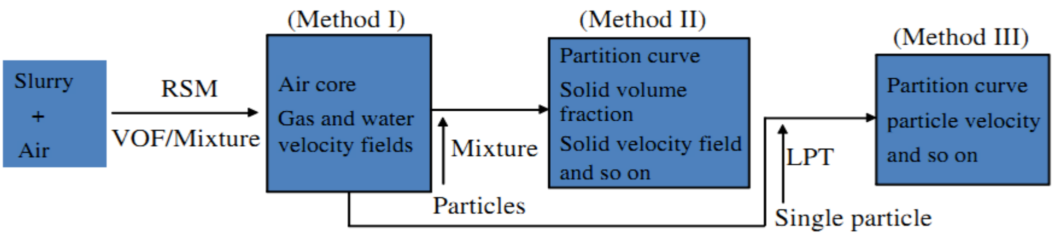

Fig. 2.18 different CFD models for hydrocyclones

2.7.3 **Model description**

The present study is based on the TFM model, facilitated by the mixture model. In the model, both fluid (liquid and air) and solid phases are treated as interpenetrating continua, respectively. Particles of different sizes or densities represent different phases. However, the mixture of gas, liquid and solids is represented by a single phase with mixture properties, and allows certain slip velocities between different phases. Note that in this study, we only consider particles of the same density, although they have different sizes. To carry out a simulation, the size distribution is divided into a series of size intervals, with each represented by a mean size in the simulation.

The flow of the mixture is calculated from the continuity and the Navier–Stokes equations based on the local mean variables over a computational cell with the consideration of slip velocities between different phases (Manninen et al., 1996b), which are given by:

$$\frac{\partial}{\partial t}(\rho_m) + \frac{\partial}{\partial x_i}(\rho_m u_m) = 0 \tag{2.21}$$

and

$$\frac{\partial}{\partial t}(\rho_m u_{mi}) + \frac{\partial}{\partial x_j}(\rho_m u_{mi} u_{mj}) = -\frac{\partial p}{\partial x_i} + \frac{\partial}{\partial x_i}(\sum_{k=3}^{n} p_k) + \frac{\partial}{\partial x_j}[\mu_m(\frac{\partial u_{mi}}{\partial x_j} + \frac{\partial u_{mj}}{\partial x_i})]$$
$$+ \frac{\partial}{\partial x_j}(-\rho_m \overline{u'_{mi} u'_{mj}}) + \frac{\partial}{\partial x_j}(\sum_{k=1}^{n} \rho_k u_{dr,ki} u_{dr,kj}) + g\rho_m \tag{2.22}$$

where g is the gravitational acceleration, p_k is the solid pressure, $u_{dr,ki}$ is the drift velocity, and $-\rho_m \overline{u'_{mi} u'_{mj}}$ is the Reynolds stress term which includes turbulence closure and must be modelled to close Eq. (2.22).

To model anisotropic turbulence problems as encountered in hydrocyclones, turbulence models like the Reynolds stress model (RSM) or Large eddy simulation (LES) should be used, which can both give results comparable to the experimental measurements (Brennan, 2006a; Wang and Yu, 2006; Mousavian and Najafi, 2009a). RSM is adopted in the present model for computational efficiency:

$$\frac{\partial}{\partial t}\left(\rho_m \overline{u'_{mi} u'_{mj}}\right) + \frac{\partial}{\partial x_k}\left(\rho_m u_{mk} \overline{u'_{mi} u'_{mj}}\right) = D_{T,ij} + P_{ij} + \phi_{ij} + \varepsilon_{ij} \tag{2.23}$$

where $D_{T,ij}$, P_{ij}, ϕ_{ij}, and ε_{ij} represent the turbulent diffusion, stress production, pressure strain, and dissipation, respectively.

In Equations (2.21) to (2.23), the mass-averaged velocity u_{mi}, density ρ_m and viscosity μ_m of a mixture are respectively defined by:

$$u_{mi} = \frac{\sum_{k=1}^{n} \alpha_k \rho_k u_{ki}}{\rho_m} \tag{2.24}$$

$$\rho_m = \sum_{k=1}^{n} \alpha_k \rho_k \tag{2.25}$$

$$\mu_m = \sum_{k=1}^{n} \alpha_k \mu_k \tag{2.26}$$

where n is the number of phases, and k represents different phases: k=1 for water (the primary phase), and 2 for air, 3−n for the kth type of particles (the secondary phases).

The volume fraction of phase α_k is obtained according to the continuity equation for phase k:

$$\frac{\partial}{\partial t}(\alpha_k \rho_k) + \frac{\partial}{\partial x_i}(\alpha_k \rho_k u_{mi}) = -\frac{\partial}{\partial x_i}(\alpha_k \rho_k u_{dr,ki}) \tag{2.27}$$

The drift velocity is determined by the algebraic slip mixture model assuming that the phases should be reached over a short spatial length (Manninen et al., 1996b):

$$u_{dr,ki} = \frac{(\rho_k - \rho_m) d_k^2}{18 \mu_1 f_{drag}} a_{k,i} - \frac{\eta_t}{\sigma_t}\left(\frac{\nabla \alpha_k}{\alpha_k} - \frac{\nabla \alpha_1}{\alpha_1}\right) - \sum_{k=1}^{n}\left(\frac{\alpha_k \rho_k u_{1k,i}}{\rho_m}\right) \tag{2.28}$$

where σ_t is the Prandtl Schmidt number set to 0.75, and η_t is the turbulent diffusivity. $a_{k,i}$ is the acceleration of phase *k*. $f_{drag}$is the drag force on particles or air bubbles, which is determined according to the well-known Ergun & Wen-Yu correlation (1952; 1966) for particles:

$$f_{drag} = \begin{cases} \frac{3}{4} C_d \frac{\alpha_1 \rho_1 |\mathbf{u}_1 - \mathbf{u}_k|}{d_k} \frac{\tau_s}{\rho_k} \alpha_1^{-2.65} \\ \frac{\tau_s}{\rho_k}\left(150 \frac{(1-\alpha_1)\mu_1}{\alpha_1 d_k^2} + 1.75 \frac{\rho_1 |\mathbf{u}_1 - \mathbf{u}_k|}{d_k}\right) \end{cases} \tag{2.29}$$

where $C_d = \begin{cases} \frac{24}{\mathrm{Re}}\left(1 + 0.15(\mathrm{Re})^{0.687}\right) & \mathrm{Re} < 1000 \\ 0.44 & \mathrm{Re} \geq 1000 \end{cases}$, $\mathrm{Re} = \frac{\alpha_1 \rho_1 d_k |\mathbf{u}_1 - \mathbf{u}_k|}{\mu_1}$, and

$$\tau_k = \frac{\rho_k d_k^2}{18 \mu_1}$$

and Schiller and Neumann correlation (1933) for air bubbles:

$$f_{drag} = \begin{cases} 1 + 0.15\,\mathrm{Re}^{0.687} & \mathrm{Re} \leq 1000 \\ 0.0183\,\mathrm{Re} & \mathrm{Re} > 1000 \end{cases} \tag{2.30}$$

In this study, the bubbles are assumed to be rigid spheres having a constant diameter. The bubble diameter is set to 10^{-5} m after some tests, so that the TFM model gives almost the same air core as obtained by a Volume of Fluid (VOF) model as reported elsewhere (Brennan, 2006a; Kuang et al., 2012b). Note that the VOF model does not need to introduce the concept of bubble size (Hirt and Nichols, 1981).

The solid viscosity μ_k in Eq. (2.22) consists of collisional viscosity arising from particle momentum exchange due to transition and collision, and kinetic viscosity:

$$\mu_k = \mu_{k,col} + \mu_{k,kin} \tag{2.31}$$

$$\mu_{k,col} = \frac{4}{5}\alpha_k \rho_k d_k g_{0,kk}(1+e_{kk})(\frac{\Theta}{\pi})^{0.5}\alpha_k \tag{2.32}$$

$$\mu_{k,kin} = \frac{\alpha_k d_k \rho_k \sqrt{\pi\Theta}}{6(3-e_{kk})}[1+\frac{2}{5}(1+e_{kk})(3e_{kk}-1)\alpha_k g_{0,kk}] \tag{2.33}$$

$$g_{0,kl} = \frac{1}{(1-\sum_{k=2}^{n}\alpha_k)} + \frac{3(\sum_{k=1}^{N}\frac{\alpha_k}{d_k})}{(1-\sum_{k=2}^{n}\alpha_k)^2(d_l+d_k)}d_l d_k \tag{2.34}$$

where e_{kk} is the coefficient of restitution set to 0.9 in the present study. Θ is the solid granular temperature, given by the solution of the algebraic model of temperature model (Syamlal et al., 1993).

$$0 = -(p_k \bar{\bar{\mathbf{I}}} + \overline{\overline{\boldsymbol{\tau}}}_k):\nabla\mathbf{u}_k - \gamma\Theta + \phi_{l,k} \tag{2.35}$$

where $-(p_k \bar{\bar{\mathbf{I}}} + \overline{\overline{\boldsymbol{\tau}}}_s):\nabla\mathbf{u}_k$ is the generation of energy by the solid stress tensor. $\gamma\Theta$ is the collisional dissipation of energy. $\phi_{l,k}$ is the energy exchange between the lth fluid or solid phase and the kth solid phase.

The solid pressure in Equation (2.22) and (2.31) is given by:

$$p_k = 2\rho_k(1+e_{kk})\alpha_k^2 g_{0,kk}\Theta_k \tag{2.36}$$

$$p_{s,total} = \sum_{k=3}^{n} p_k \tag{2.37}$$

2.7.4 **Model validation**

For the purpose of model validation, two typical experiments in literature are simulated, considering classification of limestone and coal, respectively.

The first experiment was carried out by Hsieh (1988a), which has been widely used in literature to verify the validity of different CFD models for hydrocyclones. The geometry and mesh representation of hydrocyclone are shown in Fig. 2.19 and geometrical parameters in Table 2.1.

The whole computational domain was meshed with hexahedral grids. In the vicinity of the walls and vortex finder, the grid was more detailed than the remainder of the cyclone. Trial numerical results demonstrated that the solution was independent of the mesh size used. This strategy of grid generation applies to all the simulations considered in this work.

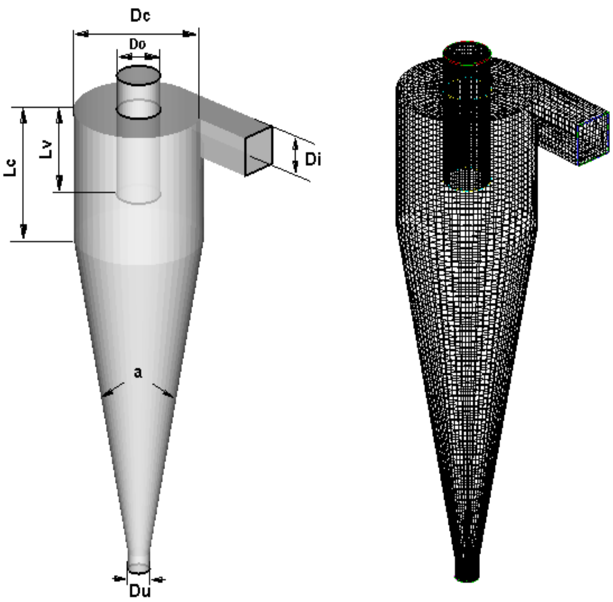

(a) (b)

Fig. 2.19 Geometry (a) and mesh (b) representation of the hydrocyclone for classification of limestone.

Table 2-1 Geometry parameters of the hydrocyclone for the classification of limestone.

Parameter	Symbol	Dimension
Diameter of the body	D_c	75mm
Diameter of inlet	D_i	25mm (same area quadrate is used)
Diameter of vortex finder	D_o	25mm
Diameter of apex	D_u	12.5mm
Length of cylindrical part	L_c	75mm
Length of vortex finder	L_v	50mm
Included angle	a	20°

Table 2-2 Operational conditions for the classification of limestone

Parameter	Symbol	Values
Inlet velocity	u	2.28 m/s (CASE I); 2.5 m/s (CASE II)
Particle material		Limestone
Particle density	ρ_p	2700 kg/m^3
Feed solid percentage	ρ_{feed}	No solid feed (CASE I); 4.14% by volume (CASE II)
Particle sizes simulated	d	35.5 25.1 17.74 12.55 8.87 6.27 4.43 3.13 1.41 mm

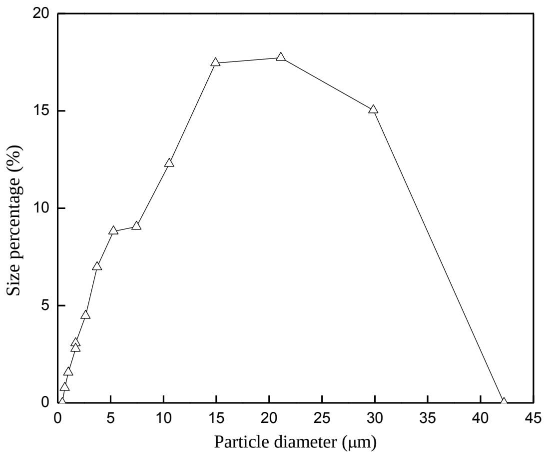

Fig. 2.20 Size distribution for the classification of limestone in Hsieh’s experiment (1988a)

Table 2.2 shows the simulated operational conditions, considering two different setups according to the data available in the Hsieh’s experiment (1988a): without solid feed (CASE I) and with a feed solid percentage 4.14% by volume (CASE II). CASE I is used to validate the prediction of water flow, while CASE II is used to validate the prediction of particle flow. The inlet water velocity is 2.28 m/s in CASE I, and the inlet water velocity and the limestone particle velocity in CASE II were both 2.5 m/s. Pressure at the two outlets (vortex finder and spigot) were 1 atm (101.325 kPa). The size distribution considered in the experiments (Hsieh, 1988) is given in Fig. 2.20, represented by nine average sizes in simulation (CASE II), as listed in Table 2.2.

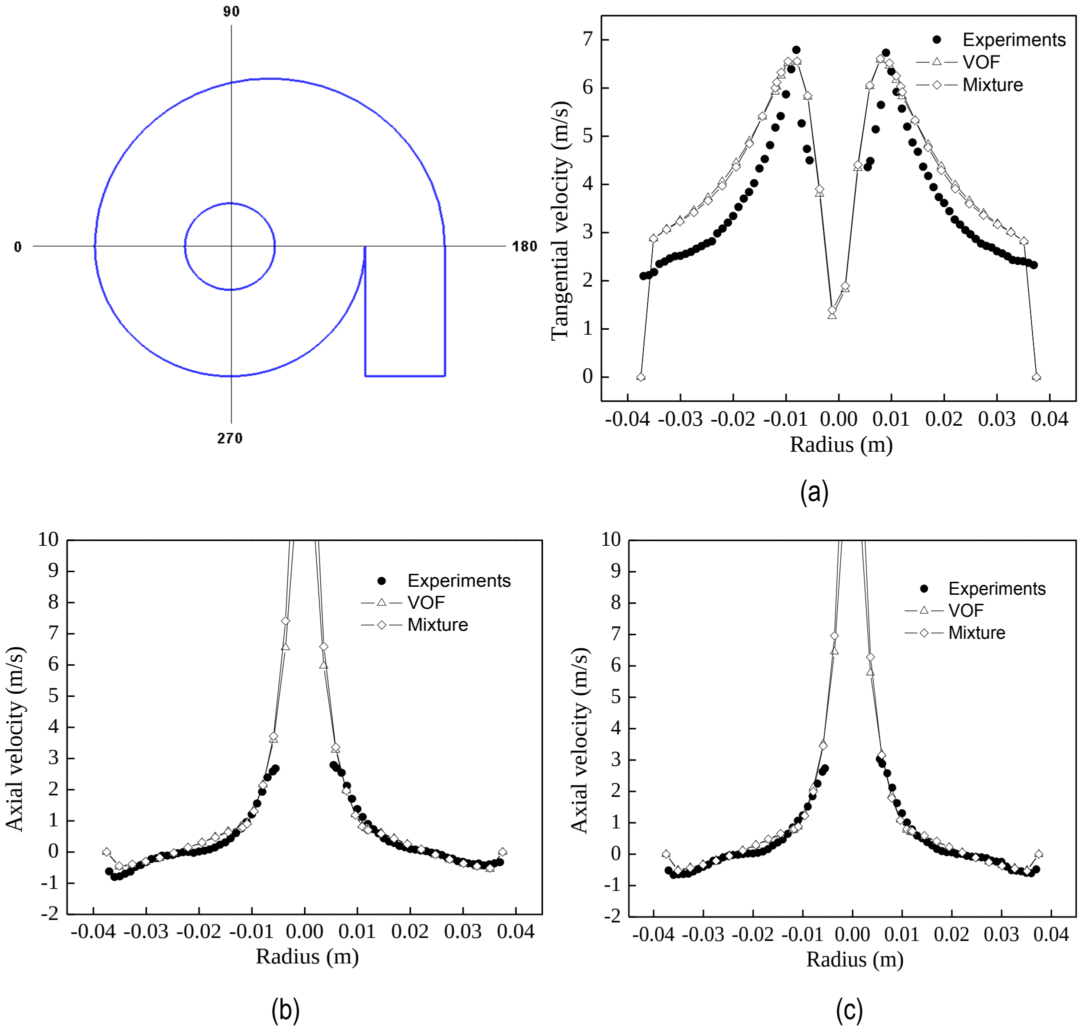

Fig. 2.21 Comparison between the measured (Hsieh, 1988a)and predicted (a) tangential and (b) axial velocities on 0° and 180° planes, and (c) axial velocities on 0° and 180° in the hydrocyclone operating without solid feed. All the planes are located 60 mm away from the top wall of the hydrocyclone.

Fig. 2.21 compares the experimental and predicted velocity profiles on the different planes located at 60mm away from the top of the hydrocyclone. Here, the interface between air and water is simulated by both volumes of fluid (VOF) and mixture models. The major difference of two models lies in that (a) the phases is interpenetrating for the mixture model, but not for the Volume of fluid model, and (b) the velocities of phases may be different in the mixture model, but not for the VOF model. Although different in principle, the hydrocyclone CFD based on the two models give almost the same results, as shown in Fig. 2.20. It can also be seen from the figure that the simulated results are in good agreement with the experimental ones, particularly for the axial velocities. The tangential velocity distribution is a Rankine vortex with a quasi-free vortex in the outer and a quasi-forced vortex in the inner part (Panton, 1996).

Table 2-3 Comparison between the measured and predicted inlet pressure and amount of water split in the hydrocyclone operating without solid feed.

	Inlet pressure drop (kPa)	Amount of water split to underflow (%)
Experiments (Hsieh, 1988a)	46.7	4.9
VOF model	48.0	4.8
Mixture model	48.2	4.7

The comparison between the experimental and numerical results has also been made for other variables in the hydrocyclone without solid feed, as given in Table 2.3. It can be seen that the Volume of fluid (VOF) and mixture models again predict the close inlet pressure drop and amount water split to under flow. Good qualitative agreement between measured and predicted results can also be observed for the two variables.

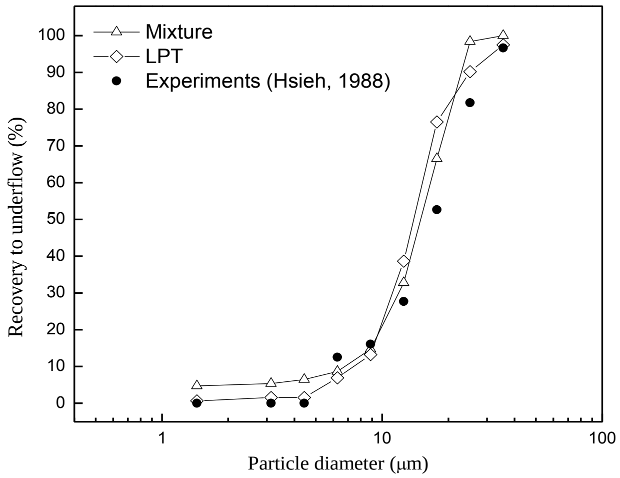

Fig. 2.22 Separation efficiency curve for the classification of limestone at feed solid percentage 4.11% (by volume).

Fig. 2.22 shows the separation efficiency curve calculated by the mixture model for the hydrocyclone operating at feed solid percentage of 4.11% (by volume). For comparison, Lagrangian particle tracking (LPT) method is here used to predict the separation efficiency. As seen for the figure that the numerical results from the mixture model and Lagrangian particle tracking (LPT) are both comparable to the experimental data obtained by Hsieh (1988a). This is expected as the two models are both valid under the considered condition.

Table 2-4 Comparison between the measured and predicted inlet pressure and amount of water for the classification of limestone at feed solid percentage 4.11% (by volume)

	Cut size d_{50} (μm)	Inlet pressure drop (Kpa)	Amount of water split to underflow (%)
Measured(Hsieh, 1988a)	16.8	69.3	4.3
Predicted(by LPT)	14.0	58.5	3.7
Predicted(by Mixture model)	15.1	57.2	4.0

Table 2-4 shows the comparison between measured and numerical results for variables including inlet pressure drop, and cut size d_{50} (the particle size at which the hydrocyclone efficiency is 50%)in the hydrocyclone operating at feed solid percentage of 4.11% (by volume). the results from the mixture model and Lagrangian particle tracking (LPT) are again comparable to the experimental measurements. Overall, the mixture model predicts cut size and water split closer to the experimental values compared to the Lagrangian particle tracking (LPT) model. The later give larger inlet pressure drop, which of value is slightly closer to the experimental value.

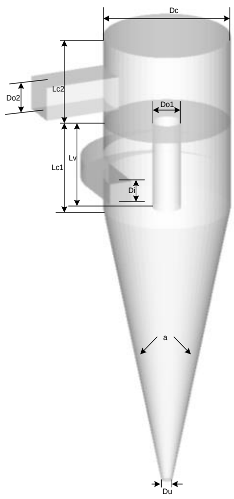

Fig. 2.23 Geometry of the hydrocyclone for the classification of coal

Besides the above results, the experimental result of Slechta and Firth (1984) who studied the classification of coal in 225 m Linatex hydrocyclone is also used in this work for our model validation. In this case, feed solid percentage is larger, which help examine the difference between Lagrangian particle tracking (LPT) and mixture model.

The geometry of the hydrocyclone is shown in Fig. 2.23 and geometrical parameters in Table 2-5.

Table 2-5 Geometry parameters of the hydrocyclone for the classification of coal

Diameter of the body	D_c	225mm
Diameter of inlet	D_i	47mm (same area quadrate is used)
Diameter of vortex finder	D_{o1}	50 mm
Diameter of outlet at the cap	D_{o2}	76 (same area quadrate is used)
Diameter of apex	D_u	19 mm
Length of cylindrical part	L_{c1}	176 mm
Length of cap	L_{c1}	176 mm
Length of vortex finder	L_v	176 mm
Included angle	a	20.8°

Table 2-6 shows the simulated operational conditions. According to the experimental result of Slechta and Firth (1984), all the particles with size larger 0.045 reports to underflow. In simulations, these sizes are treated as one size, and seven computational sizes (Table 2-6) are used to represent the size distribution in the experiment (Fig. 2.24). In addition, Slechta and Firth (1984) did not given the density distribution, and pointed out that under their considered conditions, the effect of relative density on the reduced partition curve is not significant. Thus, the density distribution is represented by mean density 1400 kg/m^{3}in the present simulations.

Table 2-6 Operational conditions for the classification of coal

Parameter	Symbol	Values
Inlet velocity	u	6.7 m/s
Particle material		coal
Mean particle density	ρ_p	1400 kg/m^3
Feed solid percentage	ρ_{feed}	9.5% (by volume)
Particle sizes simulated	d	0.355 0.25 0.18 0.125 0.09 0.063 0.045 mm

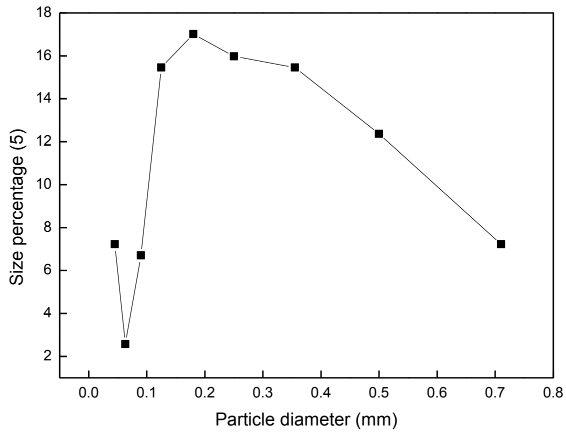

Fig. 2.24 Size distribution for the classification of coal in Slechta and Firth's experiments(1984)

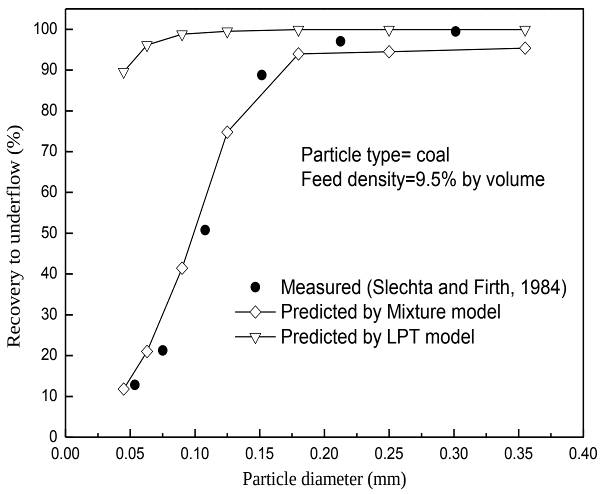

Fig. 2.25 Separation efficiency curve for the classification of coal

Fig. 2.25 shows the predicted and measured separation efficiency curve. It can be seen from the figure that the results given by the mixture model agree well with the experimental measurement. As expected, the prediction of separation efficiency by Lagrangian particle tracking (LPT) has a big deviation from that the experimental values due to the relative high feed solid percentage (9.5%) considered in this case. This highlights the importance for the development of the mixture model for hydrocyclones in coal preparation.

In summary, the mixture model discussed above can satisfactorily predict hydrocyclone flow and performance under different feed solid concentrations, but not for the widely used Lagrangian particle tracking (LPT) model. On this base, the developed model was used to examine the effects of feed solid concentrations and geometries in this thesis with extra consideration of extensive comparison between the calculated and measured results, and then modified to simultaneously study the effects density and size of particles. To date, the previous studies of hydrocyclones generally treated particle density as constant.

2.7.5 **Effect of Feed Solid Concentrations**

The feed solid concentration varying from 0 to 24.5% by volume were considered to examine how different feed solid concentrations affect hydrocyclone flow and performance, as given in Table 2-7. Here all other parameters are constant.

Table 2-7 Feed solid percentages simulated

Runs	1	2	3	4	5	6	7	8	9	10	11
Feed solid percentage (%)	0	1.04	2.07	4.14	7.07	9.94	12.8	15.7	18.7	21.6	24.5

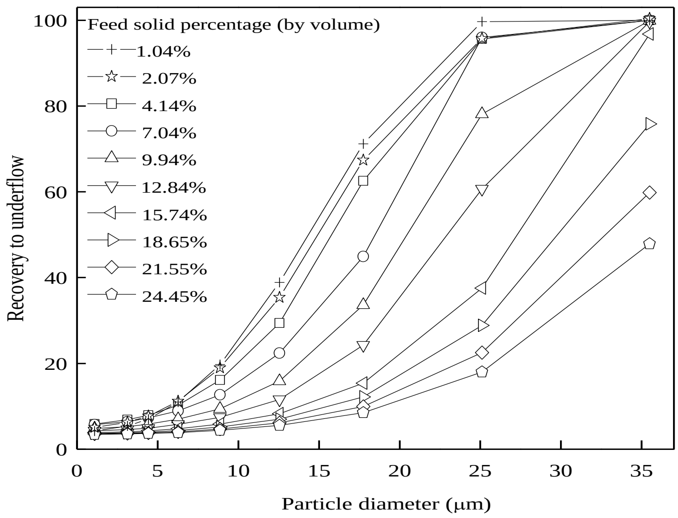

Fig. 2.26 Separation efficiency curve under different feed solid percentages at inlet velocity 2.5 m/s.

Fig. 2.26 shows the predicted separation efficiencies. It can be seen from the figure that the separation efficiency decreases with the increase of feed solid percentage. The trend is consistent with the experiment work of O'Brie*et al*. (2000) who examined the effects of two feed solids concentrations (10%and 20% by mass) on a plant scale. The figure also shows that the efficiency curves do not pass through the origin. This is in in line with the fact that the partition curve is the result of combination of two factors: a classification process and a by-pass effect; and the water reporting to the under flow entrains feed particles of all sizes which by-pass the classification process (Slechta and Firth, 1984). It should be pointed out Here that the LPT model can gives only one result for different feed solid percentages, and thus is invalid to study hydrocyclone flow and performance when solid percentage is not low, e.g. for solid percentage larger than 7.04% in the present conditions. More details of validation of the model can be found in the recent work of Kuang et al., (2012).

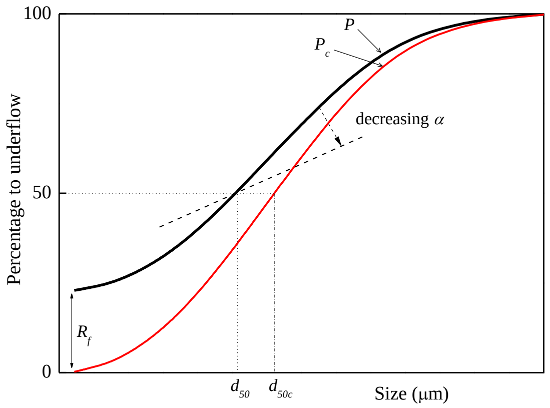

Fig. 2.27 Lynch model for describing separation efficiency

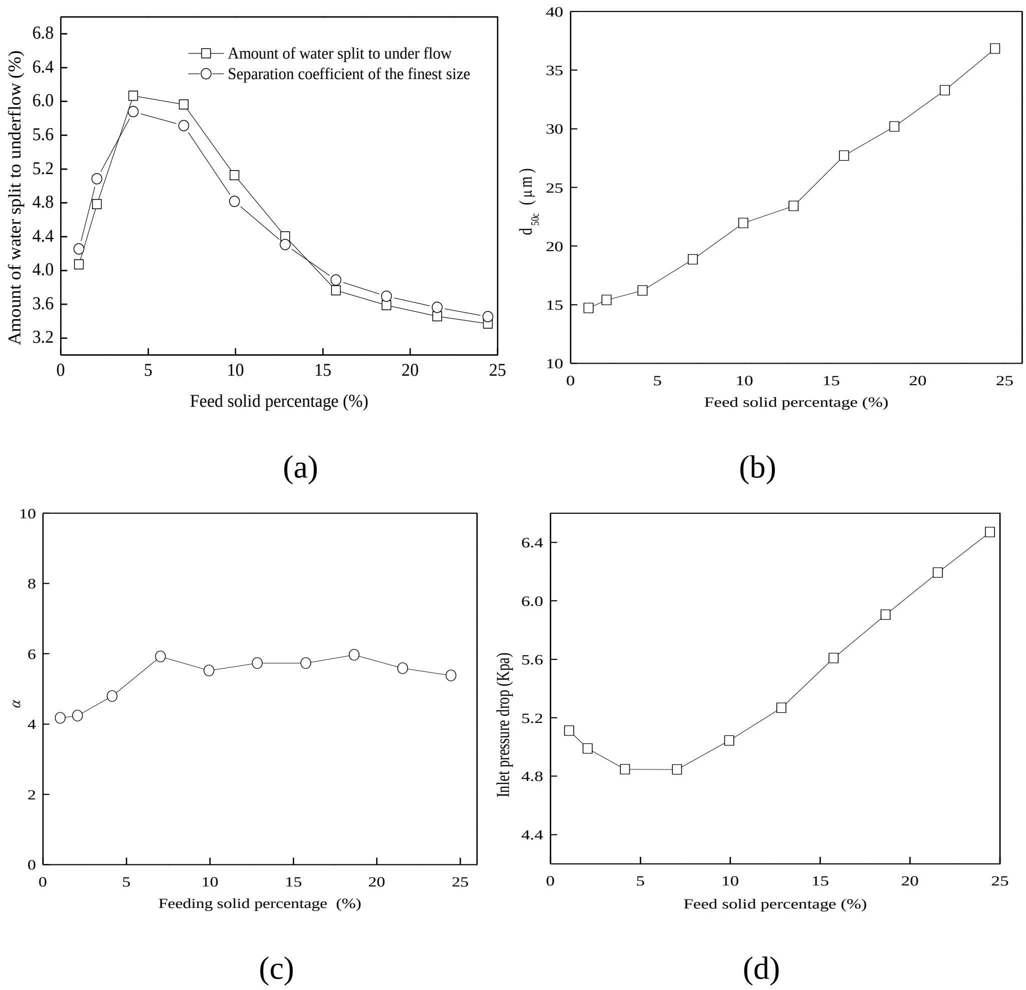

Fig. 2.28 Variations of (a) d50c, (b) inlet pressure drop and amount of water split to underflow with feed solids concentration

2.8 Objectives

The main objectives of this dissertation could be listed as below:

1- The Two fluid model (TFM) facilitated by Mixture model will be extended to describe hydrocyclone flows and performances under a wide range of flow conditions.

2- The applicability of the approach will be examined by comparing the numerical and experimental results under wide range of feed solids concentrations.

3- On this basis, a systematic study of the geometrical, operational and material variation effects on the flows and performances of hydrocyclones operated at wide range of feed solid concentrations will be carried out.

4- As the fourth objective of this study, hydrocyclones of different conical configurations will be studied under a wide range of feed solids concentrations with the aim of gaining a better understanding of the effects of conical part on the flow and performance of hydrocyclones, and identifying possible methods to improve the cyclone performance. On this base, a new hydrocyclone design will proposed.

5- The other impact of this research is controlling the flow within the pre-separation space of the cyclone by properly changing the dimension and shape of the vortex finder, with the aim of improving cyclone performance such as energy utilization and particle separation efficiency. This part of the study will be focused on the optimum dimension of the vortex finder with respect to length, diameter and shape.

6- The final contribution of this dissertation is to understand and investigate the effect of changing material properties of the coal based on density variation on the flow feature and performance of the large diameter industrial hydrocyclones. The overall aim is the evaluation of the size separation performance of a large diameter (1m) classifying cyclone under a number of different operating conditions which could be encountered in normal plant operation. The outcomes from this part of the project allow coal preparation engineers to evaluate the potential of incorporating large diameter cyclones into plant circuits, and assess the resulting processing and cost improvements

REFERENCES

Asomah, A. K., Napier-Munn, T. J., 1997. An empirical model of hydrocyclones incorporating angle of cyclone inclination. Minerals Engineering, 10 (3), 339-347.

Atkinson, B., Swanson, A., 2008, Improved efficiency of fine coal classification. ACARP report, C15059.

Azadi, M., Azadi, M., Mohebbi, A., 2010. A CFD study of the effect of cyclone size on its performance parameters. Journal of Hazardous Materials, 182 (1-3), 835-841.

B. Dabir, C. A. P., 1986. Measurement of mean velocity profiles in a hydrocyclone using laser Doppler anemometry. Chem Eng Commun, 48 (4–6), 377–388.

B.A.Wills, 1997. An Introduction to the Practical Aspects of Ore Treatment and Mineral Recovery. 6th ed, Butterworth-Heinemann, Oxford, (6th).

Bagnold, R. A., 1954. Experiments on a gravity-free dispersion of large solid spheres in a Newtonian fluid under shear. processing of the royal society, London, 225 49-63.

Baranov, D. A., Kutepov, A.M., and Lagutkin, M.G., 1996. Calculation of the Separation Process in Hydrocyclones. Teor Osn Khim Tekhnol, 30 (2), 117.

Barrientos, A., Sampaio, R., Concha, F., 1993. Effects of the air core on the performance of a hydrocyclone. In: Proc. of XVIII International. Mineral Processing Congress, 267–270.

Baskakov, A. P., Dolgov, V. N., Goldobin, Y. M., 1990. AERODYNAMICS AND HEAT-TRANSFER IN CYCLONES WITH PARTICLE-LADEN GAS-FLOW. Experimental Thermal and Fluid Science, 3 (6), 597-602.

Bennett, M. A., Williams, R. A., 2004. Monitoring the operation of an oil/water separator using impedance tomography. Minerals Engineering, 17 (5), 605-614.

Bergström, J., Vomhoff, H., Söderberg, D., 2007. Tangential velocity measurements in a conical hydrocyclone operated with a fibre suspension. Minerals Engineering, 20 (4), 407-413.

Bhaskar, K. U., Murthy, Y. R., Raju, M. R., Tiwari, S., Srivastava, J. K., Ramakrishnan, N., 2007a. CFD simulation and experimental validation studies on hydrocyclone. Minerals Engineering, 20 (1), 60-71.

Bhaskar, K. U., Murthy, Y. R., Ramakrishnan, N., Srivastava, J. K., Sarkar, S., Kumar, V., 2007b. CFD validation for flyash particle classification in hydrocyclones. Minerals Engineering, 20 (3), 290-302.

Bhattacharyya, F., 1984. The flow field inside a conventional hydrocyclone. In 2nd International Conference on Hydrocyclones, Bath, England.

Bloor, M. I. G., Ingham, D.B, 1973a. Theoretical investigation of the flow in a conical hydrocyclone. Transactions of the Institution of Chemical Engineers, 51 36-41.

Bloor, M. I. G., Ingham, D.B., 1975. Turbulent spin in a cyclone. Transactions of the Institution of Chemical Engineers 53 1 –46.

Boysan, F., Ayers, W. H., Swithenbank, J., 1982. A fundamental mathematical-modeling approach to cyclone design. Transactions of the Institution of Chemical Engineers, 60 (4), 222-230.

Bradley, D., 1965. The Hydrocyclone; Pergamon. London, 1965.

BRADLEY, D., PULLING, D. J., 1959. Flow patterns in the hydraulic cyclone and their interpretation in terms of performance. Chemical Engineering Research and Design 37 34 - 45.

Brennan, M., 2006a. CFD simulations of hydrocyclones with an air core - Comparison between large eddy simulations and a second moment closure. Chemical Engineering Research & Design, 84 (A6), 495-505.

Brennan, M., 2006b. CFD Simulations of Hydrocyclones with an Air Core: Comparison Between Large Eddy Simulations and a Second Moment Closure. Chemical Engineering Research and Design, 84 (6), 495-505.
Brennan, M. S., 2003. Multiphase CFD simulations of dense medium and classifying Cyclones. Third International Conference on CFD in the Minerals and Process Industries CSIRO, Melbourne, Australia, 10–12
Brennan, M. S., Narasimha, M., Holtham, P. N., 2007a. Multiphase modelling of hydrocyclones - prediction of cut-size. Minerals Engineering, 20 (4), 395-406.
Brennan, M. S., Narasimha, M., Holtham, P. N., 2007b. Multiphase modelling of hydrocyclones – prediction of cut-size. Minerals Engineering, 20 (4), 395-406.
Castilho, L. R., Medronho, R. A., 2000. A simple procedure for design and performance prediction of Bradley and Rietema hydrocyclones. Minerals Engineering, 13 (2), 183-191.
Castro, O., Concha, F., Montero, J., Miranda, J., Castro, J., Urizar, D.,, 1996. Air core modelling for an industrial hydrocyclone. In: Claxton,Svarovsky (Ed), Hydrocyclones '96 Thew, Mech Eng Publications Lim, London and Bury St Edmunds, UK,, 229–240.
Chang, Y. F., Ilea, C. G., Aasen, L., Hoffmann, A. C., 2011. Particle flow in a hydrocyclone investigated by positron emission particle tracking. Chemical Engineering Science, 66 (18), 4203-4211.
Chen, W., Zydek, N., Parma, F., 2000. Evaluation of hydrocyclone models for practical applications. Chemical Engineering Journal, 80 (1-3), 295-303.
Chiné, B., Concha, F., 2000. Flow patterns in conical and cylindrical hydrocyclones. Chemical Engineering Journal, 80 (1-3), 267-273.
Chu, K. W., Wang, B., Xu, D. L., Chen, Y. X., Yu, A. B., 2011. CFD-DEM simulation of the gas-solid flow in a cyclone separator. Chemical Engineering Science, 66 (5), 834-847.
Chu, K. W., Wang, B., Yu, A. B., Vince, A., 2009. CFD-DEM modelling of multiphase flow in dense medium cyclones. Powder Technology, 193 (3), 235-247.
Chu, K. W., Wang, B., Yu, A. B., Vince, A., 2012. Computational study of the multiphase flow in a dense medium cyclone: Effect of particle density. Chemical Engineering Science, 73 123-139.
Chu, K. W., Yu, A. B., 2008. Numerical simulation of complex particle–fluid flows. Powder Technology, 179 (3), 104-114.

Chu, L.-Y., Chen, W.-M., Lee, X.-Z., 2002. Effects of geometric and operating parameters and feed characters on the motion of solid particles in hydrocyclones. Separation and Purification Technology, 26 (2-3), 237-246.

Chu, L.-Y. C., W.-M., 1993. Research on the Motion of Solid Particles in a Hydrocyclone. Separation Science and Technology, 28 (10), 1875 - 1886.
Chu, L., Yu, W., Wang, G., Zhou, X., Chen, W., Dai, G., 2004. Enhancement of hydrocyclone separation performance by eliminating the air core. Chemical Engineering and Processing, 43 (12), 1441-1448.
Chu, L. Y., Chen, W. M., 1993. Research on the motion of solid particles in a hydrocyclone. Separation Science and Technology, 28 (10), 1875-1886.
Cilliers, J. J., Diaz-Anadon, L., Wee, F. S., 2004. Temperature, classification and dewatering in 10 mm hydrocyclones. Minerals Engineering, 17 (5), 591-597.
Cilliers, J. J., Hinde, A. L., 1991. An improved hydrocyclone model for backfill preparation. Minerals Engineering, 4 (7-11), 683-693.

Coelho, M. A. Z., Medronho, R. A., 2001. A model for performance prediction of hydrocyclones. Chemical Engineering Journal, 84 (1), 7-14.
Cortés, C., Gil, A., 2007. Modeling the gas and particle flow inside cyclone separators. Progress in Energy and Combustion Science, 33 (5), 409-452.
Cokljat, D., Slack, M., Vasquez, S. A., Bakker, A., Montante, G., 2006. Reynolds-Stress Model for Eulerian multiphase. Progress in Computational Fluid Dynamics, an International Journal, 6 (1), 168-178.
Concha, F., Barrientos, A., Montero, J., Sampaio, R., 1996. Air core and roping in hydrocyclones. International Journal of Mineral Processing, 44-45 743-749.
Concha, F., Castro,B.,Ovalle,E. & Romero,J., 1998. Numerical simulation of the flow pattern in a hydrocyclone. Innovation in Physical Separation Technology, 35-60.
Criner, H. E., 1950. The vortex thickener. In International conference on coal preparation, Paris.
Crowe, C. T., Troutt, T. R., Chung, J. N.,, 1996. Numerical models for two-phase turbulent flows. Annual Review of Fluid Mechanics, 28 11-43.
Cullivan, J. C., Williams, R. A., Cross, R., 2003. Understanding the Hydrocyclone Separator Through Computational Fluid Dynamics. Chemical Engineering Research and Design, 81 (4), 455-466.
Cullivan, J. C., Williams, R. A., Dyakowski, T., Cross, C. R., 2004. New understanding of a hydrocyclone flow field and separation mechanism from computational fluid dynamics. Minerals Engineering, 17 (5), 651-660.
Cullivan, J. C. W., R. A.; Cross, C. R., 2001. Verification of theoretical 3D-flow in a hydrocyclone using tomography. In Fourth World Congress for Particle Technology, Sydney, Australia, 2001.
Dai, G. Q., Chen, W. M., Li, J. M., Chu, L. Y., 1999. Experimental study of solid-liquid two-phase flow in a hydrocyclone. Chemical Engineering Journal, 74 (3), 211-216.
Davailles, A., Climent, E., Bourgeois, F., 2012a. Fundamental understanding of swirling flow pattern in hydrocyclones. Separation and Purification Technology, 92 (0), 152-160.
Davailles, A., Climent, E., Bourgeois, F., Majumder, A. K., 2012b. Analysis of swirling flow in hydrocyclones operating under dense regime. Minerals Engineering, 31 (0), 32-41.
Davidson, M. R., 1988. Numerical calculations of flow in a hydrocyclone operating without an air core. Applied Mathematical Modelling 12 (2), 119-128.
Davidson, M. R., 1995a. An adaptive method of predicting the air core diameter for numerical models of hydrocyclone flow. International Journal of Mineral Processing, 43 (3-4), 167-177.
Davidson, M. R., 1995b. An adaptive method of predicting the air core diameter for numerical models of hydrocyclone flow. International

Journal of Mineral Processing, 42 167–177.
De Souza, J. S., A 2004. Preliminary results of large eddy simulations of a hydrocyclone. Thermal Eng, 3 (168-173).
Debair, 1983. Mean Velocity Measurements in a 3 inches Hydrocyclone Using Laser Doppler Anemometry. PhD Thesis, Department of Chemical Engineering, Michigan State University, USA
Delgadillo, J. A. R., R.K 2009. Computational fluid dynamics prediction of the air-core in hydrocyclones International Journal of Computational Fluid Dynamics, 23 189-197.

Delgadillo, J. A. R., Raj K., 2005. A comparative study of three turbulence-closure models for the hydrocyclone problem. International Journal of Mineral Processing, 77 (4), 217-230.
Devulapalli, B., 1996. Hydrodynamic Modeling of Solid-liquid Flows in largeScale hydrocyclones. Ph.D. Thesis, University of Utah, Salt Lake City, UT. .
Ding, J. G., D. , 1990. Bubbling fluidization model using kinetic theory of granular flow. AIChE Journal, 36 523-538.
Doby, M. J., Nowakowski, A. F., Yiu, I., Dyakowski, T., 2008. Understanding air core formation in hydrocyclones by studying pressure distribution as a function of viscosity. International Journal of Mineral Processing, 86 (1–4), 18-25.
Driessen, M. G., 1951. Theory of flow in a cyclone. Review of Industrial Mining 1951, Special Issue, 449-461.
Dyakowski, T., Williams, R. A., 1996. Prediction of high solids concentration regions within a hydrocyclone. Powder Technology, 87 (1), 43-47.
Dyakowski, T., Williams, R. A., 1993. Modelling turbulent flow within a small-diameter hydrocyclone. Chemical Engineering Science, 48 (6), 1143-1152.
Dyakowski, T., Williams, R. A., 1996. Prediction of high solids concentration regions within a hydrocyclone. Powder Technology, 87 (1), 43-47.
Dyakowski, T., Williams, R.A., 1995. Prediction of air-core size and shape in a hydrocyclone. International Journal of Mineral Processing 43 1–14.
Dyakowski, T. W., R.A., 1992. Modeling turbulent flow within a small-diameter hydrocyclone. Chemical Engineering Science, 47 1-10.
Elsayed, K., Lacor, C., 2011. The effect of cyclone inlet dimensions on the flow pattern and performance. Applied Mathematical Modelling, 35 (4), 1952-1968.
Ergun, S., 1952. Fluid flow through packed columns. Chemical Engineering Progress, 48 (2), 89-94.
Evans, W. K., Suksangpanomrung, A., Nowakowski, A. F., 2008. The simulation of the flow within a hydrocyclone operating with an air core and with an inserted metal rod. Chemical Engineering Journal, 143 (1-3), 51-61.
Fahlstroem, P. H., 1960. Studies of a hydrocyclone as a classifier. In Proceedings International Mineral Processing Congress, Institute of Mining and Metallurgy.
Firth, B., O'Brien, M., Edward, D., Clarkson, C., 1999, Fine coal classification. ACARP report, C3084.
Fisher, M. J., Flack, R. D., 2002. Velocity distributions in a hydrocyclone separator. Experiments in Fluids, 32 (3), 302-312.
Flintoff, B. C., Plitt, L. R., Turak, A. A., 1987. Cyclone Modeling - A Review Of Present Technology. Cim Bulletin, 80 (905), 39-50.
Fraser, S. M., Abdel Razck,A.M & Abdullah,M.Z 1997. Computational and experimental investigations in a cyclone dust separator 257. Proceedings of the Institution of Mechanical Engineers, Part E: Journal of Process Mechanical Engineering, 211 247-257.
Ghodrat, M., Kuang, S. B., Yu, A. B., Vince, A., Barnett, G. D., Barnett, P. J., 2013. Computational Study of the Multiphase Flow and Performance of Hydrocyclones: Effects of Cyclone Size and Spigot Diameter. Industrial & Engineering Chemistry Research, 52 (45), 16019-16031.
Gidaspow, D., Bezburuah,R.,Ding J., 1992. Hydrodynamics of Circulating Fluidized Beds, Kinetic Theory Approach. In Fluidization VII, Proceedings of the 7th Engineering Foundation Conference on Fluidization, 75-82.

Gu, F. L., W., , 1987. Measurement and study of velocity field in various cyclones by use of laser Doppler anemometry. In 3rd International Conference on Hydrocyclones, Oxford, England.
Gupta, R., Kaulaskar, M. D., Kumar, V., Sripriya, R., Meikap, B. C., Chakraborty, S., 2008. Studies on the understanding mechanism of air core and vortex formation in a hydrocyclone. Chemical Engineering Journal, 144 (2), 153-166.
H. Schubert, T. H. N., 1980. A hydrocyclone separation model in consider-ation of the turbulent multi-phase flow. Proceedings of International Conference on Hydrocyclones BHRA, Fluid Eng, 23–36.
Hararah, M. A., Endres, E., Dueck, J., Minkov, L., Neesse, T., 2010. Flow conditions in the air core of the hydrocyclone. Minerals Engineering, 23 (4), 295-300.
He, P., Salcudean, M., Gartshore, I. S., 1999. A Numerical Simulation of Hydrocyclones. Chemical Engineering Research and Design, 77 (5), 429-441.
Hirt, C. W., Nichols, B. D., 1981. Volume of fluid (VOF) method for the dynamics of free boundaries. Journal of Computational Physics, 39 (1), 201-225.
Hirt , C. W. N., B.D 1981. Volume of fluid (VOF) method for the dynamics of free boundaries. Journal of Computational Physics, 39 201-225.
Hou, R., Hunt, A., Williams, R. A., 2002. Acoustic monitoring of hydrocyclones. . Powder Technology, 124 (3), 176-187.
Hsieh, K. T., 1988a. Phenomenological Model of the Hydrocyclone. PhD thesis, The University of Utah, Salt Lake City, UT, USA.
Hsieh, K. T., Rajamani, R. K., 1991. Mathematical model of the hydrocyclone based on physics of fluid flow. AIChE J, 37 (5), 735-746.
Hsieh, K. T., Rajamani, K., 1988b. Phenomenological model of the hydrocyclone: Model development and verification for single-phase flow. International Journal of Mineral Processing, 22 (1-4), 223-237.
Hsieh, K. T. R., R. K., 1991. Mathematical model of the hydrocyclone based on physics of fluid flow. Aiche Journal, 37 (5), 735-746.
Huang, S., 2005a. Numerical Simulation of Oil-water Hydrocyclone Using Reynolds-Stress Model for Eulerian Multiphase Flows The Canadian Journal of Chemical Engineering, 83 829-834.
Huang, S., 2005b. Numerical simulation of oil-water hydrocyclone using reynolds-stress model for Eulerian multiphase flows. Canadian Journal of Chemical Engineering, 83 (5), 829-834.
Hwang, C. C. S., H. Q.; Zhu, G.; Khonsari, M. M., 1993. On the main flow pattern in hydrocyclones. Journal of Fluids Engineering 115 (1), 21-25.
Inaki Schlaberg, H., Podd, F. J. W., Hoyle, B. S., 2000. Ultrasound process tomography system for hydrocyclones. Ultrosonics, 38 813-816.
Ishii, M. M., K., , **1984**. Two-fluid model and hydrodynamic constitutive relations. *Nuclear Engineering and Design* 82 (2-3), 107-126.
Ivanov, A. A., Ruzanov, S.R., and Lunyushkina, I.A., , 1987. Fluid Dynamics and Separation in a Hydrocyclone. Zh Prikl Khim (Leningrad), 60 (5), 1047.
Kawatra, S. K., Bakshi, A. K., Rusesky, M. T., 1996a. The effect of slurry viscosity on hydrocyclone classification. International Journal of Mineral Processing, 48 (1-2), 39-50.
Kawatra, S. K., Bakshi, A. K., Rusesky, M. T., 1996b. Effect of viscosity on the cut (d50) size of hydrocyclone classifiers. Minerals Engineering, 9 (8), 881-891.
Kelsall, D. F., 1952a. A study of the motion of solid particles in a hydraulic cyclone. Chemical Engineering Research and Design 30 87–108.

Kelsall, D. F., 1952b. A study of themotion of solid particles in a hydraulic cyclone. Trans Inst Chem Eng, 30 (30), 87–108.
Kelsall, D. F., 1953. A further study of the hydraulic cyclone. Chemical Engineering Science 2 (6), 254-272.
Kelsall, D. F., 1963. Some applications of hydraulic cyclones in hydrometallurgical processes. Transactions of the American Institute of Mining, Metallurgical and Petroleum Engineers, 226 225-231.
Knowles, S. R., Woods, D. R., Feuerstein, I. A., 1973. The velocity distribution within a hydrocyclone operating without an air core. The Canadian Journal of Chemical Engineering, 51 (3), 263-271.
Kuang, S. B., Chu, K. W., Yu, A. B., Vince, A., 2012a. Numerical study of liquid-gas-solid flow in classifying hydrocyclones: effect of feed solids concentration. Minerals Engineering, 31 17-31.
Kuang, S. B., Chu, K. W., Yu, A. B., Vince, A., 2012b. Numerical study of liquid–gas–solid flow in classifying hydrocyclones: Effect of feed solids concentration. Minerals Engineering, 31 (0), 17-31.
Launder, B. E., Reece,G.J.&Rodi,W, 1975. Progress in the development of Reynolds-Stress turbulence closure. Journal of Fluid Mechanics, 68 537-566.
Li, S. H., Zhang, H., Yang, H. R., Yang, S., Lu, J. F., Yue, G. X., 2007. Determining cyclone particle holdup by pressure drop for a CFB boiler. Chemical Engineering & Technology, 30 (12), 1726-1731.
Lilge, E. O., 1962. Hydrocyclone fundamentals. Transactions of the Institution of Mining and Metallurgy, 71 285–337.
Lim, E. W. C., Chen, Y.-R., Wang, C.-H., Wu, R.-M., 2010. Experimental and computational studies of multiphase hydrodynamics in a hydrocyclone separator system. Chemical Engineering Science, 65 (24), 6415-6424.
Luo, Q. D., C. L.; Xu, J. R.; Yu, L. X.; Xiong, G. A., 1989. Comparison of the performance of water-sealed and commercial hydrocyclones. . International Journal of Mineral Processing 25 297–310.
Lynch, A. J., 1976. Mineral crushing and grinding circuits. Elsevier, Amsterdam.
Lynch, A. J., 1977. Mineral crushing and grinding circuits, their simulation, optimisation, design and control. Elsevier, Amsterdam.
Lynch, A. J., Rao, T. C., 1968. Studies on the operating characteristics of hydrocyclone classifiers. Indian Journal of Technology 6106–114.
Ma, L., Ingham, D. B., Wen, X., 2000. Numerical modelling of the fluid and particle penetration through small sampling cyclones Journal of Aerosol Science, 31 (9), 1097-1119.
Malhotra, A., Branion, R. M. R., Hauptmann, E. G., 1994. Modelling the flow in a hydrocyclone. The Canadian Journal of Chemical Engineering, 72 (6), 953-960.
Manninen, M., Taivassalo, V., Kallio, S., 1996a. On the mixture model for multiphase flow. 288 p.
Manninen, M., Taivassalo, V., Kallio, S., 1996b. On the mixture model for multiphase flow. VTT Publications 288, Technical Research Centre of Finland.
Marins, L. P. M., Duarte, D. G., Loureiro, J. B. R., Moraes, C. A. C., Freire, A. P. S., 2010. LDA and PIV characterization of the flow in a hydrocyclone without an air-core. Journal of Petroleum Science and Engineering, 70 (3-4), 168-176.
Monredon, T. C., Hsieh, K. T.,Rajamani, R. K., 1992. Fluid flow model of the hydrocyclone: an investigation of device dimensions. International Journal of Mineral Processing, 35 (1-2), 65-83.

Mousavian, S. M., Najafi, A. F., 2009a. Influence of geometry on separation efficiency in a hydrocyclone. Archive of Applied Mechanics, 79 (11), 1033-1050.
Mousavian, S. M., Najafi, A. F., 2009b. Numerical simulations of gas-liquid-solid flows in a hydrocyclone separator. Archive of Applied Mechanics, 79 (5), 395-409.
Nageswararao, K., 1999. Normalisation of the efficiency curves of hydrocyclone classifiers. Minerals Engineering, 12 (1), 107-118.
Nageswararao, K., 2000. A critical analysis of the fish hook effect in hydrocyclone classifiers. Chemical Engineering Journal, 80 (1-3), 251-256.
Nageswararao, K., Wiseman, D. M., Napier-Munn, T. J., 2004. Two empirical hydrocyclone models revisited. Minerals Engineering, 17 (5), 671-687.
Narasimha, M., 2005. CFD modelling of hydrocyclone prediction of cut size. International Journal of Mineral Processing, 75 (1-2), 53-68.
Narasimha, M., Brennan, M., Holtham, P. N., 2007a. A review of CFD modelling for performance predicitons of hydrocyclone. Engineering Applications of Computational Fluid Mechanics, 1 (2), 109-125.
Narasimha, M., Brennan, M. S., Holtham, P. N., 2006. Numerical simulation of magnetite segregation in a dense medium cyclone. Minerals Engineering, 19 (10), 1034-1047.
Narasimha, M., Brennan, M. S., Holtham, P. N., 2012. CFD modeling of hydrocyclones: Prediction of particle size segregation. Minerals Engineering, 39 (0), 173-183.
Narasimha, M., Brennan, M. S., Holtham, P. N., Napier-Munn, T. J., 2007b. A comprehensive CFD model of dense medium cyclone performance. Minerals Engineering, 20 (4), 414-426.
Narasimha, M., Brennan,M.S.,Holtham,P.N. & Napier-Munn,T.J, 2007c. A comprehensive CFD model of dense medium cyclone performance Minerals Engineering, 20 414-426.
Nauman, E. B., 2008. Residence Time Theory. Industrial & Engineering Chemistry Research, 47 (10), 3752-3766.
Neesse, T., Dueck, J., 2007. Air core formation in the hydrocyclone. Minerals Engineering, 20 (4), 349-354.
Neesse, T., Schneider, M., Dueck, J., Golyk, V., Buntenbach, S., Tiefel, H., 2004. Hydrocyclone operation at the transition point rope/spray discharge. Minerals Engineering, 17 (5), 733-737.
Neesse, T. S., H., 1991. Praktische und theoretische aspekte der dichtstromklassierung. Aufbereitungstechnik 32 (9), 459–472.
Neesse, T. S., M.; Golyk, V.; Tiefel, H., 2004. Measuring the operating state of the hydrocyclone. Minerals Engineering 17 (5), 697-703.
Noroozi, S., Hashemabadi, S. H., 2009. CFD simulation of inlet design effect on deoiling hydrocyclone separation efficiency. Chemical Engineering and Technology, 32 (12), 1885-1893.
Nowakowski, A. F., Cullivan, J. C., Williams, R. A., Dyakowski, T., 2004. Application of CFD to modelling of the flow in hydrocyclones. Is this a realizable option or still a research challenge? Minerals Engineering, 17 (5), 661-669.
Nowakowski, A. F., Kraipech, W., Williams, R. A., Dyakowski, T., 2000. The hydrodynamics of a hydrocyclone based on a three-dimensional multi-continuum model. Chemical Engineering Journal, 80 (1-3), 275-282.

Nowakowski, A. F. C., J. C.; Williams, R. A.; Dyakowski, T., 2004. Application of CFD to modelling of the flow in hydrocyclones. Is this a realizable option or still a research challenge? . Minerals Engineering, 17 (5), 661-669.
Nunan, K. C., Keller, J. B., 1984. Effective elasticity tensor of a periodic composite. Journal of the Mechanics and Physics of Solids, 32 (4), 259-280.
O'Brien, M., Taylor, A., Nemeth, D., Firth, B., Clarkson, C., 2000, Large diameter classifying cyclones. ACARP report, C6047.
Ohashi, H. M., S.,, 1958. Motion of water in a hydraulic cyclone. . Chemical Engineering Japan, 22 200-207.
Ovalle, E., Concha, F., 2005. The role of wave propagation in hydrocyclone operations II: Wave propagation in the air–water interface of a conical hydrocyclone. Chemical Engineering Journal, 111 (2–3), 213-223.
Panton, R. L., 1996. Incompressible flow (second ed.). John Wiley & Sons, New York.
Pericleous, K. A., 1987. Mathematical simulation of hydrocyclones. Applied Mathematical Modelling, 11 242-255.
Pericleous, K. A., Rhodes, N., 1986. The hydrocyclone classifier — A numerical approach. International Journal of Mineral Processing, 17 (1-2), 23-43.
Petersen, K. R. P., Aldrich, C., Van Deventer, J. S. J., McInnes, C., Stange, W. W., 1996. Hydrocyclone underflow monitoring using image processing methods. Minerals Engineering, 9 (3), 301-315.
Petty, C. P., S.M, 2001. Flow predictions within hydrocyclones. Filtration and Separation, 38 28-34.
Piomelli, U., Scotti,A & Balaras,E 2001. Large Eddy Simulations of Turbulent Flows, from Desktop to Supercomputer. JMLM Palma et al (Eds) 551-577.
Plitt, L. R., 1976a. A mathematical model of the hydrocyclone classifier. Cim Bulletin, 69 (776), 114-123.
Plitt, R., 1976b. A Mathematical Model of the Hydrocyclone Classifier. CIM Bull,, 69 114-123.
Podd, F. J. W., 2000. Model based parameterisation of a hydrocyclone air core.
Povarov, A. I., Gidrotsyklony. Gosgortechizdat, Moskva., Puget, F.P., Melo, M.V., Massarani, G., 1961. Comparative study of flotation techniques for the treatment of liquid effluents. Environmental Technology 25 (1), 79–87.
Prandtl, L., 1925. Uber die ausgebildete Turbulenze. ZAMM, 5. .
Rajamani, R. K. M., L., 1992. Fluid-flow model of the hydrocyclone for concentrated slurry classification. Hydrocyclone, Analysis and Application, Kulwer: London, p 95–101.
Renner, V. G. C., H. E., 1978. Measurement and interpretation of size distribution of particles within a hydrocyclone. Transactions of the Institution of Mining and Metallurgy, 87 c139–c145.
Rietema, 1961. Performance and design of hydrocyclones-General considerations. Chemical Engineering Science, 15 (3-4), 298-302.
Romero, J., Sampaio, R., 1999. A numerical model for prediction of the air-core shape of hydrocyclone flow. Mechanics Research Communications, 26 (3), 379-384.
Rong, R., 2007, Industial trials of novel cyclones. ACARP report, C14067.
Saffman, P. G., 1965. The lift on a small sphere in a slow shear flow. Journal of fluid Mechanics, 22 385-400.
Schiller, L., Naumann, Z., 1933. A drag coefficienty correlation. Z Ver Deutsch Ing, 77 318-320.
Schiller, L. N., A, 1935. A drag coefficient correlation. Z Ver Dtsch Ing, 77 318-320

Schuetz, S., Chuetz,S.,Mayer,G.,Bierdel,M.& Piesche,M 2004. Investigations on the flow and separation behaviour of hydrocyclones using computational fluid dynamics International Journal of Mineral Processing, 73 229-237.
Sevilla.E.M & Branion, R. M. R., 1997. The fluid dynamics of hydrocyclones Journal of Pulp and Paper Science 23.
Slack, M. D., Prasad, R. O.,Bakker, A.,Boysan, F., 2000. Advances in Cyclone Modelling Using Unstructured Grids. Chemical Engineering Research and Design, 78 (8), 1098-1104.
Slechta, J., Firth, B. A., 1984. Classification of fine coal with a hydrocyclone. International Journal of Mineral Processing, 12 (4), 213-237.
Smagorinsky, J., 1963. General circulation experiments with the primitive equations. Monthly Weather Review, 91 99-164.
Speziale, C. G., Sarkar,S.& Gatski,T.B, 1991. Modelling the pressure-strain correlation of turbulence. An invariant dynamical systems approach. Journal of Fluid Mechanics, 227 245-272.
Sripriya, R., Kaulaskar, M., Chakraborty, S., Meikap, B., 2007. Studies on the performance of a hydrocyclone and modeling for flow characterization in presence and absence of air core☆. Chemical Engineering Science, 62 (22), 6391-6402.
Steffens, P. R., Whiten, W. J., Appleby, S., Hitchins, J., 1993. Prediction of air core diameters for hydrocyclones. International Journal of Mineral Processing, 39 (1-2), 61-74.
Suasnabar, D., J., 2000. Dense medium cyclone performance, enhancements via computational modeling of the physical process. Ph.D. Thesis, University of New South Wales, Sydney. .
Subramanian, V. S., 2002. Measuring medium segregation in the dense medium cyclone using gamma ray tomography. PhD thesis, The University of Queensland.
Svarovsky, L., 1984. Hydrocyclones. Holt, Rinehart and Winston, Sydney.
Swain, S., Mohanty, S., 2013. A 3-dimensional Eulerian–Eulerian CFD simulation of a hydrocyclone. Applied Mathematical Modelling, 37 (5), 2921-2932.
Syamlal, M., Rogers, W., O'Brien, T. J., 1993. MFIX documentation: theory guide. National Technical Information Service, Springfield, VA, DOE/METC-9411004, NTIS/DE9400087.
T. Neesse, M. S., V. Golyk, H. Tiefel, 2004. Measuring the operating state of the hydrocyclone Miner Eng 17 (5), 697–703.
T. Ohtake, M. U., T. Kadoya, 1987. A fundamental study of hydrocyclones.Part 1. Flow pattern in the hydrocyclone. Jpn Tappi J 41 (2), 60.
Tarjan, G., 1961. Some theoretical questions on classifying and separating hydrocyclones. Acta Technica (Hungary), 32 357-388.
Ternovsky, I. G., Kutepov, A.M., 1994. Gidrotsiklonirovanie. Nauka, Moskva.J.C.Wood, 1994. A performance model for coal-washing dense medium cyclones, PhD Thesis,1990, JKMRC, Univ. of Queensland.
Tsuji, Y., Tanaka, T., Ishida, T., 1992. Lagrangian numerical simulation of plug flow of cohesionless particles in a horizontal pipe. Powder Technology, 71 (3), 239-250.
Xu, B. H., Yu, A. B., 1997. Numerical simulation of the gas-solid flow in a fluidized bed by combining discrete particle method with computational fluid dynamics. Chemical Engineering Science, 52 (16), 2785-2809.
Yu, A. B., Xu, B. H., 2003. Particle-scale modelling of gas–solid flow in fluidisation. Journal of Chemical Technology & Biotechnology, 78 (2-3), 111-121.

Wang, B., Chu, K. W., Yu, A. B., 2007. Numerical study of particle-fluid flow in a hydrocyclone. Industrial & Engineering Chemistry Research, 46 (13), 4695-4705.
Wang, B., Chu, K. W., Yu, A. B., Vince, A., 2009. Modeling the Multiphase Flow in a Dense Medium Cyclone. Industrial & Engineering Chemistry Research, 48 (7), 3628-3639.
Wang, B., Yu, A. B., 2006. Numerical study of particle-fluid flow in hydrocyclones with different body dimensions. Minerals Engineering, 19 (10), 1022-1033.
Wang, B., Yu, A. B., 2008. Numerical study of the gas–liquid–solid flow in hydrocyclones with different configuration of vortex finder. Chemical Engineering Journal, 135 (1-2), 33-42.
Wang, B., Yu, A. B., 2010. Computational Investigation of the Mechanisms of Particle Separation and "Fish-Hook" Phenomenon in Hydrocyclones. Aiche Journal, 56 (7), 1703-1715.
Wen, C. Y., Yu, Y. H., 1966. Mechanics of fluidisation. Chem Eng Prog Symp Series, 62 100-111.
Wilcox, D. C., 1994. Turbulence modelling for CFD (second ed.). DCW Industries Inc: La Canada, CA, USA.
Wilcox , D. C., 1998. Turbulence modelling for CFD, Third ed DCW Industries Inc, La Canada, CA, USA.
Williams, R. A., Dickin, F. J., Gutierrez, J. A., Dyakowski, T., Beck, M. S., 1997. Using electrical impedance tomography for controlling hydrocyclone underflow discharge. Control Engineering Practice, 5 (2), 253-6.
Williams, R. A., Ilyas, O. M., Dyakowski, T., Dickin, F. J., Gutierrez, J. A., Wang, M., Beck, M. S., Shah, C., Rushton, A., 1995. Air core imaging in cyclonic separators: implications for separator design and modelling. The Chemical Engineering Journal and the Biochemical Engineering Journal, 56 (3), 135-141.
Williams, R. A., Ilyas, O.M., Dyakowski, T., 1995. Air core imaging in cyclonic coal separators using electrical impedance tomography. Coal Preparation 15 (149–163).
Williams, R. A. J., X.; West, R. M.; Wang, M.; Cullivan, J. C.; Bond, J.; Faulks, I.; Dyakowski, T.; Wang, S. J.; Climpson, N.; Kostuch, J. A.; Payton, D.,, 1999. Industrial monitoring of hydrocyclone operation using electrical resistance tomography. Minerals Engineering 12 (10), 1245-1252.
Witt PJ, M. L., Wu J,Shephero IC, 1999. Validation of a CFD model for predicting gas flow in a cyclone. In CHEMECA, Newcastle, Australia
Xu, J. R., Luo, Q., Qiu, J. C., 1991. Research on the preseparation space in hydrocyclones. International Journal of Mineral Processing, 31 (1–2), 1-10.
Xu, P., Wu, Z., Mujumdar, A. S., Yu, B., 2009. Innovative Hydrocyclone Inlet Designs to Reduce Erosion-Induced Wear in Mineral Dewatering Processes. Drying Technology, 27 (2), 201-211.
Yakhot , A., Orszag,S.A.,Yakhot,V. & Israeli,M, 1989. Renormalization group formulation of large-eddy simulations. Journal of Scientific Computing, 4 139-158.
Yoshioka, N., Hotta, Y., 1955a. Chemical Engineering Journal, 19 633.
Yoshioka, N., Hotta, Y., 1955b. Liquid cyclone as a hydraulic classifier. Chemical Engineering Japan, 19 (12), 633-641.
Yu, A. B., Xu, B. H., 2003. Particle-scale modelling of gas–solid flow in fluidisation. Journal of Chemical Technology & Biotechnology, 78 (2-3), 111-121.

Xu, B. H., Yu, A. B., 1997. Numerical simulation of the gas-solid flow in a fluidized bed by combining discrete particle method with computational fluid dynamics. Chemical Engineering Science, 52 (16), 2785-2809.
Zhang, Y., Qian, P., Liu, Y., Wang, H., 2011. Experimental study of hydrocyclone flow field with different feed concentration. Industrial and Engineering Chemistry Research, 50 (13), 8176-8184.
Zhou, Z. Y., Kuang, S. B., Chu, K. W., Yu, A. B., 2010. Discrete particle simulation of particle-fluid flow: model formulations and their applicability. Journal of Fluid Mechanics, 661 482-510.
Zhu, H. P., Zhou, Z. Y., Yang, R. Y., Yu, A. B., 2007. Discrete particle simulation of particulate systems: Theoretical developments. Chemical Engineering Science, 62 (13), 3378-3396.
Zhu, H. P., Zhou, Z. Y., Yang, R. Y., Yu, A. B., 2008. Discrete particle simulation of particulate systems: A review of mayor applications and findings. Chemical Engineering Science, 63 5728-5770.
Zughbi, H. D. S., M. P.; Turner, W. J.; Hutton, W., 1991. Numerical and experimental investigations of wear in heavy medium cyclones. Minerals Engineering 4(3-4), 245-262.

CHAPTER 3[1]

COMPUTATIONAL STUDY OF THE MULTIPHASE FLOW AND PERFORMANCE OF HYDROCYCLONES: EFFECTS OF CYCLONE SIZE AND SPIGOT DIAMETER

This chapter presents a numerical study of the multiphase flow in hydrocyclones with different configurations of cyclone size and spigot diameter. This is done by a mixture multiphase flow model which has been developed in our group (Kuang et al., 2012).The model is then further extended to describe hydrocyclone flows and performances at wide range of flow conditions. In the model, the strong swirling flow of the cyclone is modelled using the Reynolds stress model. The interface between liquid and air core and the particle flow are both modelled using the so called mixture model. The solid properties are described by the kinetic theory. The applicability of the proposed model has been verified by the good agreement between the measured and predicted results in a previous study. The model is further extended and used to study the effects of cyclone size and spigot diameter when feed solids concentration is up to 30 % (by volume), which is well beyond the range reported before. The flow features predicted are examined in terms of the flow field, pressure drop, and amount of water split to underflow, separation efficiency and underflow discharge type. The simulation results show that the multiphase flow in a hydrocyclone varies with cyclone size or spigot diameter, leading to a different performance. A smaller cyclone results in an increased cut size, a decreased pressure drop and a sharper separation, and at the same time, an increased water split (thus worse by-pass effect) and more unstable operation associated with rope discharge, particularly at relatively high feed solids concentrations. Both large and small spigot diameters may lead to poor separation performance. Accordingly, an optimum spigot diameter can be identified depending on feed solids concentration. It is

[1] Content of this chapter has been published in Industrial & Engineering Chemistry Research journal: Ghodrat, M., Kuang, S. B., Yu, A. B., Vince, A., Barnett, G. D., Barnett, P. J., 2013. Computational Study of the Multiphase Flow and Performance of Hydrocyclones: Effects of Cyclone Size and Spigot Diameter. Industrial & Engineering Chemistry Research, 52 (45), 16019-16031.”

also shown that for all the considered hydrocyclones, a better separation performance and a smoother running state can be achieved by the operation at a lower feed solid concentration.

3.1 Introduction

Hydrocyclones are widely used to separate particles by size in many industries because of their advantages such as design and operational simplicity, high capacity, low operational and maintenance costs, and compactness (Bradley, 1965; Svarovsky, 1984). In the past, a number of variations and modifications have been made to the basic design of the hydrocyclone to establish optimal models for different industrial applications, and various empirical models have been formulated to describe the equipment performance (Bradley, 1965; Svarovsky, 1984; Chen et al., 2000; Kraipech et al., 2006) However, systematic studies for better designing and controlling the hydrocyclone process are few. Moreover, the fundamentals governing the complicated liquid-gas-solid flow in a hydrocyclone are still poorly understood, particularly at different feed solids concentrations.

One big concern from industry side of view is to select proper size of cyclone for given materials to be separated effectively. Therefore, a series of cyclone sizes has been simulated based on standard case that was selected from highly-recognized experiment Hsieh (1988).The routine operation in the experiment was kept the same, while the geometry of the base cyclone was scaled up and down to achieve different body sizes within a reasonable range. With the aid of the well-defined and controlled simulations, the effect of body size was systematically assessed with respect to the flow behavior and performance indices of the hydrocyclone; so as to address the industrial demand and concern.

It is well known that to describe the solids recovery, the size classification performance is required. It is also well-known that small cyclones exhibit a fish-hook partition curve (Finch, 1983) and have a high bypass fraction. In the past decades, various experimental techniques have been developed to study the flows within hydrocyclones (Yoshioka and Hotta, 1955; Knowles et al., 1973; Hsieh and Rajamani, 1991; Chu and Chen, 1993; Dyakowski and Williams, 1996; Williams et al., 1997; Dai et al., 1999; Inaki Schlaberg et al., 2000b; Fisher and Flack, 2002; Bergström et al., 2007; Lim et al., 2010; Marins et al., 2010; Chang et al., 2011; Zhang et al., 2011a). The techniques include the Pitot tube technique, (Yoshioka and Hotta, 1955), high-speed camera, (Knowles et al., 1973) , Electrical Impedance Tomography (EIT), (Dyakowski and Williams, 1996; Williams et al., 1997), Ultrasound Tomography (UT), (Inaki Schlaberg et al., 2000b), Laser Doppler Velocimetry (LDV), (Hsieh and Rajamani, 1991; Chu and Chen, 1993; Dai et al., 1999; Fisher and Flack, 2002; Bergström et al., 2007; Marins et al., 2010; Zhang et al., 2011a), Particle Image Velocimetry (PIV), (Lim et al., 2010; Marins et al., 2010) and Positron Emission Particle Tracking (PEPT) (Chang et al., 2011). Their use has led to a better understanding of the complicated flow structures in hydrocyclones. However, such an experimental method is often difficult and expensive and only suitable for laboratory scale studies rather than for industrial tests and cyclone design. This is particularly true at relatively high feed solids concentrations where the accumulation of particles along the wall highly complicates the optical access to the flow in a hydrocyclone. A similar problem happens to opaque slurry (e.g. coal slurry) widely encountered in practice.

On the other hand, computer modeling and simulation have been recognized as a promising technique to overcome the problems associated with the experimental measurements. Based on the modeling of the solid phase, the popular mathematical models proposed thus far can be grouped into two categories: the discrete approach at a microscopic level represented by the combined approach of computational fluid dynamic and discrete element method (CFD-DEM) and the continuum approach at a macroscopic level represented by the two-fluid Model (TFM) (Zhou et al., 2010). The CFD-DEM approach has been widely accepted as an effective tool to study particle-fluid systems, (Zhu et al., 2007,2008) with recent efforts made to gas cyclone, (Chu et al., 2011) hydrocyclone, (Zhou et al., 2010) and dense medium cyclone (Chu et al., 2009,2012). However, at present, it cannot be applied to practical hydrocyclones, where the particle size involved is very small and the number of particles could be billions. To date, discrete modelling of hydrocyclones has been mainly made by the combined CFD and Lagrangian particle tracking (LPT) method (Hsieh and Rajamani, 1991; Wang and Yu, 2006; Bhaskar et al., 2007b; Mousavian and Najafi, 2009; Azadi et al., 2010). The CFD-LPT approach, which is actually a simplified CFD-DEM model, traces only a single particle, with the effect of inter-particle interactions and the reaction of particles on the fluid ignored. Because of its computational efficiency, the approach has been used to study hydrocyclones under different geometrical and operational conditions as reviewed by Nowakowski et al., (2004) and Narasimha et al., (2007a). However, it is erroneous as a general model applied to hydrocyclones which may be operated at high solids concentrations (Slechta and Firth, 1984; Dyakowski and Williams, 1996; O'Brien et al., 2000; Hararah et al., 2010; Zhang et al., 2011a).

The Two Fluid Model (TFM) approach can overcome this problem while being computationally more convenient than the CFD-DEM model. It has been increasingly used to study the flows in hydrocyclones (Nowakowski et al., 2000; Huang, 2005; Brennan et al., 2007; Noroozi and Hashemabadi, 2009; Davailles et al., 2012a; Davailles et al., 2012b; Kuang et al., 2012a; Narasimha et al., 2012; Swain and Mohanty, 2013). Generally, the previous TFM studies employ two different ways to describe the phases considered. One applies a full set of conservative equations regarding momentum and mass to each phase involved (Nowakowski et al., 2000). It was used to study particle separation (Nowakowski et al., 2000; Davailles et al., 2012a; Davailles et al., 2012b; Swain and Mohanty, 2013) and deoiling (Huang, 2005; Noroozi and Hashemabadi, 2009) in hydrocyclones. Another is based on the so called mixture model which solves only one set of governing equations for all the phases, with an algebraic slip velocity model for each phase (Manninen et al., 1996). This simplification significantly alleviates the computational loading in simulations based on a full TFM model. It has been used by various investigators to study the multiphase flow and related phenomena in hydrocyclones (Brennan et al., 2007; Kuang et al., 2012a; Narasimha et al., 2012) or in dense medium cyclones (Narasimha et al., 2007b; Chu et al., 2009; Wang et al., 2009). Kuang et al., (2012a) recently extended the mixture model to study the effect of feed solid concentration based on the cyclone used in Hsieh's experiment (1988). Good agreements between model predictions and measurements can also be found in the recent work of Narasimha et al., (2012). Therefore, the TFM facilitated with the mixture model is applicable to a wide range of hydrocyclone conditions. However, to date, comprehensive studies of the flows and performance in hydrocyclones of different geometrical configurations at different feed solids concentrations have not been found in the literature.

In this work, the mixture model reported by Kuang et al., (2012a) is extended and used to systematically study the geometrical effects on the flows and performance in hydrocyclones operated at a wide range of feed solid concentrations. The cyclone size and spigot diameter are the point of focus as they are often studied under specific conditions for the purpose of industrial applications (O'Brien et al., 2000; Rong, 2007; Atkinson and Swanson, 2008). The findings from this study should be useful not only for establishing a comprehensive picture about the effects of cyclone size and spigot diameter but also for designing and controlling hydrocyclones.

3.2 Mathematical model

3.2.1 Model description

The present study is based on the Two Fluid Model (TFM), facilitated by the mixture model. In the model, both fluid (liquid and air) and solid phases are treated as interpenetrating continua, respectively. Particles of different sizes or densities represent different phases. However, the mixture of gas, liquid and solids is represented by a single phase with mixture properties, and allows certain slip velocities between different phases. Note that in this study, we only consider particles of the same density, although they have different sizes. To carry out a simulation, the size distribution is divided into a series of size intervals, with each represented by a mean size in the simulation.

The flow of the mixture is calculated from the continuity and the Navier–Stokes equations based on the local mean variables over a computational cell with the consideration of slip velocities between different phases (Manninen et al., 1996), which were given in section 2.8.2.

3.2.2 Simulation conditions

Fig. 3.1 (a) shows the most common hydrocyclone design, which consists of seven main geometrical parameters: diameter of the cylindrical body or cyclone size D_c, diameter of inlet D_i, diameter of vortex finder D_v, diameter of spigot D_u, length of cylindrical part L_c, length of vortex finder L_v, and included angle a. These parameters affect the separation efficiency, pressure drop and water split of a hydrocyclone. The aim of this work is to quantify the effects of cyclone size and spigot diameter on hydrocyclone liquid-gas-solid flow and performance at different feed solids concentrations

Table 3-1 Geometrical and operational conditions in the base case

Parameter	Symbol	Value
Geometry parameters		
Diameter of the body (mm)	D_c	75
Diameter of inlet (mm)	D_i	25
Diameter of vortex finder (mm)	D_v	25
Diameter of spigot (mm)	D_u	12
Length of cylindrical part (mm)	L_c	75
Length of vortex finder (mm)	L_v	50
Included angle (°)	α	20
Operational conditions		
Inlet velocity (m/s)	u	2.49
Flow rate (kg/m^2)	Q	0.000621, 0.00122, 0.00244,0.00488
Particle material		Limestone
Particle density (kg/m^3)	ρ_p	2700
Feed solids concentration (% by volume)	ρ_{feed}	4.14
Particle sizes simulated (μm)	d	134.16, 114.89, 99.49, 79.37, 59.16, 45.94, 35.49, 27.31, 22.96, 19.48, 16.38, 12.54, 8.87, 6.27, 2.4

In order to compare the results with those reported elsewhere, (Wang and Yu, 2006; Kuang et al., 2012a) the same hydrocyclone and operational conditions considered in the experimental work of Hsieh (1988) are used in this work as the base case, except that a wider range of particle size is considered to cover wider operational conditions. Table 3.1 lists the base geometry.

Fig. 3.1 (b) shows an isometric view of the mesh-fitted computational domain. In the figure, only the representative parts are shown for clarity. The whole computational domain is divided by about 100,000 unstructured hexahedral grids.

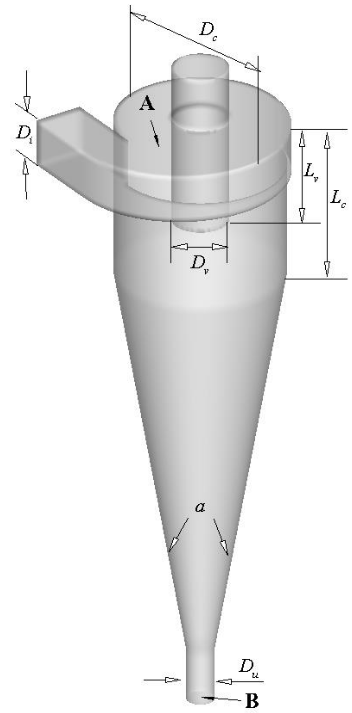

(a)

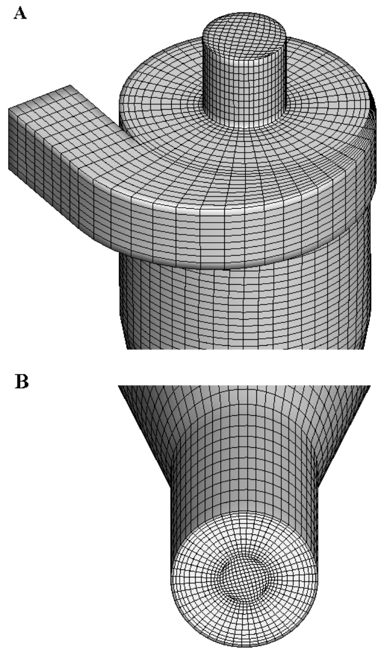

(b)

Fig. 3.1 Hydrocyclone used for the classification of limestone: (a) geometry of the hydrocyclone, and (b) representative grid arrangements in the computational domain (here the top and bottom sections viewed from different angles)

CFD mesh is of importance for obtaining meaningful numerical results. It is mainly determined by three factors: mesh type, size and arrangement. In this study, the computational domain is divided by hexahedral grids for numerical stability and efficiency, with the grid arrangement similar to those used elsewhere (Wang and Yu, 2006,2008; Chu et al., 2009; Wang et al., 2009; Kuang et al., 2012b) adopted. The grids are finer near the central region (including the vortex finder), as shown in Fig. 3.1. This allows us to reasonably capture the interface between the air and the liquid. In the vicinity of the walls, the grids are also finer because the flow usually varies more significantly there. On this basis, some preliminary tests are conducted to select fine enough meshes, so that the numerical solution becomes grid-independent. Three grid schemes of 53,028, 100,000, and 195,268 hexahedra are examined for such tests. The numerical results reveal that the flows and performance are indeed converged, independent of mesh size when mesh size is fine enough (e.g. for the last two grid schemes). Fig. 3.2 shows the representative results including the tangential velocity, pressure drop and separation efficiency of particles for the base case. Similar results can also be obtained for other cases. In addition, the computational time of the tests increases from one week to three weeks with decreasing mesh size. As such, the mesh size used in our study is similar to that of the second grid scheme.

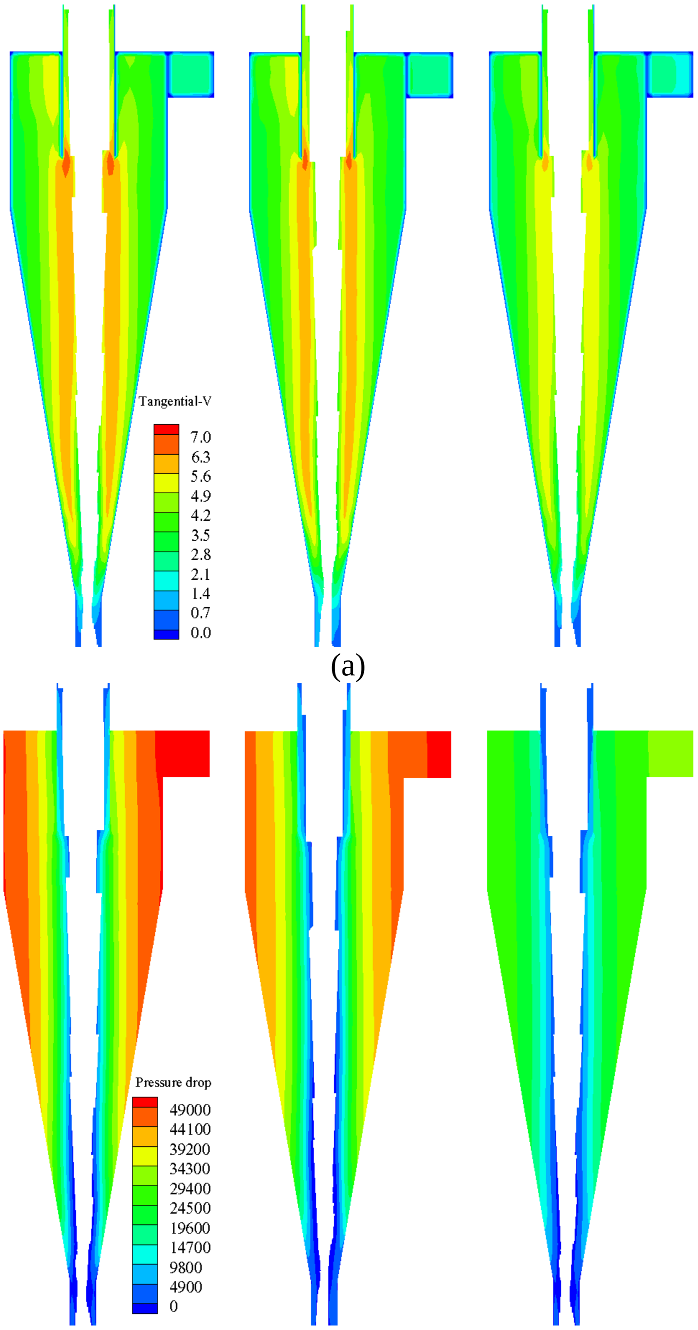

Grid density=195,268 cells 100,000 cells 53,028 cells

(b)

(to be continued)

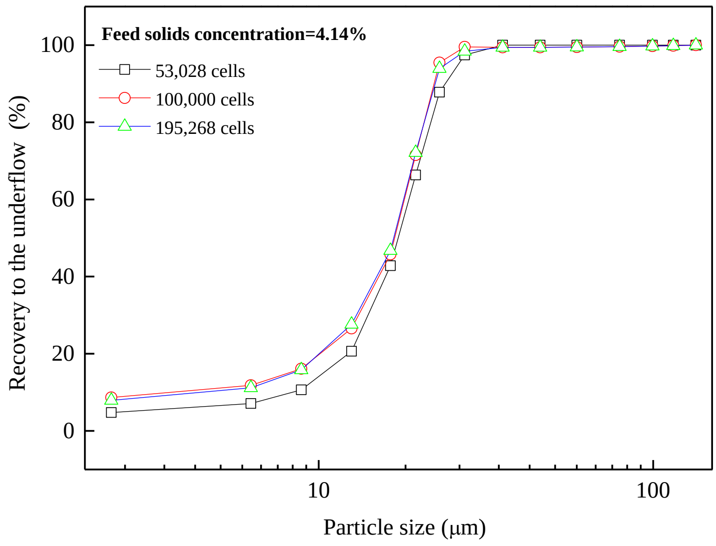

(c)

Fig. 3.2 Effects of mesh size on the calculated results for the base case: (a) tangential velocity, (b) pressure drop and (c) separation efficiency

A “velocity inlet” boundary condition is used at the cyclone inlet, and the “pressure-outlet” condition at both outlets. The inlet velocity is 2.49 m/s and the pressure at the two outlets (vortex finder and spigot) is 1 atm, corresponding to the ambient atmospheric pressure. For the particles involved, the density is 2700 kg/m^3, and the size range is between 2.4 and 134 μm. The size distribution considered here is similar to that used in the experimental work of Hsieh (1988). It is represented by 15 mean sizes in simulations. The mean sizes and their distribution are given in Table 3.1 and Fig. 3.3, respectively.

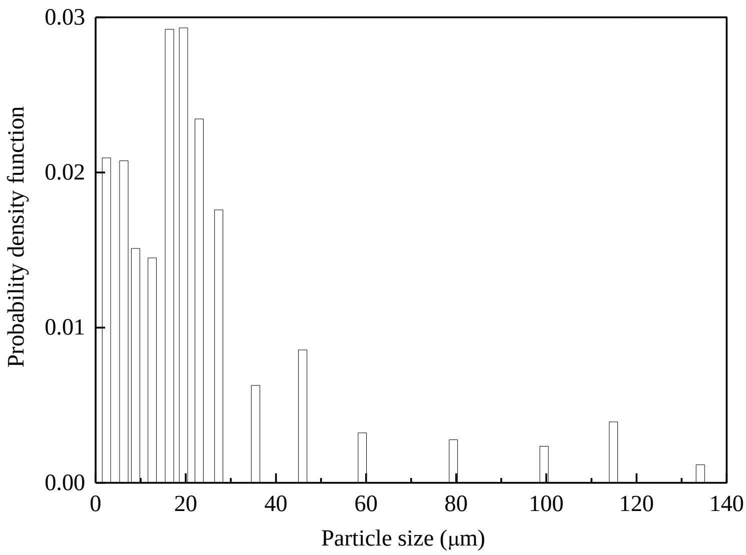

Fig. 3.3 Size distribution considered in the simulations

All the simulations were conducted using the ANSYS Fluent CFD software package (version 14) in NCI (National Computational Infrastructure) in Australia. Sixteen CPUs are assigned to each simulation, which lasts for about 14 days for computing the physical time of about 35 seconds to ensure that the steady-state flow is achieved. The steady state is identified by the feature that the macroscopic flow characteristics just fluctuate around their respective mean values. This study focuses on the steady-state results. Unless otherwise noted, all the results shown are time-averaged steady-state results.

3.2.3 **Model validation**

It is necessary to verify the mathematical model before its application for numerical experiments. This has been done by comparing the measured and calculated flow fields in terms of flow and performance under different conditions, as brought in model validation section (2.8.3) and reported in the recent work of Kuang (Kuang et al., 2012b). The comparison progressed from simple to complicated cases. First, the tangential and axial velocity distributions measured by Hsieh (1988) at different axial locations were used. The operation involves only gas-liquid flow. Overall, the trends obtained in the numerical and physical experiments are in good agreement. The prediction error is less than 10% for the axial velocities but up to 30% for the tangential velocities. Based on the same experimental conditions, the applicability of the model in predicting the inlet pressure drop and water split was also examined. The errors are less than 5%. Similar results were also reported by Wang and Yu (2006) and Brennan (2006) who considered the same experiments but used the VOF approach facilitated with the RSM model. Furthermore, Brennan (2006) reported that the LES model can better predict the tangential velocities. It however requires much finer meshes than the RSM model, computationally much more demanding. Secondly, the separation behaviours of particles of different sizes were considered for the hydrocyclones operated at both low and relatively high feed solids concentrations respectively using the experimental measurements of Hsieh (1988) and Slechta and Firth (1984). The model can successfully predict different separation behaviours when feed solids concentration and other conditions vary. The prediction errors are generally less than 10%, although being up to 20% for large and heavy particles. Thirdly, the TFM model, facilitated respectively with the LPT model (Wang et al., 2009) or the mixture model

(Kuang et al., 2013), has been extended to study the complicated multiphase flow in a dense medium cyclones (DMC). The model can reasonably predict the separation behaviours in DMCs, although it again gives larger errors for coarser particles. Such a problem should be overcome by the combined approach of CFD and DEM (discrete element model) that can describe the motion of particles at the particle scale (Chu et al., 2009). Nonetheless, the results obtained thus far for different types of cyclones suggest that the present TFM model can be used to describe hydrocyclone flow and performance, at least qualitatively. Thus, in the following, the effects of body diameter and spigot diameter are examined through a parametric study at different feed solid concentrations (see Table 3.2).

The cyclone size is varied from 37.5 to 300 mm by simultaneously changing the dimension of the base cyclone in proportion through different scale factors. The corresponding scale factor ranges from 0.5 to 4. The spigot diameter considered is from 10 to 25 mm, achieved by varying the cone length at a given included angle, following the experimental studies of spigot diameter by different investigators (Slechta and Firth, 1984; O'Brien et al., 2000; Atkinson and Swanson, 2008). For each case, only one variable/dimension is changed while the rest are the same as the base hydrocyclone.

Table 3-2 Variables considered in the present study

Parameter	Symbol	Value
Diameter of the body (mm)	D_c	(37.5,75,112.5,150,187.5,225,262.5, 300)
Spigot (apex) diameter (mm)	D_u	(10, 12.5,15,20,25)
Feed solids concentration (% by volume)	S_c	(4.14, 30)

3.3 Results and discussion

3.3.1 Effect of cyclone size

3.3.1.1 Partition curve

A typical classification curve is shown in Fig. 3.4 and 3.5. This is called the partition curve (sometimes called the grade recovery curve) and it shows the fraction of particles at a particular size that will be partitioned to the coarser fraction. The S shaped curve is typical of all practical cyclones and a variety of quantitative expressions have been used to describe the shape of the curve.

Fig. 3.4 and Fig. 3.5 illustrate how cyclone size affects the separation efficiency at different feed solids concentrations. Note that in these figures, the results are steady-state, which are identified by the feature that the macroscopic flow characteristics just fluctuate around their respective mean values. Moreover, unless otherwise noted, all the results are time averaged. It can be seen from Fig. 3.4 that the separation efficiency decreases with the increase of cyclone diameter at all the feed solids concentrations considered. A similar result was also reported by Wang and Yu (2006) who, however, considered only a low feed solids concentration using the CFD-LPT model. Fig. 3.4 and Fig. 3.5 also show that the effect of feed solids concentration on separation efficiency is significantly reflected from the following three aspects that cannot be obtained by the CFD-LPT model. Firstly, for the same cyclone, the separation efficiency decreases with the increase of feed solids concentration. However, this decrease does not occur to the very fine particles. For such particles, the separation efficiency increases with the increase of feed solids concentration (Fig. 3.5). This indicates that a higher feed solids concentration leads to a reduced recovery of fine particles to the overflow, and thus an increased loss of the product (fine particles). Secondly, the difference in the recovery to the underflow between the largest and smallest cyclones becomes smaller at a higher feed solids concentration (Fig. 3.4).

This indicates that the effect of cyclone size on separation efficiency becomes less significant at a higher feed solids concentration. Thirdly, the effect of feed solids concentration on separation efficiency becomes smaller at a larger cyclone size (Fig. 3.5). In order to understand the separation behaviours, the calculated tangential velocity (u_t) and radial acceleration (a_r) are examined. The radial acceleration represents the driving force for separation in a hydrocyclone, calculated by (Svarovsky, 1984).

$$a_r = u_t^2 / r \qquad (3.1)$$

where r is the radial distance. It can be seen from Fig. 3.6 that the tangential velocity increases with the increase of cyclone size. However, with increasing feed solids concentration, the tangential velocity decreases and slows down at relatively large cyclones, similar to those observed by Zhang et al., (2011a).

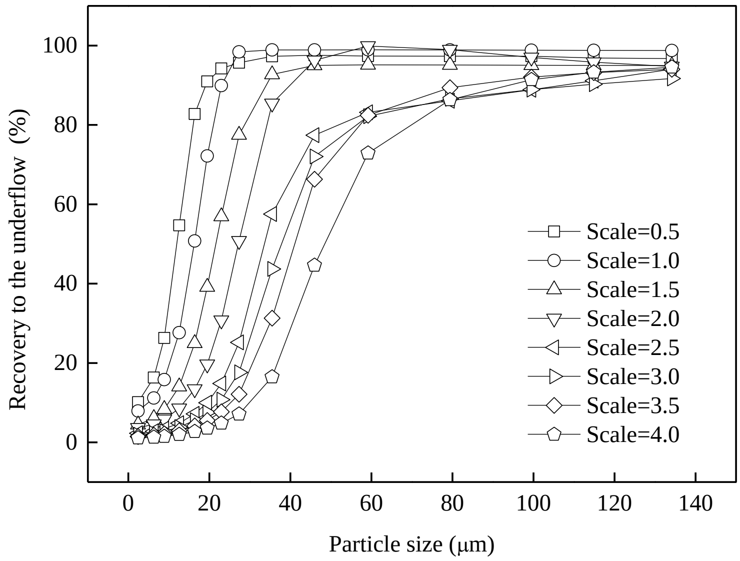

(a)

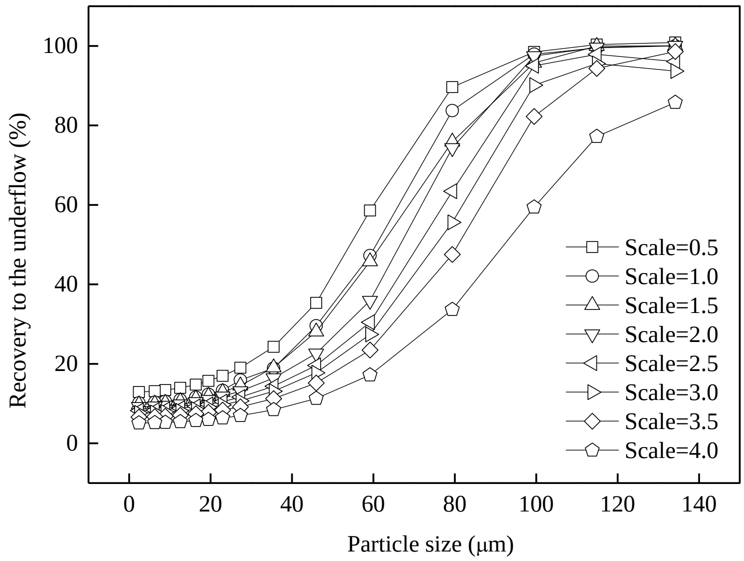

(b)

Fig. 3.4 Effect of cyclone size on separation efficiency at different feed solids concentrations: (a) 4.14%, and (b) 30%.

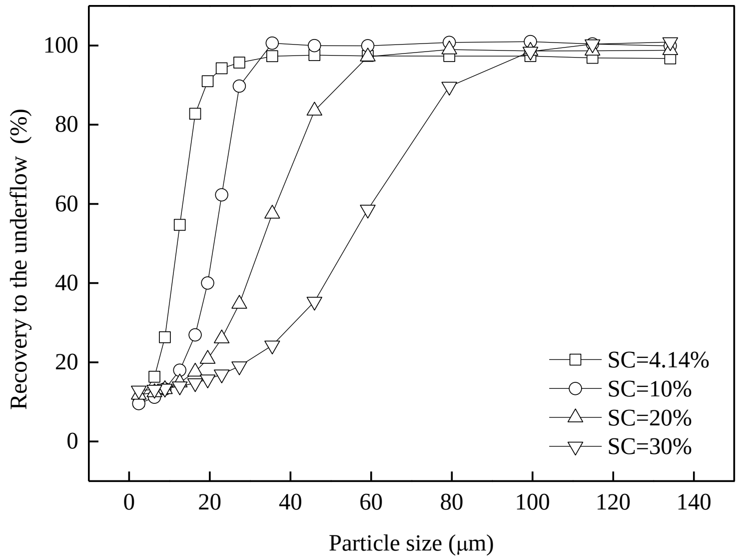

(a)

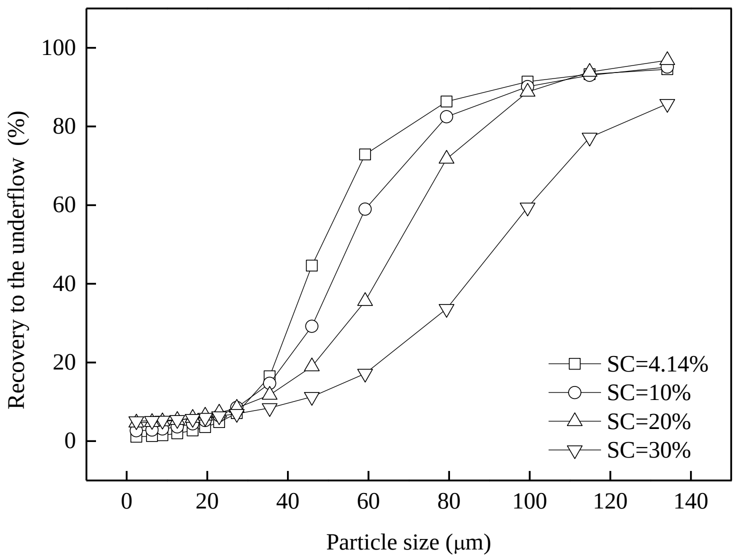

(b)

Fig. 3.5 Effect of feed solids concentration on separation efficiency for different sized cyclones: (a) scale=0.5 and (b) scale=4

Corresponding to the tangential velocity, the radial acceleration decreases with the increase of either cyclone size or feed solids concentration (Fig. 3.7). Overall, the trend of the results in Fig. 3.9 corresponds well to those in Figs. 3.4 and 3.5. This result suggests that the decrease of separation efficiency as a result of the increase in either feed solid concentration or cyclone size is essentially attributed to the decrease of radial acceleration. Clearly, tangential velocities widely used to explain cyclone separation behaviours should be valid only to cyclones with similar body sizes. For different sized cyclones, analysis of radial acceleration as proposed here is necessary. Note that in Figs. 3.6 (and 3.7, 3.9, 3.10, 3.12); all the different sized cyclones shown are scaled to the same size for comparison.

It is of interest to note that the separation efficiency is less sensitive to feed solids concentration for a large cyclone (Fig. 3.7). This is because the separation efficiency is essentially governed by the radial acceleration. As seen from Fig. 3.7, with increasing feed solids concentration, the radial acceleration is reduced more significantly for smaller cyclones. The loss of radial acceleration is particularly evident at the lower part of a cyclone, mainly caused by different particle accumulations there.

3.3.1.2 Separation efficiency parameters

To quantitatively assess cyclone performance under different conditions, we examine the separation efficiency parameters such as cut size, sharpness of partition curve and water split, as well as the inlet pressure drop. The results are respectively given in Fig. 3.8(a) to Fig. 3.8(d).

Fig. 3.8 (a) shows the inlet pressure drops which are usually thought of as an index of energy loss and reveals that when cyclone size is increased at a given feed solid concentration, the inlet pressure drop defined as the difference of the pressure at the inlet and the underflow outlet always increases. This is consistent with the experimental and numerical results of Azadi et al., (2010) who, however, focused on low feed solids concentrations. However, Fig. 3.8(a) shows that feed solids concentration significantly affects pressure drop. For small cyclones (scale=0.5 and 1), when feed solids concentration increases, the inlet pressure drop first decreases to a minimum and then increases. A similar phenomenon was also observed by Kuang et al., (2012a) who considered the same cyclone at scale=1 but much finer particles. Conversely, for larger cyclones, the inlet pressure drop monotonically increases with the increase of feed solids concentration, and this increase becomes more evident with increasing cyclone size.

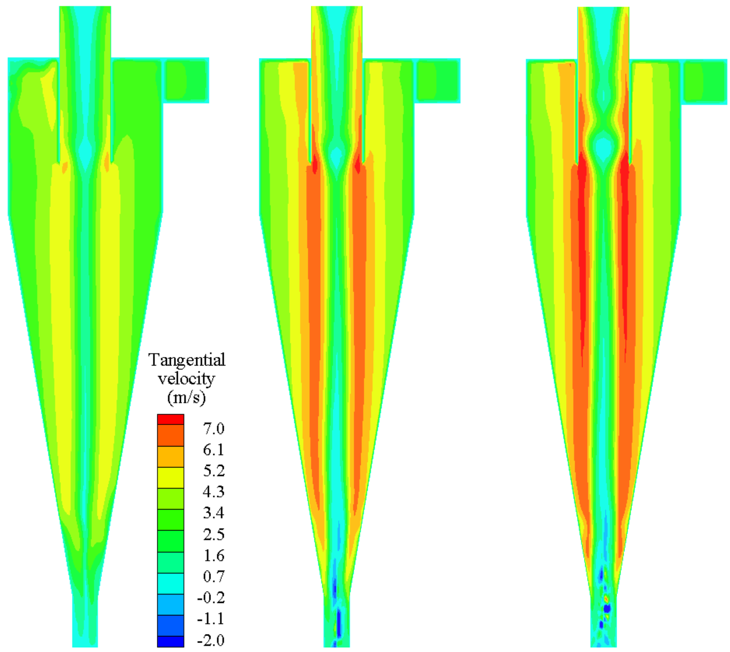

(a)

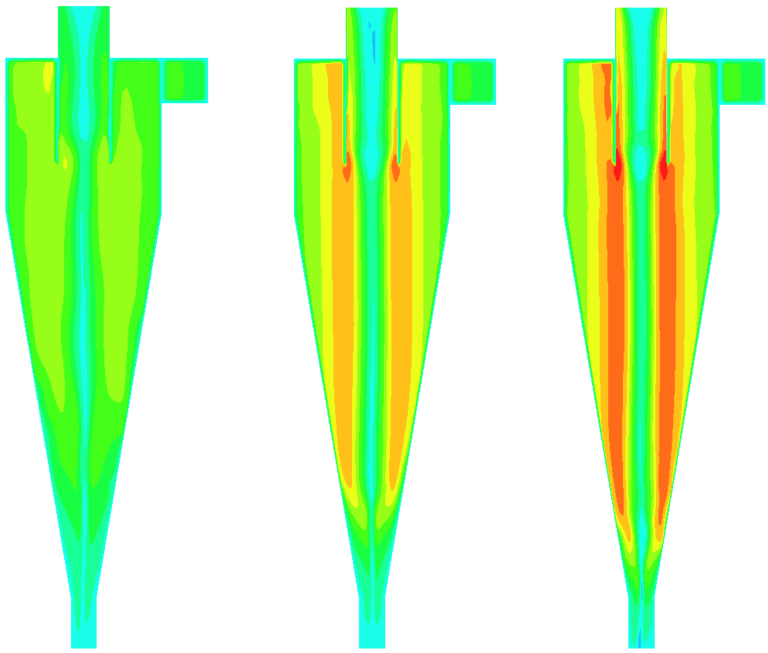

Scale=0.5 Scale=2 Scale=4

(b)

Fig. 3.6 Effect of cyclone size on spatial distribution of tangential velocities at different feed solids concentrations: (a) SC=4.14% and (b) SC=30%

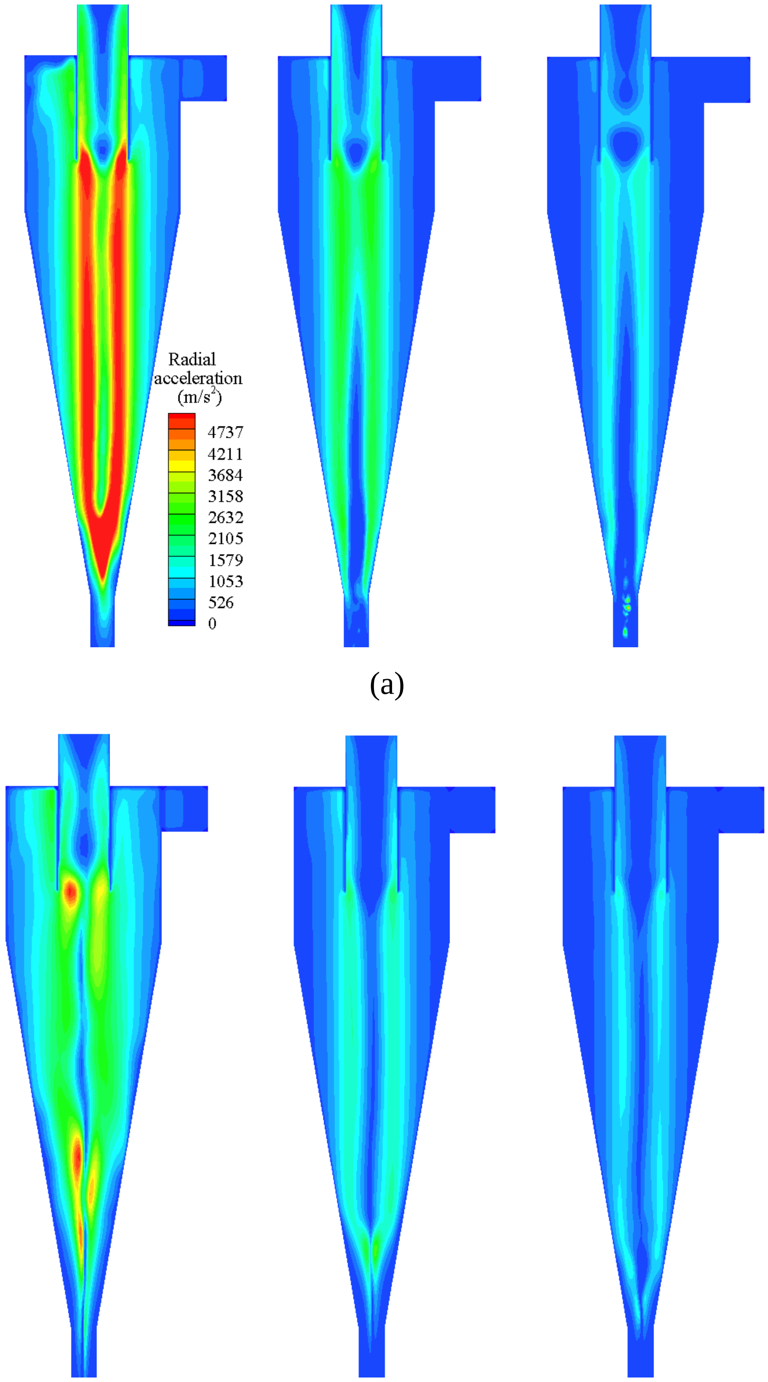

(a)

Scale=0.5 Scale=2 Scale=4

(b)

Fig. 3.7 Effect of cyclone size on spatial distribution of radial acceleration at different feed solid concentrations: (a) SC=4.14% and (b) SC=30%

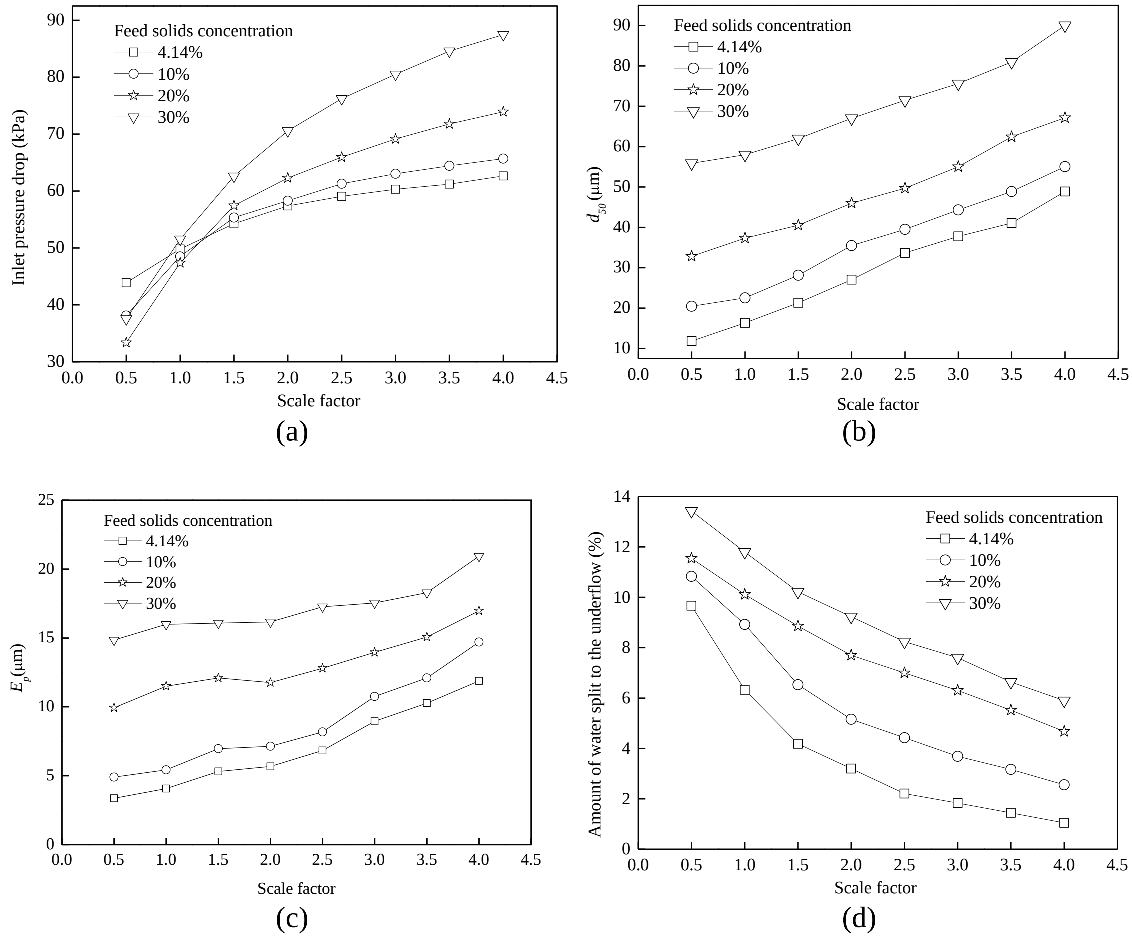

Fig. 3.8 Effects of cyclone size on separation efficiency parameters: (a) inlet pressure drop, (b) cut size, (c) Ecart probable, and (d) water split.

In general, pressure behaviours in a hydrocyclone operated in a dilute regime can be explained using tangential velocities (Narasimha et al., 2006;Wang and Yu, 2006; Bhaskar et al., 2007a). Such analysis has limitations and cannot be applied to the complicated pressure behaviour obtained here. This is overcome in this study. In accordance with the reduced Navier–Stokes equation, the radial pressure distribution in hydrocyclones can be expressed as (Hararah et al., 2010):

$$dp / dr = \rho_L \frac{u_t^2}{r} \tag{3.2}$$

where ρ_L is the liquid (or suspension) density. In a computational cell, ρ_L and u_t are usually treated as constants in a CFD model. Thus, integrating Eq. (3.2) on the computational cell i for cyclones of different scales give:

$$\Delta p_i = s\rho_{L,i}u_{t,i}^2 \ln\frac{r_{1,i}}{r_{2,i}} \qquad (3.3)$$

where s is the scale factor, Δp_i is the radial pressure drop across the considered computational cell i, and $r_{1,i}$ and $r_{2,i}$ are the radial locations in the base cyclone. Further integrating Eq. (3.3) in the radial direction gives the radial pressure drop:

$$\Delta p = s\sum_{i=1}^{N}(\rho_{L,i}u_{t,i}^2 \ln\frac{r_{1,i}}{r_{2,i}}) \qquad (3.4)$$

where N is the number of computational cells in the radial direction

Note that the inlet pressure drop is largely equal to the radial pressure drop at the inlet height level because here the pressure drop at the central line is close to that on the underflow outlet. Eq. (3.4) indicates that the inlet pressure drop should be proportional to the suspension (or mixture) density, tangential velocity and scale factor. Indeed, it is shown that the inlet pressure drop behaviours (Fig. 3.6) can be well explained by the mixture density (Fig. 3.9), tangential velocity (Fig. 3.6), and scale factor, and their roles significantly vary with the conditions considered. When cyclone size is varied for a given feed solids concentration, the mixture density has a small variation; the tangential velocity and scale factor both increasing with the increase of cyclone size, are the dominating factors, leading to an increased inlet pressure. When feed solids concentration is varied for relatively small cyclones, the mixture density and tangential velocity are the dominating factors. The increase for the mixture density and the decrease for the tangential velocity (e.g. scale=0.5 in Fig. 3.6 and Fig. 3.9) together lead to the fact that the inlet pressure drop decreases first to a minimum and then increases. When solid concentration is varied within relatively large cyclones, the mixture density remains nearly the same and the increase of inlet pressure drop is attributed to the increase of tangential velocity (e.g. scale=2 and 4 in Fig. 3.6 and Fig. 3.9). In the previous studies, (Narasimha et al., 2006; Wang and Yu, 2006; Bhaskar et al., 2007a) the effect of particles on water flow was neglected and the fluid (only water) density outside the air core is constant, thus the inlet pressure drop is dominated by the tangential velocity.

Fig. 3.8(b) shows the cut size d_{50} (corresponding to the separation efficiency of 50% in a partition curve) as a function of scale factor at different feed solids concentrations. As seen from the figure, for a given feed solids concentration, the cut size linearly increases with the increase of cyclone size. This may be due to the changed orbit radius of particles. As body diameter increases, the orbit radius increases. Consequently, the probability for particles to move to the wall of the body and then move down with the downward flow is decreased. Fig. 3.8(b) also shows that when feed solids concentration is increased for a given cyclone, the cut size increases, and the increase becomes more evident at a higher feed solids concentration. The result could be explained as follows. With increasing feed solids concentration, particles near the spigot region become denser, as experimentally observed, (Kawatra et al., 1996; Neesse and Dueck, 2007) leading to a decreased settling speed of particles (Kawatra et al., 1996). This promotes the possibility for coarse particles to reach the central region and flow up with the upward water flow and report to the overflow.

Fig. 3.8 (c) shows the sharpness of partition curve which determines the cut precision and thus the quality of the product from hydrocyclones used to classify particles by size. Note that when the focus is on the separation of particles from liquid, separation efficiency is the major concern and sharpness is not so important. It is this case for most of the previous numerical studies of hydrocyclones where sharpness was usually not considered. The partition sharpness can generally be determined by two methods. One is from the Lynch model (1976) where a function described by the sharpness coefficient, cut size and water split is used to fit the partition curve, giving the sharpness coefficient. Another is the Ecart probable E_p ($= \frac{d_{75} - d_{25}}{2}$) which is widely used to assess DMC performance, (Chu et al., 2009; Wang et al., 2009) with some applications to hydrocyclones (Pascoe, 2006). Our trial tests indicated that the sharpness coefficient given by the Lynch model (1976) sometimes cannot properly reflect the difference in sharpness between two partition curves if the data points around the cut size are not dense enough. This problem does not happen to E_p, which is hence used to describe the sharpness of partition curve in this work. Note that according to the definition, a smaller E_p corresponds to a larger sharpness and a better product quality. A zero E_p is the ideally best case where particles are exactly classified into two groups according to the cut size.

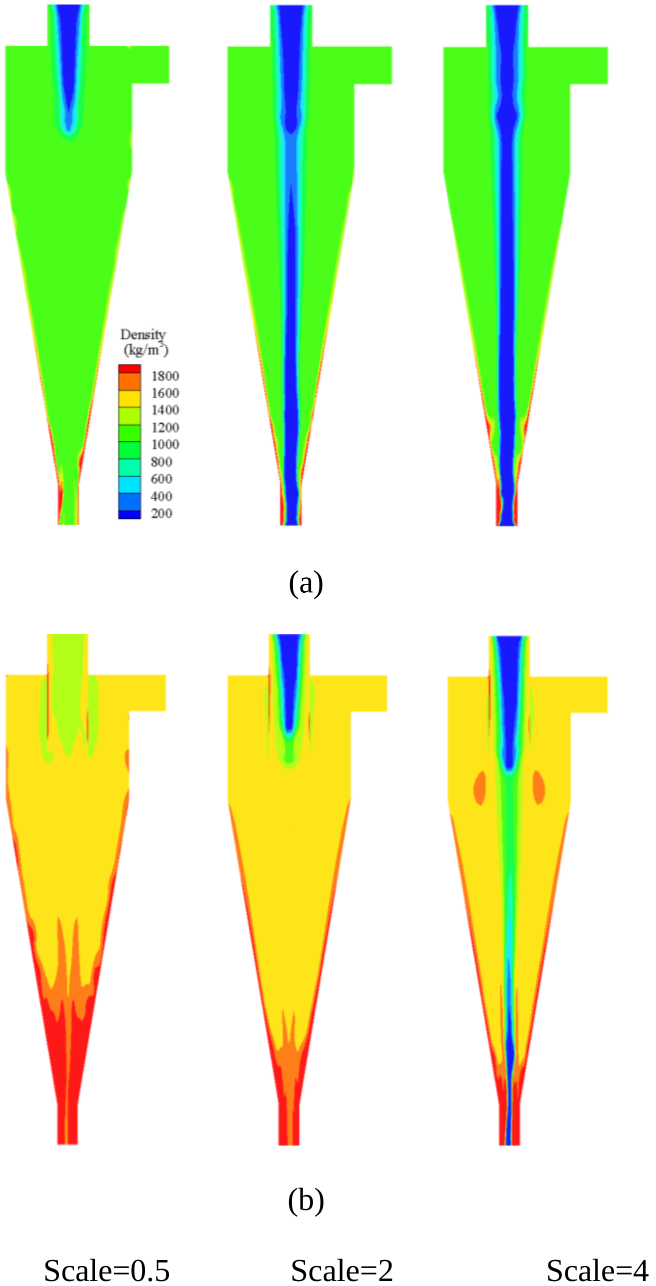

Fig. 3.9 Effect of cyclone size on spatial distribution of mixture density at different feed solids concentrations: (a) SC=4.14%, and (b) SC=30%.

It can be seen from Fig. 3.8(c) that E_p increases with the increase of either feed solids concentration or cyclone size, and the extent of the increase becomes more significant at a higher feed solids concentration or a smaller cyclone size. This result corresponds well to the partition curves in Fig. 3.4 and Fig. 3.5. Our result of the partition curve further confirms that E_p can be used to describe the sharpness of partition curve in a hydrocyclone. More importantly, Fig. 3.8(c) shows that E_p at a large cyclone or a high feed solids concentration is large, which is not favorable to the quality of the product. This phenomenon should also be attributed to the decrease of radial acceleration given in Fig. 3.7.

Fig. 3.8 (d) shows the amount of water split to the underflow. Here, the so called water split is defined as the ratio of the volumetric water flow rate of the underflow to that of the feed stream. It is known that hydrocyclones suffer from two inherent deficiencies associated with by-pass effects (Lynch, 1976; Slechta and Firth, 1984). One is the coarse particle bypass where coarse particles in the feed stream move along the boundary layer over the outside wall of the vortex finder and directly join the overflow stream within the vortex finder. It leads to the contamination of the product. Another is the fine particle bypass where fine particles flow with water and report to the underflow. This causes product loss which is normally evitable because fine particles usually do not possess sufficient drag forces to resist moving with a fluid. The previous studies revealed that the amount of fines reporting to the underflow is proportional to that of water split (Kelsall, 1953; Plitt 1976; Braun and Bohnet, 1990). It can be seen from Fig. 3.8(d) that the water split increases with the feed solids concentration, but, decreases with the increase of cyclone size. This is consistent with the experimental work of Bhaskar et al., (2007b) who demonstrated that the water split for the 75 mm cyclone is always smaller than the 50 mm cyclone. In that work, only low feed solids concentrations were considered with a focus on confirmation of capability of CFD-LPT model. The effect of feed solids concentration on water split is mainly governed by the tangential velocity. With increasing feed solids concentration, a cyclone has an increasing region with small tangential velocities at the lower part (Fig. 3.6). Consequently, the water has an increased chance to be reported to the underflow, and an increased water split is observed at a higher feed solids concentration. Conversely, the decrease of water split with the increase of cyclone size is attributed to the decrease of the magnitudes of tangential velocities near the spigot region.

Fig. 3.8 (d) indicates that a high feed solids concentration damages the product quality; conversely, a large cyclone helps improve the product quality. Notably, Fig. 3.8(c) Fig. 3.8(d) together reveal that the effect of cyclone size on product quality is actually two-sided, i.e. favourable in view of water split and unfavourable in view of partition sharpness. This may be the reason that there are some arguments on the selection of a large or medium hydrocyclone to minimize the missed placed particles in coal separation process (O'Brien et al., 2000; Atkinson and Swanson, 2008). The results also suggest that caution should be made to use a smaller cyclone to achieve high quality product, although multi-cyclone units consisting of many small cyclones are often used for high throughputs in practice. In addition, it should be pointed out that compared to our previous study, (Kuang et al., 2012a) a non-monotonic variation of water split as a result of the change in feed solids concentration is not observed in the present study. This may be due to that a wider size range is considered in the present study. This indicates that material properties also affect cyclone performance and will be considered in our future study.

The effect of cyclone size on solid viscosity and mixture slurry viscosity at different feed solids concentration is given in Fig. 3.10 and Fig. 3.11.

It can be seen from these figures that, as body diameter increases both solid viscosity and mixture slurry viscosity remain almost unchanged for relatively low feed solids concentration, however these two magnitudes change significantly with cyclone body size, while solids concentration is relatively high (30%). The key reason for this phenomenon is when we have dilute flow, the viscosity is innately low and change marginally with changing cyclone body size, but when the feed solids concentration is comparatively higher than normal practice, then increasing body size could be affected by solid and mixture viscosity in a great extent.

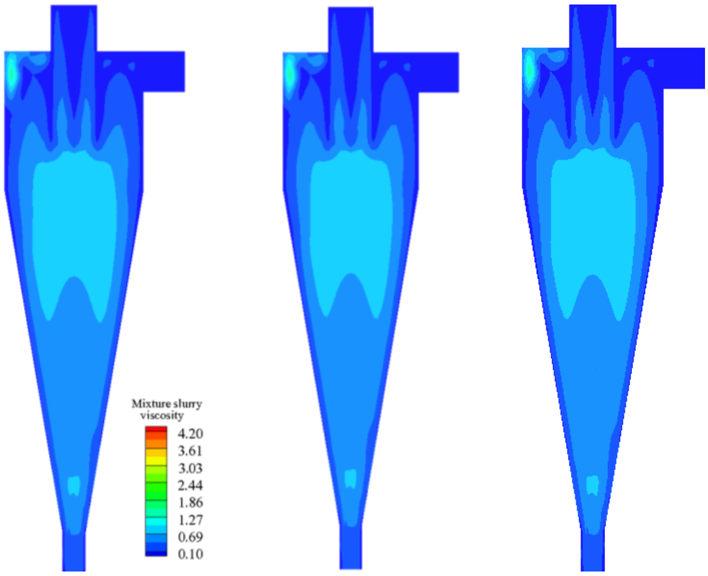

(a)

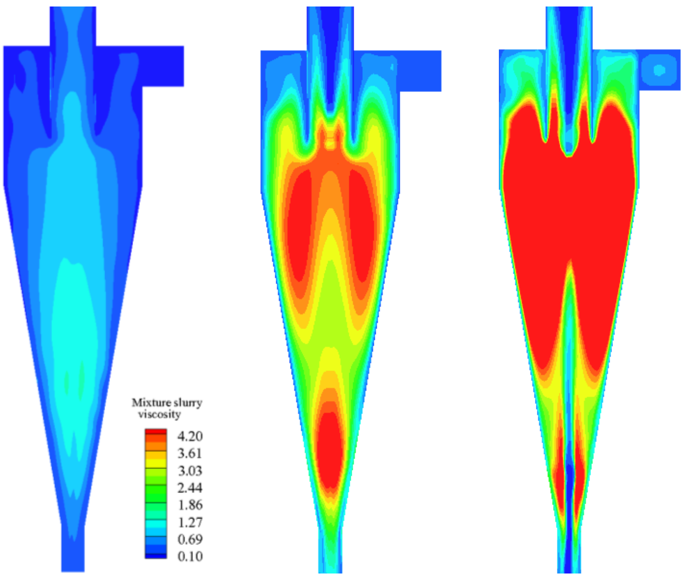

(b)

Scale=0.5 Scale=2 Scale=4

Fig. 3.10 Effect of cyclone size on mixture slurry viscosity at different feed solids concentrations: (a) SC=4.14% and (b) SC=30%.

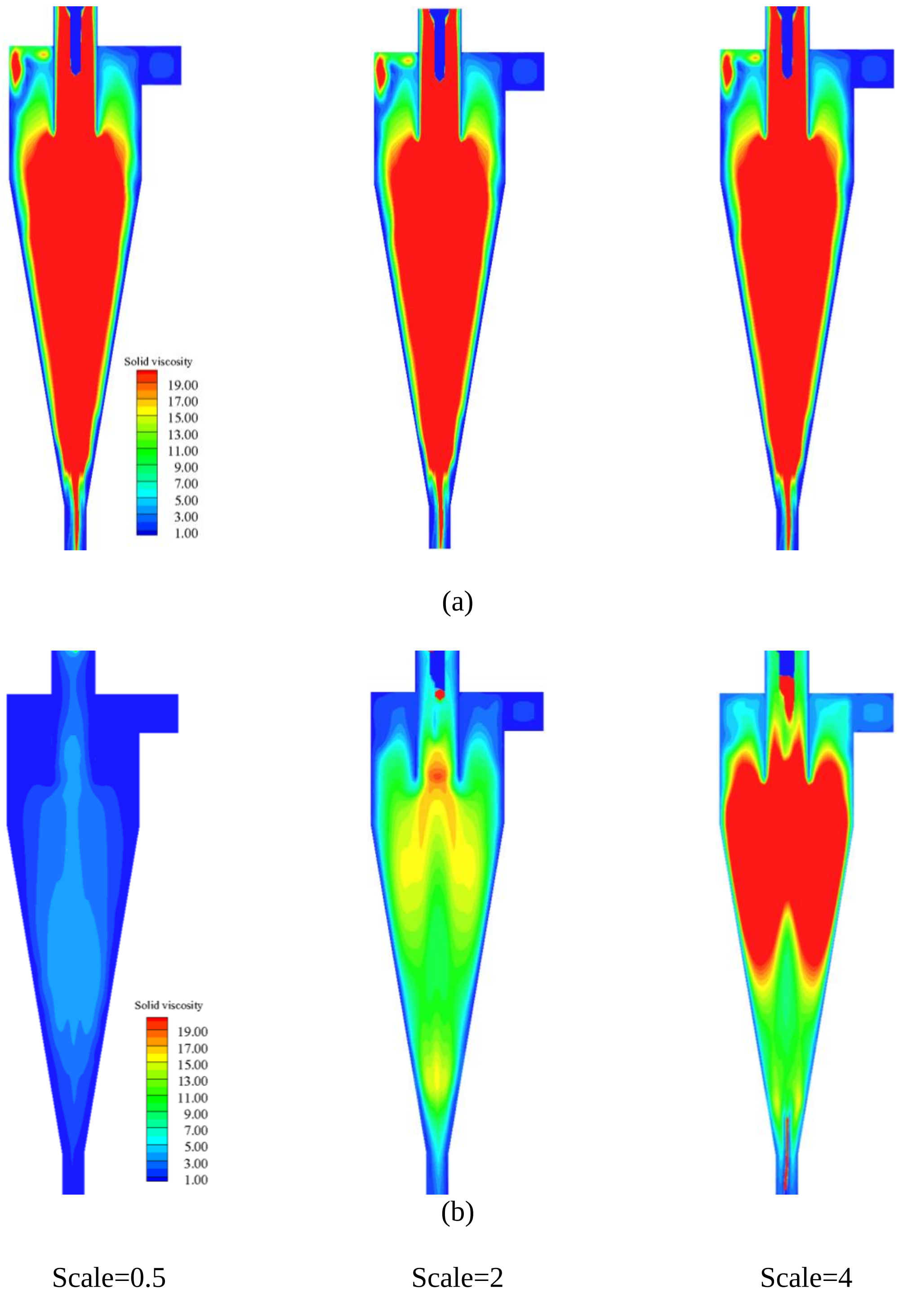

Fig. 3.11 Effect of cyclone size on solid viscosity at different feed solids concentrations: (a) SC=4.14% and (b) SC=30%.

3.3.1.3 Air core

Air is usually sucked into a hydrocyclone, flows through the central region and forms an air core due to the rotational flow which causes a lower pressure than the atmosphere pressure in the central region. Usually, the geometry and movement of the air core are identified as sensitive indicators for hydrocyclone operational state (2000a; Neesse and Dueck, 2007). Although useful, air core were rarely considered as an independent factor for designing and controlling hydrocyclones due to the lack of knowledge about it. An attempt is hence made in this work to better understand the behaviors of the air core and link them to cyclone size, spigot diameter and feed solids concentration.

Fig. 3.12 shows the representative profiles of air core inside different sized cyclones operated at different feed solids concentrations. Three types of air core can be identified. For type I, the air core is continuous and goes through the entire cyclone from the underflow to the overflow along the central region and the diameter is largely uniform (scale=2 and 4 at SC=4.14%). For type II, the air core is semi-continuous. It also goes through the cyclone but tends to be disconnected beneath the vortex finder and the diameter is not uniform.

Fig. 3.13 shows the pressure along the cyclone central line where the pressure should be lower than those on other locations at the same height level. In the figure, the pressure is given relative to the ambient atmospheric pressure (1 atm). It can be seen from Fig. 3.13 that the pressure significantly varies along the vertical axis and has the largest value inside the spigot. Expectedly, the air core can be observed only when the pressure along the central line of the cyclone is overall less than the atmospheric pressure. It is of interest to note that the presence of the air core is up to the pressure inside the spigot. For all the cases considered in this work, the air core cannot be observed when the pressure inside the spigot is larger than the atmospheric pressure.

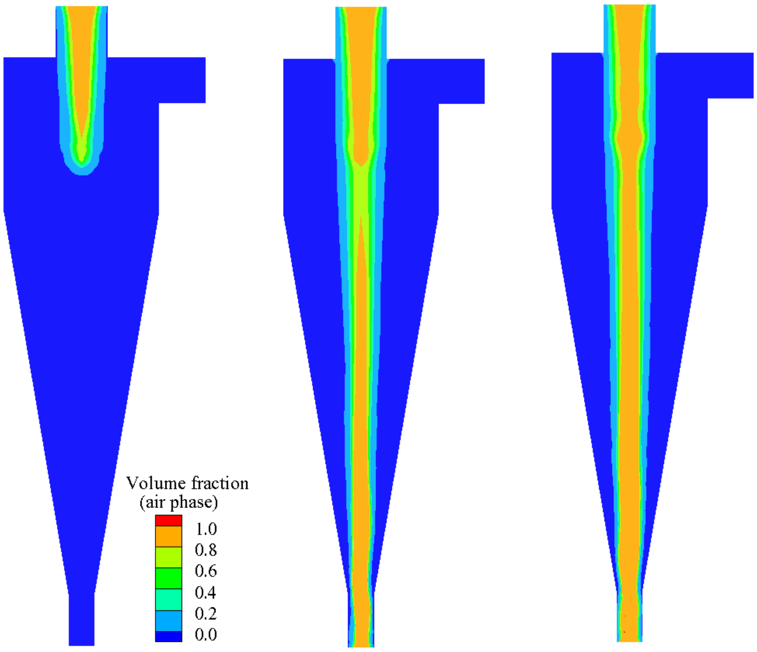

(a)

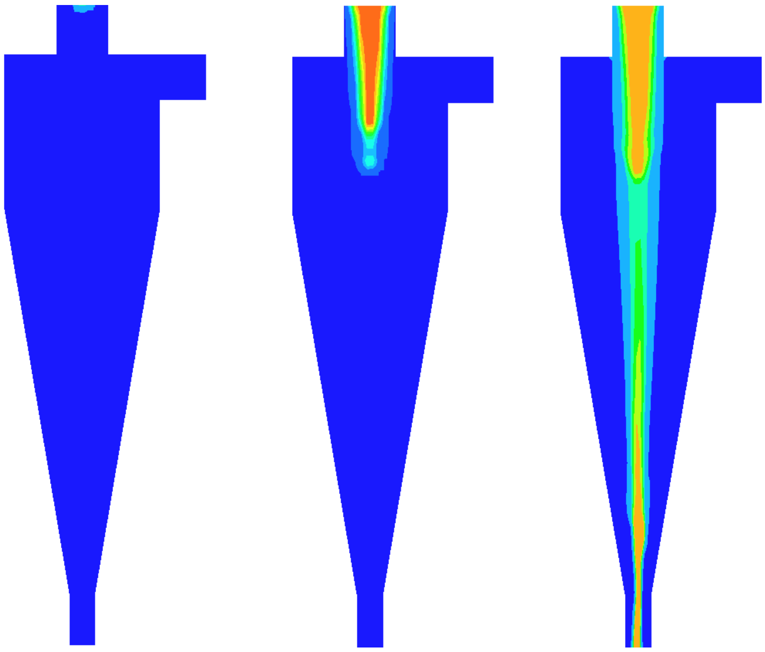

(b)

Fig. 3.12 Effect of cyclone size on air core at different feed solids concentrations: (a) SC=4.14% and (b) SC=30%.

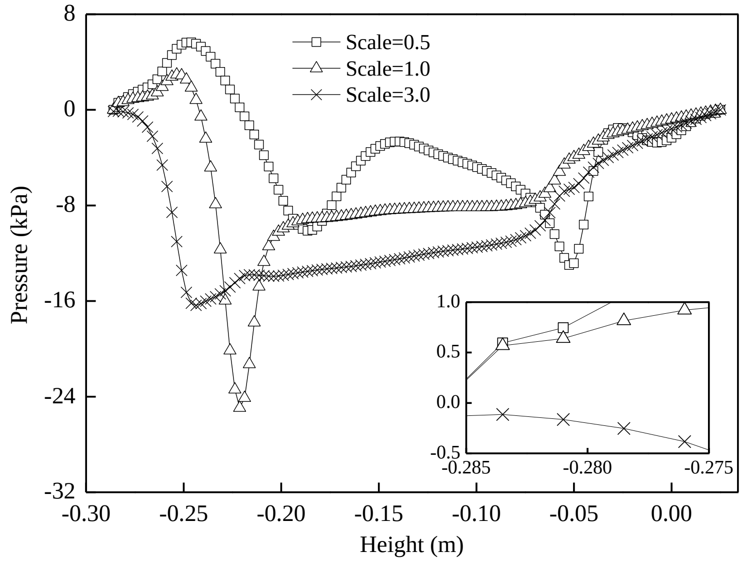

Fig. 3.13 Pressure drop along the cyclone central line at SC=30%.

Fig. 3.14 shows the flow field inside the spigot. In the figure, the downward flow corresponds to the slurry flow and the upward flow mainly to the air flow. Fig. 3.12 and Fig. 3.14 together show that the slurry flow inside the spigot is largely downward when the air core does not exist. This leads to the so-called rope discharge at the underflow. On the other hand, when the air core exists, the slurry flow is downward and inclined toward the spigot wall away from the air core, because the diameter of the air core at the spigot is larger than those on other regions due to the lowest pressure there. The so-called spray discharge is hence observed. These results are consistent with the general observation of hydrocyclone (Concha et al., 1996 ; Neesse and Dueck 2007 ; Krishna et al., 2010).

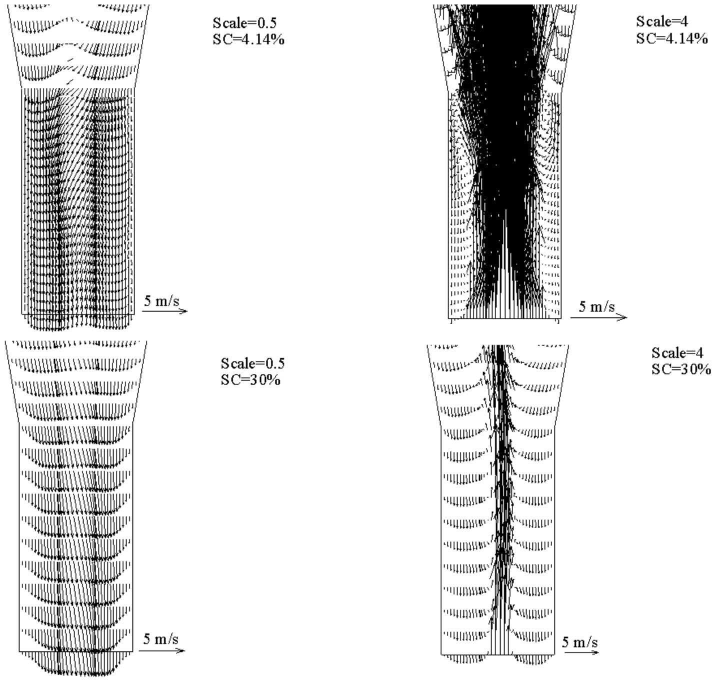

Fig. 3.14 Flow field inside the spigot for different sized cyclones operated at different feed solids concentrations.

As seen from this figure, the solid flow rate at the underflow fluctuates significantly around a constant for the rope discharge but is nearly uniform for the spray discharge. It should be pointed out that although rope discharge (or semi-discharge) is an undesirable operation, hydrocyclones should be operated under conditions as close as possible to roping discharge, to obtain the highest possible underflow concentration (or the smallest water split) in order to minimize the by-pass effect, as suggested by Concha et al (Concha et al., 1996). More importantly, based on the numerical experiments, a diagram is established to predit air core with respect to cyclone size and feed solids concentation and the results are given in Fig. 3.16. It is well established that hydrocyclones operated with the spray discharge run more smoothly than those operated with the rope discharge, and hence the operation with the rope discharge should be avoided .(Concha et al., 1996). This can be well reflected by the present model, as demonstrated in Fig. 3.15. As seen from this figure, the solid flow rate at the underflow fluctuates significantly around a constant for the rope discharge but is nearly uniform for the spray discharge. It should be pointed out that although rope discharge (or semi-discharge) is an undesirable operation, hydrocyclones should be operated under conditions as close as possible to roping discharge, to obtain the highest possible underflow concentration (or the smallest water split) in order to minimize the by-pass effect, as suggested by Concha et al .(Concha et al., 1996). More importantly, based on the numerical experiments, a diagram is established to predit air core with respect to cyclone size and feed solids concentation and the results are given in Fig. 3.16.

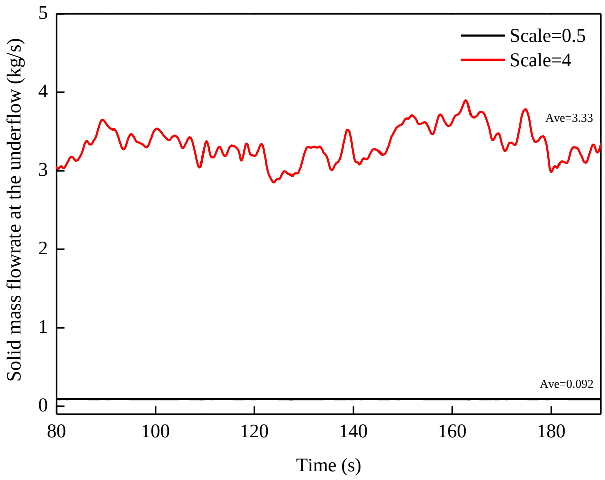

Fig. 3.15 Temporal variation of solid flow rate at the underflow at SC=30%.

Fig. 3.16 shows that three zones can be defined according to the three types of air core as discussed above, which respectively have continuous air core (type I), semi-continuous air core (type II) and no air core (type III). Correspondingly, spray (due to types I and II) and rope (due to type III) discharges should be observed. Fig. 3.16 also shows that under the considered conditions, the air core presents mainly within a larger cyclone at a lower feed solids concentration. Under such a condition, a spray discharge should be achieved and the unit can be operated smoothly.

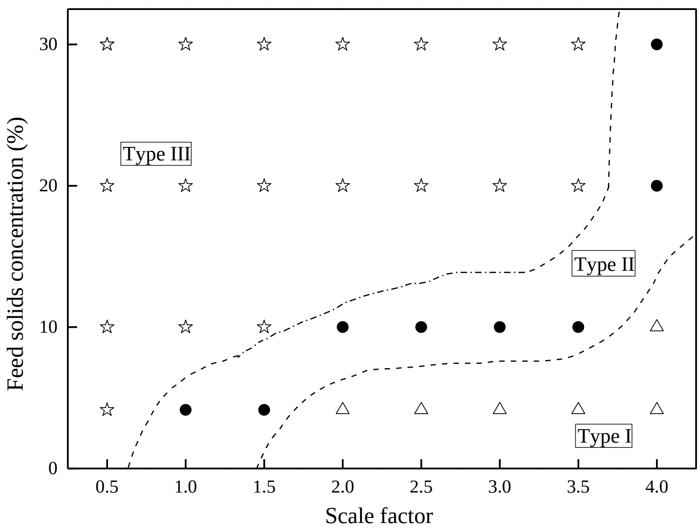

Fig. 3.16 Air core type as a function of cyclone size and feed solids concentration.

3.3.2 **Effect of spigot diameter**

3.3.2.1 Partition curve

Fig. 3.17 shows the effect of spigot diameter and reveals that the separation efficiency increases with the increase of spigot diameter or the decrease of feed solids concentration. This is consistent with the experimental work of Saengchan et al., (2009) who examined the effect of spigot diameters on the recovery of starch particles at feed solids concentrations up to 11% by volume, however, did not provide the information about flow and some key separation coefficient parameters such as partition sharpness. Fig. 3.17 also shows that the difference in the recovery to the underflow between the largest and smallest spigot diameters increases at a higher feed solids concentration. That is, the effect of spigot diameter on separation efficiency is significantly pronounced at high feed solids concentrations.

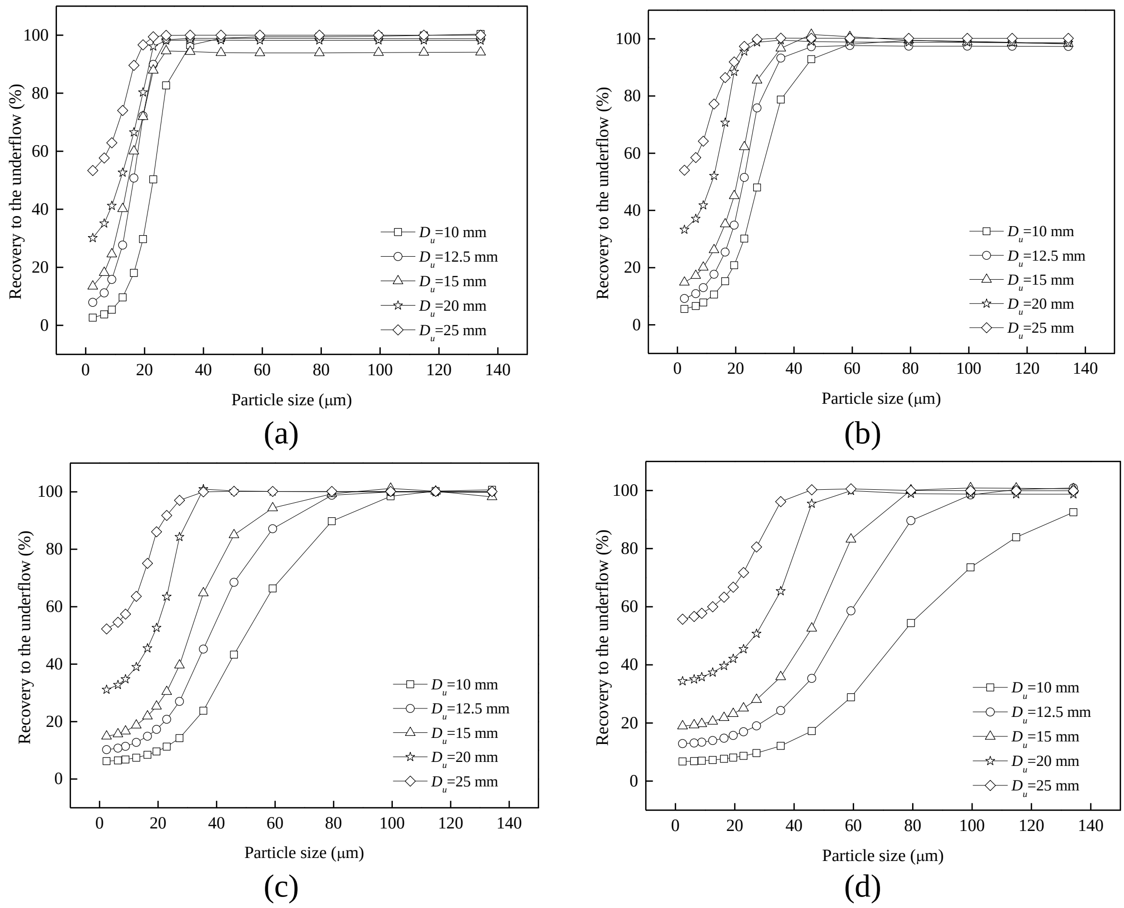

Fig. 3.17 Effect of spigot diameter on the separation efficiency at different feed solids concentrations: (a) 4.14%, (b) 10%, (c) 20%, and (d) 30%.

The above separation behaviors can also be explained by the radial acceleration (Fig. 3.19) calculated from the tangential velocity (Fig. 3.18). Fig. 3.18 shows that a larger spigot diameter leads to an increased tangential velocity. Accordingly, the radial acceleration is increased (Fig. 3.19), resulting in the increased separation efficiency (Fig. 3.17). This applies to all the results obtained here, although for brevity, Fig. 3.18 and Fig. 3.19 include the results of the highest feed solids concentration only.

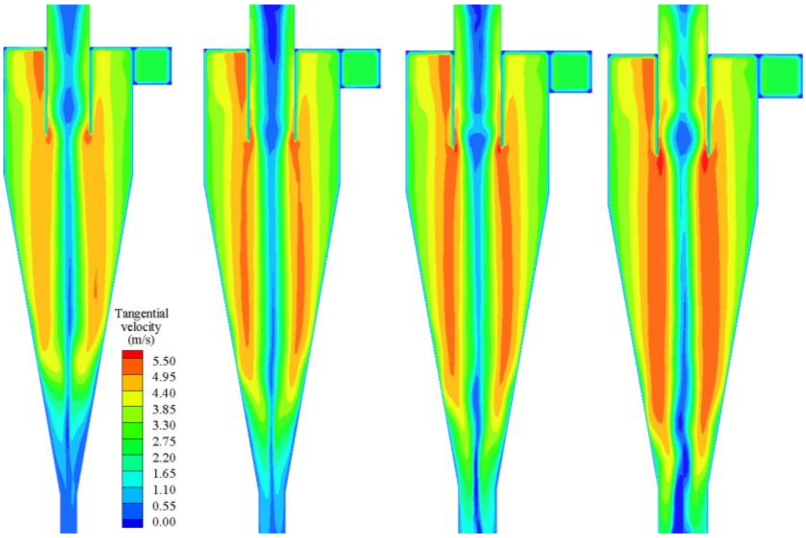

Du=10 mm Du=15 mm Du=20 mm Du= 25 mm

Fig. 3.18 Effect of spigot diameter on the spatial distribution of tangential velocities at SC=30%.

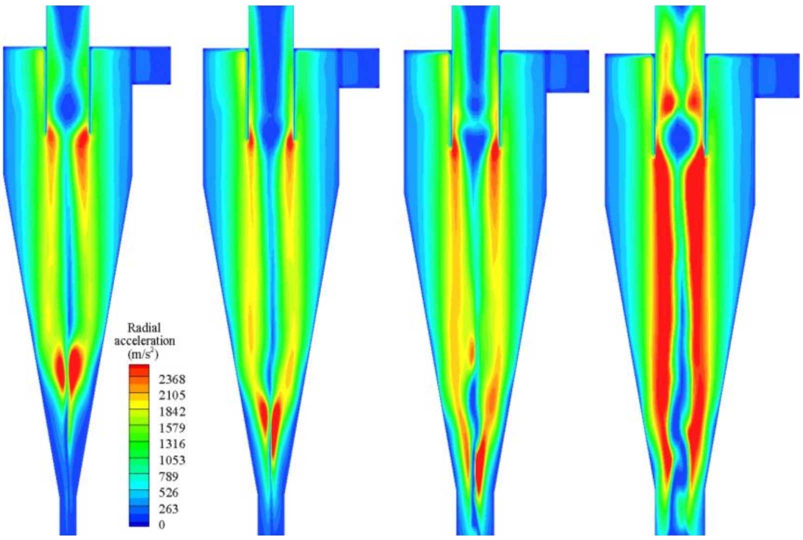

D_u=10 mm D_u=15 mm D_u=20 mm D_u= 25 mm

Fig. 3.19 Effect of spigot diameter on the spatial distribution of radial acceleration at SC=30%.

3.3.2.2 Separation efficiency parameters

Fig. 20 illustrates how the four major separation parameters including the inlet pressure drop, cut size, water split and E_p are quantitatively affected by spigot diameter at different feed solids concentrations. Fig. 20 (a) shows that for a given feed solids concentration, the inlet pressure drop is largely uniform at different spigot diameters due to the collective effect of increased tangential velocity and decreased mixture density.

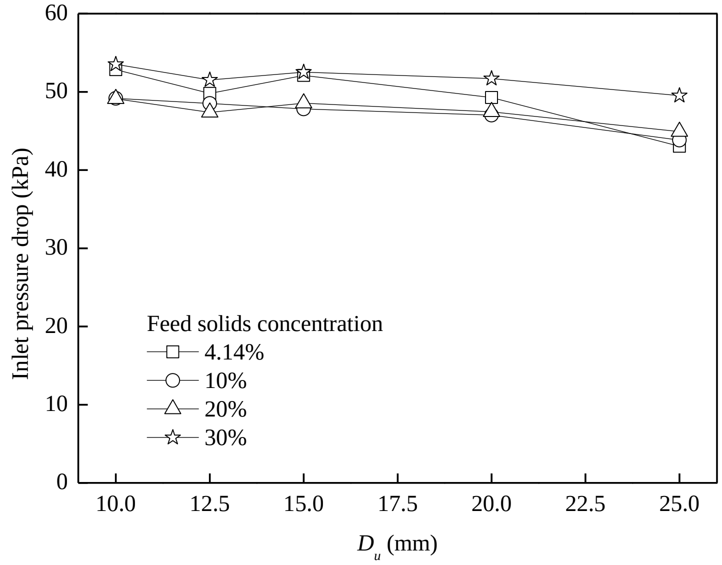

Fig. 3.20 (a) Effect of spigot diameter inlet pressure drop

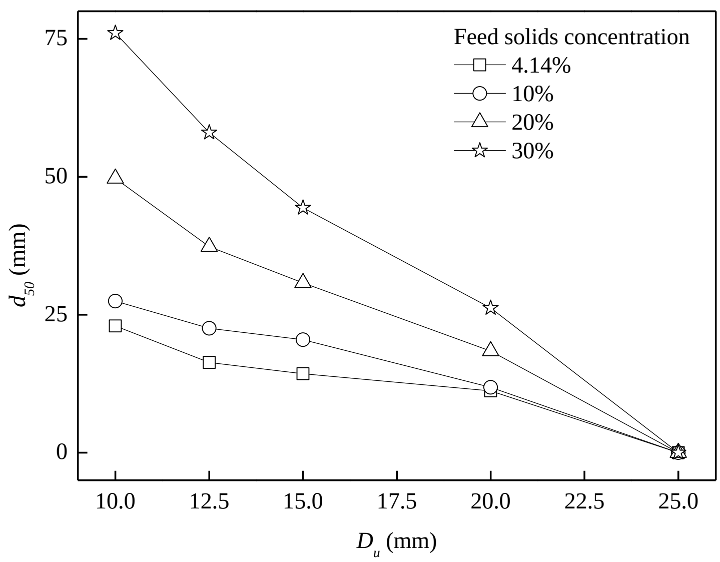

Fig. 3.20 (b) Effect of spigot diameter on cut size

This figure also shows that when the feed solids concentration is increased for a given spigot diameter, the inlet pressure drop decreases first to a minimum and then increases, because the scale factor is here equal to 1, similar to those discussed in Section 3.1.2. Fig. 20 (b) shows that the cut size decreases with the increase of spigot diameter but increases with the increase of feed solids concentration, and the effect of feed solids concentration becomes more significant with decreasing spigot diameter. Again, these results are attributed to the relatively high solids extent inside the spigot. Fig. 3.20 shows that particles become much denser at a decreased spigot diameter. This is pronounced by the increased feed solids concentration. The increased solid concentration leads to a larger settling velocity and an increased cut size, similar to those observed in different sized cyclones. Note that in Fig. 20 (b) the cut size is equal to zero at the largest spigot diameter. This is because for the cyclone with such a large spigot, the water split is larger than 50% (Fig. 20 (c)), and relatively small particles flow down with water and reports to the underflow and thus by-pass the classification process. In general, the water split increases with decreasing spigot diameter (Fig. 20 (c)). Expectedly, it increases with the increase of feed solids concentration. However, compared to spigot diameter, the effect of feed solids concentration is much less significant.

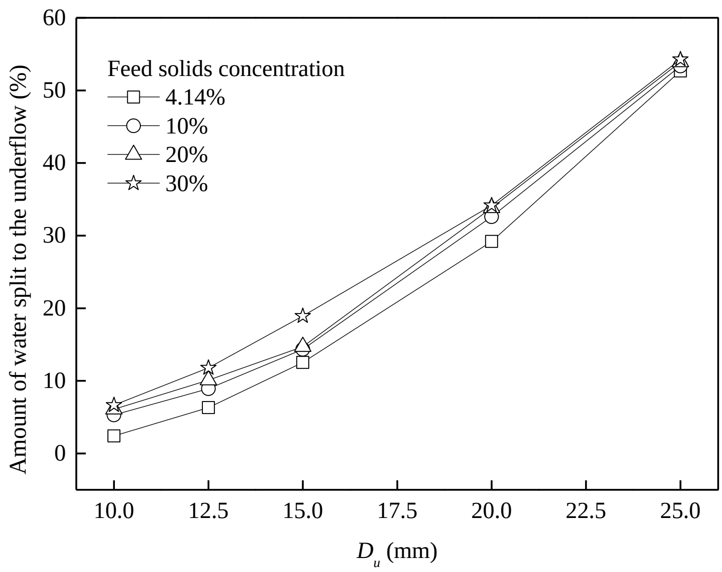

Fig. 3.20 (c) Effect of spigot diameter on amount of water split to underflow

Fig. 20 (d) shows that E_p is affected by spigot diameter in a much more complicated way compared to the cut size and water split. As seen from the figure, at a given feed solids concentration, E_p decreases first to a minimum and then increases and generally slows down. This variation becomes more significant with increasing feed solids concentration. Accordingly, the spigot diameter corresponding to the minimum E_p largely decreases. These results should be attributed to two factors: radial acceleration and by-pass effect associated with water split. When spigot diameter increases, the increased radial acceleration is the dominant factor that accounts for the decrease of E_p. With the further increase of spigot diameter, the increase in by-pass effect due to the increased water split becomes the dominant factor, leading to the increase of E_p. But a further increase in spigot diameter leads to a rapid increase in the radial acceleration (Fig. 3.19), which to a large degree cancels out the effect of the increased by-pass effect and slows down the increase of E_p. The above results suggest that both large and small spigot diameters should not be used in the design of a hydrocyclone in view of product quality, and an optimum spigot diameter exists and the optimum depends on feed solids concentration, as shown in Fig. 20 (d).

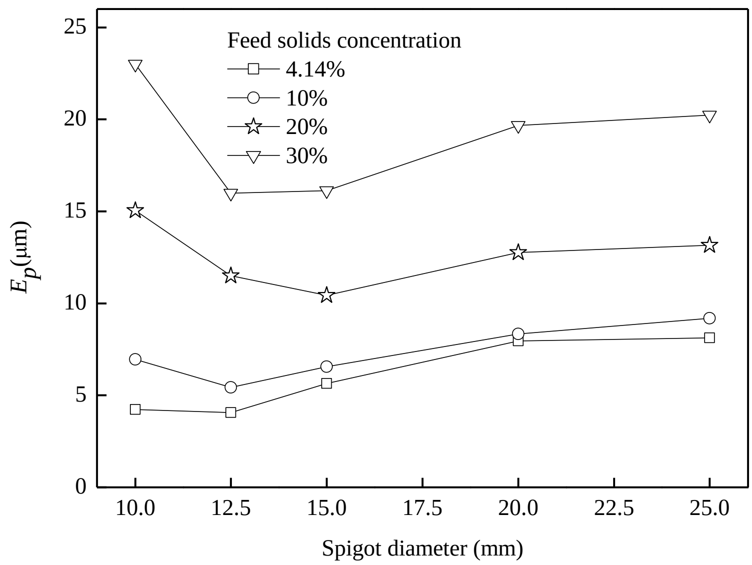

Fig. 20 (d) Effect of spigot diameter on Ecart probable

3.3.3 **Air core**

Fig. 3.21 shows the variation of the air core with spigot diameter at different feed solids concentrations. In this figure, the spigot diameter is also expressed as the ratio of spigot to vortex finder diameters D_u/D_v as this ratio dominates the behaviors of air core and underflow discharge (Concha et al., 1996). As seen from Fig. 3.21, when D_u/D_v is equal to 0.8 and 1.0, the air core exists at all the considered feed solids concentrations and the hydrocyclones can be operated smoothly, although their separation performance is not good in view of product quality (Fig. 18) When D_u/D_v=0.4 and 0.5, a semi-continuous air core is observed at the lowest feed solids concentration and no air core at other feed solids concentration. When D_u/D_v=0.6, three states including continuous air core, semi-continuous air core and no air core can be sequentially observed with increasing feed solids concentration. Corresponding to the above air core states, the operation stability of each cyclone associated with underflow discharge can largely be determined, as discussed in Section 3.1.3. In general, a large spigot can result in an air core and stable operation regardless of feed solids concentration.

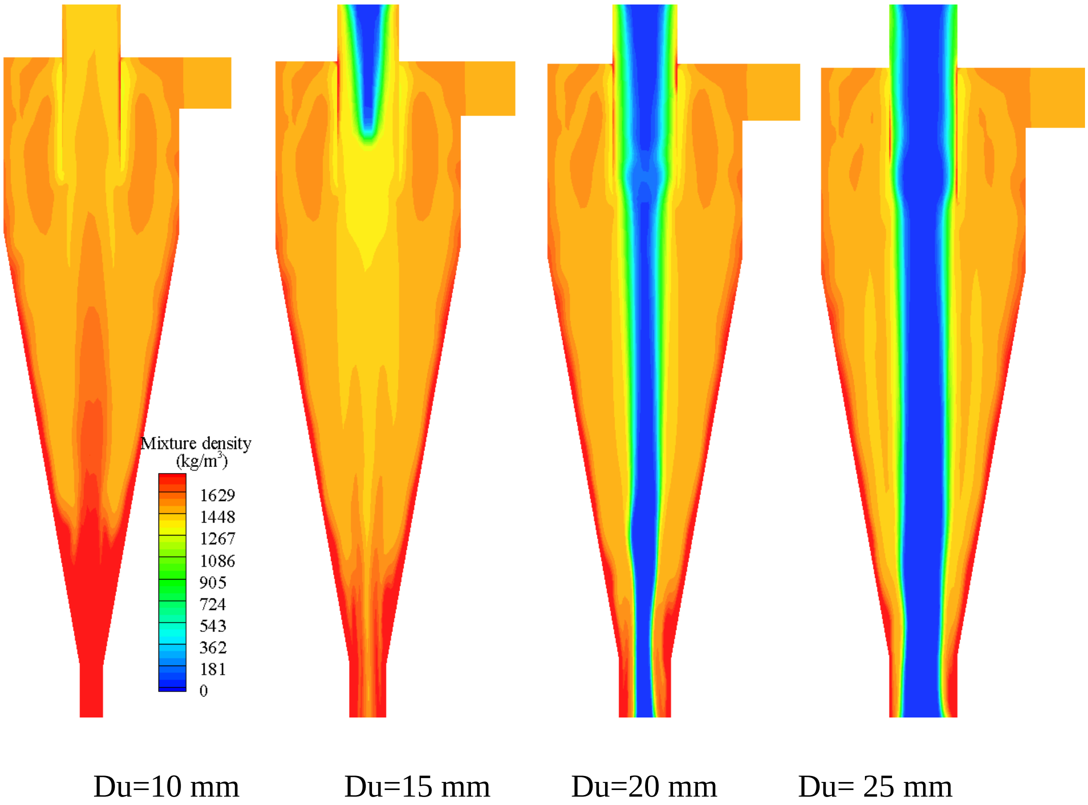

Fig. 3.20 Effect of spigot diameter on spatial distribution of mixture density at SC=30%.

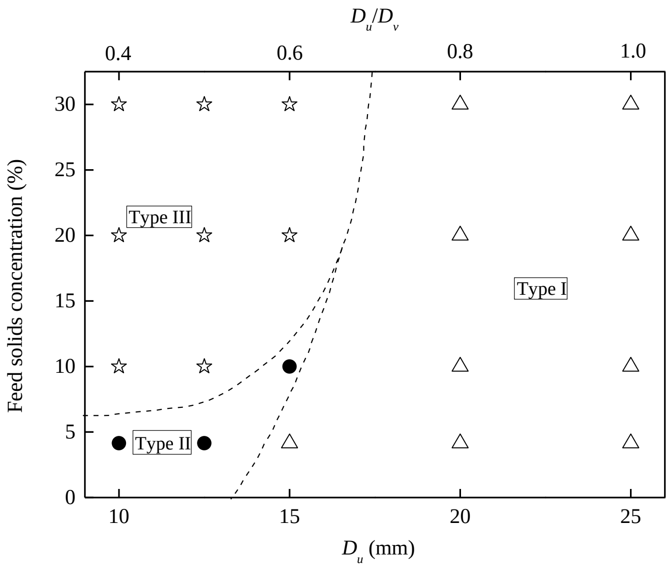

Fig. 3.21 Air core type as a function of spigot diameter and feed solids concentration.

3.4 Conclusions

The flow and performance of hydrocyclones have been numerically studied at a wide range of feed solid concentrations by means of a recently developed two fluid model facilitated by the mixture model, with special reference to the effects of cyclone size and spigot diameter. The findings from the present study are summarized as follows:

(1) The separation efficiency decreases with the increase of cyclone size or the decrease of spigot diameter. Correspondingly, the cut size increases, whereas the water split decreases and hence the by-pass flow decreases. These effects are quantitatively different at different feed solids concentrations and can be well explained by the variation of radial acceleration.

(2) The inlet pressure drop increases with the increase of cyclone size or the increase of spigot diameter. With increasing feed solids concentration, the pressure drop first decreases to a minimum and then increases for relatively small cyclones, however, monotonically increases for the relatively large cyclones. These behaviours can be attributed to the collective effect of tangential velocity, mixture density and scale factor.

(3) The separation sharpness increases with the decrease of cyclone size or feed solids concentration due to the increased radial acceleration. However, with increasing spigot

diameter, the separation sharpness decreases first and then increases and flattened out due to the increased radial acceleration and by-pass effect in proportion with water split. There exists an optimum spigot diameter under given operational conditions.

(4) The pressure drop within the spigot controls the formation of air core. Two diagrams can be established to predict air core with respect to cyclone size, spigot diameter and feed solid concentration. It is shown that air core may be suppressed by small spigot diameter, high feed solids concentration and small cyclone.

REFERENCES

Atkinson, B., Swanson, A., 2008, Improved efficiency of fine coal classification. ACARP report, C15059.
Azadi, M., Azadi, M., Mohebbi, A., 2010. A CFD study of the effect of cyclone size on its performance parameters. Journal of Hazardous Materials, 182 (1-3), 835-841.
Baskakov, A. P., Dolgov, V. N., Goldobin, Y. M., 1990. Aerodynamics and heat-transfer in cyclones with particle-laden gas flow. Experimental Thermal and Fluid Science, 3 (6), 597-602.
Bergström, J., Vomhoff, H., Söderberg, D., 2007. Tangential velocity measurements in a conical hydrocyclone operated with a fibre suspension. Minerals Engineering, 20 (4), 407-413.
Bhaskar, K., Murthy, Y., Raju, M., Tiwari, S., Srivastava, J., Ramakrishnan, N., 2007a. CFD simulation and experimental validation studies on hydrocyclone. Minerals Engineering, 20 (1), 60-71.
Bhaskar, K. U., Murthy, Y. R., Ramakrishnan, N., Srivastava, J. K., Sarkar, S., Kumar, V., 2007b. CFD validation for flyash particle classification in hydrocyclones. Minerals Engineering, 20 (3), 290-302.
Bradley, D., 1965. The Hydrocyclone; Pergamon. London, 1965.
Braun, T., Bohnet, M., 1990. Influence of feed solids concentration on the performance of hydrocyclones. Chemical Engineering & Technology, 13 (1), 15-20.
Brennan, M., 2006. CFD simulations of hydrocyclones with an air core - Comparison between large eddy simulations and a second moment closure. Chemical Engineering Research & Design, 84 (A6), 495-505.
Brennan, M. S., Narasimha, M., Holtham, P. N., 2007. Multiphase modelling of hydrocyclones - prediction of cut-size. Minerals Engineering, 20 (4), 395-406.
Chang, Y. F., Ilea, C. G., Aasen, L., Hoffmann, A. C., 2011. Particle flow in a hydrocyclone investigated by positron emission particle tracking. Chemical Engineering Science, 66 (18), 4203-4211.
Chen, W., Zydek, N., Parma, F., 2000. Evaluation of hydrocyclone models for practical applications. Chemical engineering journal, 80 (1-3), 295-303.
Chiné, B., Concha, F., 2000. Flow patterns in conical and cylindrical hydrocyclones. Chemical Engineering Journal, 80 (1–3), 267-273.
Chu, K. W., Wang, B., Xu, D. L., Chen, Y. X., Yu, A. B., 2011. CFD-DEM simulation of the gas-solid flow in a cyclone separator. Chemical Engineering Science, 66 (5), 834-847.
Chu, K. W., Wang, B., Yu, A. B., Vince, A., 2009. CFD-DEM modelling of multiphase flow in dense medium cyclones. Powder Technology, 193 (3), 235-247.
Chu, K. W., Wang, B., Yu, A. B., Vince, A., 2012. Computational study of the multiphase flow in a dense medium cyclone: Effect of particle density. Chemical Engineering Science, 73 123-139.
Chu, L. Y., Chen, W. M., 1993. Research on the motion of solid particles in a hydrocyclone. Separation Science and Technology, 28 (10), 1875-1886.
Chu, L. Y., Chen, W. M., Lee, X. Z., 2000. Effect of structural modification on hydrocyclone performance. Separation and Purification Technology, 21 (1-2), 71-86.
Chu, L. Y., Chen, W. M., Lee, X. Z., 2002. Effects of geometric and operating parameters and feed characters on the motion of solid particles in hydrocyclones. Separation and Purification Technology, 26 (2-3), 237-246.

Concha, F., Barrientos, A., Montero, J., Sampaio, R., 1996. Air core and roping in hydrocyclones. International Journal of Mineral Processing, 44-45 743-749.
Dai, G. Q., Chen, W. M., Li, J. M., Chu, L. Y., 1999. Experimental study of solid-liquid two-phase flow in a hydrocyclone. Chemical Engineering Journal, 74 (3), 211-216.
Davailles, A., Climent, E., Bourgeois, F., 2012a. Fundamental understanding of swirling flow pattern in hydrocyclones. Separation and Purification Technology, 92 (0), 152-160.
Davailles, A., Climent, E., Bourgeois, F., Majumder, A. K., 2012b. Analysis of swirling flow in hydrocyclones operating under dense regime. Minerals Engineering, 31 (0), 32-41.
Dyakowski, T., Williams, R. A., 1996. Prediction of high solids concentration regions within a hydrocyclone. Powder Technology, 87 (1), 43-47.
Fisher, M. J., Flack, R. D., 2002. Velocity distributions in a hydrocyclone separator. Experiments in Fluids, 32 (3), 302-312.
Fontein, F. J., van Kooy, J. G., Lelliger, H. A., 1962. The influence of some variables upon hydrocyclones performance. British Chemical Engineering, 7 410-421.
Ghodrat, M., Kuang, S. B., Yu, A. B., Vince, A., Barnett, G. D., Barnett, P. J., 2013a. Computational study of multiphase flow and performance of hydrocyclone: effects of cyclone size and spigot diameter. Industrial & Engineering Chemistry Research, http://dx.doi.org/10.1021/ie402267b.
Ghodrat, M., Kuang, S. B., Yu, A. B., Vince, A., Barnett, G. D., Barnett, P. J., 2013b. Computational Study of the Multiphase Flow and Performance of Hydrocyclones: Effects of Cyclone Size and Spigot Diameter. Industrial & Engineering Chemistry Research, 52 (45), 16019-16031.
Hararah, M. A., Endres, E., Dueck, J., Minkov, L., Neesse, T., 2010. Flow conditions in the air core of the hydrocyclone. Minerals Engineering, 23 (4), 295-300.
Hsieh, K. T., 1988. Phenomenological model of the hydrocyclone. PhD thesis, The University of Utah, Salt Lake City, UT, USA.
Hsieh, K. T., Rajamani, R. K., 1991. Mathematical model of the hydrocyclone based on physics of fluid flow. AIChE J, 37 (5), 735-746.
Huang, S., 2005. Numerical simulation of oil-water hydrocyclone using reynolds-stress model for Eulerian multiphase flows. Canadian Journal of Chemical Engineering, 83 (5), 829-834.
Inaki Schlaberg, H., Podd, F. J. W., Hoyle, B. S. Ultrasound process tomography system for hydrocyclones. Ultrasonics International 1999 Joint with 1999 World Congress on Ultrasonics, 29 June-1 July 1999, Netherlands,
Inaki Schlaberg, H., Podd, F. J. W., Hoyle, B. S., 2000b. Ultrasound process tomography system for hydrocyclones. Ultrosonics, 38 813-816.
Kawatra, S. K., Bakshi, A. K., Rusesky, M. T., 1996. Effect of viscosity on the cut (d50) size of hydrocyclone classifiers. Minerals Engineering, 9 (8), 881-891.
Kelsall, D. F., 1953. A further study of the hydraulic cyclone. Chemical Engineering Science, 2 (6), 254-272.
Knowles, S. R., Woods, D. R., Feuerstein, I. A., 1973. The velocity distribution within a hydrocyclone operating without an air core. The Canadian Journal of Chemical Engineering, 51 (3), 263-271.
Kraipech, W., Chen, W., Dyakowski, T., Nowakowski, A., 2006. The performance of the empirical models on industrial hydrocyclone design. International Journal of Mineral Processing, 80 (2-4), 100-115.

Krishna, V., Sripriya, R., Kumar, V., Chakraborty, S., Meikap, B. C., 2010. Identification and prediction of air core diameter in a hydrocyclone by a novel online sensor based on digital signal processing technique. Chemical Engineering and Processing: Process Intensification, 49 (2), 165-176.
Kuang, S. B., Chu, K. W., Yu, A. B., Vince, A., 2012a. Numerical study of liquid-gas-solid flow in classifying hydrocyclones: effect of feed solids concentration. Minerals Engineering, 31 17-31.
Kuang, S. B., Chu, K. W., Yu, A. B., Vince, A., 2012b. Numerical study of liquid–gas–solid flow in classifying hydrocyclones: Effect of feed solids concentration. Minerals Engineering, 31 (0), 17-31.
Kuang, S. B., Qi, Z., Yu, A. B., Vince, A., Barnett, G. D., Barnett, P. J., 2013. CFD modelling and analysis of the multiphase flow and performance of dense medium cyclones. Minerals Engineering, http://dx.doi.org/10.1016/j.mineng.2013.10.012.
Launder, B. E., Reece, G. J., Rodi, W., 1975. Progress in the development of a Reynolds-stress turbulence closure. Journal of Fluid Mechanics, 68 537-566.
Li, S. H., Zhang, H., Yang, H. R., Yang, S., Lu, J. F., Yue, G. X., 2007. Determining cyclone particle holdup by pressure drop for a CFB boiler. Chemical Engineering & Technology, 30 (12), 1726-1731.
Lim, E. W. C., Chen, Y.-R., Wang, C.-H., Wu, R.-M., 2010. Experimental and computational studies of multiphase hydrodynamics in a hydrocyclone separator system. Chemical Engineering Science, 65 (24), 6415-6424.
Lynch, A. J., 1976. Mineral crushing and grinding circuits. Elsevier, Amsterdam.
Manninen, M., Taivassalo, V., Kallio, S., 1996. On the mixture model for multiphase flow. VTT Publications 288, Technical Research Centre of Finland.
Marins, L. P. M., Duarte, D. G., Loureiro, J. B. R., Moraes, C. A. C., Freire, A. P. S., 2010. LDA and PIV characterization of the flow in a hydrocyclone without an air-core. Journal of Petroleum Science and Engineering, 70 (3-4), 168-176.
Milin, L., Hsieh, K. T., Rajamani, R. K., 1992. The leakage mechanisms in the hydrocyclone. Minerals Engineering, 5 (7), 779-794.
Min'kov, L. L., Dueck, J. H., 2012. Numerical modeling of a nonmonotonic separation hydrocyclone curve. Journal of Engineering Physics and Thermophysics, 85 (6), 1317-1326.
Mousavian, S. M., Najafi, A. F., 2009. Numerical simulations of gas-liquid-solid flows in a hydrocyclone separator. Archive of Applied Mechanics, 79 (5), 395-409.
Narasimha, M., Brennan, M., Holtham, P. N., 2006. Large eddy simulation of hydrocyclone - prediction of air-core diameter and shape. International Journal of Mineral Processing, 80 (1), 1-14.
Narasimha, M., Brennan, M., Holtham, P. N., 2007a. A review of CFD modelling for performance predicitons of hydrocyclone. Engineering Applications of Computational Fluid Mechanics, 1 (2), 109-125.
Narasimha, M., Brennan, M. S., Holtham, P. N., 2012. CFD modeling of hydrocyclones: Prediction of particle size segregation. Minerals Engineering, 39 (0), 173-183.
Narasimha, M., Brennan, M. S., Holtham, P. N., Napier-Munn, T. J., 2007b. A comprehensive CFD model of dense medium cyclone performance. Minerals Engineering, 20 (4), 414-426.
Neesse, T., Dueck, J., 2007. Air core formation in the hydrocyclone. Minerals Engineering, 20 (4), 349-354.

Noroozi, S., Hashemabadi, S. H., 2009. CFD simulation of inlet design effect on deoiling hydrocyclone separation efficiency. Chemical Engineering and Technology, 32 (12), 1885-1893.
Nowakowski, A. F., Cullivan, J. C., Williams, R. A., Dyakowski, T., 2004. Application of CFD to modelling of the flow in hydrocyclones. Is this a realizable option or still a research challenge? Minerals Engineering, 17 (5), 661-669.
Nowakowski, A. F., Kraipech, W., Williams, R. A., Dyakowski, T., 2000. The hydrodynamics of a hydrocyclone based on a three-dimensional multi-continuum model. Chemical Engineering Journal, 80 (1-3), 275-282.
O'Brien, M., Taylor, A., Nemeth, D., Firth, B., Clarkson, C., 2000, Large diameter classifying cyclones. ACARP report, C6047.
Pascoe, R. D., 2006. Investigation of hydrocyclones for the separation of shredded fridge plastics. Waste Management, 26 (10), 1126-1132.
Plitt, L. R., 1976. A mathematical model of the hydrocyclone classifier. Cim Bulletin 69 (3), 114-123.
Rong, R., 2007, Industial trials of novel cyclones. ACARP report, C14067.
Saengchan, K., Nopharatana, A., Songkasiri, W., 2009. Enhancement of tapioca starch separation with a hydrocyclone: effects of apex diameter, feed concentration, and pressure drop on tapioca starch separation with a hydrocyclone. Chemical Engineering and Processing: Process Intensification, 48 (1), 195-202.
Slechta, J., Firth, B. A., 1984. Classification of fine coal with a hydrocyclone. International Journal of Mineral Processing, 12 (4), 213-237.
Svarovsky, L., 1984. Hydrocyclones. Holt, Rinehart and Winston, Sydney.
Svarovsky, L., Thew, M. T., 1992. Hydrocyclones: analysis and applications. Kluwer Academic Publishers, MA, USA.
Swain, S., Mohanty, S., 2013. A 3-dimensional Eulerian–Eulerian CFD simulation of a hydrocyclone. Applied Mathematical Modelling, 37 (5), 2921-2932.
Wang, B., Chu, K. W., Yu, A. B., 2007. Numerical study of particle-fluid flow in a hydrocyclone. Industrial & Engineering Chemistry Research, 46 (13), 4695-4705.
Wang, B., Chu, K. W., Yu, A. B., Vince, A., 2009. Modeling the Multiphase Flow in a Dense Medium Cyclone. Industrial & Engineering Chemistry Research, 48 (7), 3628-3639.
Wang, B., Yu, A. B., 2006. Numerical study of particle-fluid flow in hydrocyclones with different body dimensions. Minerals Engineering, 19 (10), 1022-1033.
Wang, B., Yu, A. B., 2008. Numerical study of the gas-liquid-solid flow in hydrocyclones with different configuration of vortex finder. Chemical Engineering Journal, 135 (1-2), 33-42.
Wang, B., Yu, A. B., 2010. Computational investigation of the mechanisms of particle separation and "fish-hook" phenomenon in hydrocyclones. AIChE J, 56 (7), 1703-1715.
Williams, R. A., Dickin, F. J., Gutierrez, J. A., Dyakowski, T., Beck, M. S., 1997. Using electrical impedance tomography for controlling hydrocyclone underflow discharge. Control Engineering Practice, 5 (2), 253-6.
Yang, Q., Wang, H. L., Liu, Y., Li, Z. M., 2010. Solid/liquid separation performance of hydrocyclones with different cone combinations. Separation and Purification Technology, 74 (3), 271-279.
Yang, Q., Wang, H. L., Wang, J. G., Li, Z. M., Liu, Y., 2011. The coordinated relationship between vortex finder parameters and performance of hydrocyclones for separating light dispersed phase. Separation and Purification Technology, 79 (3), 310-320.

Yoshioka, N., Hotta, Y., 1955. Liquid cyclone as a hydraulic classifier. Chemical Engineering Japan, 19 (12), 633-641.
Zhang, Y., Qian, P., Liu, Y., Wang, H., 2011a. Experimental study of hydrocyclone flow field with different feed concentration. Industrial and Engineering Chemistry Research, 50 (13), 8176-8184.
Zhang, Y. H., Qian, P., Liu, Y., Wang, H. L., 2011b. Experimental study of hydrocyclone flow field with different feed concentration. Industrial and Engineering Chemistry Research, 50 (13), 8176-8184.
Zhou, Z. Y., Kuang, S. B., Chu, K. W., Yu, A. B., 2010. Discrete particle simulation of particle-fluid flow: model formulations and their applicability. Journal of Fluid Mechanics, 661 482-510.
Zhu, H. P., Zhou, Z. Y., Yang, R. Y., Yu, A. B., 2007. Discrete particle simulation of particulate systems: Theoretical developments. Chemical Engineering Science, 62 (13), 3378-3396.
Zhu, H. P., Zhou, Z. Y., Yang, R. Y., Yu, A. B., 2008. Discrete particle simulation of particulate systems: A review of mayor applications and findings. Chemical Engineering Science, 63 5728-5770.

CHAPTER 4[2]

NUMERICAL ANALYSIS OF HYDROCYCLONES WITH DIFFERENT CONICAL SECTION DESIGNS

Hydrocyclones generally follow a conventional design and may have some limitations on separation performance. This chapter presents a numerical study of hydrocyclones, with different conical configurations, using a recently developed computational fluid dynamics method. The feed solids concentration considered is up to 30 % (by volume), which is well beyond the range reported before. The numerical results show that the cyclone performance is sensitive to both the length and shape of the conical section, as well as the feed solids concentration. A longer conical section length leads to a decreased inlet pressure drop, cut size d_{50}, and Ecart probable E_p, and at the same time, an increased water split (thus larger by-pass effect). When conical shape varies from the concave to convex styles gradually, a compromised optimum performance is observed for the cyclone with a convex cone, resulting in a minimum E_p and relatively small inlet pressure drop and water split. Almost all these effects are pronounced with increasing feed solids concentration. Based on the numerical experiments, a new hydrocyclone featured with a long convex cone is proposed. It can improve the performance of the conventional cyclone at all the feed solids concentrations considered.

---

[2] Content of this chapter published in Minerals Engineering 2014, Ghodrat, M., Kuang, S. B., Yu, A. B., Vince, A., Barnett, G. D., Barnett, P. J., 2014. Numerical analysis of hydrocyclones with different conical section designs. Minerals Engineering, 62 (0), 74-84

4.1 Introduction

Hydrocyclones are widely used to classify solids by size in many industries due to their design simplicity, high capacity, low maintenance and operational costs. However, there are different problems associated with such a separator, such as high energy loss, misplaced particles in both the overflow and underflow, and limited sharpness of the cut in particle sizes between the fine and coarse streams. To date, how to overcome these problems is still a challenge.

The structure of the hydrocyclone affects cyclone performance depending on operational conditions and materials to be handled. Such effects should be known for practical applications of hydrocyclones. In this respect, various studies have been carried out in the past to investigate the flow and performance of hydrocyclones with different conical configurations. For example, based on studies of a series of variables, Fontein et al., (1962) suggested that the conical section should be as long as possible, but the cylindrical section is retained for the purpose of providing a convenient feed opening, especially in small cyclones. Similarly, Svarosky (1984) reported that the cylindrical section may be short or even omitted, whereas the conical section is essential. Chiné and Concha (2000) compared the conical and cylindrical hydrocyclones and revealed that the tangential velocities of the liquid phase within the two cyclones are similar but the axial velocities are different. Chu et al., (2000) assessed different structural modifications and showed that the modification of the conical part affects the cyclone performance. In that work, two specific conical shapes were considered and it was found that both the concave and convex designs lead to increased separation sharpness and cut size, compared to the conventional design. However, only the convex design caused a decreased energy loss and flow split. Chu et al., (2002) also observed that the particle radial velocity, which determines the separation efficiency, is higher for a hydrocyclone with a conical section of longer length, at a given cone angle. Recently, Wang and Yu (2006) quantified the effects of conical section length and other geometrical variables on separation efficiency and flow characteristics. Their results confirmed the importance of the conical part as reported by Fontein et al., (1962) and Svarosky (1984). Yang et al. (2010) introduced a two-cone combination instead of the conventional single cone, and showed that the modification can lead to a better hydrocyclone performance. All these studies mainly based on experiments, suggest that a better design of the conical part should be beneficial to the cyclone performance. However, most of them focused on operations at low feed solids concentrations. To date, the effects of the conical part on the flow and performance of hydrocyclones are not clear, particularly when hydrocyclones are operated at different feed solids concentrations as widely used in practice (see, e.g., Slechta and Firth, 1984; Dyakowski and Williams, 1996; O'Brien et al., 2000; Hararah et al., 2010; Zhang et al., 2011b). Also, systematic studies of geometrical variables including those related to the conical part are lacking. Usually, hydrocyclones are designed on the basis of empirical models. The most widely known model is Plitt model, which however may be unbound to practical limits and yield unrealistic results (Svarovsky and Thew, 1992). In principle, these problems can be overcome by numerical simulations which are often carried out under well controlled conditions for a wide range of applications. Although numerical simulations provide insight and potential solution, the proposed designs are required to be tested for industrial applications.

In recent years, various numerical studies have been done for better designing and controlling hydrocyclones (see, for example, the reviews by Nowakowski et al., (2004) and Narasimha et al., (2007a). The numerical models were mainly based on CFD-LPT (Computational Fluid Dynamics-Lagrangian Particle Tracking) and TFM (Two-Fluid Model) approaches. In the former, the motion of discrete particles is obtained by LPT which applies Newton's laws of motion to a particle, and the flow of continuum fluid is described by the local averaged Navier–Stokes equations that can be solved by the traditional CFD. However, it traces only the motion of a single particle, and the effect of inter-particle interactions and the reaction of particles on the fluid are ignored. Therefore, although widely used in the previous studies, CFD-LPT is applicable only to dilute-phase flows or very low feed solids concentrations, hence has significant limitations in applied research.

In the TFM approach, on the other hand, both the fluid and solid phases are treated as interpenetrating continuum media at a computational cell scale that is much larger than individual particles but still smaller compared to the size of the process equipment. Further, the flows of continuum fluids are described by the local averaged Navier-Stokes equations that can be solved by CFD, with the coupling of fluid and solid phases being considered through the interactions between the particles and the fluid. It can, to a large extent, overcome the problems associated with the CFD-LPT model and has been increasingly used to study hydrocyclones in dense and/or dilute regimes by different investigators (Nowakowski et al., 2000; Huang, 2005; Brennan et al., 2007; Noroozi and Hashemabadi, 2009; Davailles et al., 2012b; Kuang et al., 2012a; Min'kov and Dueck, 2012; Narasimha et al., 2012; Swain and Mohanty, 2013). However, while confirming the capability of the TFM approach, the previous studies have not covered the geometrical effects on the hydrocyclone flow and performance.

In this chapter, hydrocyclones of different conical configurations have been studied in a wide range of feed solids concentrations using a recently developed TFM model (Kuang et al., 2012a). This aims at gaining a better understanding of the effects of the conical part on the flow and performance of hydrocyclones, and identifying possible methods to improve the cyclone performance. First, the effects of the length and shape of the conical section are studied. On this basis, a new hydrocyclone design is proposed by replacing the conventional cone with a long convex cone. The results show that the new hydrocyclone has a better performance compared to the conventional cyclone at all the feed solids concentrations considered.

4.2 Simulation method and conditions

The present section is based on the Two Fluid Model (TFM), facilitated with the mixture model which has been proved to be valid for hydrocyclones (Kuang et al., 2012a; Ghodrat et al., 2013a). The detail of the model has been discussed in section 2.7.3. For completeness, only the key features of the model are described below.

In the model, both the fluid (liquid and air) and solid phases are treated as interpenetrating continua. Particles of different sizes or densities represent different phases. In this study, the density is considered constant, while the size is specified according to the size distribution given. To carry out a simulation, the size distribution is divided into a series of size intervals, with each represented by a mean size in the simulation. The flow of liquid-gas-solid mixture (as a single phase) is calculated from the continuity and the Navier–Stokes equations based on the local mean variables over a computational cell, considering slip velocities between different phases (Manninen et al., 1996). This gives the interface between the liquid and air core and the flows of liquid and particles of different sizes. The turbulent flow of the liquid-gas-solid mixture is modelled using the Reynolds stress model (Launder et al., 1975). The solid properties are described by the kinetic theory based on the algebraic temperature model (Syamlal et al., 1993). The applicability of the model has been verified by the good agreement between the measured and calculated results in terms of hydrocyclone flow and performance at different feed solids concentrations, as discussed elsewhere (Kuang et al., 2012a). Here, the model is directly used to conduct numerical experiments to study the effects of different conical configurations.

The present operational and geometrical conditions, as listed in Table 4.1, follow Hsieh's experimental work (1988), whose measurements have been widely used in the literature to validate various numerical models including the present model.

Table 4-1 Geometrical and operational conditions used in the simulations

Parameter	Symbol	Value*
Geometrical parameters		
Diameter of the body	D_c	75 mm
Diameter of inlet	D_i	25 mm
Diameter of vortex finder	D_o	25 mm
Diameter of apex	D_u	12.5 mm
Length of cylindrical part	L_c	75 mm
Length of conical part	L_{co}	186 (35-385) mm
Length of vortex finder	L_v	50 mm
Cone angle	α	20°
Conical shape factor	n	1.4 (0.3-3)
Operational conditions		
Inlet velocity	u	2.49 m/s
Particle material		Limestone
Particle density	ρ_p	2700 kg/m^3
Feed solids concentration	SC	4.14 (4.14-30) % by volume
Particle sizes simulated	d	2.4~134 μm

*for the base case, with their varying ranges in the brackets

Two geometrical variables are considered here: length and shape of the conical section. The conical section length L_{co} is varied from 35 mm to 385 mm at a fixed spigot diameter, selected according to the work of Wang and Yu (2006) for comparison, who studied the effect of conical section length in a dilute regime. Note that both dilute and dense regimes are considered for the two geometrical variables in this study by varying the feed solids concentration SC from 4 to 30% by volume. The shapes include concave, straight (conventional design), and convex types. The function of $z=(r-D_c/2)^n/(D_u/2)$ was proposed to describe all the shapes, where z was the vertical distance of the conical surface away from the spigot bottom, r was the radial distance of the conical surface away from the central line of the cyclone; D_c and D_u were the cylinder and spigot diameters, respectively; and n was referred to as the conical shape factor and varies between 0.3 and 3. By definition, the cone was concave at $n<1$, convex at $n>1$ and straight at $n=1$ (see Fig. 4.1). All the cyclones considered have the same inlet, cylinder, and vortex finder as those of the base case. The same grid scheme as used and tested elsewhere (Wang and Yu, 2006,2008,2010; Kuang et al., 2012a) is applied to all the cyclones considered, so that the solutions are independent of the mesh size used. A "velocity inlet" boundary condition is used at the cyclone inlet, and the "pressure-outlet" condition at both outlets. The inlet velocity is 2.49 m/s, and the pressure at the two outlets (vortex finder and spigot) is 1 atm, corresponding to the ambient atmospheric pressure. For particles, their (true) density is 2700 kg/m^3, and size range lies between 2.4 and 134 μm based on the same size distribution as used in the experiments (Hsieh, 1988). The distribution is represented by 15 sizes in the simulations.

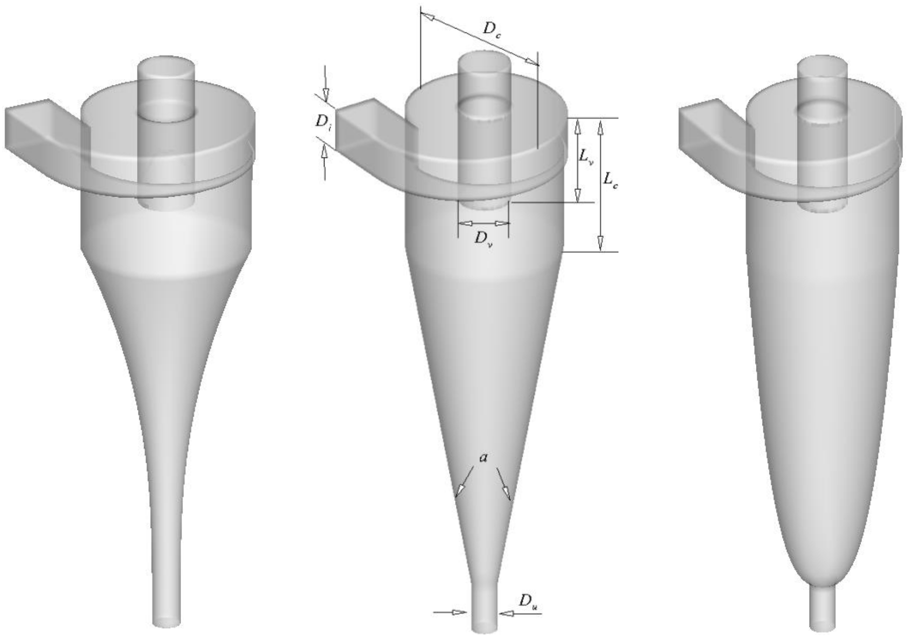

n=0.3 (concave) n=1 (standard) n=3 (convex)

Fig. 4.1 Hydrocyclones with cones of different shapes

All the simulations were conducted using the ANSYS Fluent CFD software package (version 14) in NCI (National Computational Infrastructure) in Australia. Sixteen CPUs were assigned to each simulation, which lasts for about 14 days for computing the physical time of about 35 seconds to ensure that the steady-state flow was achieved. The steady state was identified by the feature that the macroscopic flow characteristics just fluctuate around their respective mean values. This study focuses on the steady-state results. Unless otherwise noted, all the results shown are time-averaged.

4.3 Results and discussion

4.3.1 Effect of conical section length

Fig. 4.2 shows the effect of the conical section length on the separation efficiency at high (*SC*=30%) and low (*SC*=4.14%) feed solids concentrations. It can be seen from the figure that for a given feed solids concentration, the cut size of the separation efficiency increases with the increase of conical section length. The increase is overall smooth at *SC*=4.14% but not at *SC*=30%, particularly when the conical section length is not long enough. In general, for the cyclone operated at a low feed solids concentration (*SC*=4.14%), the results obtained here are similar to those reported by Wang and Yu (2006) based on the CFD-LPT simulations which, however, cannot give the results at the higher feed solids concentrations.

Fig. 4.3 shows the effects of feed solids concentration on the cyclones with different conical section lengths. As seen from this figure, the separation efficiency decreases with the increase of feed solids concentration when the conical section length is long enough (Fig. 4.3b), as observed experimentally by O'Brien et al. (2000) and Milin et al., (1992). Conversely, when the conical section length is too short, with increasing feed solids concentration, the separation efficiency initially drops drastically, and then varies within a relatively narrow range (Fig. 4.2a).

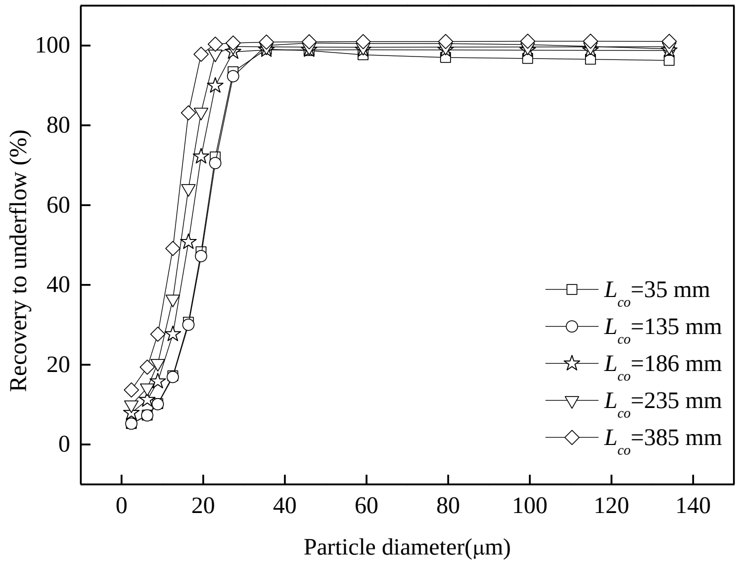

(a)

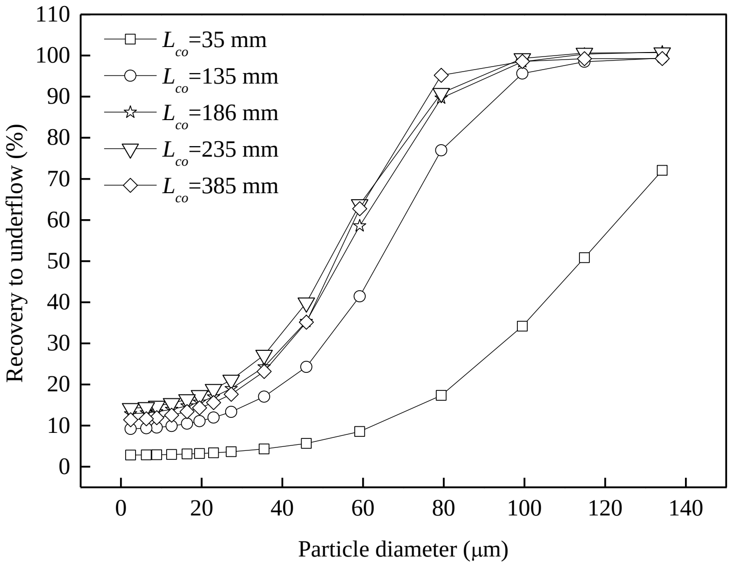

(b)

Fig. 4.2 Effect of conical section length on separation efficiency at the feed solids concentration of: (a) SC=4.14% and (b) SC=30%.

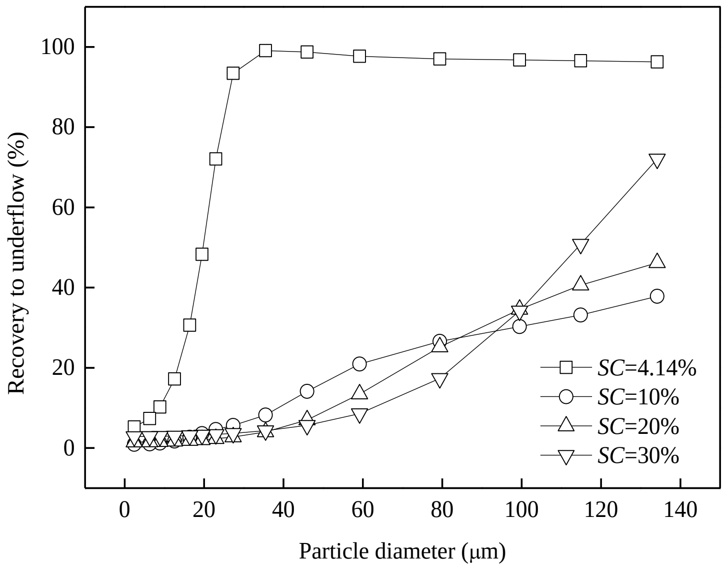

(a)

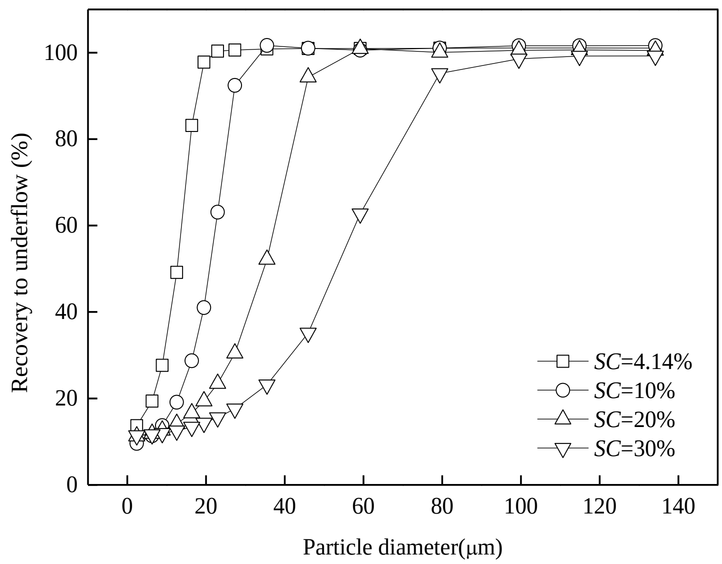

(b)

Fig. 4.3 Effect of feed solids concentration on separation efficiency for the cyclone with the conical section length of: (a) L_{co}=35 mm, and (b) L_{co}=385 mm.

In order to quantitatively assess the cyclone performance under different conditions, the parameters such as cut size, sharpness of partition curve, water split, and inlet pressure drop (an index of energy loss) are examined and the results are given in Fig. 4.4. In such studies, an optimum performance is identified when all the performance indices are at their best. Also, the concept of a compromised optimum performance is introduced to represent the situation where some indices are at their best while the remaining ones are reasonably good. Here, the water split is defined as the portion of water reported to the underflow. The inlet pressure drop is the difference of average pressures at the inlet and underflow outlet. Note that the pressures at the underflow and overflow outlets are the same, equal to the ambient atmospheric pressure. Both the cut size d_{50} and Ecart probable E_p are determined from a partition curve. d_{50} is the size corresponding to the separation efficiency of 50% in the partition curve. E_p is calculated by $(d_{75}\text{-}d_{25})/2$, where d_{75} and d_{25} are the sizes respectively corresponding to the separation efficiencies of 75% and 25%. E_p represents the sharpness of partition curve or separation precision. It is used for both hydrocyclones and dense medium cyclones (Pascoe, 2006; Chu et al., 2009; Wang et al., 2009).

Fig. 4.4 (a) shows that with increasing conical section length, the inlet pressure drop sharply decreases and then flattened. It is of interest to note that when the feed solids concentration increases, the inlet pressure drop increases sharply for the cyclones with the shortest conical section; but it decreases first to a minimum and then increases for the cyclones with longer cones. The non-monotonic variation is better shown by the inset in Fig. 4.4a, which re-plots the inlet pressure drop as a function of feed solids concentration. Such a phenomenon was experimentally observed for gas cyclones (Baskakov et al., 1990; Li et al., 2007). Overall, the inlet pressure drop is found to be sensitive to the feed solids concentration, mainly when the conical section length is relatively small.

Fig. 4.4 (b) indicates that when conical section length is increased, d_{50} sharply decreases and then slows down. Moreover, d_{50} increases with the increase of feed solids concentration. This increase becomes particularly evident at relatively short conical section lengths. These results can be explained as follows. As the conical section length increases at a given feed solids concentration, the orbit radius of particles decreases. Consequently, the probability of particles to move to the wall and then move down with the downward water flow is increased. This leads to a decreased cut size for a longer cone. Conversely, when feed solids concentration is increased for a given conical section length, the spigot region become denser with particles, leading to a decreased settling speed of particles (Kawatra et al., 1996). This promotes the possibility for coarse particles to reach the central region and flow up with the upward water flow and report to the overflow. Therefore, d_{50} increases with an increase in the feed solids concentration. Similar to d_{50}, E_p increases with an increase in the feed solids concentration; however, it sharply decreases first and then slows down with increasing conical section length (Fig. 4.4c). Note that by definition, a lower E_p corresponds to a sharper partition, leading to better product quality.

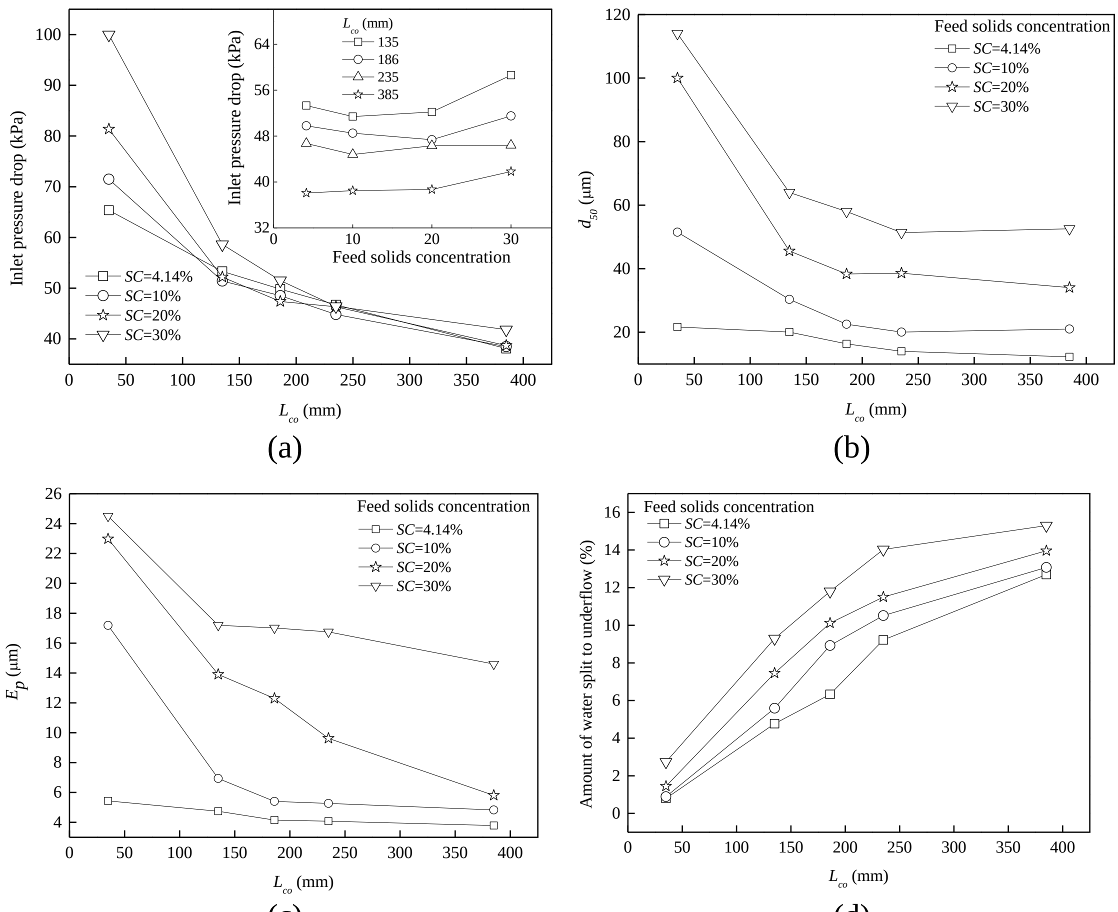

Fig. 4.4 Inlet pressure drop (a), d_{50} (b), E_p (c), and water split (d) as a function of conical section length at different feed solids concentrations.

Fig. 4.4 c shows that the water split increases with an increase in the conical section length or feed solids concentration. It is generally known that in hydrocyclones, some particles (regardless of being coarse or fine) flow with water and by-pass the classification process (Lynch, 1976; Slechta and Firth, 1984). Hence, fine particles that are supposed to report to the overflow may flow with water and report to the underflow. Similarly, coarse particles that are supposed to report to the underflow may be found at the overflow. Such misplaced particles lead to the contamination and loss of the product and need to be avoided in applications of hydrocyclones (O'Brien et al., 2000; Atkinson and Swanson, 2008). Based on this understanding, water split should be small. Fig. 4.4c and Fig. 4.4d together reveal that a longer cone is desirable in view of E_p but undesirable in view of water split. In addition, an operation with a high feed solids concentration leads to a large water split and E_p. It may degrade the product quality, but can be beneficial in terms of high throughput.

Fig. 4.5 presents the representative distributions of tangential velocities at different conical section lengths and feed solids concentrations. In this figure (and Figs. 4.6, 4.10 and 4.11), the white region corresponds to the area occupied by the air core, whose velocities (or solid volume fraction) are not shown because the properties of air and liquid-solid mixture are quite different. Such a representation has been used in other studies (Wang and Yu, 2006; Wang et al., 2007; Wang and Yu, 2008,2010), and offers a convenience for better showing the flow properties that govern the separation process and the profile of the air core. For all the feed solids concentrations considered, the tangential velocity distributions predicted are a Rankine vortex with a quasi-free vortex in the outer part and a quasi-forced vortex in the inner part, as previously observed numerically and experimentally (see, for example, the studies of Hsieh, 1988; Milin et al., 1992; Wang et al., 2007; Wang and Yu, 2008; Yang et al., 2011; Kuang et al., 2012a). Overall, the tangential velocities decrease with the increase of conical section length or feed solids concentration. Note that this velocity is proportional to the radial acceleration which represents the driving force for separation in a hydrocyclone (Svarovsky, 1984). Therefore, a cyclone with a larger separation region characterised by large tangential velocities should be favourable for gaining better separation efficiency. This relationship between tangential velocities and separation performance can be observed in Fig. 4.4 (c) and Fig. 4.5.

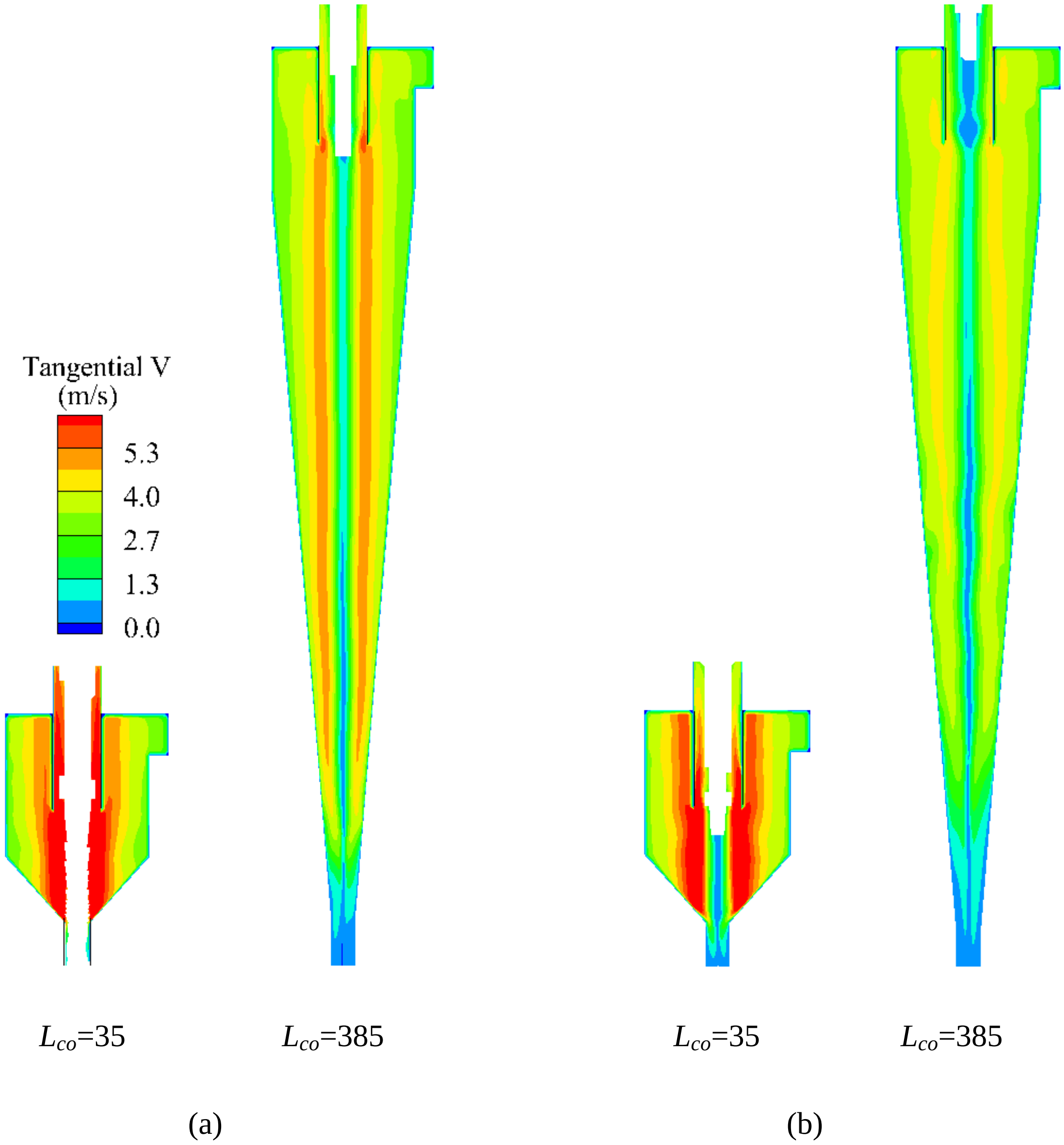

Fig. 4.5 Distributions of tangential velocities in the cyclones with different Lco at the feed solids concentration of: (a) SC=4.14%, and (b) SC=30%.

As seen from these two figures, at a given feed solids concentration, a cyclone with a longer cone has a rather large separation region identified by relatively large tangential velocities. The increased E_p as a result of the decrease of conical section length is mainly attributed to the decreased separation region due to a decreasing physical space. Conversely, the increased E_p due to the increase of feed solids concentration is attributed to two factors. One is that tangential velocities in the separation region are generally decreased. Another is related to the increased amount of particles accumulation around the spigot region, which causes the tangential velocities there to decrease significantly, leading to an increase of particle-particle interactions and a decrease of separation region. In addition, the tangential velocities can also be used to explain the behavior of water split shown in Fig. 4.4(d). When conical section length or feed solids concentration is increased, tangential velocities around the spigot region become smaller, leading to weaker rotation of water flow there. Consequently, the water has a higher chance to be reported to the underflow. Thus, an increased water split is observed.

Fig. 4.6 shows the distributions of solid volume fraction, corresponding to Fig. 4.5. It is shown that when feed solids concentration or conical section length is increased, the solid volume fraction increases, especially around the spigot region. Since particle density is constant in this study, the variations of solid volume fraction and mixture density are consistent. Note that in hydrocyclones, the radial pressure drop is proportional to the mixture density and tangential velocity (Hararah et al., 2010). The inlet pressure drop can be approximated by the radial pressure drop at the inlet height level because here the pressure drop at the central line is close to that on the underflow outlet. Thus, the inlet pressure drop is proportional to the mixture density (thus volume fraction) and tangential velocity. As such, the complicated behaviors of inlet pressure shown in Fig. 4.4(a) are explained using the tangential velocity and solid volume fraction shown in Fig. 4.5 and Fig. 4.6. At a given feed solids concentration when the conical section length increases, both the tangential velocity and solid volume fraction decrease. This accounts for the decrease in the inlet pressure drop. For the cyclone with the shortest cone, when feed solids concentration increases, the solids volume fraction increases significantly due to the narrower space of the cyclone, while the tangential velocity decreases slightly. Thus, the increase of the inlet pressure drop is mainly attributed to the increase of the solids volume fraction. Conversely, when feed solids concentration is increased for the cyclones with longer cones, the opposite variations of solids volume fraction and tangential velocity (increase for the former and decrease for the latter) contribute to the observed behavior of the inlet pressure drop which decreases first to a minimum and then increases (Fig. 4.4a).

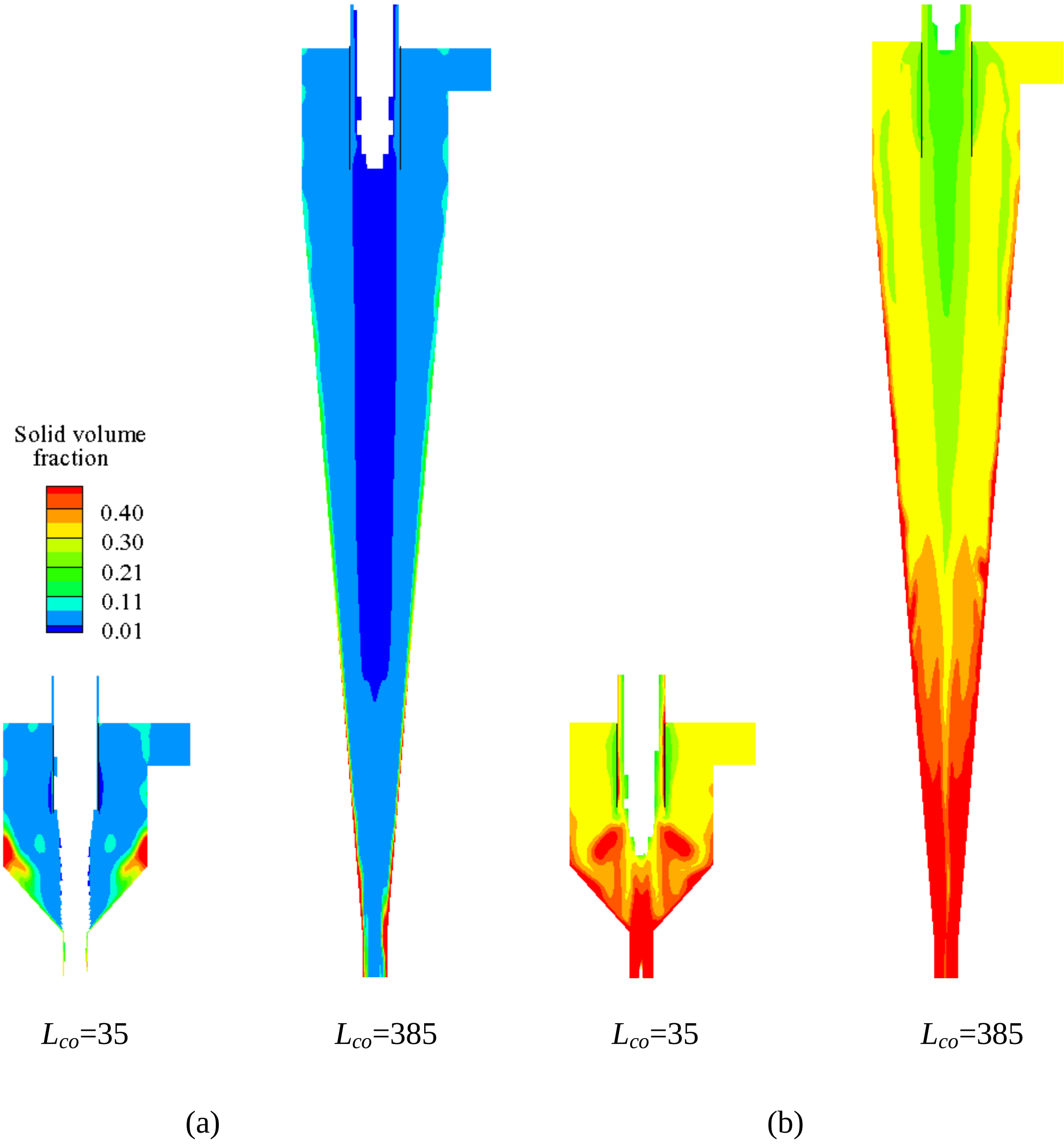

Fig. 4.6 Distributions of solid volume fraction in the cyclones with different Lco at the feed solids concentration of: (a) SC=4.4%, and (b) SC=30%.

Fig. 4.5 and Fig. 4.6 also show that the air core is observed mainly for a short cone for the cyclone operated at a low feed solids concentration. Note that the geometry and movement of the air core are sensitive to hydrocyclone operational state. Two general features associated with the air core were experimentally observed (Concha et al., 1996; Neesse and Dueck, 2007): (a) the operation with an air-core corresponds to a spray discharge, while the one without an air-core to a rope discharge; and (b), the spray discharge operation is more stable than the rope discharge operation. They can also be obtained by the present model, as detailed elsewhere (Ghodrat et al., 2013a). Based on this understanding, a longer cone is not desirable for a stable operation because such a design has an increased difficulty to achieve a stable spray discharge operation, as indicated by the behaviors of air core shown in Fig. 4.5 and Fig. 4.6.

4.3.2 **Effect of cone shape**

Fig 4.7 shows how conical shape factor (*n*) affects the separation efficiencies at different feed solids concentrations. As seen from the figure, with increasing conical shape factor, the separation efficiency increases and then decreases. The variation is quantitatively different at different feed solids concentrations. This can be clearly observed in Fig. 4.8 which shows the effect of feed solids concentration on the separation efficiency at two representative conical shape factors.

As seen from Fig. 4.8, with increasing feed solid concentration, the separation efficiency decreases; however, for coarse particles, the separation efficiency increases, particular at relatively small conical shape factors and relatively high feed solids concentrations. The behavior of coarse particles can be explained as follows. The decrease of separation efficiency with the increase of feed solids concentration is attributed to the decreasing settling speed of particles as a result of the particle accumulation, similar to those discussed in Section 4.3.1. However, when the feed solids concentration exceeds a certain value (20% in this study) at relatively small conical shape factors, the spigot region becomes so dense with particles that the water amount there decreases significantly. The entrainment of particles by fluid hence becomes negligible, and the particle flow is dominated by gravity. Accordingly, the coarse particles, which have more tendencies to reside inside the spigot region, are easier to report to the underflow, particularly when the feed solids concentration is further increased. This accounts for the increased separation efficiency of coarse particles with the increase of feed solids concentration.

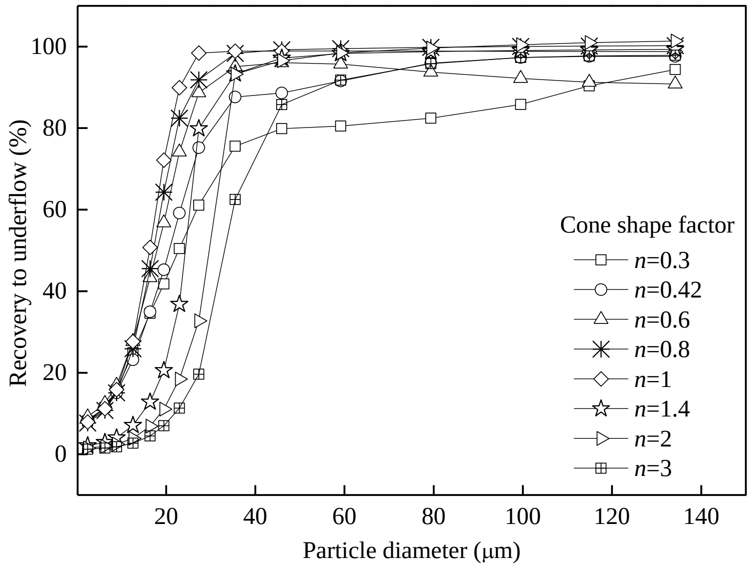

(a)

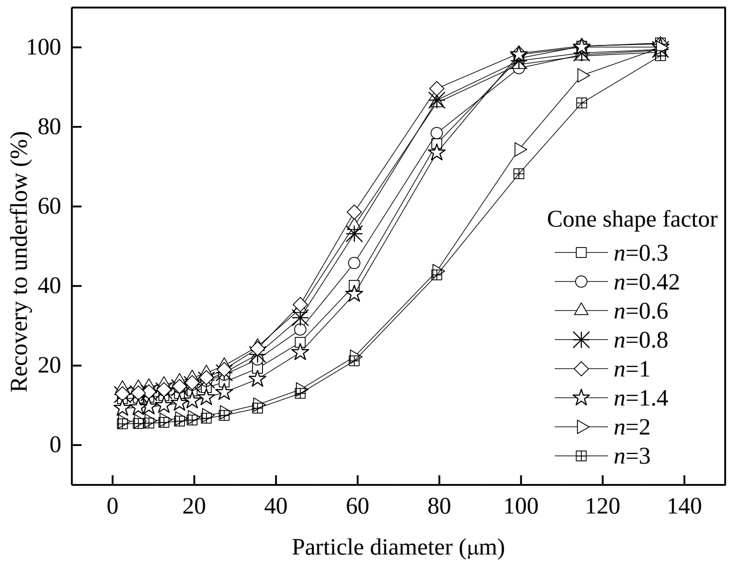

(b)

Fig. 4.7 Effect of conical shape factor on separation efficiency at the feed solids concentration of: (a) *SC*=4.14% and (b) *SC*=30%.

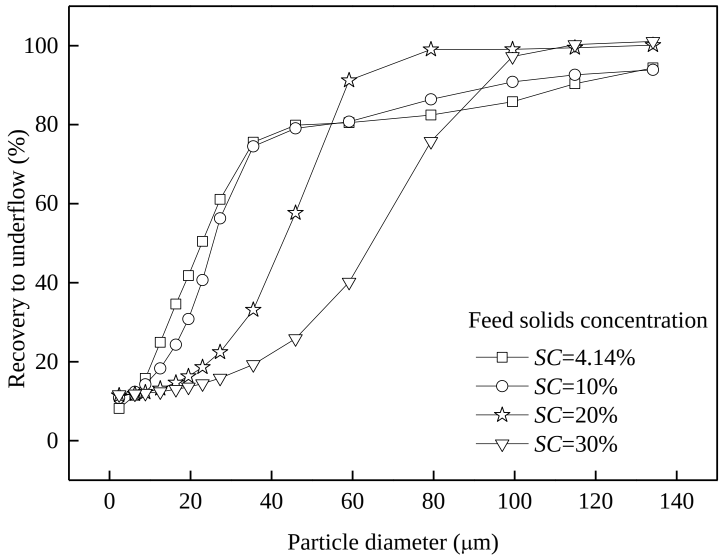

(a)

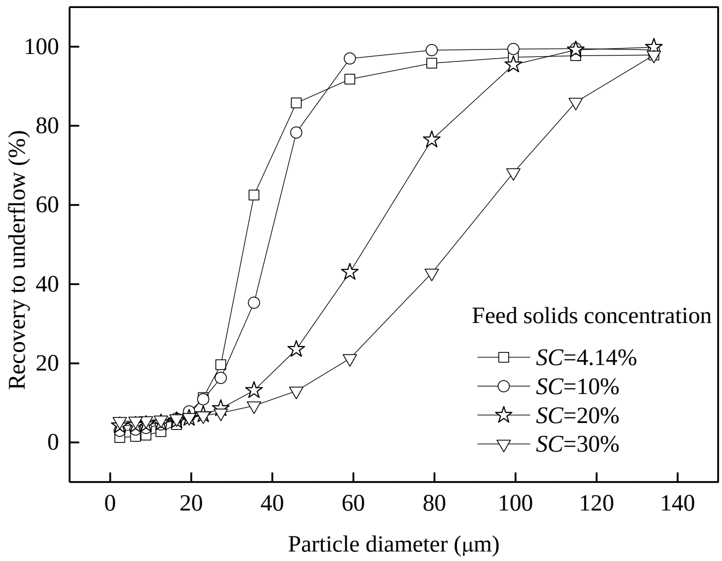

(b)

Fig. 4.8 Effect of feed solids concentration on separation efficiency in the cyclone with the conical shape factor of: (a) n=0.3 and (b) n=3.

Fig. 4.9 plots the inlet pressure drop, d_{50}, E_p and water split as a function of conical shape factor at different feeds solids concentrations. It can be seen from this figure that when the conical shape factor is increased, the inlet pressure-drop decreases. However, both d_{50} and E_p decrease first to a minimum and then increase. The water split increases to a maximum and then decreases. Note that all these performance parameters increase with the increase of feed solids concentration. Consequently, a compromised optimum performance can be identified at the conical shape factor close to n=1.4, showing a minimum E_p and relatively small inlet pressure drop and water split.

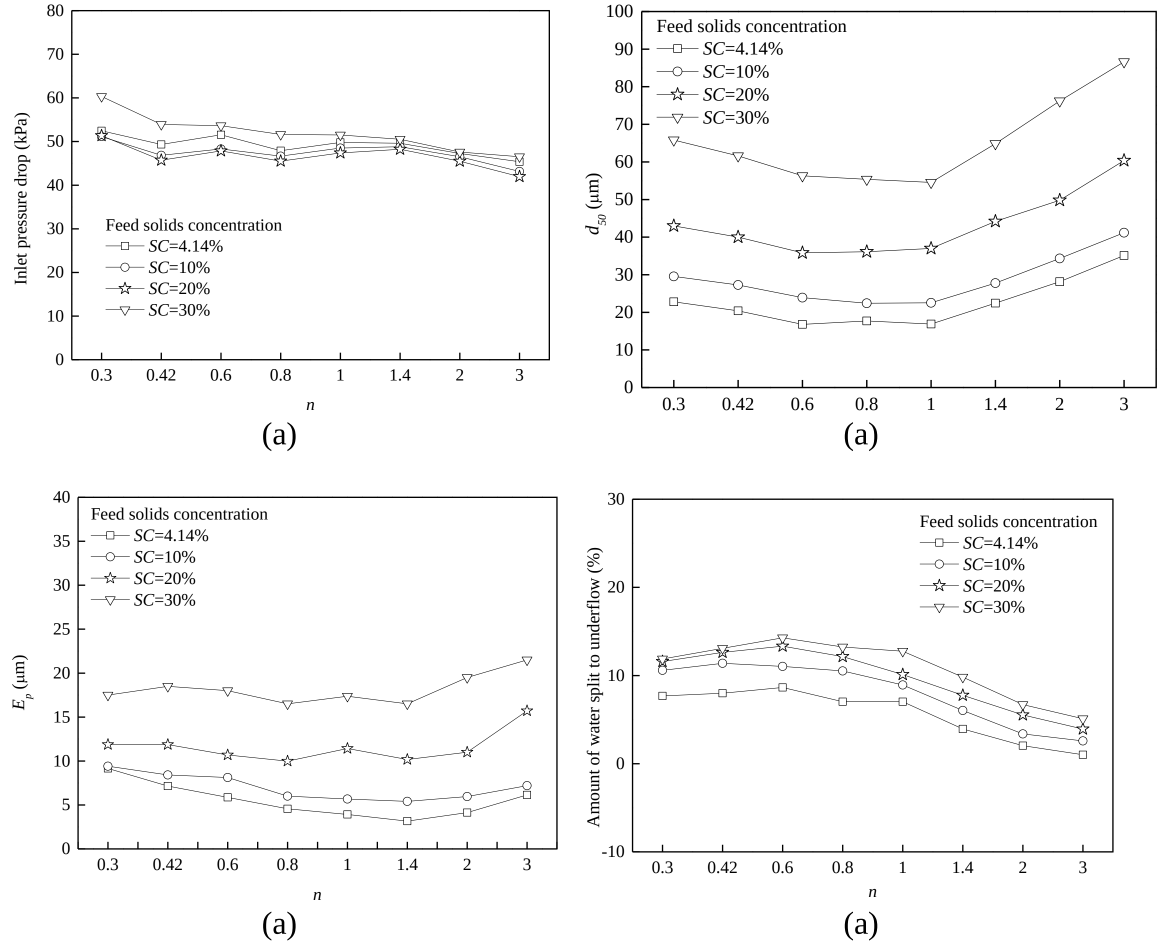

Fig. 4.9 Inlet pressure drop (a), d_{50} (b), E_p (c) and water split (d) as a function of n at different feed solids concentrations

Fig. 4.10 shows representative distributions of tangential velocities at different conical shape factors and feed solids concentrations. It shows that the tangential velocities generally decrease with the increase of conical shape factor or feed solids concentrations. Moreover, with increasing conical shape factor, the separation region becomes larger for two reasons. One is the increased physical separation region with large tangential velocities, and another is related to the decreased amount of particles accumulation around the spigot region.

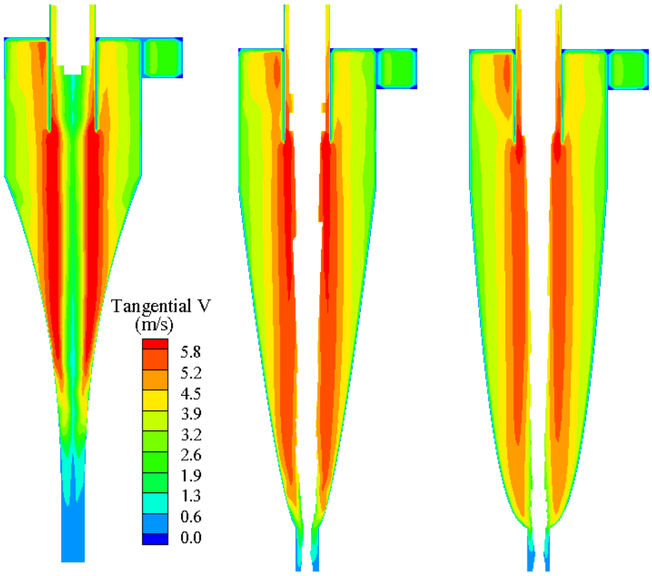

(a)

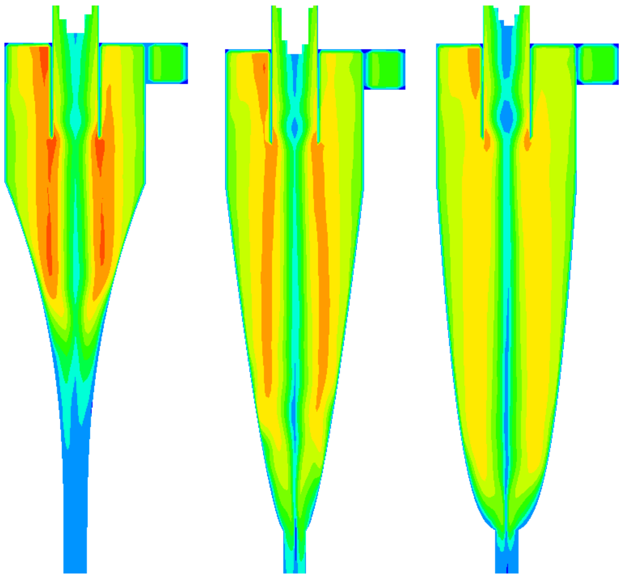

n=0.42 *n*=1.4 *n*=3

(b)

Fig. 4.10 Distributions of tangential velocities in the cyclones with different n at the feed solids concentration of: (a) SC=4.143%, and (b) SC=30%.

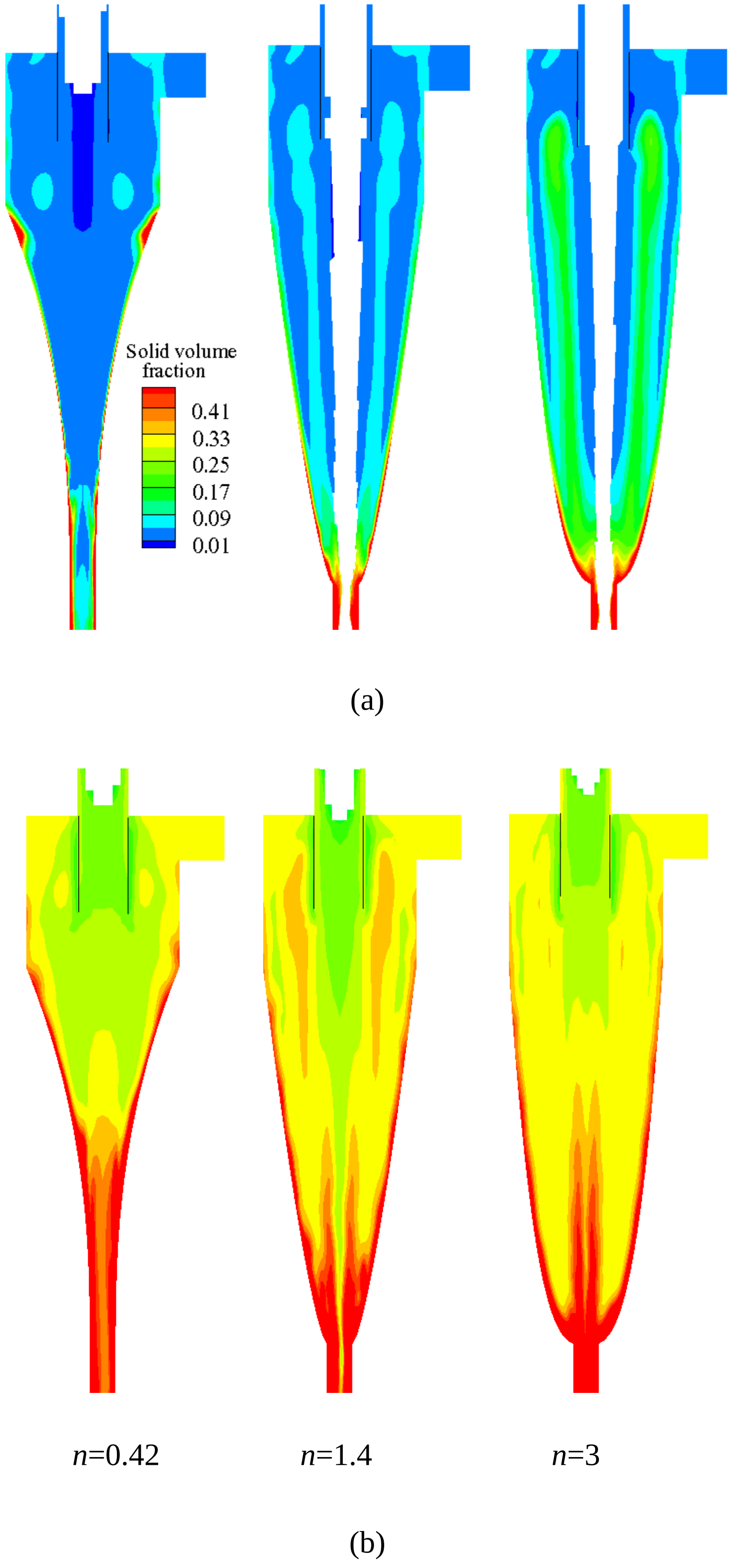

Fig. 4.11 Distributions of solid volume fraction in the hydrocyclones with different *n* at the feed solids concentration of: (a) *SC*=30%, and (b) *SC*=4.143%.

The opposite variations of the separation region and tangential velocities (increase for the former and decrease for the latter) account for the complicated behavior of E_P which decreases first to a minimum and then increases, as shown in Fig. 4.9(c). The variation of tangential velocity also accounts for the variation of water split in Fig. 4.9(d), similar to those discussed in Section 4.3.1. It is not discussed here for brevity.

Fig. 4.11 shows the distribution of solids volume fraction, corresponding to Fig. 4.10. It can be observed that with increasing conical shape factor or feed solids concentration, the solids volume fraction increases, particularly around the central and spigot regions. This variation is opposite to that of the tangential velocity shown in Fig. 4.10. Consequently, the contributions of solids volume fraction and tangential velocity to the inlet pressure drop are, to some degree, cancelled out by each other. As such, the inlet pressure drop varies gradually when the feed solids concentration or conical shape factor varies (Fig. 4.9a). Notably, Fig. 4.10 and Fig. 4.11 also show that the air core is observed at relatively large conical shape factors for cyclones operated at a low feed solids concentration. It suggests that a cyclone with a large conical shape factor is beneficial to achieving a spray discharge operation and thus a stable operation.

4.3.3 **A new cyclone design**

The results in Sections 4.3.1 and 4.3.2 reveal that selection of an optimum conical section length or conical shape factor can only improve some aspects of the cyclone performance. In this case, a new cyclone is proposed by combining a long cone (L_c=385 mm) and a convex cone ($n=1.4$) considering that both designs show certain compromised performances under their optimum conditions. Note that a longer cone may also be selected based on the present results and others (Fontein et al., 1962; Svarovsky, 1984; Wang and Yu, 2006). However, the focus here is the confirmation of the concept. For such a purpose, the performance of the new cyclone is assessed against the conventional cyclone at different feed solids concentrations.

Fig. 4.12 compares the partition curves for the new and conventional cyclones at different feed solids concentrations. As seen from this figure, the new cyclone has two favourable features compared to the conventional cyclone: at all the feed solids concentrations considered, its partition curve is sharper and the separation efficiencies of fine particles are much smaller, and thus there is less by-pass effect for such particles.

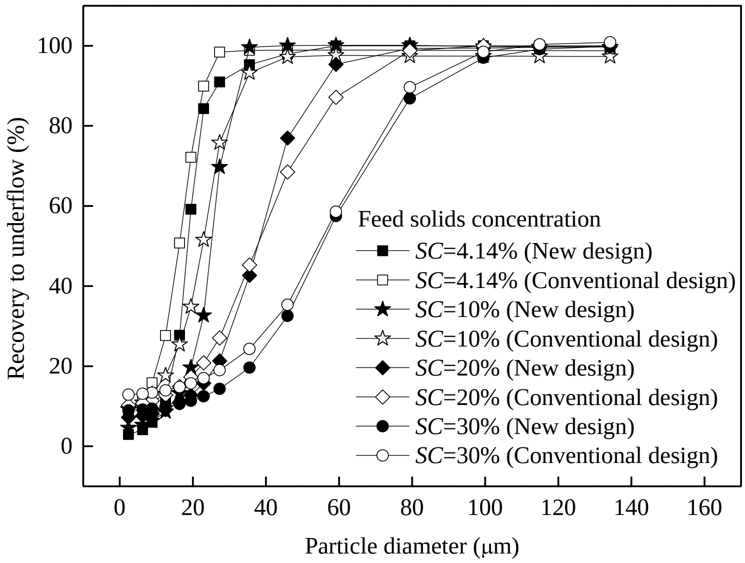

Fig. 4.12 Comparison of the separation efficiencies of the new and conventional cyclones at different feed solids concentrations

In order to be quantitative in the comparison, Fig. 4.13 plots the performance of the new and conventional cyclones such as d_{50}, water split, inlet pressure drop and E_p. It is shown that the new and conventional cyclones have nearly the same d_{50} which increases with the increase of feed solids concentration (Fig. 4.13a). This suggests that the two cyclones can be used to classify particles of the same size range. More importantly, smaller water split and inlet pressure drops are observed for the new cyclone (Figs. 4.13b and 4.13c). This leads to less by-pass effect and energy input. The new design has a decreased E_p compared to the conventional design (Fig. 4.13d). The decrease is more evident in the middle range of the feed solids concentrations considered and becomes very small at the highest solid concentration.

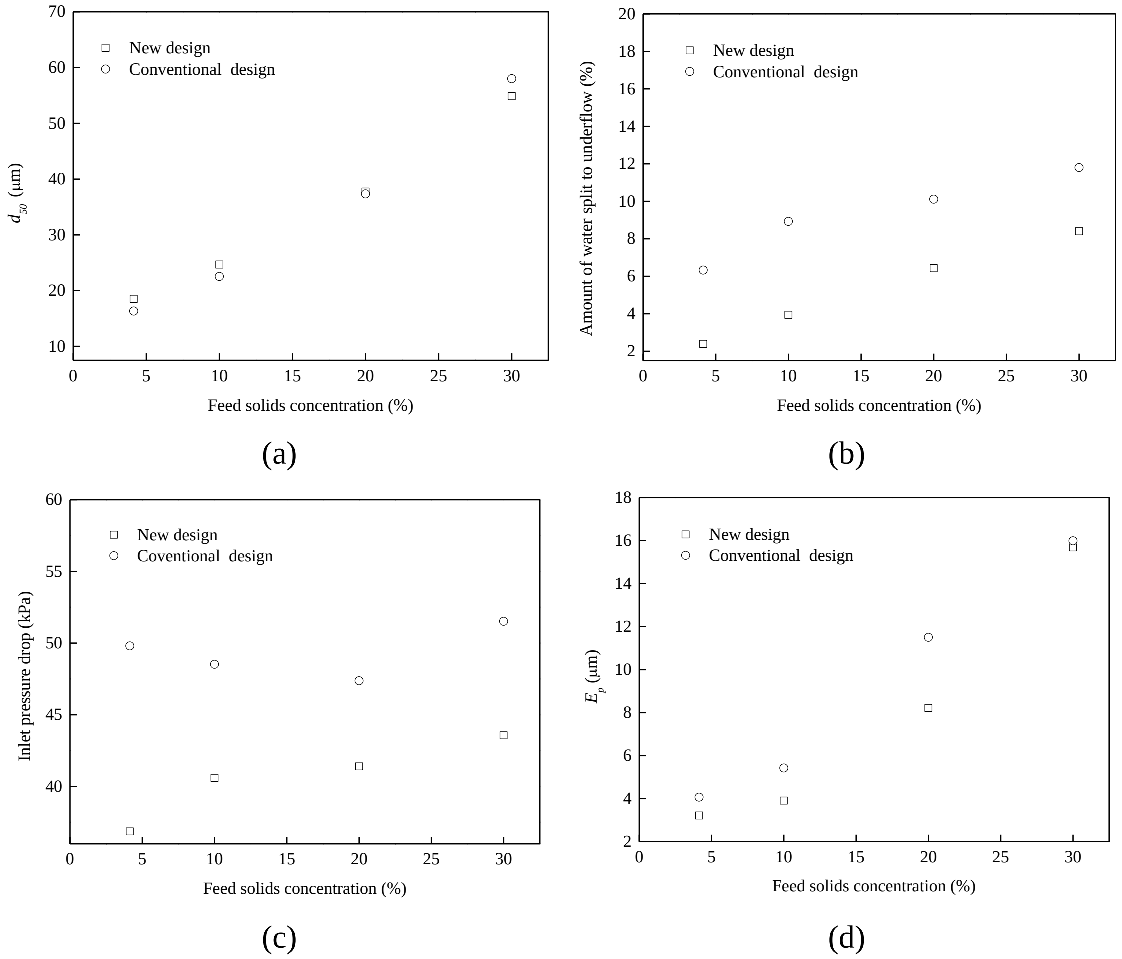

Fig. 4.13 Comparison of the performance indices of the new and conventional cyclones at different feed solids concentrations: (a) d_{50}, (b) water split, (c) inlet pressure drop, and (d) E_p.

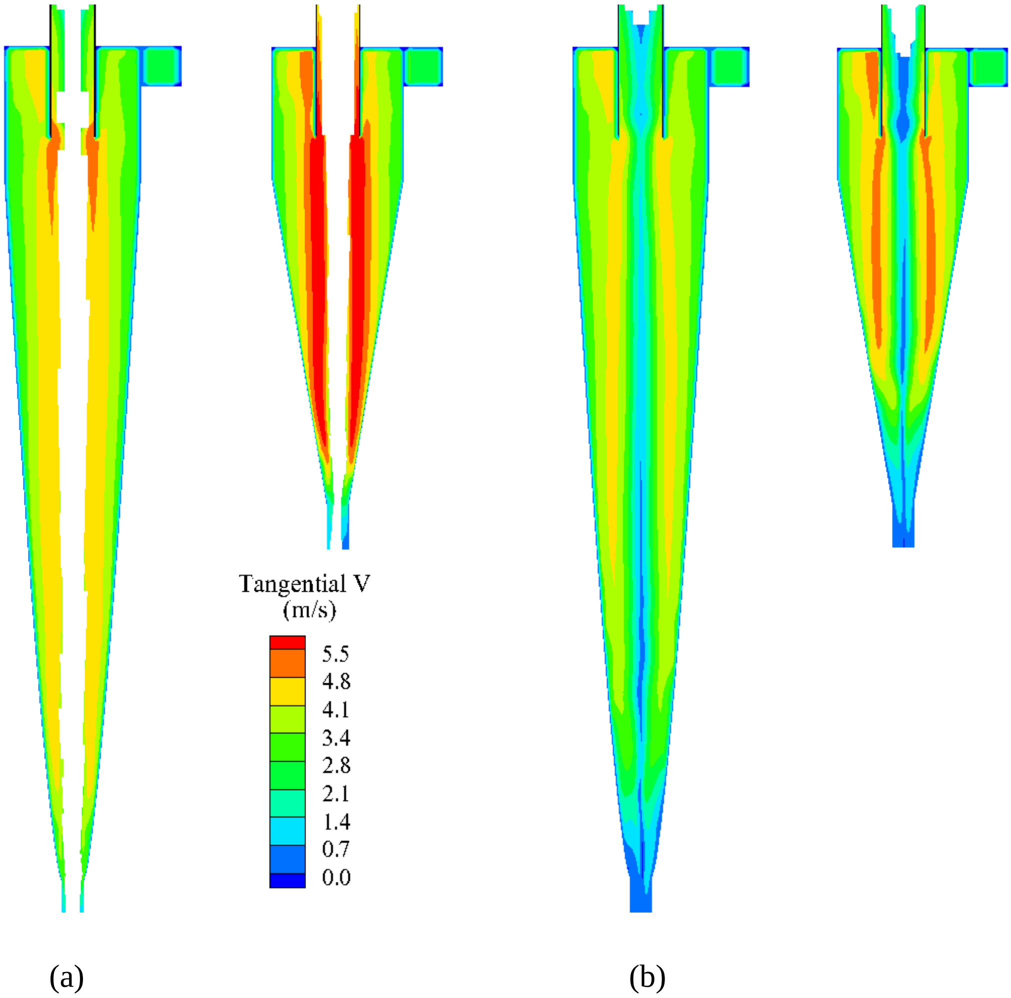

Fig. 4.14 Comparison of the tangential velocities of the new (long) and conventional (short) cyclones at the feed solids concentration of: (a) *SC*=4.14%, and (b) *SC*=30%.

Fig. 4.14 compares the tangential velocities within the new and conventional cyclones at low and high feed solids concentrations. As seen from this figure, the tangential velocities within the new cyclone are smaller compared to the conventional cyclone at the same feed solids concentration, leading to a smaller inlet pressure drop. Overall, the separation region with relatively large tangential velocities in the new cyclone is much larger due to the long length and convex shape of the conical part. Thus, the value of E_p is lower for the new cyclone design. Note that in both cyclones, particles accumulate around the spigot region (Fig. 4.15), where the tangential velocities decrease rapidly and the separation region is hence reduced. This is pronounced at the highest feed solid concentration, particularly for the new cyclone where the region with relatively dense particles is much larger compared to the conventional cyclone. As a result, the difference in E_p between the two cyclones becomes the smallest at the highest feed solids concentration (Fig. 4.15b). In addition, compared to the conventional cyclone, the tangential velocities around the spigot region are larger in the new cyclone, which accounts for the smaller water split. On the other hand, it is of interest to note that an air core is observed in both the cyclones operated at a low feed solids concentration (Fig. 4.14 and Fig. 4.15). However, the air core size is generally larger in the new cyclone than that of the conventional cyclone due to larger tangential velocities around the spigot region. This indicates that it is more likely that the new cyclone achieves a stable operation.

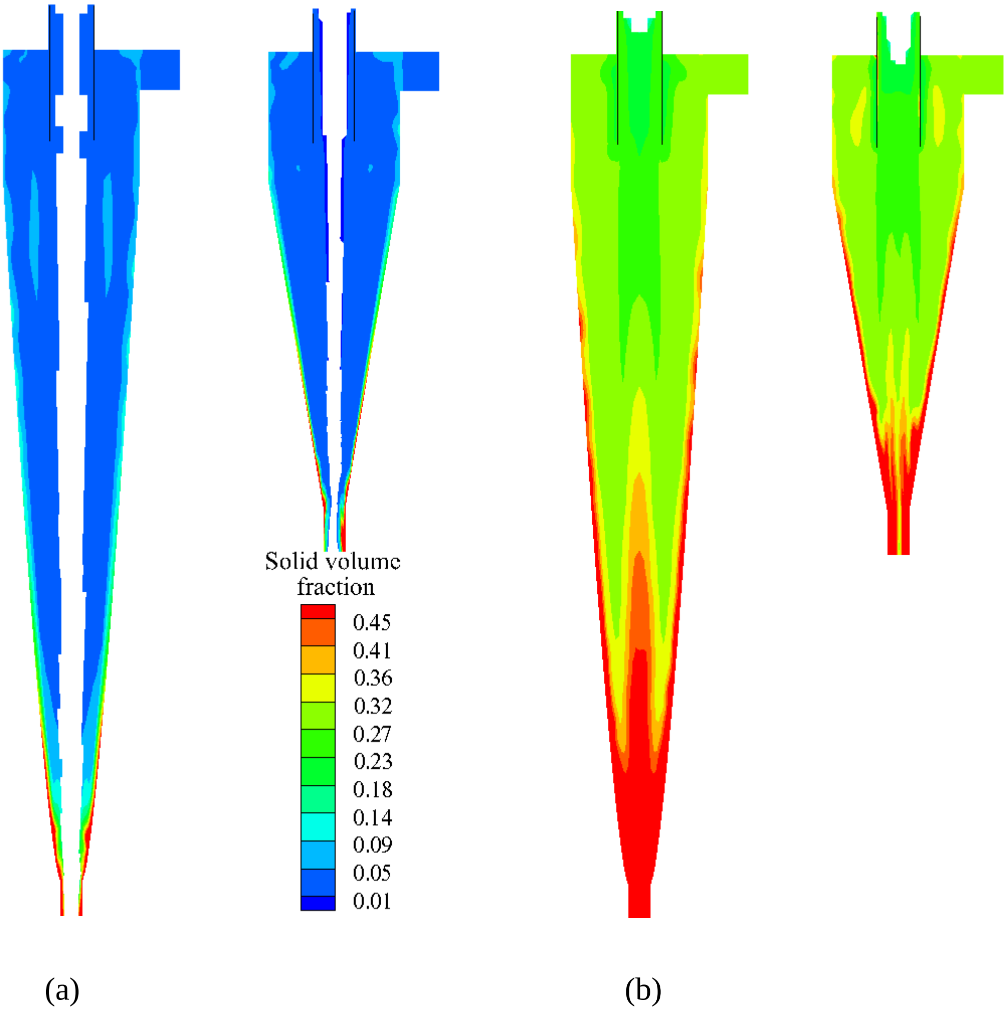

Fig. 4.15 Comparison of the solid volume fraction of the new (long) and conventional (short) cyclones at the feed solids concentration of: (a) *SC*=4.14%, and (b) *SC*=30%.

4.4 Conclusions

Conical geometry affects hydrocyclone flow and performance significantly. In this work, the recently developed CFD model (Kuang et al., 2012a) has been used to study the multiphase flow and performance of hydrocyclones, focusing on the effects of length and shape of conical section at a wide range of feed solids concentrations. The results from this study can be summarised as follows:

(1) A longer conical section length leads to decreased inlet pressure drop, d_{50} and E_p, and at the same time, an increased water split (thus larger by-pass effect). These effects are pronounced with increasing feed solids concentration considered. However, the inlet pressure drop is sensitive to the feed solids concentration mainly at relatively short conical section lengths.

(2) The effect of cone shape including concave and convex styles has been studied. A compromised optimum performance is observed for the cyclone with a convex cone at all the feed solids concentrations considered, resulting in a minimum E_p and relatively small inlet pressure drop and water split. These performance parameters increase with the increase of feed solids concentration.

(3) Based on the CFD results, a new improved cyclone design has been proposed by introducing a long convex cone design. Compared to the conventional cyclone, the new cyclone has a larger separation region with smaller tangential velocities, however, with larger tangential velocities around the spigot region. Its inlet pressure drop, water split and E_p are hence smaller.

REFERENCES

Atkinson, B., Swanson, A., 2008, Improved efficiency of fine coal classification. ACARP report, C15059.
Baskakov, A. P., Dolgov, V. N., Goldobin, Y. M., 1990. Aerodynamics and heat-transfer in cyclones with particle-laden gas flow. Experimental Thermal and Fluid Science, 3 (6), 597-602.
Brennan, M. S., Narasimha, M., Holtham, P. N., 2007. Multiphase modelling of hydrocyclones - prediction of cut-size. Minerals Engineering, 20 (4), 395-406.
Chiné, B., Concha, F., 2000. Flow patterns in conical and cylindrical hydrocyclones. Chemical Engineering Journal, 80 (1–3), 267-273.
Chu, L. Y., Chen, W. M., Lee, X. Z., 2000. Effect of structural modification on hydrocyclone performance. Separation and Purification Technology, 21 (1-2), 71-86.
Chu, L. Y., Chen, W. M., Lee, X. Z., 2002. Effects of geometric and operating parameters and feed characters on the motion of solid particles in hydrocyclones. Separation and Purification Technology, 26 (2-3), 237-246.
Concha, F., Barrientos, A., Montero, J., Sampaio, R., 1996. Air core and roping in hydrocyclones. International Journal of Mineral Processing, 44-45, 743-749.
Davailles, A., Climent, E., Bourgeois, F., Majumder, A. K., 2012. Analysis of swirling flow in hydrocyclones operating under dense regime. Minerals Engineering, 31 (0), 32-41.
Dyakowski, T., Williams, R. A., 1996. Prediction of high solids concentration regions within a hydrocyclone. Powder Technology, 87 (1), 43-47.
Fontein, F. J., van Kooy, J. G., Lelliger, H. A., 1962. The influence of some variables upon hydrocyclones performance. British Chemical Engineering, 7, 410-421.
Hararah, M. A., Endres, E., Dueck, J., Minkov, L., Neesse, T., 2010. Flow conditions in the air core of the hydrocyclone. Minerals Engineering, 23 (4), 295-300.Hsieh, K. T., 1988. Phenomenological model of the hydrocyclone. PhD thesis, The University of Utah, Salt Lake City, UT, USA.Huang, S., 2005. Numerical simulation of oil-water hydrocyclone using reynolds-stress model for Eulerian multiphase flows. Canadian Journal of Chemical Engineering, 83 (5), 829-834.Kawatra, S. K., Bakshi, A. K., Rusesky, M. T., 1996. Effect of viscosity on the cut (d50) size of hydrocyclone classifiers. Minerals Engineering, 9 (8), 881-891.Kuang, S. B., Chu, K. W., Yu, A. B., Vince, A., 2012. Numerical study of liquid-gas-solid flow in classifying hydrocyclones: effect of feed solids concentration. Minerals Engineering, 31, 17-31.Launder, B. E., Reece, G. J., Rodi, W., 1975. Progress in the development of a Reynolds-stress turbulence closure. Journal of Fluid Mechanics, 68, 537-566.Li, S. H., Zhang, H., Yang, H. R., Yang, S., Lu, J. F., Yue, G. X., 2007. Determining cyclone particle holdup by pressure drop for a CFB boiler. Chemical Engineering & Technology, 30 (12), 1726-1731.Lynch, A. J., Mineral crushing and grinding circuits, their simulation, optimisation, design and control, 1977, Elsevier, Amsterdam.Milin, L., Hsieh, K. T., Rajamani, R. K., 1992. The leakage mechanisms in the hydrocyclone. Minerals Engineering, 5 (7), 779-794.Min'kov, L. L., Dueck, J. H., 2012. Numerical modeling of a nonmonotonic separation hydrocyclone curve. Journal of Engineering Physics and Thermophysics, 85 (6), 1317-1326.

Narasimha, M., Brennan, M., Holtham, P. N., 2007. A review of CFD modelling for performance predicitons of hydrocyclone. Engineering Applications of Computational Fluid Mechanics, 1 (2), 109-125.

Narasimha, M., Brennan, M. S., Holtham, P. N., 2012. CFD modeling of hydrocyclones: Prediction of particle size segregation. Minerals Engineering, 39 (0), 173-183.
Noroozi, S., Hashemabadi, S. H., 2009. CFD simulation of inlet design effect on deoiling hydrocyclone separation efficiency. Chemical Engineering and Technology, 32 (12), 1885-1893.
Nowakowski, A. F., Cullivan, J. C., Williams, R. A., Dyakowski, T., 2004. Application of CFD to modelling of the flow in hydrocyclones. Is this a realizable option or still a research challenge? Minerals Engineering, 17 (5), 661-669.
Nowakowski, A. F., Kraipech, W., Williams, R. A., Dyakowski, T., 2000. The hydrodynamics of a hydrocyclone based on a three-dimensional multi-continuum model. Chemical Engineering Journal, 80 (1-3), 275-282.
O'Brien, M., Taylor, A., Nemeth, D., Firth, B., Clarkson, C., 2000, Large diameter classifying cyclones. ACARP report, C6047.
Slechta, J., Firth, B. A., 1984. Classification of fine coal with a hydrocyclone. International Journal of Mineral Processing, 12 (4), 213-237.
Svarovsky, L., Hydrocyclones, 1984, Holt, Rinehart and Winston, Sydney.
Svarovsky, L., Thew, M. T., Hydrocyclones: analysis and applications, 1992, Kluwer Academic Publishers, MA, USA.
Swain, S., Mohanty, S., 2013. A 3-dimensional Eulerian–Eulerian CFD simulation of a hydrocyclone. Applied Mathematical Modelling, 37 (5), 2921-2932.
Wang, B., Chu, K. W., Yu, A. B., 2007. Numerical study of particle-fluid flow in a hydrocyclone. Industrial & Engineering Chemistry Research, 46 (13), 4695-4705.
Wang, B., Yu, A. B., 2006. Numerical study of particle-fluid flow in hydrocyclones with different body dimensions. Minerals Engineering, 19 (10), 1022-1033.
Wang, B., Yu, A. B., 2008. Numerical study of the gas-liquid-solid flow in hydrocyclones with different configuration of vortex finder. Chemical Engineering Journal, 135 (1-2), 33-42.
Wang, B., Yu, A. B., 2010. Computational investigation of the mechanisms of particle separation and "fish-hook" phenomenon in hydrocyclones. AIChE J, 56 (7), 1703-1715.
Yang, Q., Wang, H. L., Liu, Y., Li, Z. M., 2010. Solid/liquid separation performance of hydrocyclones with different cone combinations. Separation and Purification Technology, 74 (3), 271-279.
Yang, Q., Wang, H. L., Wang, J. G., Li, Z. M., Liu, Y., 2011. The coordinated relationship between vortex finder parameters and performance of hydrocyclones for separating light dispersed phase. Separation and Purification Technology, 79 (3), 310-320.
Zhang, Y. H., Qian, P., Liu, Y., Wang, H. L., 2011. Experimental study of hydrocyclone flow field with different feed concentration. Industrial and Engineering Chemistry Research, 50 (13), 8176-8184.

CHAPTER 5[3]

NUMERICAL ANALYSIS OF HYDROCYCLONES WITH DIFFERENT VORTEX FINDER CONFIGURATIONS

This chapter presents a numerical study of the multiphase flow and performance of hydrocyclone by means of two-fluid model, with special reference to the effects of diameter, length and shape of vortex finder at a wide range of feed solids concentrations. The considered shapes include the conventional cylindrical style and the new conical and inverse conical styles. The simulation results are analysed with respect to cyclone flow and performance in term of cut size d_{50}, water split, Ecart probable E_p and inlet pressure drop. It is shown that when vortex finder diameter or shape varies, a compromised optimum performance can be identified, resulting in relatively small inlet pressure drop, E_p, and water split. Both d_{50} and E_p are more sensitive to feed solids concentration than inlet pressure drop and water split. Overall, the effect of vortex finder length on the separation efficiency of particles is much less significant than diameter and shape, which shows opposite trends at low and high feed solids concentrations. All these results can be well explained using the predicted tangential and axial velocities and solids volume fraction.

---

[3] Content of this chapter published in Minerals Engineering 2014, Ghodrat, M., Kuang, S. B., Yu, A. B., Vince, A., Barnett, G. D., Barnett, P. J., 2014. Numerical analysis of hydrocyclones with different vortex finder configurations. Minerals Engineering, 63 (0), 125-138.

5.1 Introduction

Hydrocyclones are widely used to separate particles by size in many industries such as chemical, mineral, coal preparation, and powder processing industries. Some advantages associated with such a separator include design simplicity, high capacity, low maintenance and operational costs. On the other hand, the disadvantages of the cyclone include high energy loss and unsatisfactory separation efficiencies such as misplaced particles at both the overflow and underflow, and limitations on separation performance in terms of the sharpness of the cut and the range of operating cut size (Svarovsky, 1984). To date, finding applicable solutions to overcome these deficiencies is still a challenge, particularly at different feed solids concentrations.

The internal space within a hydrocyclone can be largely divided into three parts: the pre-separation space between the vortex finder and the column wall, the main separation space below the vortex finder, and the space occupied by the air core. It is known that by properly changing the dimension and shape of the vortex finder, the flow in the pre-separation space can be controlled to improve cyclone performance such as energy utilization and particle separation efficiency. In the past decades, various experimental and numerical studies have been made in this direction. The vast majority of such studies focused on the optimum dimension of the vortex finder with respect to the length, diameter and the wall thickness (Kelsall, 1953; Xu et al., 1991; Olson and Van Ommen, 2004; Martinez et al., 2007,2008; Wang and Yu, 2008; Motsamai, 2010; Kilavuz and Gulsoy, 2011; Yang et al., 2011; Murthy and Bhaskar, 2012). Some design modifications on the shape of the vortex finder have also been made continuously (Kelsall, 1952; Duijn and Rietema, 1983; Arato, 1984; Rajamani, 1987; Chu and Luo, 1994; Wang and Yu, 2008; Silva et al., 2012). However, the previous vortex finder shapes were considered at specific dimensions. Their geometrical configurations are generally complex, which are not desirable for equipment manufacturer and wear prevention. Another deficiency associated with the previous studies is that the effect of vortex finder was often investigated at relatively low feed solids concentrations. However, hydrocyclones are often operated at different feed solids concentrations in practice and show different performance (Slechta and Firth, 1984; Dyakowski and Williams, 1996; O'Brien et al., 2000; Hararah et al., 2010; Zhang et al., 2011). To date, a comprehensive study of the vortex finder configuration at different feed solids concentrations has not been found in the literature.

Computer modelling and simulation can provide an insight into a hydrocyclone concerning the complicated inner multiphase flows that govern the equipment performance but are difficult to measure, especially for opaque slurry and/or at a relatively high feed solids concentration. It has been widely used to study hydrocyclones in recent years (see, for example, the reviews by Nowakowski et al., 2004; Narasimha et al., 2007a). Generally speaking, the numerical models used can be classified into two groups: CFD-LPT (Computational Fluid Dynamics-Lagrangian Particle Tracking) and TFM (Two-Fluid Model). The previous numerical studies of vortex finder were mainly based on the CFD-LPT approach (Olson and Van Ommen, 2004; Wang and Yu, 2008; Motsamai, 2010; Murthy and Bhaskar, 2012). However, such an approach traces only the motion of a single particle, and ignores the effect of inter-particle interactions and the reaction of particles on the fluid. Therefore, it is largely limited to hydrocyclones operated at a low feed solids concentration or in a dilute flow regime. Conversely, in the TFM approach, both the fluid and solid phases are treated as interpenetrating continuum media, considering the interactions between particles and between particles and fluid. It can, to a large extent, overcome the problems associated with the CFD-LPT approach. Therefore, the TFM approach has been increasingly used to study hydrocyclones in both dense and/or dilute regimes by different investigators (Nowakowski et al., 2000; Huang, 2005; Brennan et al., 2007; Noroozi and Hashemabadi, 2009; Kuang et al., 2012b; Narasimha et al., 2012; Swain and Mohanty, 2013). However, while confirming the capability of TFM approach, the previous TFM studies were rarely used to investigate the effects of geometrical variables on hydrocyclone flow and performance.

In this study, the flow in hydrocyclones is studied by means of the TFM model recently developed by Kuang et al. (2012). The emphasis is given to the influences of the diameter, length and shape of vortex finder on the flow and performance at different feed solids concentrations. This is different from the previous study that focused on model development and validation for a given geometry (Kuang et al., 2012b). The vortex finders of the hydrocyclones considered here include the conventional cylindrical style and the new conical and inverse conical styles, as illustrated in Fig. 5.1. The new vortex finder shapes affect the flow and thus separation performance due to the different pre-separation space at the lower part of vortex finder. This may be in principle similar to the other shapes reported in the literature (Kelsall, 1952; Duijn and Rietema, 1983; Arato, 1984; Rajamani, 1987; Chu and Luo, 1994; Wang and Yu, 2008; Silva et al., 2012). But the shapes considered in this work are simpler and more effective in practical application. Through the study of different vortex finder configurations, various methods for controlling the pre-separation space can be examined for operations at either low or high feed solids concentrations. The findings can be useful not only for establishing a comprehensive picture about the effect of vortex finder but also for designing and controlling hydrocyclones.

5.2 Simulation method and condition

5.2.1 **Model description**

The present model is based on the TFM model, facilitated with the mixture model which has been proved to be valid for hydrocyclones.The detail of the model has been discussed in section 2.7.3.

It should be pointed out that the mixture model given in section 2.7.3 is primarily intended to model multiphase flow where a dispersed phase is mixed with a continuous fluid phase (Manninen et al., 1996). However, it can also be directly applied to describe the gas-liquid flow and predict the gas-liquid interface (and thus air core) in a hydrocyclone, as demonstrated by different investigators (Brennan et al., 2007; Narasimha et al., 2007b; Wang et al., 2009; Kuang et al., 2012a). Thus, it is here used to describe air core. The bubble size used in the mixture model is set to 10^{-5} m after some tests, so that this model gives almost the same air core as that by a Volume of Fluid (VOF) model (Hirt and Nichols, 1981) that was widely used in the literature to predict the air core in a hydrocyclone.

5.2.2 **Simulation conditions and boundary conditions**

The present operational and geometrical conditions as listed in Table 5.1 follow the experimental work of Hsieh (1988), which has been widely used to validate various numerical models in the past. A 75-mm hydrocyclone is hence considered, which consists of seven main geometrical parameters following the most common design (see Fig. 1): diameter of the cylindrical body (D_c), diameter of inlet (D_i), diameter of vortex finder (D_o), diameter of apex (D_u), length of cylindrical part (L_c), length of vortex finder (L_v) and included angle (a). These parameters, together with operational conditions and material properties, characterize the pressure drop, particle separation efficiency, and water split of a hydrocyclone (Bradley, 1965; Svarovsky, 1984). Three geometrical variables are considered: shape, diameter, and length of vortex finder. Each simulation considers only one variable while others are the same as those for the base case. The diameter of vortex finder D_v varies from 10 to 50 mm, and the length L_v from 0 to 150 mm. This is selected according to the work of Wang and Yu (2008) for comparison, who systematically studied the effect of vortex finder dimension in a dilute regime and demonstrated their results are consistent with those predicted by the well-known Plitt empirical model (Plitt, 1976). Note that in this study, both dilute and dense regimes are considered for the three geometrical variables by varying feed solids concentration *SC* from 4 to 30% by volume. The vortex finder shapes include conical, inverse conical and cylindrical styles. These shapes are described by two factors determined based on the geometry of vortex finder, i.e, the ratios of bottom entrance diameter (D_b) to top exit diameter (D_t): D_b/D_t (=0.4-2), and cylindrical section length (L_t) to the conical or inverse conical section length (L_b): L_t/L_b (=0.25-4) (see Fig. 5.1). Vortex finder is conical at D_b/D_t<1, cylindrical (the conventional one) at D_b/D_t=1, and inverse conical at D_b/D_t>1. For convenience, D_b/D_t is referred to as cone ratio. All the cyclones considered have the same inlet, cylinder, cone and spigot as those of the base case.

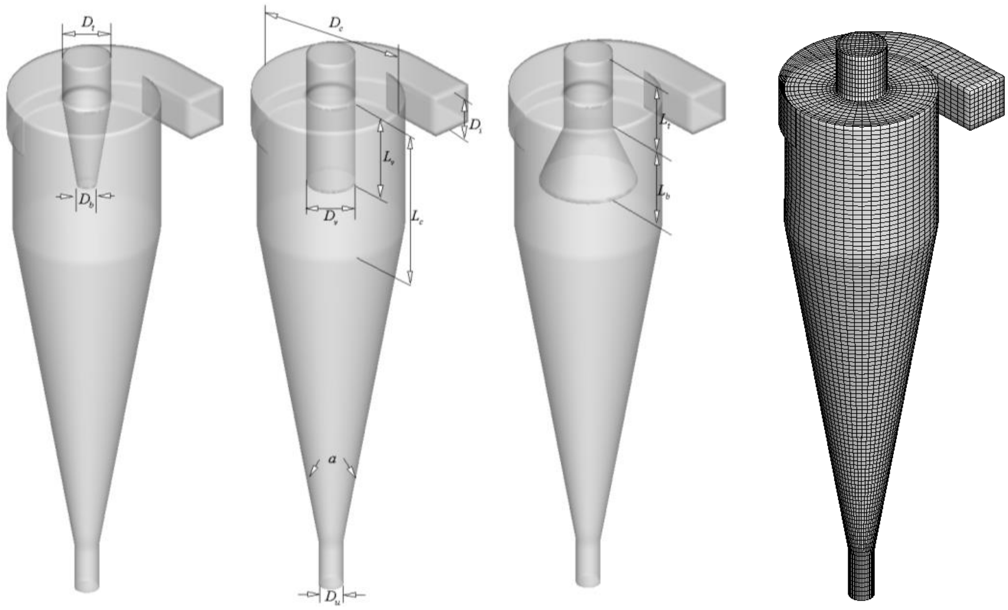

D_d/D_t=0.4 (cone) 1 (cylinder) 1.6 (inverse cone) 1

Fig. 5.1 Vortex finder of different shapes simulated and mesh for the base case.

The grid is finer in the vicinity of the walls and vortex finder than in the remainder of the cyclone. Preliminary test results confirm that the computational results, such as the flows of different phases and the resulting separation behaviors are converged ones, independent of the mesh size used. This is the case for all conditions considered in this work. A “velocity inlet” boundary condition is used at the cyclone inlet, and the “pressure-outlet” condition at both the outlets. The pressure at the two outlets (vortex finder and spigot) is 1 atm, corresponding to the ambient atmospheric pressure, and the inlet water velocity and particle velocity are both 2.49 m/s. Limestone particles are injected at the inlet at a given flow rate. For the particles involved, the density is 2700 kg/m^3, and the size range is between 2.4 and 134 μm. The size distribution considered here is similar to that used in the experimental work of Hsieh of (1988). It is represented by 15 mean sizes in simulations. The mean sizes and their distribution are given in Table 5.1. To effect a simulation, the original distribution of particle size is divided into a series of size intervals. Each size interval is represented by a mean size in simulations. This treatment could also apply to particle density. In this work, following the experiments,(1988) fifteen mean particle sizes as listed in Table 5.1 are simulated at a given particle density.

Table 5-1 Geometrical and operational conditions used in the simulations

Parameter	Symbol	Value*
Geometrical parameter		
Diameter of the body (mm)	D_c	75
Diameter of inlet (mm)	D_i	25
Diameter of vortex finder (mm)	D_v	25 (10-50)
Diameter of spigot (mm)	D_u	12
Length of cylindrical part (mm)	L_c	75
Vortex finder cone ratio	D_b/D_t	1 (0.4-2)
Length ratio of cylinder and cone	L_t/L_b	1 (0.25-4)
Length of vortex finder (mm)	L_v	50 (0-150)
Included angle (°)	A	20
Operational condition		
Inlet velocity (m/s)	U	2.49
Particle material		Limestone
Particle density (kg/m^3)	ρ_p	2700
Feed solids concentration (% by volume)	ρ_{feed}	10 (4.14-30)
Particle sizes simulated (μm)	D	134.16, 114.89, 99.50, 79.37, 59.16, 45.94, 35.50, 27.32, 22.97, 19.49, 16.39, 12.55, 8.87, 6.27, 2.40

* for the base case, with their varying ranges in the brackets.

All the simulations are conducted using the ANSYS Fluent CFD software package (version 14) in NCI (National Computational Infrastructure) in Australia. Sixteen CPUs are assigned to each simulation, which lasts for about 14 days for computing the physical time of about 35 seconds to ensure that the steady-state flow is achieved. The steady state is identified by the feature that the macroscopic flow characteristics just fluctuate around their respective mean values. This study focuses on the steady-state results. Unless otherwise noted, all the results shown are time-averaged steady-state results.

5.3 Results and discussion

5.3.1 Effect of vortex finder diameter

Fig. 5.2 shows the effect of vortex finder diameter on partition curve at high (*SC*=30%) and low (*SC*=4.14%) feed solids concentrations. It reveals that at a given feed solids concentration, the separation efficiency of particles increases with the decrease of vortex finder diameter for the 25-mm spigot used in the 75-mm cyclone. Note that unlike the previous studies (Moder and Dahlstrom, 1952; Kelsall, 1953; Rietema, 1961; Svarovsky, 1984; Concha et al., 1996), the ratio of vortex finder to spigot diameters is not considered as a variable in this study, because the ratio may be kept constant by changing appropriate dimensions of spigot and vortex finder diameter but their effects are likely different, as recently reported by Shah et al. (2006).

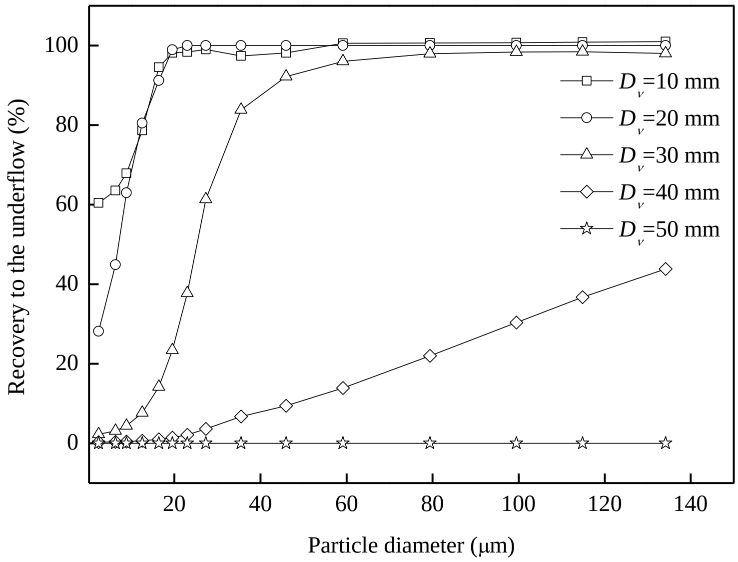

(a)

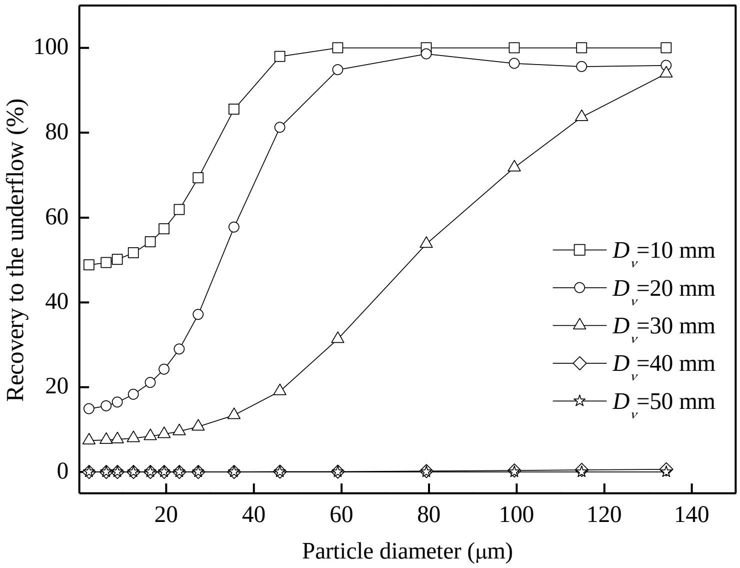

(b)

Fig. 5.2 Effect of vortex finder diameter on the separation efficiency at the feed solids concentration of: (a) *SC*=4.14% and (b) *SC*=30%.

Note that, the effect of spigot diameter was separately studied by the same mathematical model, as reported elsewhere (Ghodrat et al., 2013a). Fig. 5.2 indicates that when the diameter is too big, the separation efficiency decreases to zero. All these phenomena have been observed by Wang and Yu (2008) in their CFD-LPT study of hydrocyclone operated at a low feed solid concentration. However, Fig. 5.2 also shows that increasing feed solids concentration decreases the separation efficiency and critical vortex finder diameter. This cannot be obtained by the CFD-LPT approach due to its inherent deficiency. Here, the critical diameter is the diameter at which the separation does not occur in the hydrocyclone.

A partition curve can be characterised by cut size, sharpness of partition curve, and water split (Plitt, 1976). These three parameters together with inlet pressure drop (an index of energy loss) are used to judge cyclone performance in our study. This helps quantitatively to examine the effects of vortex finder configurations at all the feed solids concentrations considered. In the following, an optimum performance is identified once all the performance indices are at their best. Also, the concept of a compromised optimum performance is introduced to represent the situation where some indices are at their best while the remaining ones are reasonably good. Here, the cut size d_{50} is the size corresponding to the separation efficiency of 50% in a partition curve. The sharpness of the partition curve is described by the Ecart probable E_p, calculated by $(d_{75}\text{-}d_{25})/2$, where d_{75} and d_{25} are the sizes corresponding to the separation efficiency of 75% and 25%, respectively. A lower E_p corresponds to a more accurate partition, leading to better product quality. The so called water split is defined as the ratio of the volumetric water flow rate of the underflow to that of the feed stream. By definition, both d_{50} and E_p can be extracted from the partition curve, while the water split directly is obtained from the simulation output.

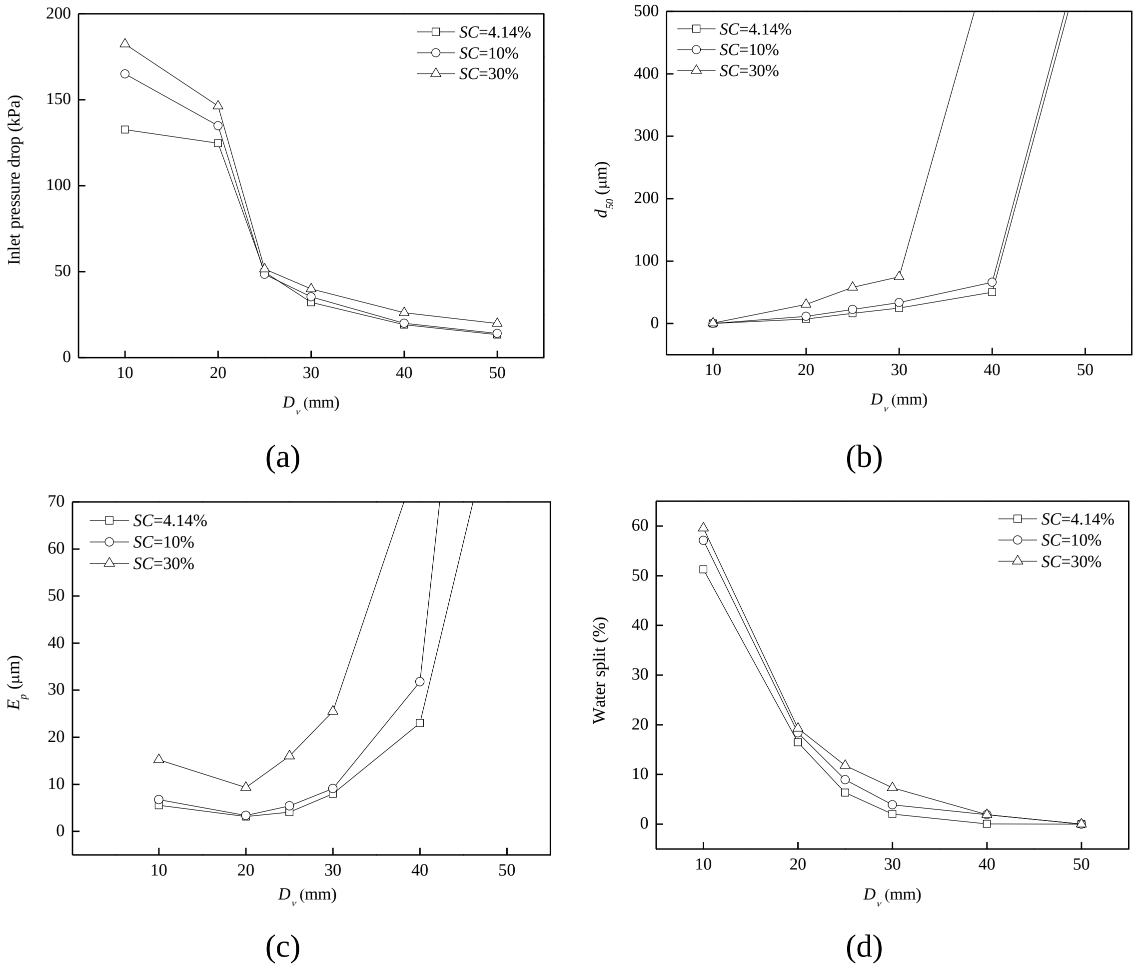

Fig. 5.3 Performance parameters as a function of vortex finder diameter at different feed solids concentrations: (a) inlet pressure drop, (b) d_{50}, (c) E_p, and (d) water split.

Fig. 5.3a shows that with increasing vortex finder diameter, the inlet pressure drop defined as the difference in the average pressures at the inlet and underflow outlet initially decreases sharply and then slows down. It monotonically increases with the increase of feed solids concentration but mainly at a thin vortex finder. These results are consistent with the experimental observation of Xu et al. (1991). On the other hand, the overall, d_{50} increases with the increase in the vortex finder diameter or feed solids concentration, although it almost remains the same when feed solids concentration is low and vortex finder diameter is small (e.g. *SC*=4.14% and D_v=10 mm) (Fig. 5.3b). Here, when the separation efficiency is zero, d_{50} is set to an infinite value by definition. This also applies to E_p. It is of interest to note that E_p decreases first to a minimum and then increases, and this variation is generally more evident at a higher feed solids concentration (Fig. 5.3c). However, the amount of water split to the underflow decreases with increasing vortex finder or decreasing feed solids concentration (Fig.

5.3d). Note that when hydrocyclones are used to classify particles, the water split should be insignificant because it largely reflects the amount of particles (regardless of being coarse or fine) which flow with the water, by-pass the classification process, and finally misplace at the underflow and overflow outlets (Lynch, 1976; Slechta and Firth, 1984). All of the results shown in Fig. 5.3 suggest that a compromised optimum vortex finder diameter can be identified based on the minimum E_p and relatively small water split and inlet pressure drop which is around 20 mm under the present condition. It should be pointed out that the selection criterion for determining the compromised optimum may have different focuses depending on applications.

In hydrocyclones, the radial acceleration a_r represents the driving force for separation (Svarovsky, 1984), calculated by:

$$a_r = u_t^2 / r \tag{5.10}$$

The acceleration drives particles towards the wall while the particles join in right flow streams. When it is not large enough, some relatively coarse particles join in the upward flow stream and report to the overflow. However, a too large radial acceleration brings relatively fine particles to join in the downward flow stream and report to the underflow. Both cases lead to deteriorated sharpness of the cut and thus large E_p. As such, the tangential velocity or radial acceleration is often used to explain different phenomena observed in hydrocyclones (see, e.g., Wang and Yu, 2006,2008; Davailles et al., 2012 ; Davailles et al., 2012; Ghodrat et al., 2013). In this study, the tangential velocities and associated properties such as axial velocities and solids volume fraction are examined to link their variations to those of performance indices shown in Fig. 5.3 for better understanding the effect of vortex finder configuration. The resulting representative results are given in Figs. 4 to7. In these figures, the white region corresponds to the area occupied by the air core, which is not shown for clarity because the properties of air and liquid phases are fairly different. This treatment is already adopted in all contours maps.

Fig. 5.4 shows that for the cyclones of different vortex finder diameters, the separation region characterized with relatively large tangential velocities is mainly located near the zone beneath the tip of the vortex finder. When the vortex finder diameter is increased at a constant feed solids concentration, the separation region shifts towards the wall and the velocity magnitudes generally decrease in that area. This can be observed more clearly in Fig. 5.5, which plots the tangential velocities in two representative regions in the same figure for cyclones of different vortex finder diameters. Because of the longer radial distance and smaller magnitudes of the tangential velocities, the radial acceleration decreases with the increase of vortex finder diameter according to Eq. (5.10). This leads to a lower E_p value. However, when the vortex finder is too thin (e.g. $D_v=10$), the upward flow cannot be developed at the lower part of the cyclone because the strong swirling flow causes the large tangential velocities there (see Fig. 5.6). Accordingly, at the lower part of the cyclone, fine particles cannot join the upward flow stream and report to the overflow as expected, even when these particles are properly separated in the radial direction. This deteriorates the sharpness of the cut and results in a relatively large E_p at the thinnest vortex finder. Consequently, a non-monotonic variation of E_p with vortex finder is observed (Fig. 5.3c). On the other hand, when the feed solids concentration is increased for the same cyclone design, the tangential velocities near the spigot region rapidly decrease due to the particles accumulated there (see Fig. 5.7). This leads to a decreased separation region and hence an increased E_p at a higher feed solids concentration.

Fig. 5.6 shows when the vortex finder becomes thinner, the locus of zero axial velocity generally moves towards the center and there is an increased portion of the downward flow characterized by negative axial velocities. As such, the water split increases, as shown in Fig. 5.3d. Fig. 5.6 also shows that the effect of feed solids concentration on the locus of zero axial velocity is much smaller than that of the vortex finder. This is consistent with the predicted result that the water split is influenced slightly by the feed solids concentration.

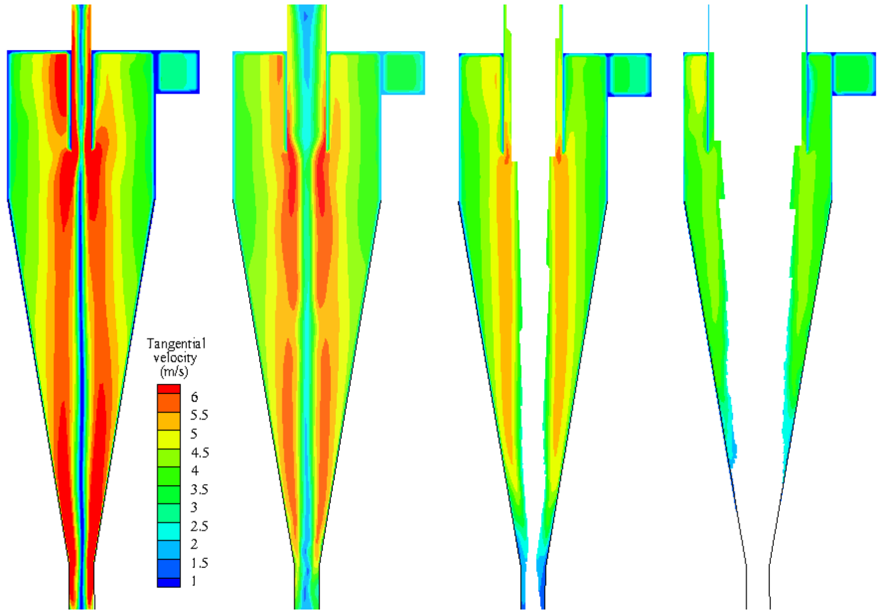

(a)

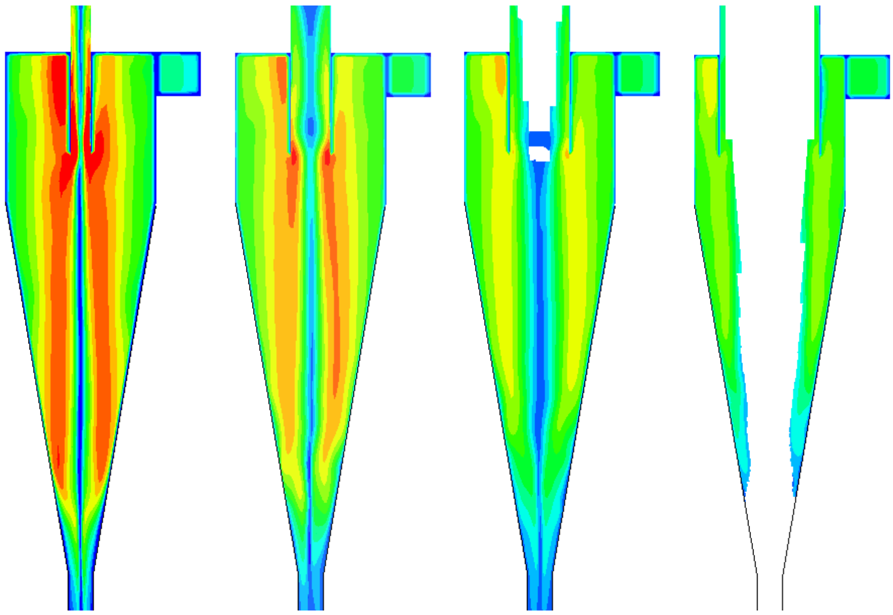

D_v=10 mm 20mm 30 mm 50 mm

(b)

Fig. 5.4 Spatial distribution of tangential velocities in the hydrocyclones with different vortex finder diameters at the feed solids concentration of: (a) *SC*=4.14%, and (b) *SC*=30%.

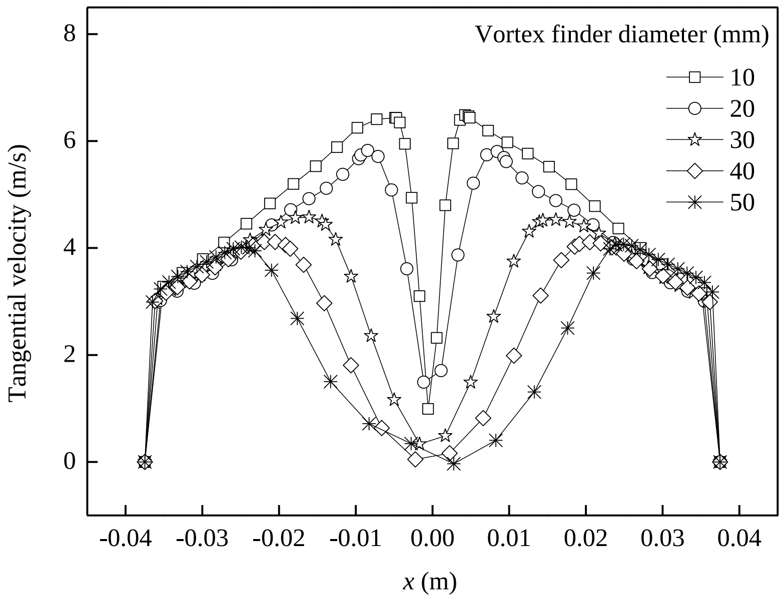

(a)

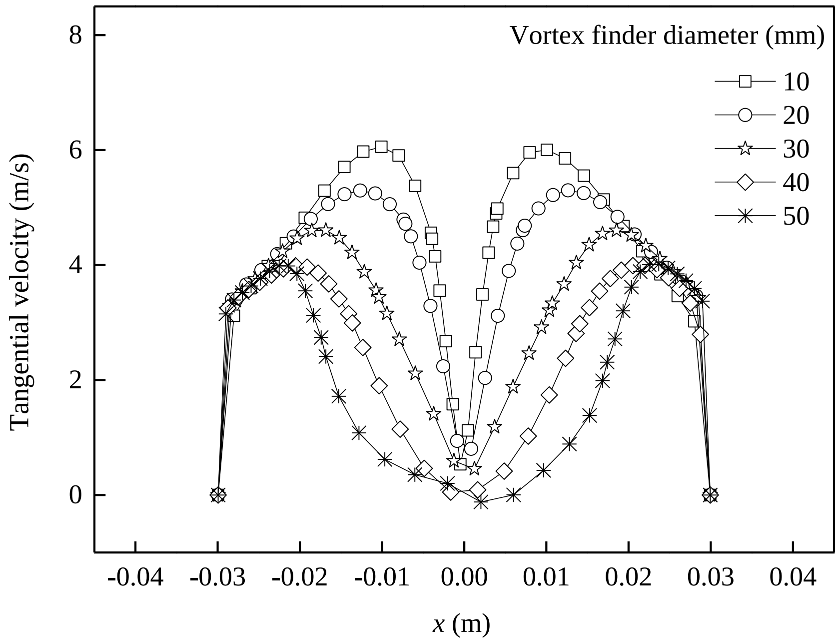

(b)

Fig. 5.5 Radial distribution of the tangential velocities in the horizontal plane located at (a) 60 mm and (b) 120 mm away from the roof of the hydrocyclones with different vortex finder diameters at the feed solids concentration of 30%.

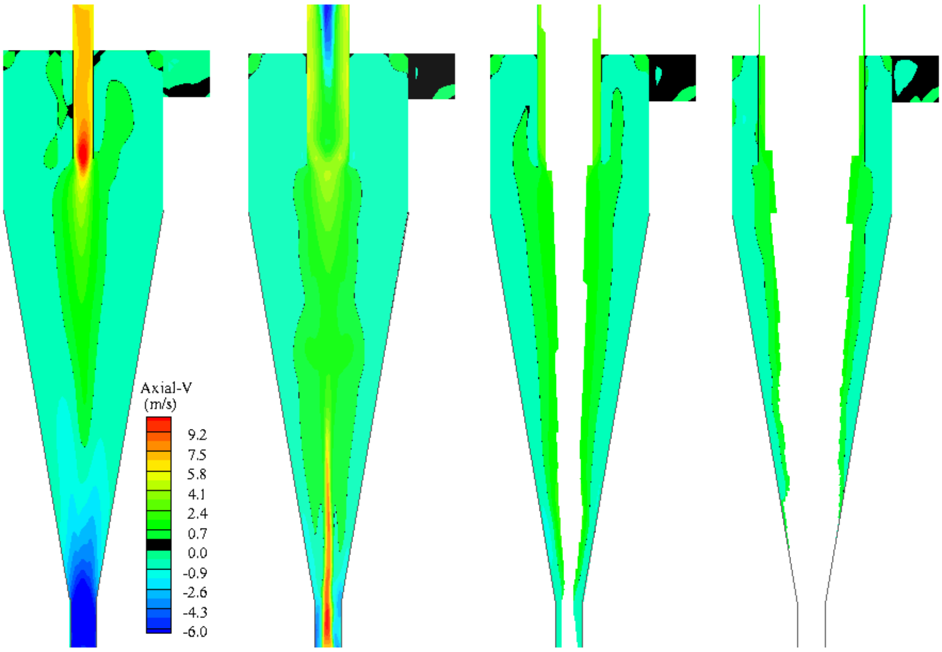

(a)

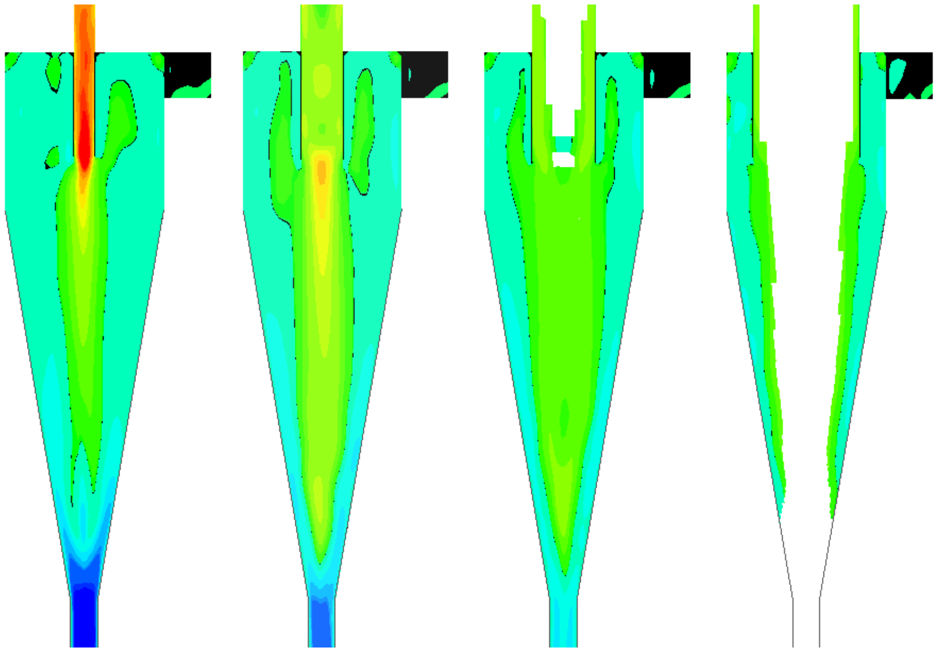

D_v=10 mm 20 mm 30 mm 50 mm

(b)

Fig. 5.6 Spatial distribution of axial velocities in the hydrocyclones with different vortex finder diameters at the feed solids concentration of: (a) *SC*=4.14%, and (b) *SC*=30%.

Fig. 5.7 reveals that when the vortex finder diameter or feed solids concentration increases, the solid volume fraction increases, especially near the wall and spigot regions. Rietema (1961) suggested that in the range of practical application, the pressure drop of a hydrocyclone may be determined only by the centrifugal head near the inlet region, which is expressed as:

$$\Delta p = \int_0^{D_c/2} \rho_m \frac{u_t^2}{r} dr \tag{5.11}$$

Therefore, the variations of tangential velocity (Fig. 5.4) and solids volume fraction (Fig. 5.7) are examined to understand how they affect the behavior of the inlet pressure drop (Fig. 5.4Fig. 5.4a) at varying feed solids concentration or vortex finder diameter. In the following discussion, the solid volume fraction is considered because it represents the mixture density when the particle density is constant. When the vortex finder diameter is increased for the same feed solids concentration, the tangential velocities near the inlet region generally decrease, while the variation of solids volume fraction is insignificant. This corresponds to the decreased inlet pressure drop at a wider vortex finder, which is consistent with Eq. (5.11) and the correlation of tangential velocities proposed by Neesse and Dueck (2007) for cyclones operated with water only. Similar numerical results were also obtained by different investigators for cyclones operated with water only (Narasimha et al., 2006; Wang and Yu, 2006; Bhaskar et al., 2007). Conversely, when the feed solids concentration is increased, for the same vortex finder contour, the tangential velocities near the inlet region increase slightly but mainly at relatively thin vortex finders, while the corresponding solids volume fraction generally increases. Accordingly, the increase of inlet pressure drop is significant only when the vortex finder is relatively thin. All these results suggest that under the conditions considered, the increase in the tangential velocities or solids volume fraction near the inlet region leads to the increase of inlet pressure drop. And, the effect of solids volume fraction is less significant. However, it should be pointed out that the distribution and magnitudes of tangential velocities may vary significantly with those of the solids volume fraction, as discussed above.

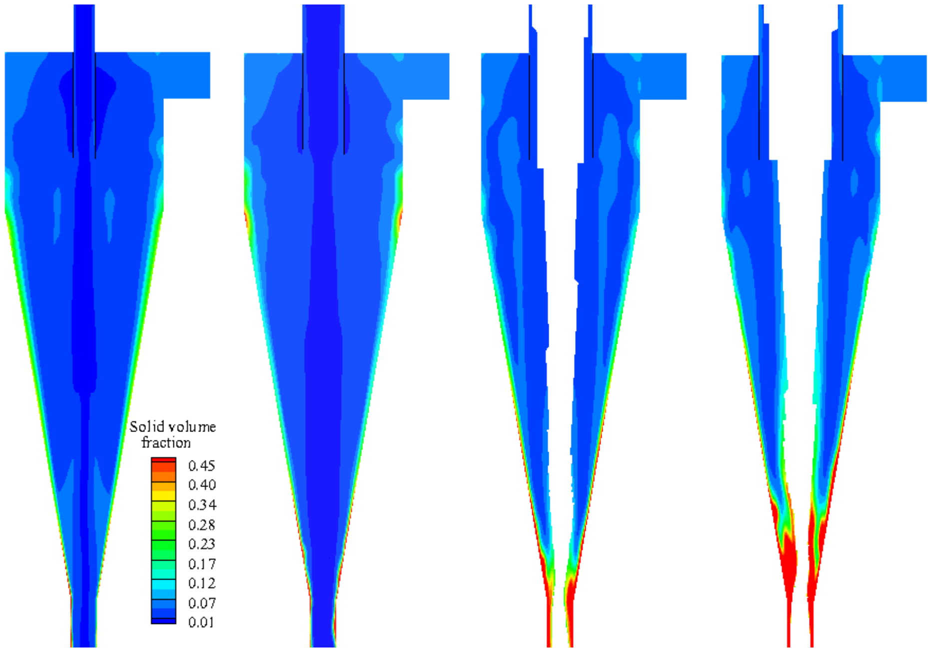

(a)

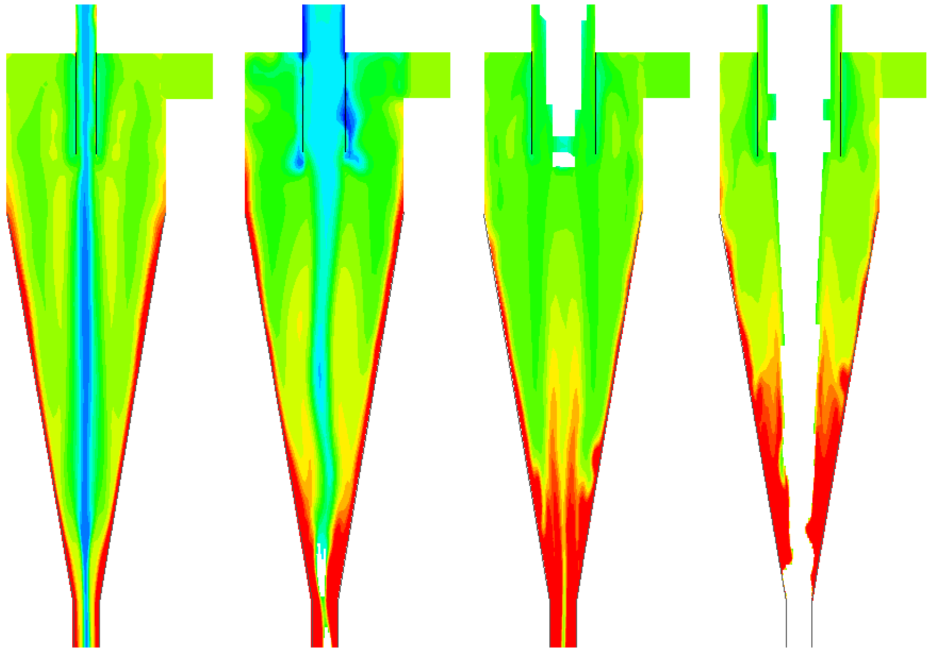

(b)

D_v=10 mm 20 mm 30 mm 50 mm

Fig. 5.7 Spatial distribution of solid volume fraction in the hydrocyclones with different vortex finder diameters at the feed solids concentration of: (a) *SC*=4.14%, and (b) *SC*=30%.

5.3.2 **Effect of vortex finder length**

Fig. 5.8 shows how the vortex finder length affects the separation efficiency at different feed solids concentrations. Here, the vortex finder length L_v is the distance between the tip of the vortex finder and the roof of the hydrocyclone, as illustrated in Fig. 5.1. Overall, the effect of the vortex finder length is much smaller than the vortex finder diameter. When feed solids concentration is low, with increasing vortex finder length, the separation efficiency decreases slightly for fine particles, however, increases for coarse particles (Fig. 5.8a). A similar result has also been reported by Wang and Yu (2008) in their CFD-LPT study of hydrocyclones operated in a dilute regime. However, the separation efficiency shows a different behavior at high feed solids concentration: it increases with the increase of vortex finder length (Fig. 5.8Fig. 5.8b). In addition, it is of interest to note that an unsmooth variation of separation efficiency with vortex finder length occurs at a high feed solids concentration. This may be explained as follows. The variations of separation region size and their tangential velocity magnitudes are intensified by both the variation of vortex finder length and the particles accumulation at the lower part of the cyclone for certain vortex finder lengths. This leads to a relatively sharp variation of partition curve for a small change in vortex finder length. These results at high feed solids concentrations have not been reported in the literature.

To understand the complicated separation behaviors shown in Fig. 5.8, we examine the distribution of tangential velocities and the results given in Fig. 5.9. It can be seen from this figure that at a low feed solids concentration, the region with large tangential velocities is located beneath the tip of vortex finder wall within the main separation space. Such a region decreases with the increases of vortex finder length, where the tangential velocities generally increase. The decrease of separation region should account for the decrease of separation efficiency as shown in Fig. 5.8a. When the vortex finder length is short or absent, the effect of the physical barrier to prevent coarse particles from reporting directly to the overflow as a result of the inertia effect is small or does not exist. This problem becomes worse at a low feed solids concentration, because the driving force for particles moving towards the wall is smaller as a result of the decreased peak of tangential velocities at a shorter vortex finder (Fig. 5.9a). Consequently, the corresponding separation efficiency of relatively coarse particles is worse (Fig. 5.8a). On the other hand, Fig. 5.9 shows that when the vortex finder length is increased at a high feed solids concentration, the separation region with large tangential velocities is located in the per-separation and main separation space, and its portion within the per-separation increases. When the separation region is gradually limited to the pre-separation space, it is more difficult for particles to move towards the center, flow with the upward flow, and report to the overflow. As such, the separation efficiency increases, as shown in Fig. 5.8b.

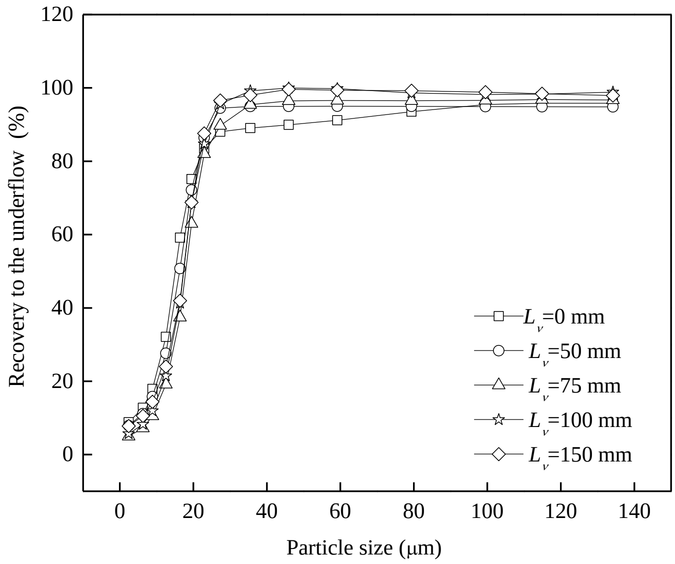

(a)

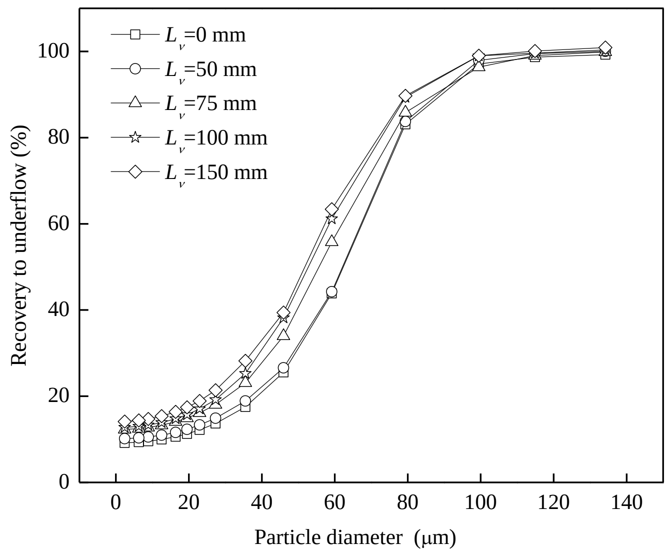

(b)

Fig. 5.8 Effect of vortex finder length on the separation efficiency at the feed solids concentration of: (a) *SC*=4.14% and (b) *SC*=30%.

The results given in Fig. 5.8 and Fig. 5.9 suggest that the absence of a vortex finder is not desirable, although it may result in high separation efficiency of relatively fine particles. Two problems can be identified when the vortex finder is absent. One is the separation efficiency of coarse particles is less than 100% (Fig. 5.8 a). This suggests that some coarse particles report to the overflow and thus are misplaced, leading to the contamination of product in practical application. This result is consistent with the experimental work of Kelsall (1953) who observed that the separation efficiency increases for fine particles but decreases for coarse particles at shorter vortex finders. Another problem is that the air core is found to be twisted when the vortex finder is absent (Fig. 5.9). This indicates the flow may be unstable, leading to more misplaced particles.

5.3.3 **Effect of vortex finder shape**

Fig. 5.10 shows how the cone ratio of the vortex finder D_b/D_t affects the separation efficiency at two representative feed solids concentrations. As seen from the figure, with increasing cone ratio, the separation efficiency decreases at all the feed solids concentrations considered. This variation becomes sharper with increasing feed solids concentration. Here, the operation with a zero separation for relatively large vortex finder diameters is not observed. Note that in this study, the maximum bottom entrance diameter for the inverse conical vortex finder is the same as the maximum diameter of the cylindrical vortex finder. In addition, the effect of the cylindrical section length (L_t) to the conical or inverse conical section length (L_b), L_t/L_b on separation efficiency for different vortex finder shapes (see Fig. 5.1) is also examined at both low and high feed solids concentrations, and the results are given in Fig. 5.11. As seen from the figure, such an effect is largely negligible and not analyzed further in the following.

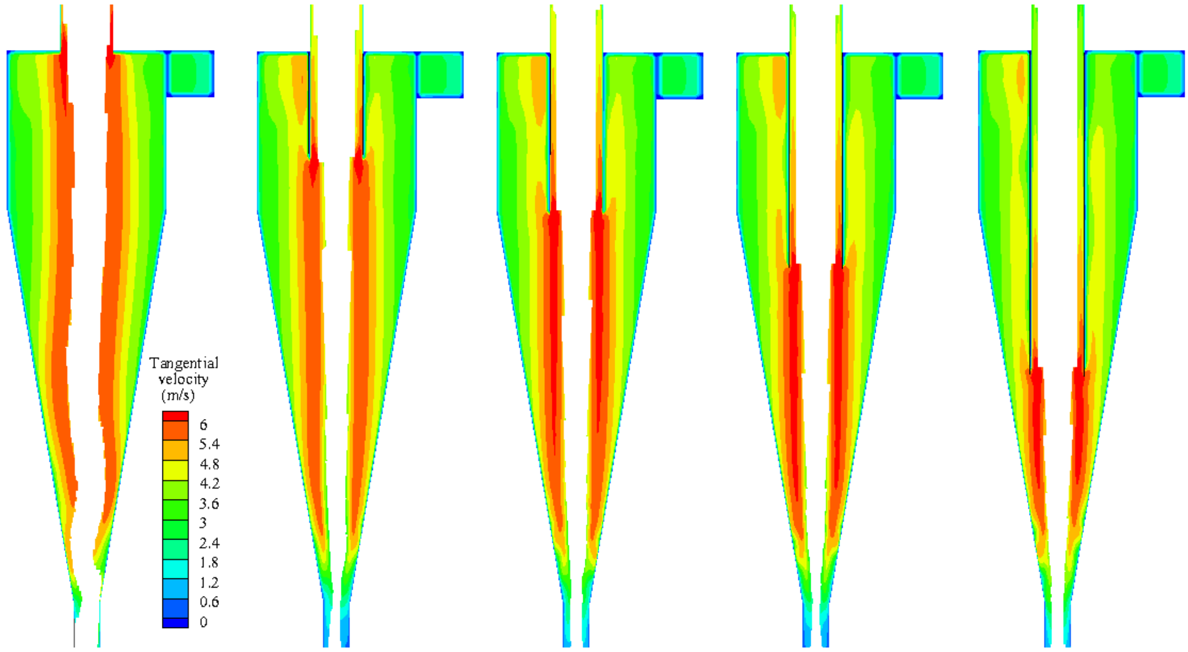

(a)

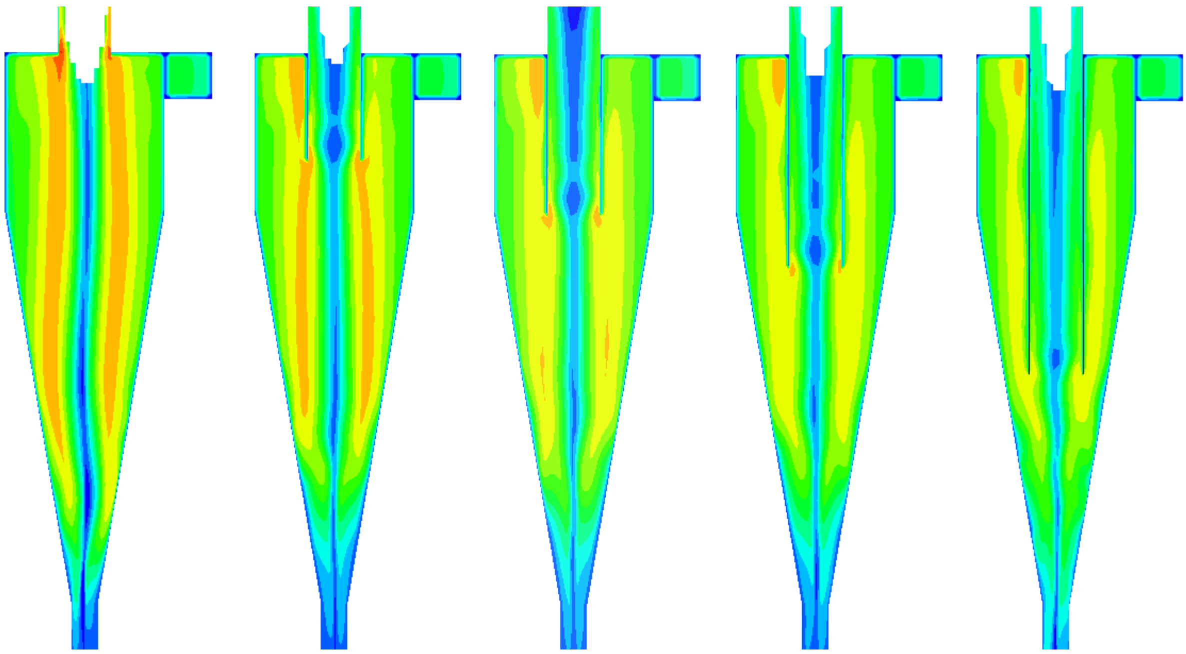

L_v=0 mm 50 mm 75 mm 100 mm 150 mm

(b)

Fig. 5.9 Spatial distribution of tangential velocities in the hydrocyclones with different vortex finder lengths at the feed solids concentration of: (a) SC=4.14%, and (b) SC=30%.

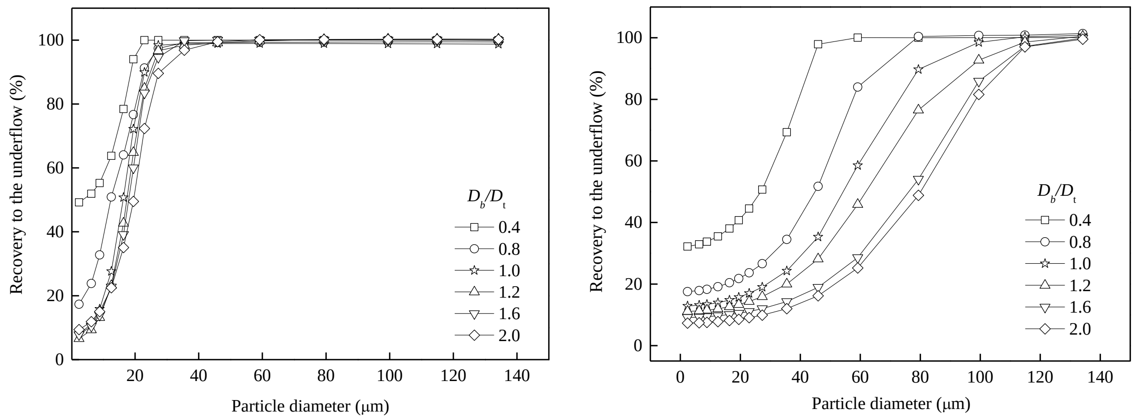

(a) (b)

Fig. 5.10 Effect of vortex finder shape on the separation efficiency at the feed solids concentration of: (a) *SC*=4.14% and (b) *SC*=30%.

Fig. 5.12 shows the effects of the cone ratio of the vortex finder on the four performance parameters at different feed solids concentrations. As seen from this figure, with increasing cone ratio, both the water split and inlet pressure drop initially decrease and then slow down, and at the same time, the d_{50} increases, but the E_p decreases first to a minimum and then increases gradually. The four parameters largely increase with the increase of feed solids concentration. But, under some conditions, the variations are very small and negligible. Overall, the water split and inlet pressure drop are much less sensitive to the feed solids concentration than the d_{50} and the E_p. Based on these results, a compromised performance can also be identified with relatively small inlet pressure drop, water split, and E_p. This compromised performance happens at the inverse conical vortex finder ratio around D_b/D_t=1.2 under the present condition.

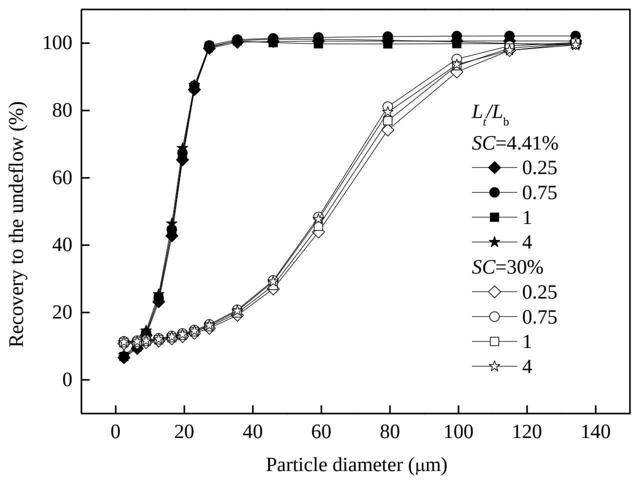

Fig. 5.11 Effect of Lt/L_b on the sepatation efficiency at D_b/D_t=1.2.

It should be pointed out that although an optimum design is obtained here, the four performance parameters generally vary smoothly for all the inverse conical vortex finders proposed.

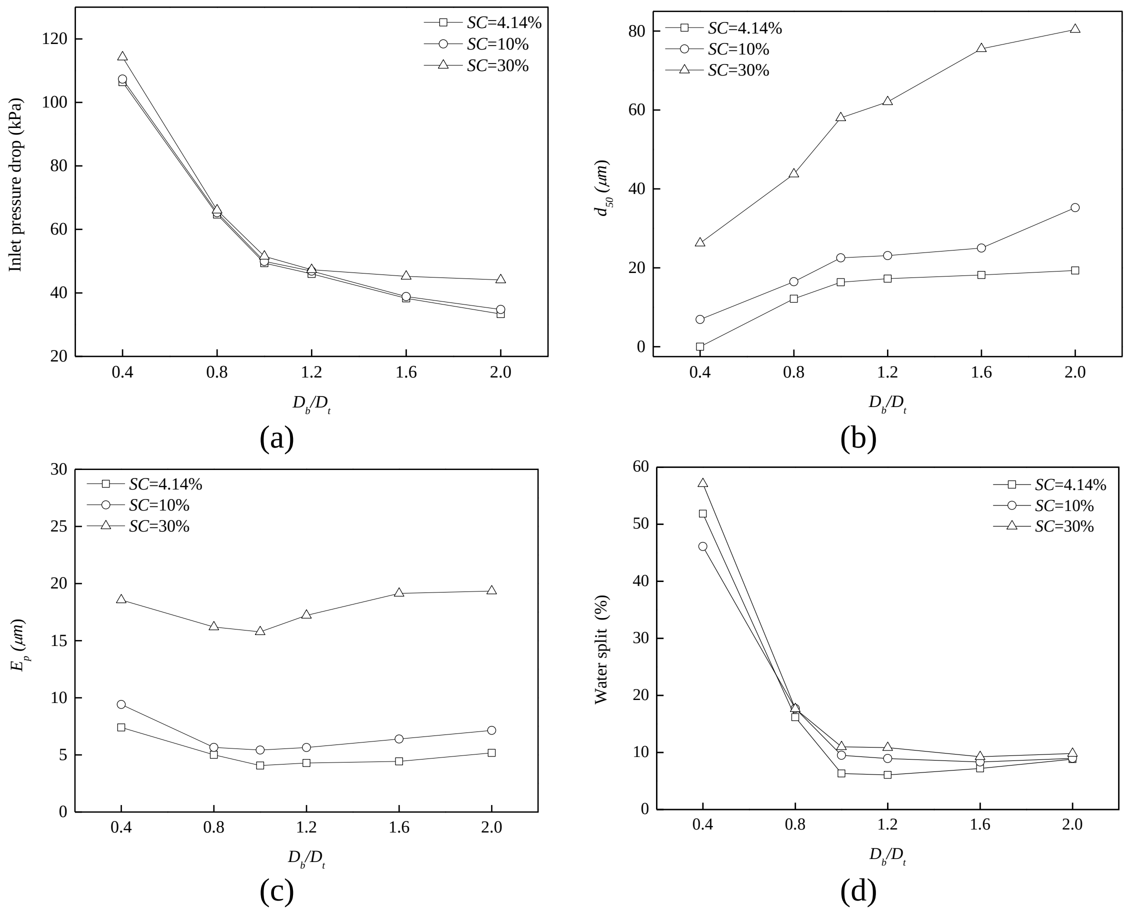

Fig. 5.12 Performance parameters as a function of cone ratio at different feed solids concentrations: (a) pressure drop, (b) d_{50}, (c) E_p, and (d) water split.

Similar to those discussed in Section 3.1, the performance behavior shown in Fig. 5.12 can also be explained by the corresponding tangential and axial velocities and solids volume fraction, which are given in Figs. 5.12-5.15, respectively. Fig. 5.13 shows that the magnitudes of tangential velocities in the separation zone generally decrease with the increase in the cone ratio. Also, at relatively small cone ratios (e.g. D_b/D_t=0.4), the downward flow cannot be developed at the lower part of the cyclone. The features of tangential and axial velocities account for the non-monotonic variation of E_p with cone ratio in Fig. 5.12c, similar to the effect of the vortex finder diameter. It is of interest to note that for a conical vortex finder, the location of the separation region corresponds to the large tangential velocities moves towards the cyclone wall with decreasing the bottom entrance diameter D_b of the vortex finder. However, for an inverse conical vortex finder, the location of the separation region is located beneath the tip of the wall of the cylindrical part. This feature of inverse-conical vortex finder limits the shift of separation zone towards the wall, and avoids the failure of separation. Fig. 5.13 also shows that both the size of the separation region and the magnitudes of the tangential velocities there decrease with the increase of the feed solids concentration. This should be the reason why E_p considerably increases at a higher feed solids concentration (Fig. 5.12c). Notably, a "stationary zone" at the largest cone ratio (highlight by a red circle in Fig. 5.13) is observed at all the feed solids concentrations considered. In such a zone, the tangential velocities decrease to zero or even change in direction. The flow from the inlet would pass around the "stationary zone", leading to energy dissipation. Accordingly, the peak in the tangential velocity is reduced and the intensity of the vortex is weakened. This result suggests that a vortex finder cone ratio cannot be too large in order to avoid the presence of the "stationary zone".

Fig. 5.14 shows that with increasing cone ratio of vortex finder, the locus of zero axial velocity initially moves rapidly towards the wall and then slows down. The influence of feed solids concentration is much less significant and the main difference comes from the spigot region where the locus of zero axial velocity moves upwards because of a significant amount of the particles accumulated there. These results account for the behavior of the water split shown in Fig. 5.12d: the water split rapidly decreases and then slows down with increasing vortex finder cone ratio; however, it increases with increasing feed solids concentration. Fig. 5.14 also shows that at the largest cone ratio, the locus of zero axial velocity twists. It indicates that the operation of such a design may not be stable. Thus, a large cone ratio is not desirable.

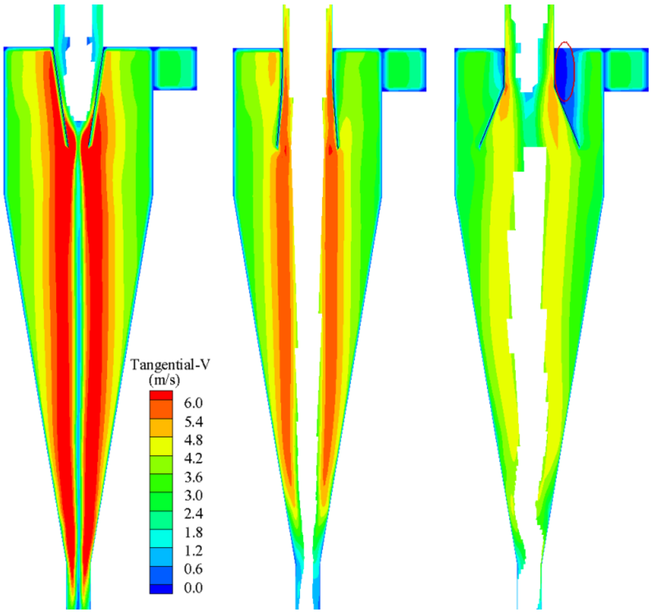

(a)

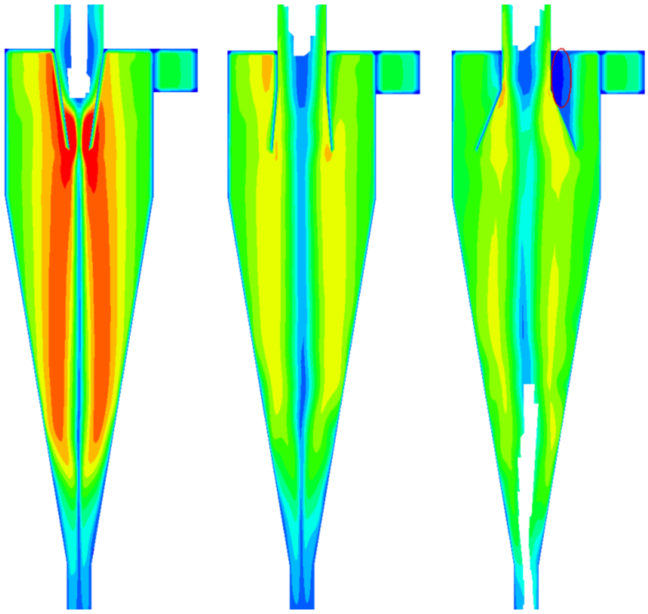

D_b/D_t=0.4 1.2 2

(b)

Fig. 5.13 Spatial distribution of tangential velocities in the hydrocyclones with different cone ratios at the feed solid concentration of: (a) *SC*=4.14%, and (b) *SC*=30%.

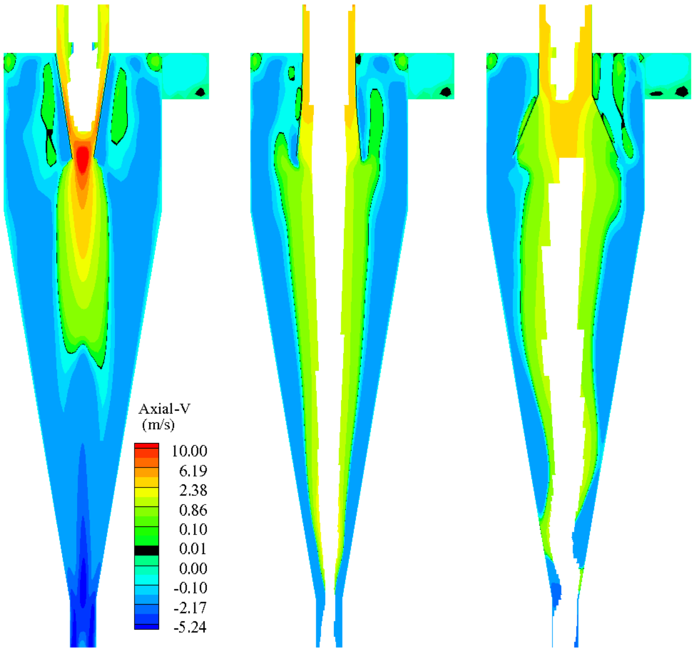

(a)

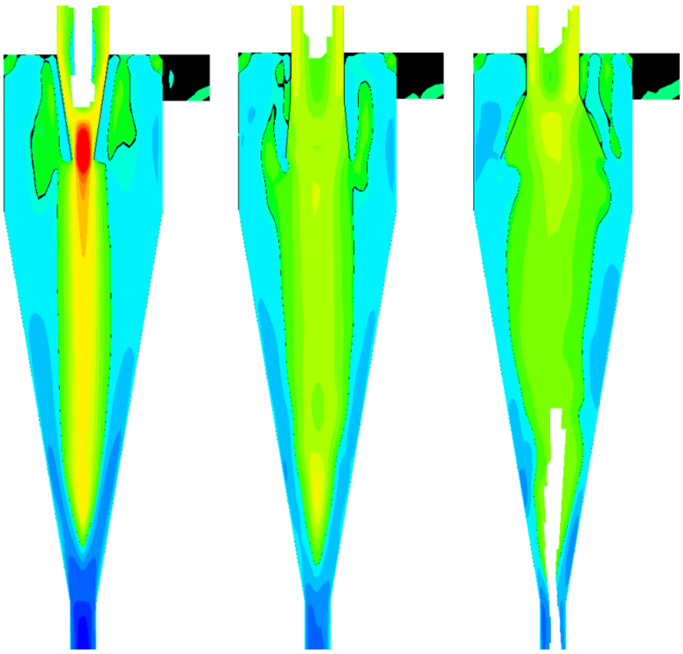

D_b/D_t=0.4 1.2 2

(b)

Fig. 5.14 Spatial distribution of axial velocities in the hydrocyclones with different cone ratios at the feed solids concentration of: (a) *SC*=4.14%, and (b) *SC*=30%.

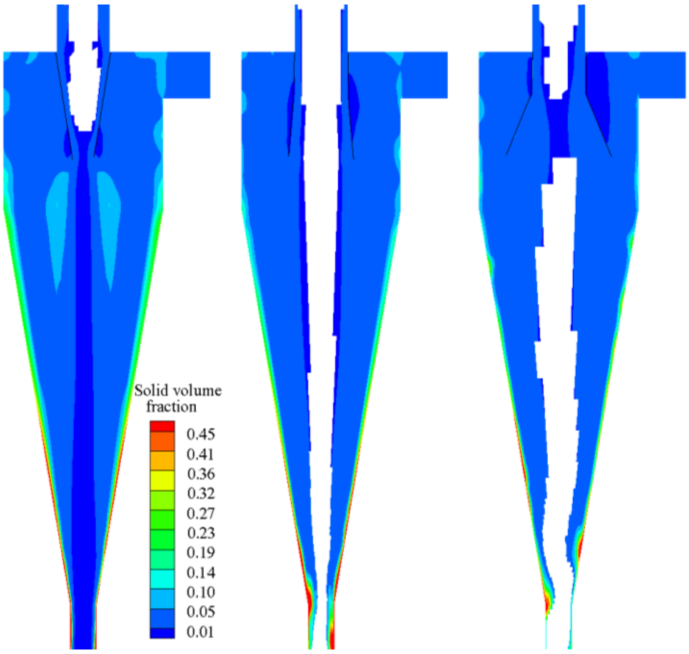

(a)

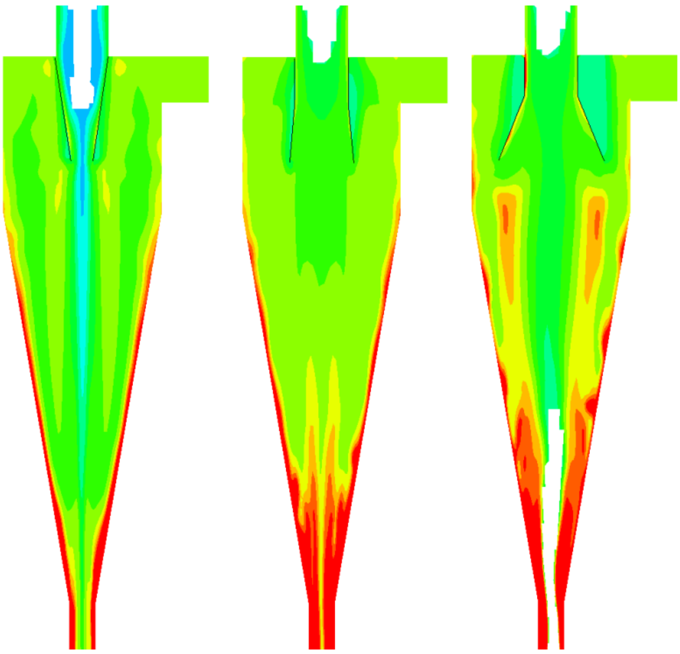

D_b/D_t =0.4 1.2 2

(b)

Fig. 5.15 Spatial distribution of solid volume fraction in the hydrocyclones with different cone ratios at the feed solids concentration of: (a) *SC*=4.14%, and (b) *SC*=30%.

Fig. 5.15 shows that with increasing cone ratio or feed solids concentration, the solid volume fraction increases, particularly near the wall and spigot regions. Similar to those discussed in Section 3.1, the inlet pressure drop shown in Fig. 5.12a can be explained together by the solids volume fraction (Fig. 5.15) and tangential velocities (Fig. 5.13). Based on the same analysis, which is not included here for brevity, we can conclude that the variation in the inlet pressure drop as a result of the change of cone ratio is mainly attributed to the variation of tangential velocities near the inlet region. Because the variation of tangential velocity is small and the contribution of solids volume fraction variation to inlet pressure drop variation is not significant, the variation of inlet pressure drop is small when the feed solids concentration is varied.

5.4 Conclusions

Vortex finder configuration plays an important role in the separation of particles in hydrocyclones. The flow and performance of the hydrocyclone have been studied by the recently developed CFD model (Kuang et al., 2012b), with special reference to diameter, length and shape of vortex finder. The shapes include the conventional cylindrical style and the proposed conical and inverse conical styles. The findings of this study can be summarised as follow:

(1) When the vortex finder diameter or shape varies, a compromised optimum performance can be identified with relatively small inlet pressure drop, d_{50}, E_p, and water split. The optimum shape is inverse conical style. In addition, at a large vortex finder diameter the separation function of the cyclone decreases, however, does not happen to the proposed vortex finders. Overall, both d_{50} and E_p are found to be more sensitive to feed solids concentration than inlet pressure drop and water split at different vortex finder configurations.

(2) The effect of the vortex finder length on the separation efficiency is much less significant than those of diameter and shape, which shows opposite trends at low and high feed solids concentrations due to different magnitudes and locations of large tangential velocities.

(3) The influences of vortex finder dimension and shape on cyclone performance are essentially governed by axial and tangential velocities and solids volume fraction. The tangential velocity and solids volume fraction near the inlet region determine the inlet pressure drop, while the portion of downward flow is characterised by the downward axial velocities which influences the water split. The size and location of the separation region with large tangential velocities and magnitude of the tangential velocities together govern the separation sharpness. These flow properties can, to some degree, be controlled by varying vortex finder configuration.

REFERENCES

Arato, E. G., 1984. Reducing head or pressure losses across a hydrocyclone. Filtration & Separation, 21 (3), 181-182.
Bhaskar, K., Murthy, Y., Raju, M., Tiwari, S., Srivastava, J., Ramakrishnan, N., 2007. CFD simulation and experimental validation studies on hydrocyclone. Minerals Engineering, 20 (1), 60-71.
Bradley, D., 1965. The Hydrocyclone; Pergamon. London, 1965.
Brennan, M. S., Narasimha, M., Holtham, P. N., 2007. Multiphase modelling of hydrocyclones - prediction of cut-size. Minerals Engineering, 20 (4), 395-406.
Chu, L. Y., Luo, Q., 1994. Hydrocyclone with high sharpness of separation. Filtration & Separation, 31 (7), 733-736.
Concha, F., Barrientos, A., Montero, J., Sampaio, R., 1996. Air core and roping in hydrocyclones. International Journal of Mineral Processing, 44-45 743-749.
Davailles, A., Climent, E., Bourgeois, F., 2012a. Fundamental understanding of swirling flow pattern in hydrocyclones. Separation and Purification Technology, 92 (0), 152-160.
Davailles, A., Climent, E., Bourgeois, F., Majumder, A. K., 2012b. Analysis of swirling flow in hydrocyclones operating under dense regime. Minerals Engineering, 31 (0), 32-41.
Duijn, G. V., Rietema, K., 1983. Performance of a large-cone-angle hydrocyclone—I: Hydrodynamics. Chemical Engineering Science, 38 (10), 1651-1661.
Dyakowski, T., Williams, R. A., 1996. Prediction of high solids concentration regions within a hydrocyclone. Powder Technology, 87 (1), 43-47.
Ghodrat, M., Kuang, S. B., Yu, A. B., Vince, A., Barnett, G. D., Barnett, P. J., 2013a. Computational study of multiphase flow and performance of hydrocyclone: effects of cyclone size and spigot diameter. Industrial & Engineering Chemistry Research, 52 16019-16031.
Ghodrat, M., Kuang, S. B., Yu, A. B., Vince, A., Barnett, G. D., Barnett, P. J., 2013b. Numerical analysis of hydrocyclones with different conical section designs. Minerals Engineering, http://dx.doi.org/10.1016/j.mineng.2013.12.003.
Hararah, M. A., Endres, E., Dueck, J., Minkov, L., Neesse, T., 2010. Flow conditions in the air core of the hydrocyclone. Minerals Engineering, 23 (4), 295-300.
Hirt, C. W., Nichols, B. D., 1981. Volume of fluid (VOF) method for the dynamics of free boundaries. Journal of Computational Physics, 39 (1), 201-225.
Hsieh, K. T., 1988. Phenomenological model of the hydrocyclone. PhD thesis, The University of Utah, Salt Lake City, UT, USA.
Huang, S., 2005. Numerical simulation of oil-water hydrocyclone using reynolds-stress model for Eulerian multiphase flows. Canadian Journal of Chemical Engineering, 83 (5), 829-834.
Kelsall, D. F., 1952. A study of the motion of solid particles in a hydraulic cyclone. Trans Inst Chem Engrs, 30 87.
Kelsall, D. F., 1953. A further study of the hydraulic cyclone. Chemical Engineering Science, 2 (6), 254-272.
Kilavuz, F. S., Gulsoy, O. Y., 2011. The effect of cone ratio on the separation efficiency of small diameter hydrocyclones. International Journal of Mineral Processing, 98 (3-4), 163-167.

Kuang, S. B., Chu, K. W., Yu, A. B., Vince, A., 2012a. Numerical study of liquid-gas-solid flow in classifying hydrocyclones: effect of feed solids concentration. Minerals Engineering, 31 17-31.
Kuang, S. B., Chu, K. W., Yu, A. B., Vince, A., 2012b. Numerical study of liquid–gas–solid flow in classifying hydrocyclones: Effect of feed solids concentration. Minerals Engineering, 31 (0), 17-31.
Lynch, A. J., 1976. Mineral crushing and grinding circuits. Elsevier, Amsterdam.
Manninen, M., Taivassalo, V., Kallio, S., 1996. On the mixture model for multiphase flow. VTT Publications 288, Technical Research Centre of Finland.
Martinez, L. F., Lavin, A. G., Mahamud, M. M., Bueno, J. L., 2007. Improvements in hydrocyclone design flow lines stabilization. Powder Technology, 176 (1), 1-8.
Martinez, L. F., Lavin, A. G., Mahamud, M. M., Bueno, J. L., 2008. Vortex finder optimum length in hydrocyclone separation. Chemical Engineering and Processing, 47 (2), 192-199.
Moder, J. J., Dahlstrom, D. A., 1952. Fine-size, close-specific-gravity solid separation with the liquid-solid cyclone. Chemical Engineering Progress, 48 (2), 75-88.
Motsamai, O. S., 2010. Investigation of the Influence of Hydrocyclone Geometric and Flow Parameters on Its Performance Using CFD. Advances in Mechanical Engineering.
Murthy, Y. R., Bhaskar, K. U., 2012. Parametric CFD studies on hydrocyclone. Powder Technology, 230 36-47.
Narasimha, M., Brennan, M., Holtham, P. N., 2006. Large eddy simulation of hydrocyclone - prediction of air-core diameter and shape. International Journal of Mineral Processing, 80 (1), 1-14.
Narasimha, M., Brennan, M., Holtham, P. N., 2007a. A review of CFD modelling for performance predicitons of hydrocyclone. Engineering Applications of Computational Fluid Mechanics, 1 (2), 109-125.
Narasimha, M., Brennan, M. S., Holtham, P. N., 2012. CFD modeling of hydrocyclones: Prediction of particle size segregation. Minerals Engineering, 39 (0), 173-183.
Narasimha, M., Brennan, M. S., Holtham, P. N., Napier-Munn, T. J., 2007b. A comprehensive CFD model of dense medium cyclone performance. Minerals Engineering, 20 (4), 414-426.
Neesse, T., Dueck, J., 2007. Air core formation in the hydrocyclone. Minerals Engineering, 20 (4), 349-354.
Noroozi, S., Hashemabadi, S. H., 2009. CFD simulation of inlet design effect on deoiling hydrocyclone separation efficiency. Chemical Engineering and Technology, 32 (12), 1885-1893.
Nowakowski, A. F., Cullivan, J. C., Williams, R. A., Dyakowski, T., 2004. Application of CFD to modelling of the flow in hydrocyclones. Is this a realizable option or still a research challenge? Minerals Engineering, 17 (5), 661-669.
Nowakowski, A. F., Kraipech, W., Williams, R. A., Dyakowski, T., 2000. The hydrodynamics of a hydrocyclone based on a three-dimensional multi-continuum model. Chemical Engineering Journal, 80 (1-3), 275-282.
O'Brien, M., Taylor, A., Nemeth, D., Firth, B., Clarkson, C., 2000, Large diameter classifying cyclones. ACARP report, C6047.
Olson, T. J., Van Ommen, R., 2004. Optimizing hydrocyclone design using advanced CFD model. Minerals Engineering, 17 (5), 713-720.
Plitt, L. R., 1976. A mathematical model of the hydrocyclone classifier. Cim Bulletin 69 (3), 114-123.

Rajamani, K., 1987. Improvements in the classification efficiency of a hydrocyclone with an impeller installation around the vortex finder. Particulate Science and Technology, 5 (1), 83-94.
Rietema, K., 1961. Performance and design of hydrocyclones—II : Pressure drop in the hydrocyclone. Chemical Engineering Science, 15 (3–4), 303-309.
Shah, H., Majumder, A. K., Barnwal, J. P., 2006. Development of water split model for a 76 mm hydrocyclone. Minerals Engineering, 19 (1), 102-104.
Silva, D. O., Facanha, J. M. F., Vieira, L. G. M., Barrozo, M. A. S. 2012. Experimental Study of the Influence of Vortex Finder Geometry on Hydrocyclones Performance. In: Salgado L., Ambrozio F., editors. Advanced Powder Technology Viii, Pts 1 and 2. Stafa-Zurich: Trans Tech Publications Ltd. p 1848-1853.
Slechta, J., Firth, B. A., 1984. Classification of fine coal with a hydrocyclone. International Journal of Mineral Processing, 12 (4), 213-237.
Svarovsky, L., 1984. Hydrocyclones. Holt, Rinehart and Winston, Sydney.
Swain, S., Mohanty, S., 2013. A 3-dimensional Eulerian–Eulerian CFD simulation of a hydrocyclone. Applied Mathematical Modelling, 37 (5), 2921-2932.
Wang, B., Chu, K. W., Yu, A. B., Vince, A., 2009. Modeling the Multiphase Flow in a Dense Medium Cyclone. Industrial & Engineering Chemistry Research, 48 (7), 3628-3639.
Wang, B., Yu, A. B., 2006. Numerical study of particle-fluid flow in hydrocyclones with different body dimensions. Minerals Engineering, 19 (10), 1022-1033.
Wang, B., Yu, A. B., 2008. Numerical study of the gas-liquid-solid flow in hydrocyclones with different configuration of vortex finder. Chemical Engineering Journal, 135 (1-2), 33-42.
Xu, J. R., Luo, Q., Qiu, J. C., 1991. Research on the preseparation space in hydrocyclones. International Journal of Mineral Processing, 31 (1-2), 1-10.
Yang, Q., Wang, H. L., Wang, J. G., Li, Z. M., Liu, Y., 2011. The coordinated relationship between vortex finder parameters and performance of hydrocyclones for separating light dispersed phase. Separation and Purification Technology, 79 (3), 310-320.
Zhang, Y. H., Qian, P., Liu, Y., Wang, H. L., 2011. Experimental study of hydrocyclone flow field with different feed concentration. Industrial and Engineering Chemistry Research, 50 (13), 8176-8184.

CHAPTER 6

CFD STUDY OF THE EFFECTS OF COAL DENSITY ON MULTIPHASE FLOW AND PERFORMANCE OF A HYDROCYLONE

A numerical model has been extended and modified to study the effect of various density flows in fine coal classification within a hydrocyclone of 1000 mm body diameter. In the model, the Reynolds Stress Model (RSM) is adopted to describe the anisotropic turbulence flow of the liquid–gas–solid mixture. The interface between the liquid and air core, and particle flow are both modelled using the mixture multiphase model under different conditions. The simulated flow features allow estimates to be made of the pressure drop, amount of water split, and partition curves for coal particles of different sizes and densities. These estimates are compared favourably with industrial scale measurements of a 1000 mm hydrocyclone operating under similar conditions. On this base, the effect of the particle density distribution that represents the foremost difference between several major coal types is studied. The results are analysed in terms of flow patterns, partition performance and energy consumption indices.

6.1 INTRODUCTION

The hydrocyclone has met the production requirements of the coal industry in the 1970s and 1980s. Its popularity is a result of its simplicity, flexibility of operation and the high capacity. But the actual physical principles which determine its performance are complex and not well understood. The presence of misplaced fine particles as a result of inefficiencies in the operation of the hydrocyclone, decrease the separation efficiency of the subsequent unit operations used for cleaning the coal, such as dense medium cyclones, spirals and flotation. The efficiency of the subsequent dewatering process is also reduced due to the high surface area of the tramp ultrafine particles. A large body of information is available in the technical literature. But "In the entire field of mineral processing another unit operation can hardly be found where the development has been slower than in classification sizing of finely divided solids" (Hukki, 1968).

Although hydrocyclones provide a cost effective method of classification, two problems with the device are identified, first the ultra-fine particles report to the oversize flow stream in proportion to the water split, and second the coarse coal particles report to the undersize flow stream due to the adverse effect of the wide range of particle densities found in fine coal feeds. Approaches to overcome the first problem such as using two cyclones in series tend to exacerbate the density effect problem and result in unacceptable loss of coarser coal particles. Overall coal preparation involves three sequential processes. Classification of the plant feed into different sizes, separation of the coal from the high ash material, by a process selected for its efficiency in treating a particular size fraction, and dewatering of the coal product.

The classification of coal at coarse sizes (0.5mm and above) is considered to be relatively efficient, and no technical challenges are apparent with current equipment. The development and use of the hydrocyclone in the 1950's, and the introduction of improved screen surfaces (wedge -wire in the 60's and polyurethane in the 80's) provided adequate technology for the plant metallurgists to meet the production requirements of the coal industry in the 1970's and 1980's. Hence classification technology has changed little since this time. Much of the coal preparation research over the last forty years has been aimed at improving the efficiency of the actual cleaning process. More recently it has been recognised that the classification process has a large effect on process efficiency, and in particular, the classification of fine particles is no longer considered satisfactory. The presence of misplaced fine particles, both coal and clay has been shown to decrease the separation efficiency of subsequent unit operations such as dense medium cyclones and baths, spirals and particularly flotation. The efficiency of the subsequent dewatering process is also reduced due to the high surface area of the ultra-fine particles, and the decrease in the permeability of material beds. It is now apparent that further improvements in the yield/ash/moisture content relationship which a coal preparation plant can achieve will require increased efficiency in this size separation step. Current classification technology is largely inadequate and efforts should be made to improve the capability, and a more general industry attitude that a better understanding of the impact of fine classification in current plant practice is required. The objective of this part of the work is to enhance coal recovery by applying a new developed computational fluid dynamics method for fine coal classification.

The development that has taken place in hydraulic classification since the first hydrocyclone by Bretney (1891) and the first rake classifier by Dorr in 1904 has concerned almost constructional improvements in the apparatus. During more than half a century, however, these developments have not yet produced the desired improvement in the sharpness (efficiency) of the separation process itself. For the classification of fine coal at separation sizes less than 0.5mm hydraulic drag type classifiers, such as the Dorr and the Akins units, were the common type of device used in the early period of coal preparation. Heiskanen (1996) recently identified a number of the problems which have limited separation of the device these include: non-linearity of the equations, non-symmetry of the flows, boundary conditions, turbulent energy dissipation, particle-particle interactions and the coupling of the flow field and local particle concentration. There have been a large number of papers published on the experimental investigation of one or more of the factors which can influence the cyclone performance. This has resulted in a number of empirical models being defined and refined over the last twenty five years. With all experimental work there are errors in sampling, processing and measurement. When a number of samples are taken around a particular circuit and there is an excess of measured values to the number of values which define the current operational state of the circuit, this results in a conflict between the calculated values of a particular parameter depending on the calculation pathway and the measured values.

For plants which require a size separation step between 0.25 and 0.1 mm, a large diameter hydrocyclone will similarly have distinct advantages over more traditional designs in terms of reducing capital and maintenance costs, and simplifying plant layout. The elimination of the subdivision step, required by multiple smaller units operated in parallel, would also lead to improved cleaning efficiency by avoiding different cut points in the parallel units. Where a higher cut point is appropriate, single large diameter cyclones could be used. Unfortunately, there is no operational information on the performance of this type of unit in classifying coal feeds due to the prodigious sampling difficulties at the one site where they have been installed. In a recent plant upgrade at another site, this issue has prevented the selection of a large diameter cyclone.

The concept of using large cyclone units, to overcome particular deficiencies is not new; for example Williams et al., (1994) provides a list of published papers in this area. But the issue of particle density effect has not been addressed, and no information on the operation at realistic cyclone sizes indicated. Firth et al., (1995) tried to maximise the amount of clean coal which can be presented to the spiral. Besides Plitt (1976) found that the solids content of the feed was the variable which had the greatest influence on the d_{50c} value. It was believed that this was due to the increase in slurry viscosity, but did draw attention to hindered settling and overcrowding in the region of the spigot (Fahlstrom, 1963) as other potential factors.

The experimental work of Fahlstrom (1963) considered slurries with high solids concentrations (up to 20% by volume). The results from this work were used by Fahlstrom to develop a crowding theory for the operation of cyclones. The underlying physics controlling the density effect in hydrocyclones is still not understood in a quantitative manner. Hence further fundamental research work is required since an improved understanding could provide further applications for this type of device which is low cost with regard to capital and operation. The potential use of large classification cyclones needs to be investigated in detail since these provide the opportunity for the circuit to be implemented in the simplest possible manner.

So in this chapter, hydrocyclones with feed slurries of different densities have been studied at two feed solids concentrations by a recently developed TFM model facilitated by extending the mixture model of (Kuang et al., 2012a), to better understand the effects of density variation on flow regime and performance of hydrocyclones.

6.2 SIMULATION METHOD AND CONDITIONS

6.2.1 Model description

The TFM model facilitated by the mixture model which has been discussed in detail in section 2.8.2 also in the recent work of Kuang (2012b), has been extended in this chapter to examine the effect of feed density variation on flow and performance of hydrocyclones . For avoid repetition, only the key features of the model are outlined below.

In the model as indicated in section 2.8.2, both the fluid (liquid and air) and solid phases are treated as interpenetrating continua. Particles of different sizes or densities represent different phases. In this chapter, coal density is considered as a variant while the coal sizes are specified according to a size range given in Table 6.1. To effect a simulation, the size distribution is divided into a series of size intervals. Each size interval is represented by a mean size in the simulation. The flow of liquid-gas-solid mixture (as a single phase) is calculated from the continuity and the Navier–Stokes equations based on the local mean variables over a computational cell considering slip velocities between different phases (Manninen et al., 1996). This gives both the interface between the liquid and air core and the flows of liquid and different sized particles. The turbulent flow of liquid-gas-solid mixture is modelled using the Reynolds stress model (Launder et al., 1975). The solid properties are described by the kinetic theory based on the algebraic temperature model (Syamlal et al., 1993). The detail of the used model has been elaborated in section 2.8.2.

6.2.2 Simulation conditions and boundary conditions

A 1m diameter Multotec cyclone from Ludowici mineral Processing Equipment was used in this study. The geometry and mesh representation of the hydrocyclone are shown in Fig. 6.1 while the geometric parameters are given in Table 6.1. The cyclone is divided into 95153 hexahedral cells. The angle between the cyclone and the horizontal, i.e. the orientation angle, is 10 degrees. The feed density varies between 1275 to 2200 kg/m^3. The operational parameters used in the simulation are summarised in Table 6.1. Feed solids concentration varies between 6.6 and 13.4 % by volume which is equal to 10 and 20% by mass. The pressure at the two outlets (vortex finder and spigot) is 1 atm (101.325 kPa). The size distribution and mass fraction of coal particles of different densities are deduced from the industrial data determined at the time of testing (O'brin et al., 2001). The simulations are undertaken by firstly allowing the slurry flow to attain steady state. Coal particles are then injected continuously from the inlet. The number of particles injected in a given time is calculated so as to match that determined during the industrial tests. For simplicity, all particles are assumed to be spherical. Totally 22 cases were simulated to study the effect of density. The simulated particle size is the same in each case, as shown in Table 6-1.

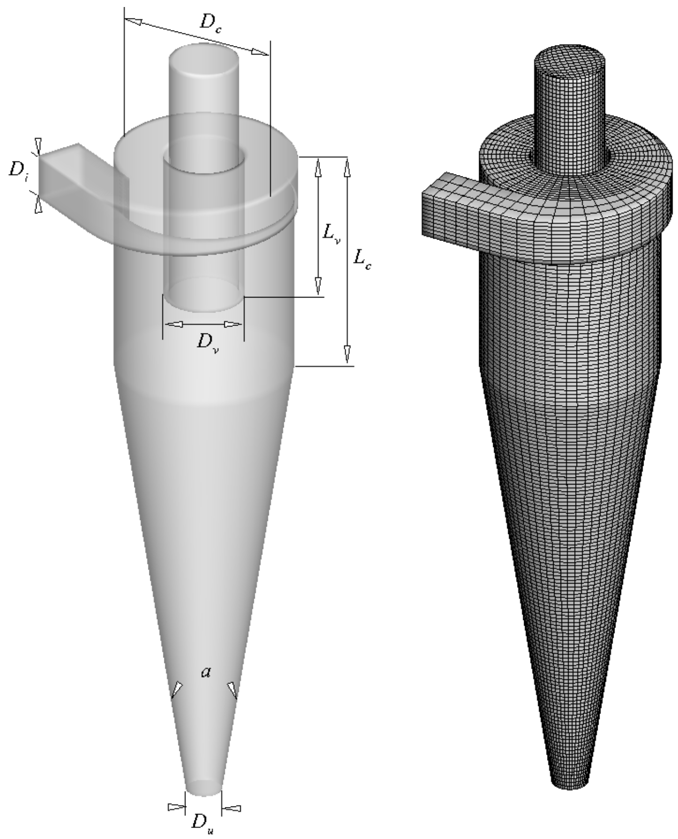

Fig. 6.1 the geometry and mesh representation of the hydrocyclone

Table 6-1 Geometrical and operational conditions used in the simulations

Parameter	Symbol	Value*
Geometrical parameter		
Diameter of the body (mm)	D_c	1000
Diameter of inlet (mm)	D_i	335
Diameter of vortex finder (mm)	D_v	390
Diameter of spigot (mm)	D_u	200
Length of cylindrical part (mm)	L_c	1158
Length of conical part (mm)	L_{co}	2330
Length of vortex finder (mm)	L_v	250
Cone angle (°)	a	20°
Inclination angle (°)	b	15°
Operational condition		
Inlet velocity (m/s)	U	3.3
Particle material	-	Coal
Particle density (kg/m^3)	ρ_p	1275,1350,1500,1885,2200
Feed solids concentration (% by volume)	ρ_{feed}	(6.6% - 13.4%)
Particle sizes simulated (mm)	D	1.41,0.71,0.42,0.3,0.21,0.15,0.115,0.08,0.045

A 1-m diameter hydrocyclone is hence considered, which consists of seven main geometrical parameters (see Fig. 6.1): diameter of the cylindrical body (D_c), diameter of inlet (Involute entry of the feed) (D_i), diameter of vortex finder (D_o), diameter of apex (D_u), length of cylindrical part (L_c), length of vortex finder (L_v) and cone angle (a) and inclination angle (b). The flow rate of the feed to the cyclone could not be varied since it was taking all of the fine coal which the plant was processing and was being fed by a fixed speed centrifugal pump. The design feed rate to the cyclone was approximately 290 L/s. One unusual feature with the simulations is the unusually high solids content of the feed to the cyclones. At 20% by mass, it was not optimum for cyclone performance, but it allowed the opportunity to investigate the impact of varying coal solids content on cyclone flow and performance. All the simulations are conducted using the ANSYS Fluent CFD software package (version 14) at the National Computational Infrastructure in Australia. 32 CPUs are assigned to each simulation. It lasts for about 14 days for each run of simulations to ensure that the flow simulated can achieve a steady state at which the macroscopic flow characteristics do not change much with time. Unless otherwise noted, all the results shown are time-averaged.

6.3 RESULTS AND DISCUSION

6.3.1 Effect of particle density on the partition curve

The role of changing particle relative density on cyclone efficiency and performance is considered in this section. The lack of a comprehensive set of experimental results means that the effect can only be analysed in a semi-quantitative manner. (b)

Fig. 6.2 compares the calculated partition curves and measured results, obtained according to the mass portions of particle recovery to the underflow. In this figure, the particle density is expressed as the relative density (RD), defined as the ratio of relative particle density to water density. This applies to all the results obtained here. In addition, the calculated results from this study are generated by the multiphase mixture model in which particles considered are classified according to particle density, as done in the experimental measurement of O'Brine (2001) and the density distribution in each set of simulation is represented by a mean density, while the size distribution is signified by nine mean sizes plus two liquid and air phases. Ten independent simulations are then conducted at different densities and two feed solids concentrations. Fig. 6.2 shows the effect of relative density on partition curve at different feed solids concentrations (SC=6.6 % and *SC*=13.4% by volume). It reveals that at a given feed solids concentration, the separation efficiency of particles increases with the increase of coal relative density. Note that unlike the previous studies (Chu et al., 2002), the ratio of vortex finder to spigot diameter is not considered as a variable in this study, because the ratio may be kept constant by changing appropriate dimensions of spigot and vortex the finder diameter but their effects are likely different, as recently reported by Shah et al., (2006). Fig. 6.2 indicates that when the coal density is higher, the separation efficiency is higher and the overall partition curve is sharper. Fig. 6.2 also shows that the magnitude of the density effect decreases with the solids concentration and the partition curve of both lighter and heaver material moves to lower separation sizes. The lighter the material then the lower the solids content at which the density effect starts. This can be interpreted as being due to the crowding of the particles at the spigot being heavily influenced by the volume fraction of solids which can effectively pass into the oversize stream.

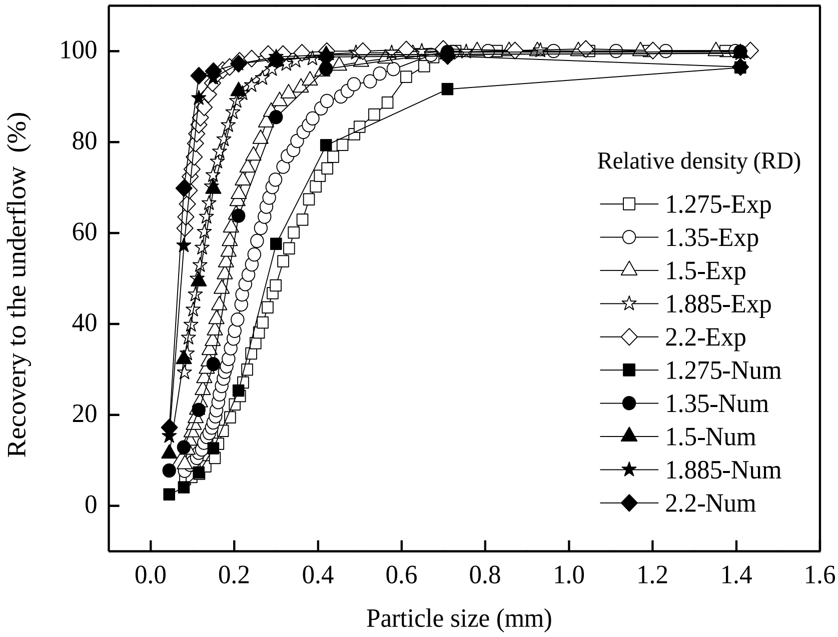

(a)

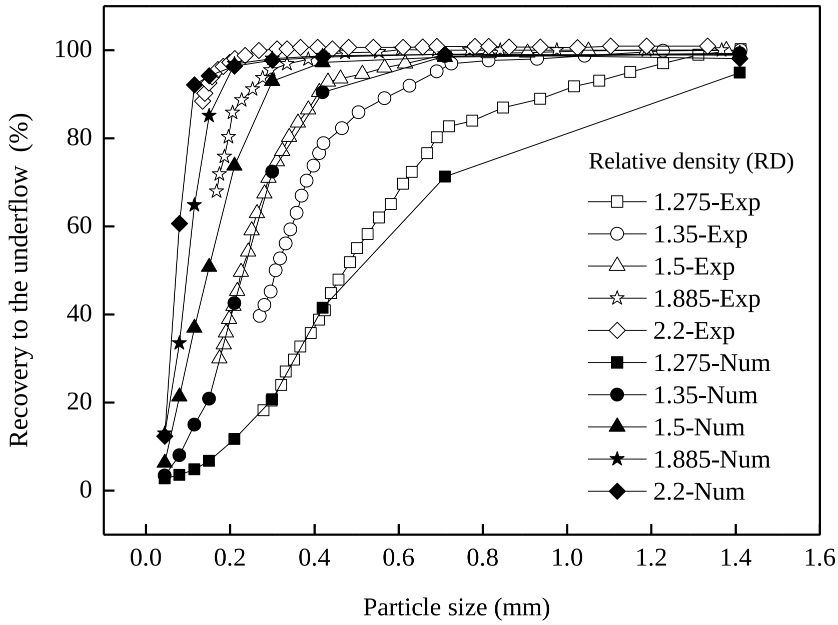

(b)

Fig. 6.2 Effect of particle relative density on the separation efficiency at the feed solids concentration of: (a) SC=6.6% and (b) SC=13.4%.(b)

Fig. 6.2 also shows that there are some differences between the simulated and experimental results. These differences may be due to the following reasons. First, the current model contains some assumptions that may not correctly represent the reality including the use of parcel particles. Secondly, only a rough estimate of the size distribution is available. That is, the particle size distribution in the simulation is not exactly the same as that used in the experiment. Finally, the common practice of measuring a particle size distribution is not capable of precisely defining a size that can be used in the simulation. For example, a particle with diameter of 2mm may not pass through screen size of 2 mm. Thus, the particles used in the simulation may be larger than those used in the experiment. How these factors affect the computed results and hydrocyclone performance is not clear, and needs to be addressed in the future. Nonetheless, the showed results suggest that the present approach can produce results that can be at least used qualitatively.

6.3.2 **Effect of particle density on separation efficiency parameters**

A partition curve can be characterised by cut size, sharpness of partition curve, and water split as stated by Plitt (1976). These three parameters together with inlet pressure drop (an index of energy loss) are used to judge cyclone performance in our study. This helps quantitatively to examine the effects of density at different feed solids concentrations. Fig. 6.3 shows that with increasing relative density, the inlet pressure drop defined as the difference of average pressures at the inlet and underflow outlet, initially decreases sharply and then slowly increases. It monotonically increases with the increase of feed solids concentration. The results can also be confirmed by the pressure drop contours presented in Fig. 6.5 (b).

The decreasing trend of pressure drop with increasing relative density fraction at a typical feed solids concentration is evident in this figure. In order to better understand the particle behaviors at different density fraction, we examine representative distributions of particles of different static pressure, tangential and axial velocity on the vertical 2–2 plane defined in Fig. 6.4. The results are given in Fig. 6.5 and Fig. 6.7.

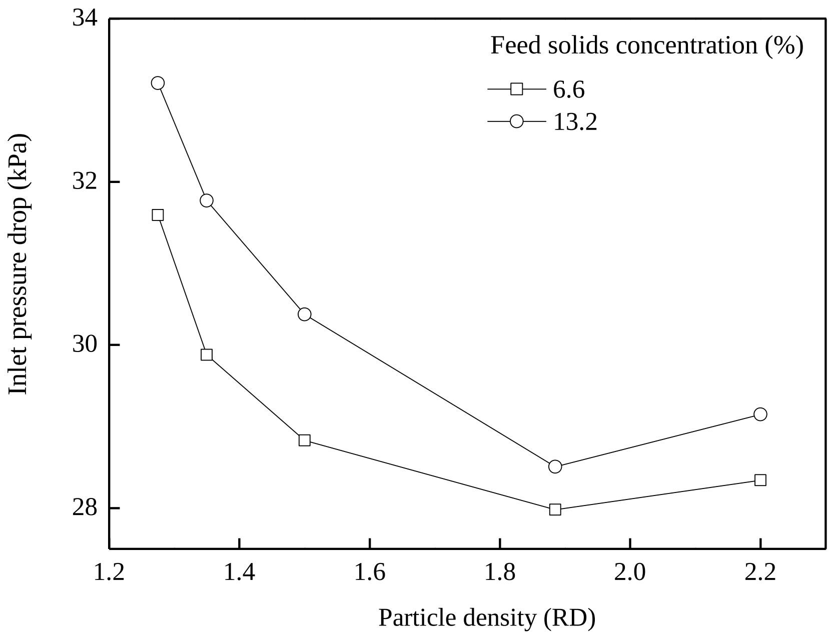

Fig. 6.3 Effects of relative density on pressure drop.

In these figures (and Fig. 6.11 to 6.12), the white region corresponds to the area occupied by the air core, which is not shown for clarity as the properties of air and liquid phases are basically different.

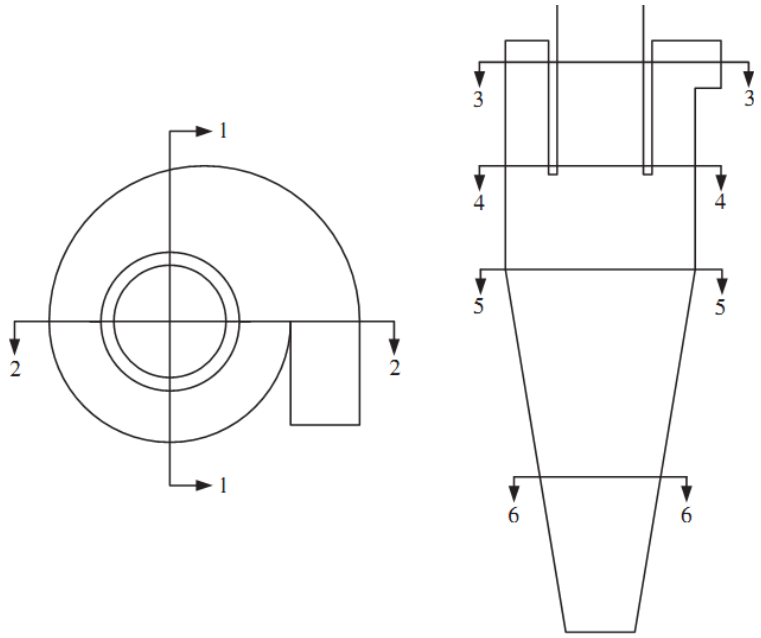

Fig. 6.4 Definitions of the sections used in this work.

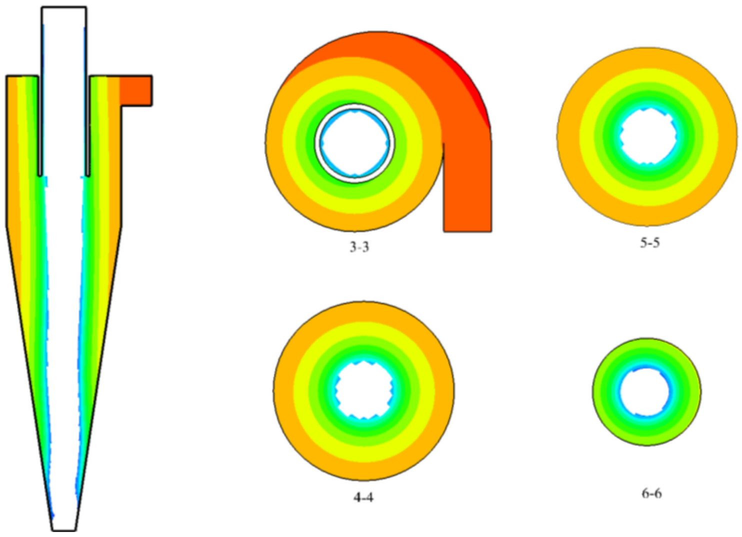

(a)

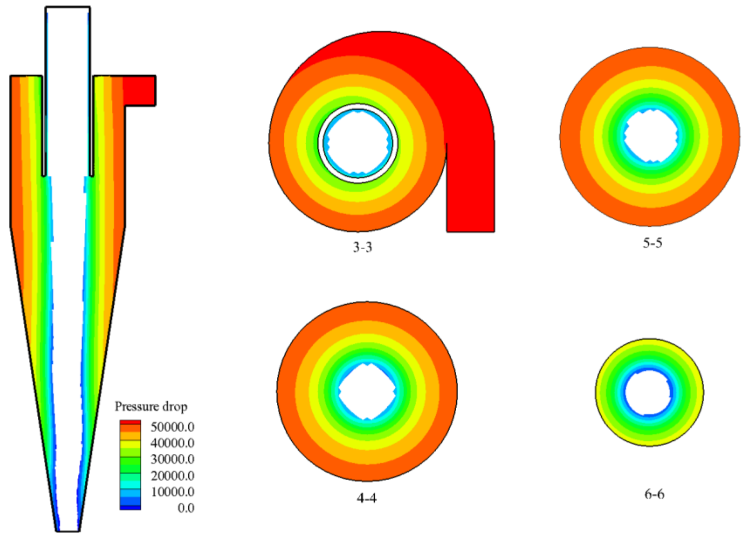

(b)

Fig. 6.5 Effect of particle relative density on spatial distribution of mixture pressure drop at different feed solids concentrations: (a) SC=6.6% and (b) SC=13.4%.

Fig. 6.6 shows that for a given feed solids concentration, the cut size linearly decreases with the increase of density although it almost remains the same when density is relatively high (e.g. RD=2.2 and 1.885). The reason for this behaviour is as density increases the settling speed of particles decreases (Kawatra et al., 1996) which promote the possibility of coarse particles to reach to the central region and move with the upward water flow and report to the overflow.

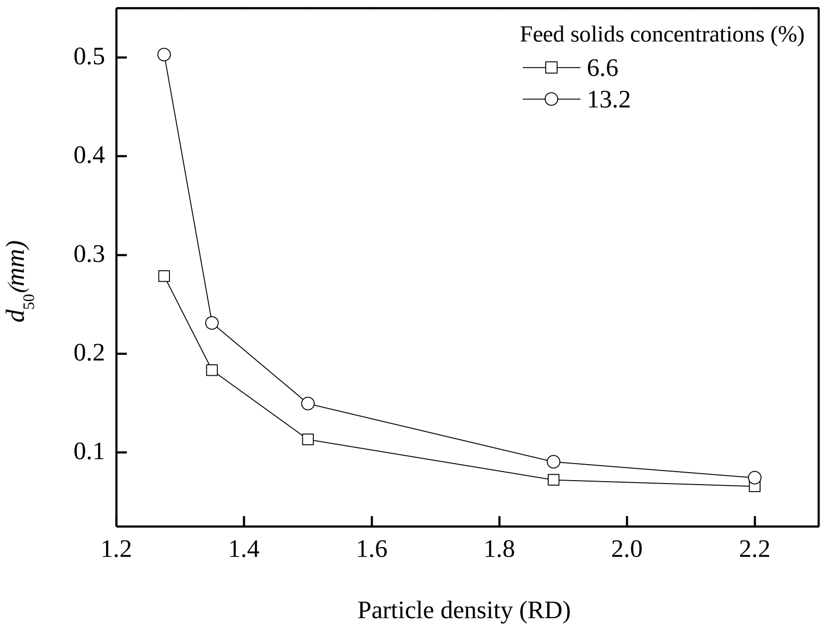

Fig. 6.6 Effects of relative density on cut size.

Fig. 6.7 shows that the tangential velocity of the particle phase decreases with the increase of the averaged particle density, especially in the middle of the conical region of the cyclone. The decrease in the tangential velocity represents the loss of swirling energy and contributes to the drop of pressure as shown in Fig. 6.3.

Fig. 6.9 shows the effect of different density fractions on the amount of water split to underflow. The WS value (defined as the ratio of the volumetric water flow rate of the underflow to that of the feed stream) increases with increasing coal density to a maximum and then decreases. The partitioning of the higher density particles (RD=2.2) is relatively unaffected by solid concentration. However, the misplaced lighter particles reporting to the overflow stream are notably in a far more dilute environment.

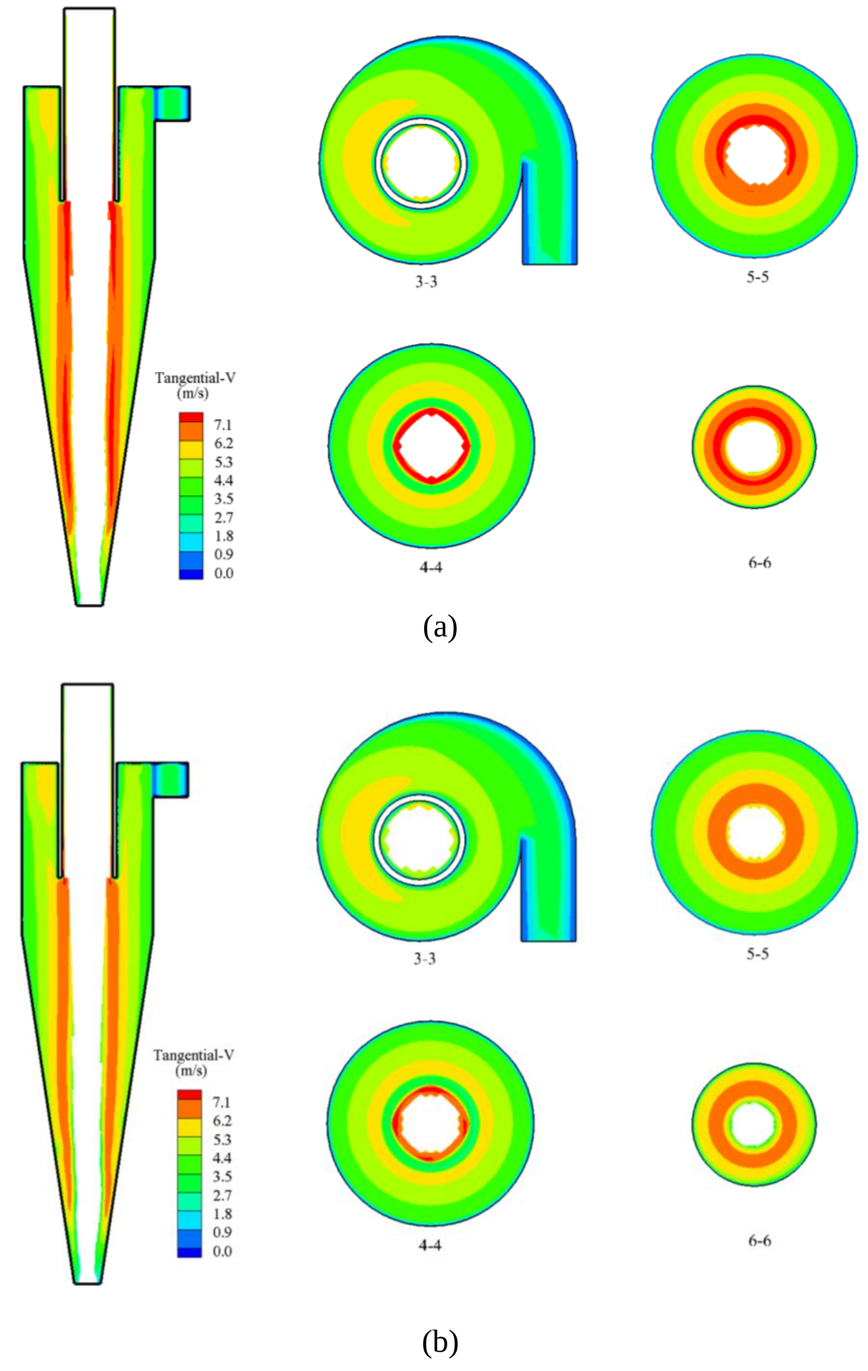

Fig. 6.7 Effect of relatively high particle relative density (RD=1.275) on spatial distribution of tangential velocities at different feed solids concentrations: (a) SC=6.6%, (b) SC=13.4%

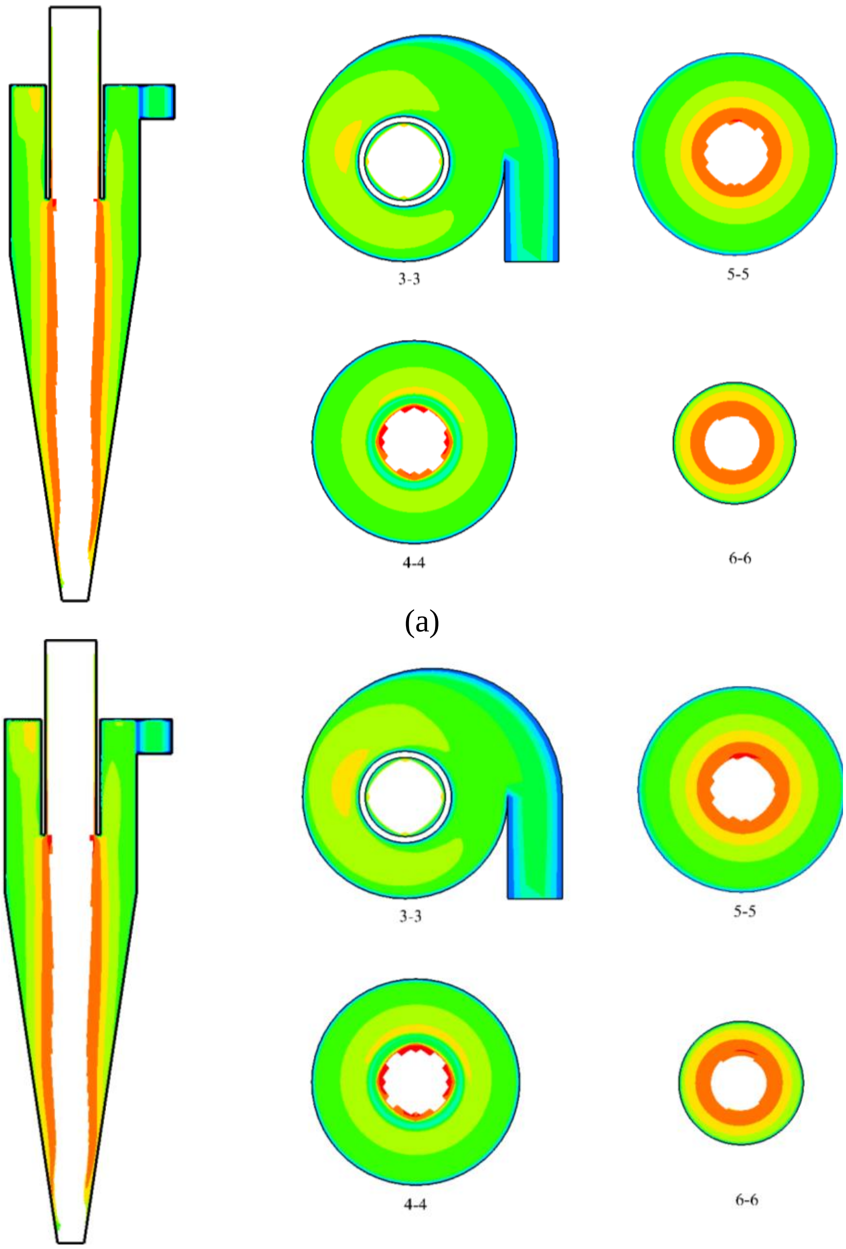

(b)

Fig. 6.8 Effect of relatively high particle relative density (RD=2.2) on spatial distribution of tangential velocities at different feed solids concentrations: (a) SC=6.6%, (b) SC=13.4%

It is well known that in particle classification within a hydrocyclone, the water split should as low as possible. This is because it largely reflects the amount of particles (regardless of being coarse or fine) which flow with water, by-pass the classification process, and finally misplace at the underflow and overflow outlets as found by (Lynch, 1976; Slechta and Firth, 1984). Here, the tangential velocities and associated properties such as axial velocities and solids volume fraction are tested to link their variation with performance indices which have been shown in. Fig. 6.11 and Fig. 6.12.

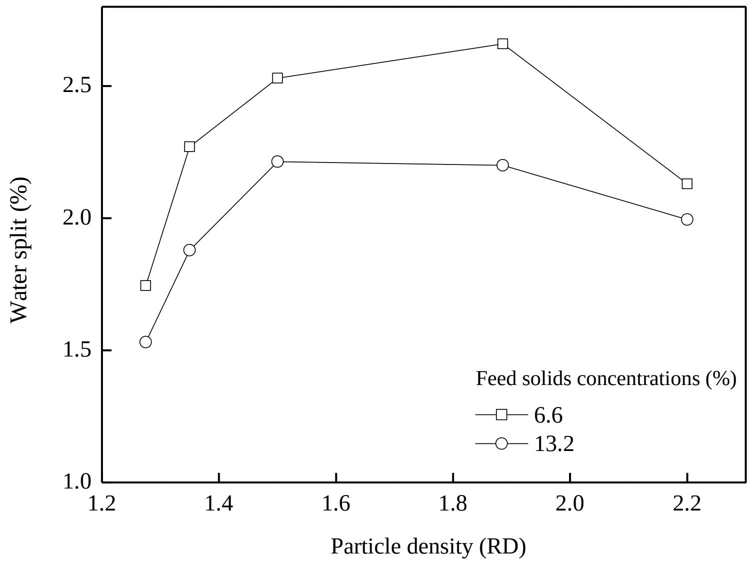

Fig. 6.9 Effects of particle relative density on water split.

In hydrocyclones, radial acceleration characterizes the driving force required for separation (Svarovsky, 1984). This acceleration drives particles to move towards the wall and join the right flow streams. When this acceleration is not large enough, some comparatively coarse particles join the upward flow stream and report to the overflow. However, fairly large radial acceleration makes relatively fine particles to join in the downward flow stream and report to the underflow. Both cases cause sharpness deterioration and thus large E_p. In essence, tangential velocity and radial acceleration are usually used to describe different phenomena observed in hydrocyclones (see, e.g., Wang and Yu, 2006,2008; Davailles et al., 2012a & b; Davailles et al., 2012b; Ghodrat et al., 2013a,b). In this section, tangential velocities and correlated properties such as axial velocities and solids volume fraction are studied to connect their variations to those of performance indices shown in Fig. 6.3, Fig. 6.6, Fig. 6.9 and Fig. 6.10 better understanding the effect of relative density.

Fig. 6.7 shows that for the cyclone of different particle density fractions, the separation region, characterized with relatively large tangential velocities, is mainly located near the central region of the cyclone below the tip of vortex finder. When density fraction is increased at a constant feed solid concentration, the separation region become restricted and the velocity magnitudes generally decrease. This can be observed more clearly in the plan view 6-3 to 6-6 which plots the tangential velocities in four representative heights in the same figure for cyclones of different densities. Because of smaller magnitudes of the tangential velocities, the radial acceleration decreases with the increase of density according to radial acceleration equation ($a_r=u_t^2/r$). This results in the decreased of the E_p value. However, when relative density is low the strong swirling flow causes the large tangential velocities at the upper part of the cyclone (see Fig. 6.7(a)). Consequently, at the lower part of the cyclone, fine particles cannot join the upward flow stream and report to the overflow as predicted even when these particles are properly separated in the radial direction. This deteriorates the sharpness of the cut and results in a relatively large E_p at the low density fractions. For low densities when feed solids concentration increased, the tangential velocities near the spigot region declines (see Fig. 6.7 (b)). This velocity reduction leads to a decreased separation region and hence a higher E_p. The variation of E_p with feed solids concentration for higher relative densities is negligible as shown in Fig. 6.9.

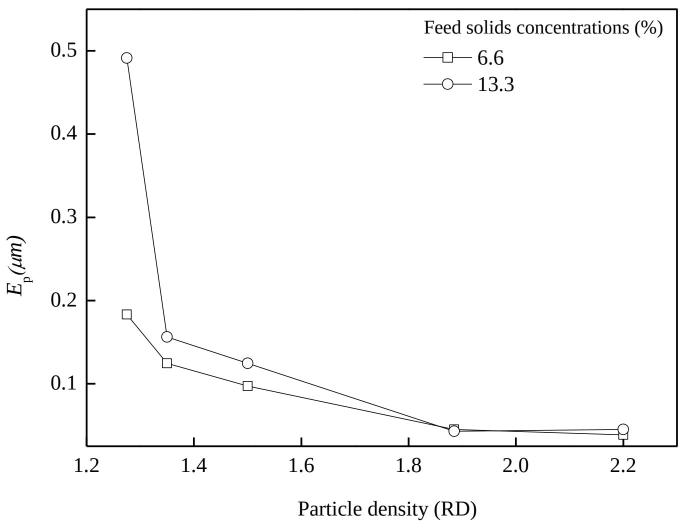

Fig. 6.10 Effects of particle relative density on sharpness of separation

Fig. 6.11 shows that when the relative density of coal particles increases, the locus of zero axial velocity moves towards the center and there is an increased portion of the downward flow characterized by negative axial velocity up to RD=1.35. For relatively high feed solids concentration (Fig. 6.11 b) water split reach to its maximum amount, thereafter the trend remain mostly unchanged and water split slowly decreases as shown in Fig 6.10.

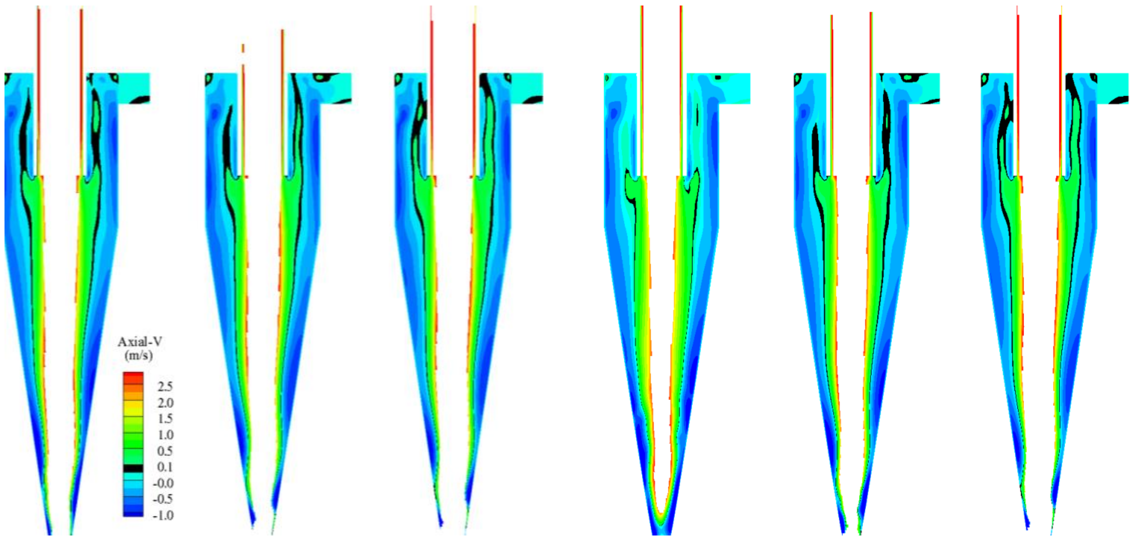

1.275(RD) 1.350(RD) 2.2(RD) 1.275(RD) 1.350(RD) 2.2(RD)

(a) (b)

Fig. 6.11 Effect of particle density fraction on spatial distribution of axial velocity at different feed solid concentrations: (a) SC=6.6% and (b) SC=13.4%.

Fig. 6.11 also shows that the effect of the feed solids concentration on the locus of zero axial velocity is smaller than that of coal density especially for relatively low (RD=1.275) and high (RD=2.2) feed solids concentrations. This is consistent with the predicted result that the water split is influenced by feed solids concentration. (Fig. 6.9) Solids volume fraction contours can be used to explain particle density variation behaviour as shown in Fig. 6.12 and Fig. 6.13.

Fig. 6.12 illustrates the distributions of coal particles of different densities inside the hydrocyclone, and when particle diameter is 1.4 mm. It is evident from this figure that for clean coal (e.g. RD = 1.275 and 1.350) more particles accumulate on the wall and flow down to join the underflow stream within the spigot.

For particles with densities around the cut density (e.g. RD = 1.500) and heavy particles (e.g. RD = 1.850 and 2.200) aggregation around the wall decreases and particles spiral down to the underflow. The helical path of particles on the wall can be observed for both medium and heavy densities under the present condition (see Fig. 6.12b), which should account for the wear phenomenon.

Fig. 6.13 also shows the distribution of coal particles of different density fractions while particles size is relatively fine (0.045 mm). It is shown that with increasing coal density more particles gather close to the center of the cyclone around the air core and vortex finder area as well as the cyclone wall particularly near the spigot. The helical path of particles on the wall is not as evident as in Fig. 6.12 b.

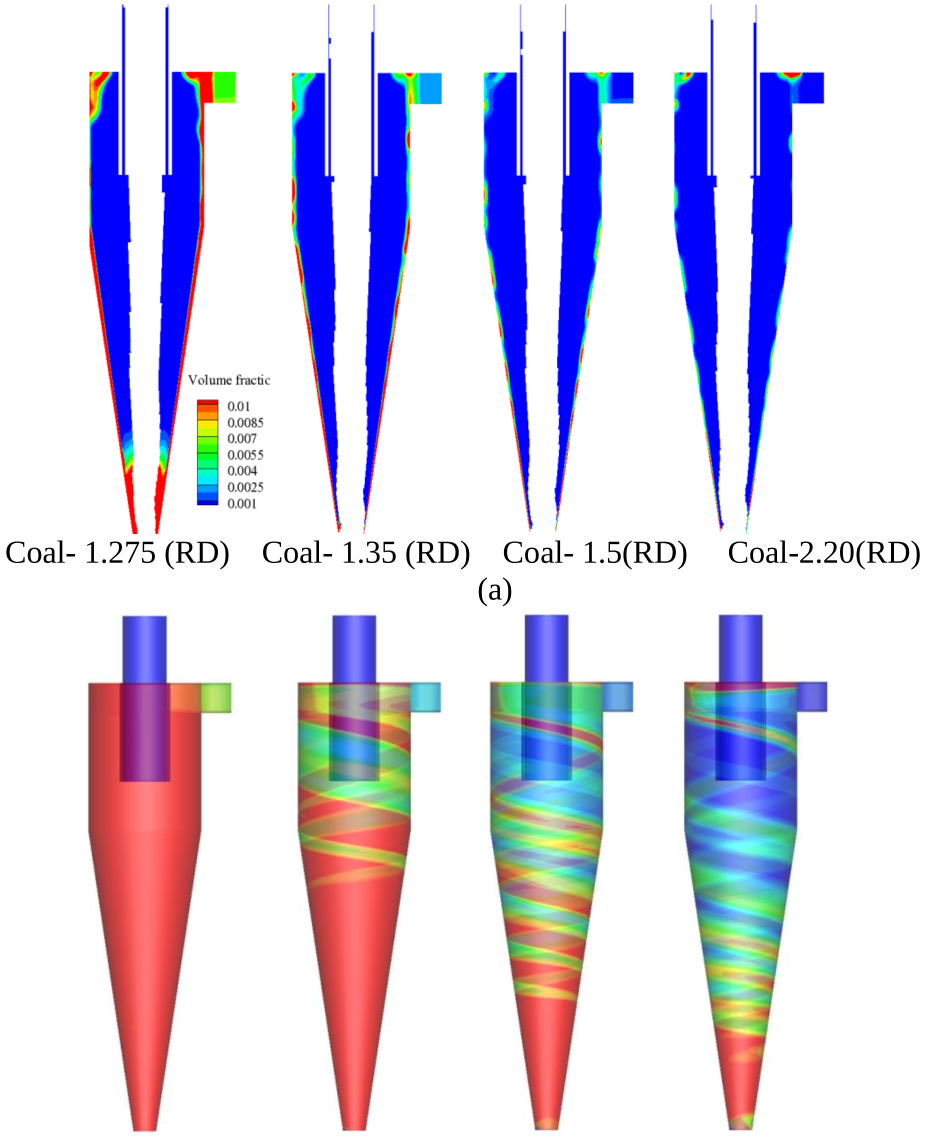

(b)

Fig. 6.12 Distributions of coal particles of different densities: (a) inside the hydrocyclone, and (b) on the wall when particle diameter is 1.4 mm.

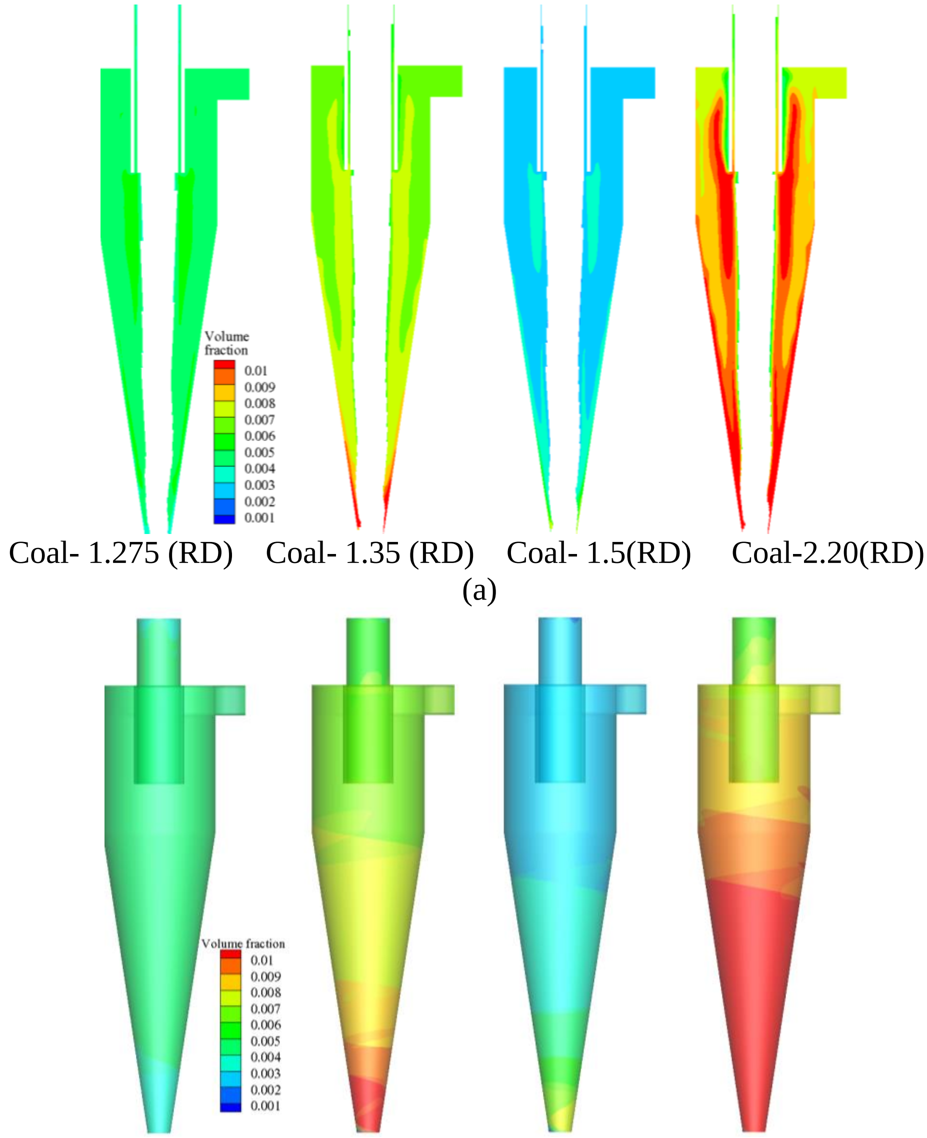

(b)

Fig. 6.13 Distributions of coal particles of different densities: (a) inside the hydrocyclone, and (b) on the wall when particle diameter is 0.045 mm.

As can be seen from Fig. 6.11 the upward axial velocities in the spigot region are stronger at smaller density fractions and thus the rejects are more difficult to move out of the spigot. Consequently, particles may accumulate in the spigot region, and fall down with the aid of gravity till it reaches a certain amount. This leads to significant fluctuation of mass flow at the underflow, which can be reflected in the results shown in. Fig. 6.14. It can be seen from this figure that the mass flow rate fluctuates more significantly with lower relative density. This suggests that the operation at a smaller density may be less stable.

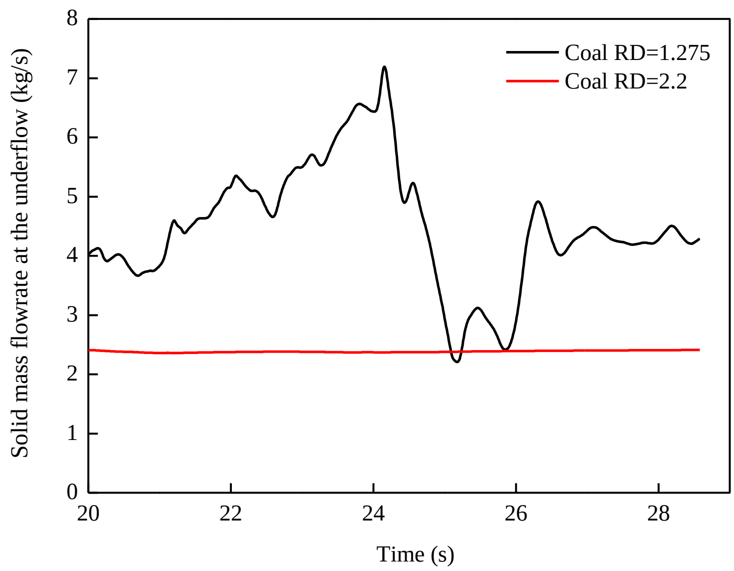

Fig. 6.14 Temporal variation of mass flow rate at the underflow for two relative density fractions

6.4 Conclusions

Feed density variation plays an important role in the separation of particles in hydrocyclones. A TFM approach facilitated by the mixture model has been extended and used to study the effect of density. The performance indices such as water split, sharpness of separation and cut size along with different flow profiles have been used to explain the underlying phenomena. The findings of this study can be summarised as follows:

- When feed density increases, both cut size and sharpness of separation are shown to have a descending trend. The amount of water reporting to the underflow stream as a key indicator of the fine particle loss, decreases for low densities (Coal (RD) =1.275) and deteriorates for the middle range densities (RD=1.5, 1.850).
- The influences of feed density fraction on cyclone performance are essentially governed by axial and tangential velocities and solid volume fraction. When density fraction is increased at a constant feed solid concentration, the separation region is restricted and the velocity magnitudes generally decrease which leads

to a decreased radial acceleration and hence a decreased sharpness of separation (E_p).

- It has been found that when the particles density is relatively high, more particles accumulate close to the wall, then flow down to join the underflow stream within the spigot. This phenomenon results in the erosion of wall surface.
- At lower relative density the upward axial velocity in the spigot region is stronger and particles accumulate in the lower part of the cyclone and fall down with the aid of gravity. This leads to significant fluctuation of mass flow at the underflow. It is also shown that the mass flow rate fluctuates more significantly with lower relative density. This suggests that the operation with too many light particles may be less stable.

REFERENCES

Bretney, E., 1891. ‘Water Purifier’. US Patent No. 453 105.
Chu, L.-Y., Chen, W.-M., Lee, X.-Z., 2002. Effects of geometric and operating parameters and feed characters on the motion of solid particles in hydrocyclones. Separation and Purification Technology, 26 (2–3), 237-246.
Davailles, A., Climent, E., Bourgeois, F., 2012a. Fundamental understanding of swirling flow pattern in hydrocyclones. Separation and Purification Technology, 92 (0), 152-160.
Davailles, A., Climent, E., Bourgeois, F., Majumder, A. K., 2012b. Analysis of swirling flow in hydrocyclones operating under dense regime. Minerals Engineering, 31 (0), 32-41.
Fahlstrom, P., 1963. Studies of the Hydrocyclone as a Classifier. Mineral Processing, Proc 6th Intl Congress, Cannes, 87-113.
Firth, B., Edward, D, Clarkson, C and O’Brien, M, 1995. “The Impact of Fine Classification on Coal Preparation Performance”. in Smitham, J (ed)Proc 7th Australian Coal Preparation Conference, Paper E2.
Ghodrat, M., Kuang, S. B., Yu, A. B., Vince, A., Barnett, G. D., Barnett, P. J., 2013a. Computational study of multiphase flow and performance of hydrocyclone: effects of cyclone size and spigot diameter. Industrial & Engineering Chemistry Research, 52 16019-16031.
Ghodrat, M., Kuang, S. B., Yu, A. B., Vince, A., Barnett, G. D., Barnett, P. J., 2013b. Numerical analysis of hydrocyclones with different conical section designs. Minerals Engineering, http://dx.doi.org/10.1016/j.mineng.2013.12.003.
Heiskanen, K., 1996. Developments in Wet Classifiers. Int J of Mineral Processing, 44-45 (29-42).
Hukki, R. T., 1968. "AN ANALYSIS OF MILL AND CLASSIFIER PERFORMANCE." VIII Int. Transactions AIME, 238 233.
Kawatra, S. K., Bakshi, A. K., Rusesky, M. T., 1996. Effect of viscosity on the cut (d50) size of hydrocyclone classifiers. Minerals Engineering, 9 (8), 881-891.
Kuang, S. B., Chu, K. W., Yu, A. B., Vince, A., 2012a. Numerical study of liquid-gas-solid flow in classifying hydrocyclones: effect of feed solids concentration. Minerals Engineering, 31 17-31.
Kuang, S. B., Chu, K. W., Yu, A. B., Vince, A., 2012b. Numerical study of liquid–gas–solid flow in classifying hydrocyclones: Effect of feed solids concentration. Minerals Engineering, 31 (0), 17-31.
Launder, B. E., Reece, G. J., Rodi, W., 1975. Progress in the development of a Reynolds-stress turbulence closure. Journal of Fluid Mechanics, 68 537-566.
Lynch, A. J., 1976. Mineral crushing and grinding circuits. Elsevier, Amsterdam.
Manninen, M., Taivassalo, V., Kallio, S., 1996. On the mixture model for multiphase flow. 288 p.
O'brin, M., A.Taylor, Nemeth, D., B.Firth, C.Clarkson, 2001. Investigation into the performance of large diameter classifying cyclones. ACARP.
Plitt, R., 1976. A Mathematical Model of the Hydrocyclone Classifier. CIM Bull,, 69 114-123.
Shah, H., Majumder, A., Barnwal, J., 2006. Development of water split model for a 76mm hydrocyclone. Minerals Engineering, 19 (1), 102-104.
Slechta, J., Firth, B. A., 1984. Classification of fine coal with a hydrocyclone. International Journal of Mineral Processing, 12 (4), 213-237.

Svarovsky, L., 1984. Hydrocyclones. Holt, Rinehart and Winston, Sydney.
Syamlal, M., Rogers, W., O'Brien, T. J., 1993. MFIX documentation: theory guide. National Technical Information Service, Springfield, VA, DOE/METC-9411004,NTIS/DE9400087.
Wang, B., Yu, A. B., 2006. Numerical study of particle-fluid flow in hydrocyclones with different body dimensions. Minerals Engineering, 19 (10), 1022-1033.
Wang, B., Yu, A. B., 2008. Numerical study of the gas-liquid-solid flow in hydrocyclones with different configuration of vortex finder. Chemical Engineering Journal, 135 (1-2), 33-42.
Williams, R. A., Albarran de Garcia Colon, I.L., Lee, M.S., and Roldan Villasana, E.J., 1994. Design Targeting of Hydrocyclone Netwrks. Minerals Engineering, Nos, 5/6 561-576.

CHAPTER 7

Conclusions and Future Works

7.1 Conclusions

This research is intended to study the gas-liquid-solid flow in hydrocyclones using a Computational Fluid Dynamics (CFD) numerical model. The applied CFD model covered a wide range of feed solids concentration and included the effects of key variables related to geometry, operational conditions, and material properties on the cyclone flow and performance. Referring to the achieved results, the following concluding remarks can be drawn:

- The geometrical parameters play an important role in the hydrocyclone performance. The separation efficiency decreases with an increase of cyclone size or the decrease of spigot diameter. Correspondingly, the cut size increases, whereas the water split decreases and hence the by-pass flow decreases. These effects are quantitatively different at different feed solids concentrations and can be well explained by the variation of radial acceleration. The inlet pressure drop increases with the increase of cyclone size or spigot diameter. With increasing feed solids concentration, the pressure drop first decreases to a minimum and then increases for relatively small cyclones, however, monotonically increases for the relatively large cyclones. These behaviours are attributed to the collective effect of tangential velocity, mixture density and scale factor. The separation sharpness increases with a decrease of cyclone size or feed solids concentration due to the increased radial acceleration. However, with increasing spigot diameter, the separation sharpness decreases first and then increase and flattens out due to the increased radial acceleration and the by-pass effect in proportion with water split. The optimum spigot diameter, where the sharpness of separation has the minimum value, can be found for given operational conditions. In addition, it is revealed that the pressure drop within the spigot controls the formation of air core. Two diagrams can be established to predict air core with respect to cyclone size, spigot diameter and feed solids concentration. It is shown that air core is suppressed by small spigot diameter, high feed solids concentration and small cyclone.

- The conical geometry affects hydrocyclone flow and performance significantly. The length and shape of the conical section have been shown to have a substantial effect on the hydrocyclone flow regime and performance under wide range of feed solids concentrations. A longer conical section length leads to decreased inlet pressure drop, d_{50} and E_p, and at the same time, increased water split (thus larger by-pass effect). These effects are pronounced by increasing feed solids concentration. However, the inlet pressure drop is sensitive to feed solids concentration mainly at relatively short conical section lengths. In addition, cone shape including concave and convex styles plays key effect on cyclone performance. Based on this concept a compromised optimum performance is perceived for the cyclone with a convex cone at all the feed solids concentrations. The compromised optimum performance involves a minimum E_p and relatively small inlet pressure drop and water split. These performance parameters increase with the increase of feed solids concentration. Based on the CFD results, new improved cyclone design has been proposed by introducing a long convex cone design. Compared to the conventional cyclone, the new cyclone has a larger separation region with smaller tangential velocities, however, larger tangential velocities around the spigot region. Its inlet pressure drop, water split and Ep are hence lower in value.

- Through the dynamic analysis, it has been found that the vortex finder configuration as an important geometrical variable plays the main role in the separation of particles in hydrocyclones. The flow and performance of hydrocyclone have been studied by the proposed multiphase mixture model, with the special reference to the shape and dimension of vortex finder. The shapes include the conventional cylindrical style and the proposed conical and inverse conical styles. It has been perceived that when the vortex finder diameter or shape varies, a compromised optimum performance is identified with relatively small inlet pressure drop, cut size, sharpness of separation, and water split. The optimum shape is an inverse conical style. In addition, a larger vortex finder diameter leads to lower separation function in cyclone, which, however, does not happen to the proposed vortex finders. Overall, both d_{50} and E_p are found to be more sensitive to feed solids concentration than inlet pressure drop and water split at different vortex finder configurations. The effect of vortex finder length on the separation efficiency is much less significant than those of diameter and shape, which shows an opposite trend at low and high feed solids concentrations due to different magnitudes and locations of large tangential velocities. The influences of vortex finder dimension and shape on cyclone performance are essentially governed by axial and tangential velocities and solids volume fraction. The tangential velocity and solid volume fraction near the inlet region determine the inlet pressure drop, while the portion of downward flow characterised by the downward axial velocities influences the water split. The size and location of the separation region with large tangential velocities and magnitude of the tangential velocities together govern separation sharpness. These flow properties can, to some degree, be controlled by varying the vortex finder configuration.

- Same TFM approach has been subsequently used to study and quantify the effect of different coal densities on performance and flow regime of hydrocyclones. The results are found to be qualitatively consistent with the experiments. The performance indices such as water split, sharpness of separation and cut size along with different flow profiles have been used to explain the underlying phenomena. Both cut size and sharpness of separation are shown to have a descending trend with increasing coal density. The amount of water reporting to the underflow stream as a key indicator of the fine particle loss decreases for low densities (Coal (RD) =1.275) and increases for the middle range densities (RD=1.5, 1.850). It has been shown that the operation of large diameter cyclones is less stable at lower coal densities. The influences of feed density fraction on cyclone performance are essentially governed by axial and tangential velocities and solid volume fraction. The results of numerical simulation revealed that at a constant feed solids concentration, when the particles density fraction is increased, the separation region is restricted, and the particles velocity magnitudes decrease, which leads to a decrease in radial acceleration and sharpness of separation (E_p). It has been found that when the particles density is relatively high, more particles accumulate close to the wall, then flow down to join the underflow stream within the spigot. This phenomenon results in the erosion of wall surface.

At lower relative density, the upward axial velocity in the spigot region is stronger, and particles accumulate in the lower part of the cyclone. These particles then fall with the aid of gravity. This leads to significant fluctuation of mass flow at the underflow. It is also shown that the mass flow rate fluctuates more significantly in lower relative density. This suggests that the operation with too many light particles may be less stable.

7.2 Future works

In this research, significant strides have been made to study the complicated liquid-gas-solid flow in hydrocyclones under a wide range of conditions. The predicted flow features were examined in terms of the flow behaviour and performance indices. Based on these works, the main areas can be considered for future studies are listed as follows:

- The effect of the inlet design, both size and shape on hydrocyclone flow and performance under a wide range of feed solids concentration is an area, which could be thought-provoking especially for large diameter industrial hydrocyclones. This research area could be carried out in parallel with inlet velocity variation effects on flow and performance

- The motion of particles and the "fish-hook" phenomenon in hydrocyclones should be further studied to mitigate the adverse effect of this phenomenon especially under dense flow regime. The outcomes are beneficial to apply in numerical simulation of multiphase flow in terms of flow behaviour analysis in the hydrocyclones.

- The effect of apex water injection in improving hydrocyclone classification efficiency is another field of study, which is noteworthy to follow. The main motivation is to achieve ultrafine particle size separations in industrial applications. The inherent deficiencies of the current industrial designs of hydrocyclone include particle density effects in multi-component suspension and ultrafine particle short circuiting to the underflow stream due to hydraulic entertainment. The recently developed TFM facilitated by mixture model could be utilized to evaluate the benefit of tangential water injection into the apex a cyclone for minimizing the ultrafine by-pass.

- There is a limited number (up to 20) of phases that can be simulated in the ANSYS Fluent for numerical stability, which brings difficulty to the simulation of operations involving a wide distribution of particle size/density or a strong interplay among particle properties. This problem can be overcome by combing the CFD- DEM model for coarse coal and the mixture model for fine coal. Further studies are necessary for the future to decide the criteria for the combination and identify the resulting benefits about prediction accuracy and computational efficiency.

- To date the effect of inlet velocity variation on hydrocyclones flow behaviour and performance indices is largely carried out for dilute regime, and few experimental or numerical investigations exist for dense regime. A dedicated broad study should be considered to examine the special distribution of flow indices within the hydrocyclone.

- Effect of viscosity on flow regime and performance of hydrocyclone is a constructive field of research which could shed light in classification efficiency improvement of the device. The necessity for monitoring slurry viscosity in order to improve cyclone efficiency, and moreover that the control strategies based on inferential sizing techniques (Seitz and Kawatra, 1984) must be modified to allow for the observed behaviour. Further work must be done to improve the quality of on-line viscosity measurements of mineral slurries.

- Using "Hydrocyclones in series" method for overcoming misplaced particle could be an effective approach and further investigation is required at an industrial scale.

LIST OF PUBLICATIONS

JOURNAL PAPERS

1. M. Ghodrat, S. B. Kuang , A. B. Yu , A. Vince , G. D. Barnett , and P. J. Barnett., Computational Study of the Multiphase Flow and Performance of Hydrocyclones: Effects of Cyclone Size and Spigot Diameter. *Published in Industrial & Engineering Chemistry Research, 2013, 52, 16019-16031*

2. M. Ghodrat, S. B. Kuang, A. B. Yu, Andrew Vince., "Numerical analysis of hydrocyclones with different conical section designs" , *Minerals Engineering ,Volume 62, July 2014, Pages 74–84*

3. M. Ghodrat, S. B. Kuang, A. B. Yu, Andrew Vince., "Numerical analysis of hydrocyclones with different vortex finder configurations" , *Minerals Engineering, Volume 63, August 2014, Pages 125–138*

4. M. Ghodrat, S. B. Kuang, A. B. Yu, A. Vince "CFD study of the effect of coal density on multiphase flow and performance of hydrocyclone" .To be submitted.

CONFERENCE PAPERS

5. M. Ghodrat, S. B. Kuang, A. B. Yu, A. Vince, G. D. Barnett, P. J. Barnett, 'CFD study of the multiphase flow in classifying hydrocyclone: Effect of cone geometry', *Ninth International Conference on CFD in the Minerals and Process Industries, CSIRO*, **Melbourne, Australia**, 10-12 December 2012.

6. M. Ghodrat, S.B. Kuang, A.B. Yu, A. Vince, G.D. Barnett and P.J. Barnett., 'Numerical analysis of hydrocyclones with different conical section designs'. In *MEI* Conferences: Physical Separation '13: Falmouth, Cornwall, UK, 2013

7. M. Ghodrat, S.B. Kuang, A.B. Yu, A. Vince, G.D. Barnett and P.J. Barnett., 'Numerical analysis of hydrocyclones with different vortex finder designs' In MEI Conferences: Computational modeling '13: Falmouth, Cornwall, UK, 2013

8. M. Ghodrat, S.B. Kuang, A.B. Yu, A. Vince “CFD study of the effect of coal density on the multiphase flow and performance in large diameter classifying”, the second Australia-China Joint Symposia on Minerals and Metallurgy”, Sydney ,Australia , 23-25 July, 2014.